Synthesis and Characterization of Novel Polyethers and Polypeptides for Use in Biomedicine and Magnetic Resonance Imaging

Jue Liang

Dissertation submitted to the Faculty of Virginia Polytechnic Institute and State University in partial fulfillment of the requirements for the degree of

Doctor of Philosophy

in

Chemistry

Judy S. Riffle, Committee Chair
Richey M. Davis
S. Richard Turner
Webster L. Santos

December 9, 2013
Blacksburg, VA

Key words: functional polyethers, poly(glutamic acid), iron oxide, poly(ethylene oxide), poly(propylene oxide), heterobifunctional polyethers, superoxide dismutase

Synthesis and Characterization of Novel Polyethers and Polypeptides for Use in Biomedicine and Magnetic Resonance Imaging

Jue Liang

Department of Chemistry, Virginia Polytechnic Institute and State University, Blacksburg, VA 24061-5976, USA

Abstract

Copolymers that contain terminal or pendent functional groups have great potential in the biomedical area due to their biocompatibility and tunable properties.[1-3] In this research, two vinyl functional epoxides, vinyldimethylsilylpropyl glycidyl ether (VSiGE) and ethoxy vinyl glycidyl ether (EVGE), were synthesized. These heterobifunctional monomers were polymerizable via the epoxide groups and can be functionalized via thiol-ene reactions through the pendent vinyl groups. A series of amphiphilic block copolyethers based on poly(ethylene oxide) and poly(1,2-butylene oxide) that incorporate VSiGE or EVGE were synthesized and characterized. The vinyl ether and vinyl silane functional groups were functionalized after polymerization and the functional polymers formed pH-sensitive micelles in aqueous medium. The copolyethers were loaded with ritonavir yielding well-controlled nanoparticles.

Poly(L-glutamic acid) is comprised of naturally occurring L-glutamic acid repeating units that are linked together with amide bonds. In this research, we have prepared magnetic block ionomer complexes based on poly(ethylene oxide)-*b*-poly(L-glutamic acid) copolymers. This is of interest due to the biocompatibility and biodegradable nature of the poly(L-glutamic acid) component of the backbone. Allyl- and thiol-functional poly(ethylene oxide)-*b*-poly(L-glutamic acid) copolymers were also synthesized and coated onto the surface of iron oxide nanoparticles. Allyl- and thiol-tipped single particles were reacted with each other to prepare magnetic clusters.

Transverse relaxivities of the clusters were found to be significantly higher than that of single particles.

One major problem in commercial development of therapeutic proteins is their poor transport across cellular membranes and biological barriers such as the blood-brain barrier (BBB). One solution to this problem is to modify proteins with amphiphilic block copolymers such as PEO-*b*-PPO-*b*-PEO, Pluronics®. However, it isn't possible to independently tune the two PEO block lengths with commercial Pluronics® since a difunctional PPO macroinitator is utilized to grow both PEO blocks simultaneously (HO-EO_n-*b*-PO_m-*b*-EO_n-OH). Another challenge is introducing functional group which allows post-polymerization functionalization for specific applications. In this study, a series of heterobifunctional asymmetric amino-EO_{n1}-*b*-PO_m-*b*-EO_{n2}-OH block copolymers (APs) with different molecular weights of each block were synthesized and the amino terminal group was conjugated to an antioxidant enzyme, Cu/Zn superoxide dismutase (SOD1). The conjugates were characterized and their cellular uptake was investigated.

Acknowledgements

First and foremost, I would like to express my deepest gratitude to my advisor Dr. Judy S. Riffle for her support, guidance, encouragement and trust throughout my graduate studies. She has given me the opportunity to work on challenging and interesting research projects in the area of polymer science, and guided me through reading, thinking, presenting and writing to grow as a research scientist. I sincerely appreciate all her contributions of time, ideas, and funding to make my Ph.D. experience joyful and stimulating.

It is also my honor to be advised by a group of prominent and brilliant committee members, Dr. Richey M. Davis, Dr. S. Richard Turner, and Dr. Webster L. Santos. All of whom I have my utmost respect for.

I would like to extend my very great appreciation to all my group members. Dr. Philip P. Huffstetler introduced me to the research topic. Dr. Yin-nian Lin, who was a research scientist with many years of lab experiences, has provided numerous comments to improve the quality of my research. And Dr. Sue Mecham, Dr. Nikon Pothayee, Dr. Nipon Pothayee, Oguzhan Celebi, Nan Hu, Suzanne Barnes, Ran Liu, Rui Zhang all of whom offered me support and invaluable advice whenever I need a practice presentation, encounter a bottleneck in my research, or seek a general discussion on our research, work and life. I cherish the hardworking environment in which we could learn from each other.

I was lucky enough to collaborate with several other research teams. Dr. Davis and Sharavanan Balasubramaniam have made great contribution to the synthesis and characterization of my nanoparticles. Dr. Kabanov Dr. Xiang Yi and Dr. Jing Tong offered great collaboration on my projects. Without them, this thesis couldn't be completed. I really appreciate their contributions.

I have also had the privilege to talk and discussion with a number of talented individual in

Department of Chemistry at Virginia Tech. Thank you all the professors for your inspiring courses and guidance. Thank you all my friends for your generous collaboration and discussion that widened my vision. I also would like to thank all staff of Department of Chemistry for the selfless support of the students.

Lastly, I would like to thank my beloved family, for their great and never-ending support. None of this would be possible without the love of my family.

Table of Contents

CHAPTER 1: DISSERTATION OVERVIEW 1

CHAPTER 2. LITERATURE REVIEW: FUNCTIONAL AND AMPHIPHILIC COPOLYMERS IN BIOMEDICINE 3

2.1 Introduction **3**
2.1.1 Polymeric materials for application in biotechnology 3
2.1.2 The enhanced permeability and retention (EPR) effect 3

2.2 Micelles based on PEO-containing copolymers **6**
2.2.1 Formation and dimensions of polymeric micelles with core/shell nanostructures 6
2.2.2 Unique properties of PEO-containing copolymers 8
2.2.3 PEO-polyester copolymers 9
2.2.4 PEO-PPO-PEO copolymers 13
2.2.5 PEO-poly(amino acid) copolymers 20

2.3 Stimuli-sensitive copolymers **22**
2.3.1 Multifunctional copolyethers based on tailor-made epoxides 22
2.3.2 Thermosensitive polymers 26

2.4 References: **33**

CHAPTER 3. DESIGN AND SYNTHESIS OF FUNCTIONAL AMPHIPHILIC COPOLYETHERS 41

3.1 Introduction **41**

3.2 Experimental **43**
3.2.1 Materials 43
3.2.2 Characterization 44
3.2.3 Synthesis of Ethoxy Vinyl Glycidyl Ether (EVGE) 46
3.2.4 Polymerization of Ethoxy Vinyl Glycidyl Ether 46
3.2.5 Synthesis of a Tapered mPEG-b-P(EVGE-co-BO) Copolymer 47
3.2.6 Synthesis of a Triblock mPEG-b-PEVGE-b-PBO Copolymer 48
3.2.7 Functionalization of pendent vinyl ether groups with mercaptoacetic acid 48
3.2.8 Functionalization of pendent vinyl ether groups with BOC-cysteamine 49
3.2.9 Synthesis of vinyl dimethyl silyl propyl glycidyl ether (VSiGE) 50
3.2.10 Synthesis of a tapered mPEG-b-poly[VSiGE-co-(1,2-BO)] copolymer 52
3.2.11 Functionalization of pendent vinyl silane groups with cysteamine hydrochloride 52
3.2.12 Synthesis of poly(butylene oxide) homopolymer 53
3.2.13 Critical aggregation concentrations measurements 53
3.2.14 Preparation of block copolymer-stabilized ritonavir nanoparticles 54

3.3 Results and discussion **54**
3.3.1 Synthesis of epoxy-functional monomers 54
3.3.2 Synthesis of copolyethers with pendent vinyl ethers 57
3.3.3 Functionalization of copolyethers with pendent vinyl ethers 62
3.3.4 Synthesis and functionalization of copolyethers with pendent vinyl silanes 68
3.3.5. Solution properties of functional copolyethers 72

3.3.6 Preparation of block copolymer micelles containing ritonavir 76

3.4 Conclusions **80**

3.5 Acknowledgement **81**

3.6 References **81**

CHAPTER 4. POLY(ETHYLENE OXIDE)-*B*-POLY(L-GLUTAMIC ACID) IONIC-NONIONIC BLOCK COPOLYMERS AND THEIR MAGNETIC COMPLEXES 86

4.1 Introduction **86**

4.2 Experimental **87**
4.2.1 Materials 87
4.2.2 Characterization 88
4.2.3 Synthesis of 3-hydroxypropyldimethylvinylsilane (3-HPMVS). 90
4.2.4 Synthesis of ammonium-PEO-CH_3. 91
4.2.5 Synthesis of the N-carboxyanhydride (NCA) of γ-benzyl-L-glutamate 93
4.2.6 Synthesis of poly(ethylene oxide)-b-poly(L-glutamic acid) 93
4.2.7 Synthesis of magnetic iron oxide nanoparticles 94
4.2.8 Adsorption of poly(ethylene oxide)-b-poly(L-glutamic acid) onto iron oxide nanoparticles 95
4.2.9 Synthesis of a heterobifunctional ammonium-PEO-allyl 96
4.2.10 Synthesis of allyl- and thiol-poly(ethylene oxide)-b-poly(L-glutamic acid) (allyl-PEO-PG and thiol-PEO-PG) 96
4.2.11 Synthesis of diallyl- and dithiol-PEO. 98
4.2.12 Synthesis of magnetic clusters 98
4.2.13 Measurements of transverse relaxivities 100

4.3 Results and discussion **100**
4.3.1 Synthesis of amino-functional PEO macroinitiators 100
4.3.2 Synthesis of poly(ethylene oxide)-b-poly(L-glutamic acid) 103
4.3.3 Synthesis of diallyl- and dithiol-functional PEO 111
4.3.4 Synthesis of allyl- and thiol-poly(ethylene oxide)-b-poly(L-glutamic acid) 114
4.3.5 Adsorption of poly(ethylene oxide)-b-poly(L-glutamic acid) onto iron oxide nanoparticles 120
4.3.6 Synthesis of magnetic clusters. 125
4.3.7 Magnetic Properties of iron oxide/PEO-b-poly(L-glutamic acid) complexes 127

4.4 Conclusions **131**

4.5 Acknowledgements **131**

4.6 References **132**

CHAPTER 5. SYNTHESIS AND CHARACTERIZATION OF HETEROBIFUNCTIONAL TRIBLOCK COPOLYETHERS 135

5.1 Introduction **135**

5.2 Experimental **136**
5.2.1 Materials 136

5.2.2 Instrumentation 137
5.2.3 Synthesis of 3-hydroxypropyldimethylvinylsilane (3-HPMVS) 138
5.2.4 Synthesis of dimethylvinylsilylpropyl-PEO-PPO-PEO-OH 139
5.2.5. Ammonium functionalization of dimethylvinylsilylpropyl-PEO-PPO-PEO-OH 141
5.2.6. Synthesis and characterization of SOD1-polymer conjugates 142
5.2.7 Cellular uptake of SOD1-polymer conjugates 144

5.3 Results and discussion **144**
5.3.1 Synthesis of 3-hydroxypropyldimethylvinylsilane (3-HPMVS) 144
5.3.2 Synthesis and characterization of asymmetric triblock copolymers 147
5.3.3 Synthesis of triblock amino-PEO-PPO-PEO-OH copolymers 153
5.3.4 Synthesis and characterization of SOD1-polymer conjugates 154
5.3.5 Cellular uptake of SOD1-polymer conjugates 157

5.4 Conclusions **158**

5.5 References **159**

CHAPTER 6: CONCLUSIONS AND RECOMMENDATIONS 162

List of Figures

Figure 2.1.2.1. (A) Concentrations of Evans blue dye-complexed albumin in: (○), blood plasma; (△), tumor uptake; and (×, □) normal muscle and skin tissues, respectively. (B) Intratumor accumulation of various ^{51}Cr-tagged proteins in solid tumor-bearing mice: (○) neocarzinostatin (NCS) (12 kDa); (●) SMANCS (16 kDa, but known to bind to albumin); (▲) ovomucoid (29 kDa); (□) bovine serum albumin (69 kDa); (■) mouse serum albumin (68 kDa); (△) mouse immunoglobulin G (160 kDa). Radio labeled proteins were injected *i.v.* at time zero. Values are based on radioactivity. The tumor model in both A and B was solid sarcoma S-180 in mice. 5
Figure 2.1.2.2. Illustration of the differences in extravasation from (A) normal tissue and (B) tumor tissue. 6
Figure 2.2.1.1. Configuration of polymeric micelles. 7
Figure 2.2.3.1. The in vitro release rates of ^{3}H-FK506 alone and PCL_{20}-*b*-PEO_{44} micelle-incorporated-3H-FK506. 10
Figure 2.2.3.2. a. The biodistribution of radiolabeled micelle incorporated FK506 (in terms of % of total dose). **b.** The biodistribution of radiolabeled micelle incorporated FK506 (in terms of total dose/g tissue) 11
Figure 2.2.3.3. Illustration of synthesis of DOX-P(DLLA-co-GA)-b-PEO conjugate. ... 12
Figure 8. Release profiles of doxorubicin from polymeric micelle 13
Figure 2.2.4.1. Illustration of synthesis of lipiodol-encapsulating nanocapsules. 15
Figure 2.2.4.2. (A) Release profile of paclitaxel from nanocapsules w/ or w/o lipiodol. (B) Cytotoxicities of different formulations of paclitaxel. 17
Figure 2.2.4.3. Illustration of pH-dependent release of doxorubicin from a P85-*b*-PAA copolymer. 18
Figure 2.2.4.4. (A) Crosslinking degrees of DAE, DAB and EDBEA. (B) Schematic illustration of crosslinking. 19
Figure 2.2.5.1. Schematic illustration of synthesis of DOX-conjugated PEO-P(Asp). ... 21
Figure 2.2.5.2. Structure of PEO-b-poly(α, β-aspartic acid)/DOX complex. 22
Figure 2.3.2.1. Schematic illustration of temperature-sensitive dissolution of PNIPAAM. 27
Figure 2.3.2.2. LCSTs of poly(*N*-substituted acrylamide)s. 28
Figure 2.3.2.3. LCSTs of PNIPAAM copolymers. 28
Figure 2.3.2.4. Schematic illustration of thermosensitive drug release from micelles with PNIPAAM as the shell-forming segments. 29
Figure 2.3.2.5. Comparison of release rates of prednisone acetate from PNIPAAM-*b*-PMMA micelles at temperatures below and above the LCST of PNIPAAM 30
Figure 2.3.2.6. Structures and LCSTs of PNIPAAM and PHPMAM copolymers. 32
Figure 2.3.2.7. pH-sensitive release of doxorubicin from P(NIPAAM-*co*-DMAAM-*co*-UA) micelles at 37 °C. 33
Figure 3.3.1.1. ^{1}H NMR spectrum of ethoxy vinyl glycidyl ether monomer. 56
Figure 3.3.1.2. ^{1}H NMR spectrum of vinyldimethylsilylpropyl glycidyl ether monomer. 57
Figure 3.3.2.1. ^{1}H NMR of a tapered 2k mPEG-*b*-P(0.9k EVGE-co-3.9 BO) copolymer. 60
Figure 3.3.2.2. Monomer conversions during copolymerization of EVGE with BO. 60
Figure 3.3.2.3. Representative SEC chromatograms of copolyethers. 62
Figure 3.3.3.1. ^{1}H NMR of a carboxylic acid-functional tapered 2k mPEG-*b*-P(0.9k EVGE-co-3.9k BO) copolymer 64

Figure 3.3.3.2. ^{1}H NMR of a *boc*-cysteamine-functional tapered 2k mPEG-*b*-P(0.9k EVGE-co-3.9k BO) copolymer..... 65
Figure 3.3.3.3. ^{1}H NMR spectrum confirmed successful removal of *boc* group..... 66
Figure 3.3.3.4. A representative titration curve of carboxylate-functional tapered 2k mPEG-*b*-P(0.9k EVGE-co-3.9k BO). 67
Figure 3.3.4.1. ^{1}H NMR of a diblock 5k mPEG-*b*-0.8k PVSiGE copolymer..... 70
Figure 3.3.4.2. ^{1}H NMR spectrum of a tapered 5k mPEG-*b*-P(0.7k EVGE-*co*-4.4k BO) copolymer. 71
Figure 3.3.4.3. ^{1}H NMR spectrum of an amino-functional tapered 5k mPEG-*b*-P(0.7k EVGE-*co*-4.4k BO) copolymer..... 72
Figure 3.3.5.1. Count rates from DLS of an amino-functional tapered 2K mPEG-P(0.9K EVGE-*co*-3.9K BO) copolymer..... 74
Figure 3.3.6.1. Molecular structure of ritonavir..... 77
Figure 3.3.6.2 Drug loading of ritonavir nanoparticles stabilized with 5k PEO-b-9k PBO and 2k homoPBO at various targeted RTV loadings in the range of 10-30 wt %. Error bars represent standard deviations from three measurements. 79
Figure 4.3.1.1. ^{1}H NMR of a 3.5k vinylsilane-PEO-OH. 102
Figure 4.3.1.2. ^{1}H NMR of a 3.5k amino-PEO-OH. 102
Figure 4.3.1.3. ^{1}H NMR of a 3.5k amino-PEO-OCH_3. 103
Figure 4.3.2.1. ^{1}H NMR of benzyl-L-glutamate. 105
Figure 4.3.2.2. ^{1}H NMR spectrum of the NCA of γ-benzyl-L-glutamate in d_6-DMSO. 106
Figure 4.3.2.3. ^{1}H NMR spectrum of the PEO-*b*-poly(γ-benzyl-L-glutamate) in d_6-DMSO. 109
Figure 4.3.2.4. ^{1}H NMR spectra of a PEO-*b*-poly(L-glutamic acid) in d_6-DMSO (acid form, top) and in D_2O (salt form, bottom). 110
Figure 4.3.2.5. SEC trace of a 3.5 K PEO-*b*-10.9 K poly(γ-benzyl-L-glutamate)..... 111
Figure 4.3.3.1. ^{1}H NMR of a 2k diallyl-PEO..... 113
Figure 4.3.3.2. ^{1}H NMR of a 2k dithiol-PEO. 114
Figure 4.3.4.1. ^{1}H NMR of a 2.5k amino-PEO-allyl. 117
Figure 4.3.4.2. ^{1}H NMR spectrum of an allyl-PEO-*b*-poly(γ-benzyl-L-glutamate) in d_6-DMSO. 118
Figure 4.3.4.3. ^{1}H NMR spectra of an allyl-PEO-*b*-poly(L-glutamic acid) in d_6-DMSO.119
Figure 4.3.4.4. ^{1}H NMR of a thiol-poly(ethylene oxide)-*b*-poly(L-glutamic acid). 120
Figure 4.3.5.2. Colloidal stability in phosphate buffered saline of iron oxide-PEO-*b*-poly(L-glutamic acid) complexes made in organic solvents..... 122
Figure 4.3.5.2. Colloidal instability in phosphate buffered saline of the iron oxide-PEO-*b*-poly(L-glutamic acid) complexes made in water at pH 9. 123
Figure 4.3.5.3. TEM of magnetic single particles made from the mixed chloroform/DMSO solvents and size analysis from a lognormal fit. 124
Figure 4.3.6.1. TEM of magnetic clusters 3..... 126
Figure 4.3.6.2. Colloidal stability in phosphate buffered saline at 25 °C of magnetic clusters. 126
Figure 4.3.7.1. Hysteresis loop of oleic acid-coated iron oxide nanoparticles at 300K. 127
Figure 4.3.7.2. Transverse relaxivities of the single iron oxide-PEO-*b*-poly(L-glutamic acid) complexes made from the mixed solvent (D_I=40 nm) and from chloroform (D_I=81 nm).129

Figure 4.3.7.3. Transverse relaxivities (top) and longitudinal relaxivities (bottom) of the iron oxide-PEO-*b*-poly(L-glutamic acid) clusters. 130
Figure 5.3.1.1. ^{1}H NMR spectrum of 3-chloropropyldimethylvinylsilane. 146
Figure 5.3.1.2. ^{1}H NMR spectrum of 3-iodopropyldimethylvinylsilane. 146
Figure 5.3.1.3. ^{1}H NMR spectrum of 3-hydroxypropyldimethylvinylsilane. 147
Figure 5.3.2.1. ^{1}H NMR of a 2.7k vinyl-PEO-OH. 148
Figure 5.3.2.2. ^{1}H NMR of a vinyl-2.7k PEO-2.0k PPO-OH. 149
Figure 5.3.2.3. ^{1}H NMR spectrum of a vinyl-2.7k PEO-2.0k PPO-0.5k PEO-OH. 151
Figure 5.3.2.4. ^{19}F NMR spectra of polyether trifluoroacetate esters. 152
Figure 5.3.3.1. ^{1}H NMR spectrum of an amino-2.9k PEO-2.5k PPO-0.5k PEO-OH. .. 154
Figure 5.3.4.1 (A) SDS-PAGE of SOD1 and SOD1-polymer conjugates (left) and (B) a mass spectrum of SOD1-AP2 conjugates (right). 155
Figure 5.3.5.1. Cellular uptake of SOD1 and SOD1-polymer conjugates. 158

List of Schemes

Scheme 2.3.1.1. Isomerization of allyl group to propenyl group in the presence of strong base. 23
Scheme 2.3.1.2. Synthesis of polyether-doxorubicin conjugation. 24
Scheme 2.3.1.3. Two types of post-polymerization modifications of vinyl ether groups: (1) acetal-formation with alcohols and (2) thiol-ene addition with thiols. 25
Scheme 2.3.1.4. Synthesis of catechol-P(EO-*co*-glycidyl amine)..... 26
Scheme 3.3.1.1. Synthesis of ethoxy vinyl glycidyl ether monomer. 56
Scheme 3.3.1.2. Synthesis of vinyldimethylsilylpropyl glycidyl ether monomer..... 57
Scheme 3.3.2.1. Synthesis of a tapered 2k mPEG-*b*-P(0.9k EVGE-co-3.9k BO) copolymer. 59
Scheme 3.3.3.1. Thiol-ene addition of mercaptoacetic acid to a tapered 2k mPEG-*b*-P(0.9k EVGE-co-3.9k BO) copolymer. 63
Scheme 3.3.3.2. Thiol-ene addition of *boc*-cysteamine to a tapered 2k mPEG-*b*-P(0.9k EVGE-co-3.9k BO) copolymer. 65
Scheme 3.3.3.3. Removal of *boc* group..... 66
Scheme 3.3.4.1. Synthesis of a diblock 5k mPEG-*b*-0.8k PVSiGE copolymer..... 69
Scheme 3.3.4.2. Synthesis of a tapered 5k mPEG-*b*-P(0.7k EVGE-*co*-4.4k BO) copolymer. 70
Scheme 3.3.4.3. Thiol-ene addition of cysteamine hydrochloride to a tapered 5k mPEG-*b*-P(0.7k EVGE-*co*-4.4k BO) copolymer. 72
Scheme 4.3.1.1. Synthesis of an amino-PEO-OCH_3. 101
Scheme 4.3.2.1. Synthesis of an NCA of γ-benzyl-L-glutamate..... 104
Scheme 4.3.2.2. Synthesis of a poly(ethylene oxide)-*b*-poly(L-glutamic acid)..... 108
Scheme 4.3.3.1. Synthesis of dially-PEO and dithiol-PEO..... 112
Scheme 4.3.4.1. Synthesis of an allyl-poly(ethylene oxide)-*b*-poly(L-glutamic acid) and a thiol-poly(ethylene oxide)-*b*-poly(L-glutamic acid). 116
Scheme 4.3.5.1. Synthesis of magnetic block ionomer complexes..... 121
Scheme 5.3.1.1. Synthesis of 3-hydroxypropyldimethylvinylsilane (3-HPMVS)..... 145
Scheme 5.3.2.1. Synthesis of a 2.7k vinyl-PEO-OH..... 148
Scheme 5.3.2.2. Synthesis of a vinyl-2.7k PEO-2.0k PPO-OH. 149
Scheme 5.3.2.3. Synthesis of a vinyl-2.7k PEO-2.0k PPO-0.5k PEO-OH. 150
Scheme 5.3.2.4. A representative reaction of a polyether with trifluoroacetic anhydride.151
Scheme 5.3.3.1. A thiol-ene reaction of a vinyl-2.9k PEO-2.5k PPO-0.5k PEO-OH with cysteamine hydrochloride. 153
Scheme 5.3.4.1 Synthesis of SOD-polyether conjugates. 155
Scheme 5.3.4.2 Reaction of primary amine with 2,4,6-trinitrobenzenesulfonic acid (TNBS). 156

List of Tables

Table 2.2.3.1. Effective diameters and loading efficiency of doxorubicin polymeric micelles. 13
Table 2.2.4.1. Particle size, paclitaxel loading efficiency and loading content of nanocapsules with or without Lipiodol 16
Table 3.3.2.1. Molecular weights of functional copolyethers. 61
Table 3.3.3.1. Quantification of functional groups on the copolymers. 68
Table 3.3.5.1. CMC's of pH-sensitive functional copolyethers in HCl or KOH solutions at 25 ºC. 75
Table 3.3.5.2. CMC's of Pluronic® triblock copolyethers in water at 25 ºC 75
Table 3.3.5.3. Micellar diameters (intensity-average) measured in aqueous dispersions at 25 ℃. 76
Table 3.3.6.1 Hydrodynamic diameters and polydispersities of ritonavir nanoparticles stabilized with 5k PEO-*b*-9k PBO and 2k homoPBO in a 1:10 (v/v) THF-water mixture. 78
Table 3.3.6.2 Hydrodynamic diameters and polydispersities of ritonavir nanoparticles stabilized with 5k PEO-*b*-0.76k PEVGE-*b*-9.4k PBO. 80
Table 4.3.2.1. Molecular weights of the PEO-*b*-poly(γ-benzyl-L-glutamate)s. 111
Table 4.3.5.1. Properties of the iron oxide/PEO-*b*-PG complexes. 123
Table 4.3.7.1. Sizes, transverse relaxivities and longitudinal relaxivities of the iron oxide-PEO-*b*-poly(L-glutamic acid) complexes. 131
Table 5.3.2.1. Characterization of asymmetric triblock copolyethers. 152
Table 5.3.4.1. Characteristics of SOD1-polymer conjugates. 156
Table 5.3.4.2. Residual activities of SOD1-polymer conjugates with various degrees of modification. 157

Chapter 1: Dissertation Overview

A major development in the biomedical area in the last decades is developing and utilizing novel polymeric materials to enhance biocompatibility and biological activity of therapeutic and diagnostic agents. The second chapter of this thesis reviews core-shell drug nanoparticles based on PEO-containing copolymers and stimuli-sensitive polymers for targeted drug delivery.

The third chapter describes a synthetic route for preparing multi-functional amphiphilic copolyethers based on poly(ethylene oxide) and poly(1,2-butylene oxide) that incorporate pendent vinyl ethers or vinyl silanes. It includes an in-depth look into the microstructures of functional blocks via kinetic studies of the anionic ring-opening copolymerizations. Post-polymerization functionalization of the vinyl functional groups via thiol-ene additions were also described. Comparisons of the critical micellar concentrations of the functional copolymers under different environmental pH were probed via DLS. These materials formed well-controlled nanoparticles containing ritonavir micelles in aqueous media. Drug loading efficiencies were investigated in collaboration with Sharavanan Balasubramaniam and Prof. Davis.

Chapter 4 describes preparation of magnetic block ionic nanoparticles based on poly(ethylene oxide)-*b*-poly(L-glutamic acid) copolymers. This is of interest due to the biocompatibility and biodegradable nature of the poly(L-glutamic acid) component of the backbone. The synthetic method for introducing terminal thiol and allyl groups to the copolymers is described. Biodegradable magnetic clusters were prepared using the thiol- and allyl-functional copolymers. Colloidal stabilities in physiological media of the

magnetic nanoparticles made from aqueous dispersion or organic solvents were compared via DLS. Magnetic properties of the single particles and the clusters were determined and compared.

The fifth chapter decribes the synthesis and characterization of a series of heterobifunctional asymmetric amino-EO_{n1}-*b*-PO_m-*b*-EO_{n2}-OH block copolymers with different molecular weights of each block. In collaboration with Prof. Kabanov's group, the amino terminal groups was conjugated to an antioxidant enzyme, Cu/Zn superoxide dismutase (SOD1). Effect of the amounts of polymers attached to the protein on enzymatic activities were investigated. Cellular uptake properties of the conjugations with different polymer block lengths were examined.

Chapter 6 describes the conclusions drawn from the previous chapters and proposed future work associated with this research.

Chapter 2. Literature Review: Functional and amphiphilic copolymers in biomedicine

2.1 Introduction

2.1.1 Polymeric materials for application in biotechnology

Recently, polymeric materials have received much attention for biological purposes due to their biocompatibility, biodegradability, biological activity and high capacity for drug delivery, tissue engineering, bone repair, implantation of medical devices and artificial organs and so on.[1-9] Using polyion complex micelles as novel carriers for gene delivery is also an attractive area.[4] Hydrogels based on hydrophilic copolymers have great potential for components of biosensors as well.[10]

As generally acknowledged, polymeric materials that are used for biomedical applications are expected to have the following features. First of all, there should not be any evidence of harmful influence caused by introducing these materials into the body. Secondly, these polymers should be cleared out from the body and biodegradation can promote this process. Furthermore, biodegradable polymers should not generate toxic byproducts and there should be a mechanism for eliminating the products of biodegradation from the body. Special functional groups can be utilized to enhance the interactions between polymers and cell membranes.[10]

2.1.2 The enhanced permeability and retention (EPR) effect

The enhanced permeability and retention (EPR) effect can be extremely important for drug delivery to tumors. Enhanced vascular permeability provides the possibility for polymeric drug delivery vehicles to selectively target tumor cells. Because tumor cells

propagate much faster than normal cells, they have much greater demands for nutrients and oxygen. The enhanced vascular permeability can satisfy those demands.[11] It also results in drugs reaching the tumor tissues more efficiently by permeating through the leaky vasculature.

Besides the enhanced permeability, the lymph drainage system in solid tumors is immature as well. Therefore, the extravasation of macromolecules from tumor tissues is much slower than that from the normal tissues. As a result, macromolecules can stay in the tumor tissues for a longer time and a higher concentration of macromolecules in the tumors can be built up.[12]

In summary, these two facts are termed as the tumor-selective enhanced permeability and retention (EPR) effect of macromolecules and lipidic particles.[11] While small molecules cannot discriminate tumor tissues from normal tissues, macromolecules can accumulate in tumor tissues at much higher concentration than in the normal tissues and plasma due to the EPR effect (Figure 2.1.2.1).

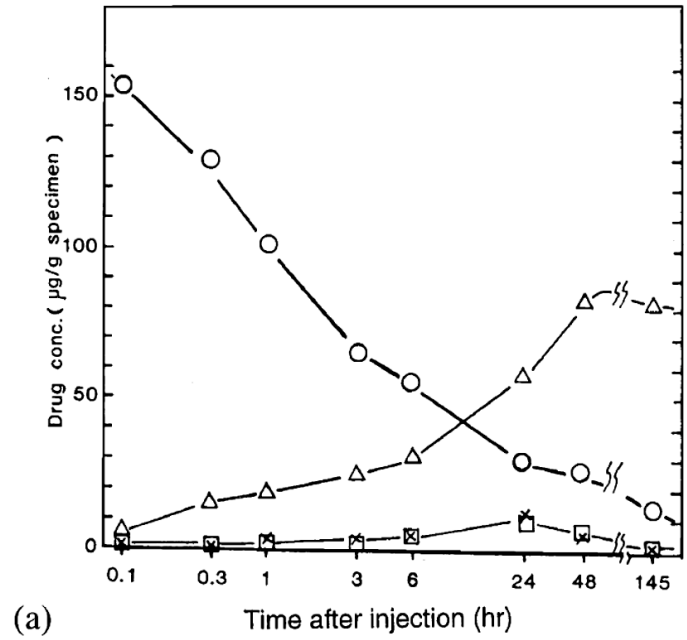

(a)

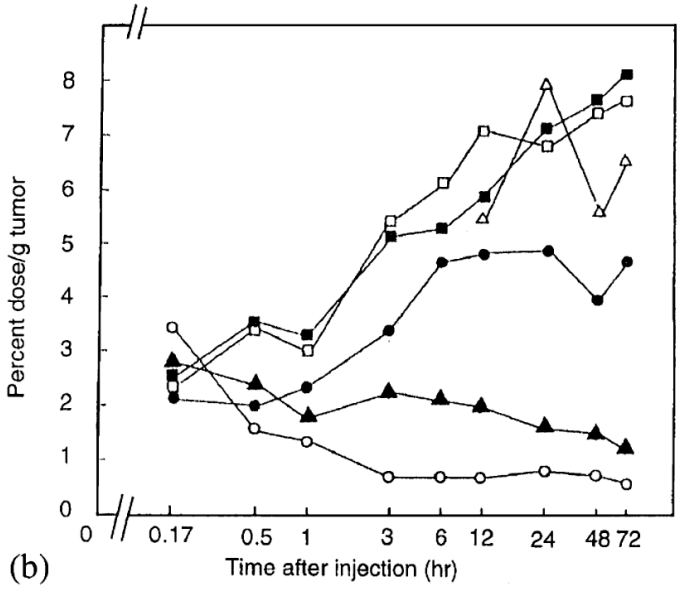

(b)

Figure 2.1.2.1. (A) Concentrations of Evans blue dye-complexed albumin in: (○), blood plasma; (△), tumor uptake; and (×, □) normal muscle and skin tissues, respectively. (B) Intratumor accumulation of various ^{51}Cr-tagged proteins in solid tumor-bearing mice: (○) neocarzinostatin (NCS) (12 kDa); (●) SMANCS (16 kDa, but known to bind to albumin); (▲) ovomucoid (29 kDa); (□) bovine serum albumin (69 kDa); (■) mouse serum albumin (68 kDa); (△) mouse immunoglobulin G (160 kDa). Radio labeled proteins were injected *i.v.* at time zero. Values are based on radioactivity. The tumor model in both A and B was solid sarcoma S-180 in mice.[13]

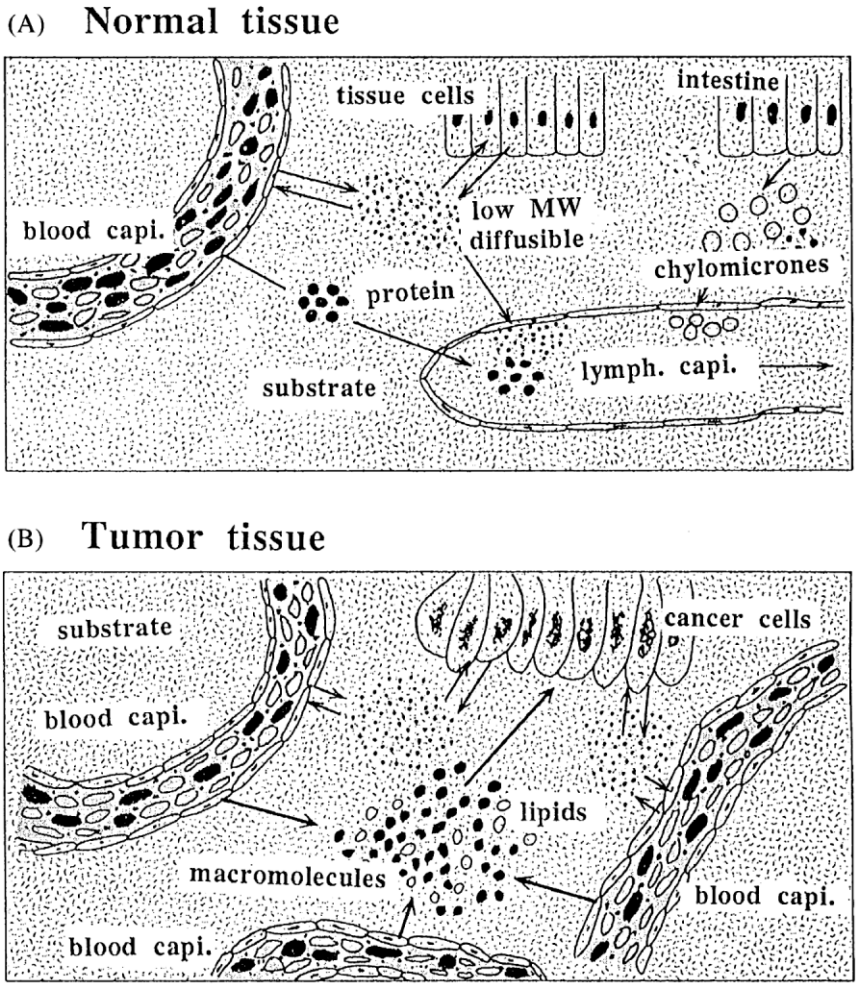

Figure 2.1.2.2. Illustration of the differences in extravasation from (A) normal tissue and (B) tumor tissue.[13]

2.2 Micelles based on PEO-containing copolymers

2.2.1 Formation and dimensions of polymeric micelles with core/shell nanostructures

Polymeric micelles generally are comprised of hydrophobic blocks and hydrophilic blocks. These micelles have a core/shell nanostructure with the hydrophobic segments isolated from the aqueous continuous phase to form an interior core and the hydrophilic segments forming the shells to stabilize the hydrophobic core (Figure 2.2.1.1). The unique architecture of this type of micelles is of great interest for drug delivery because water-insoluble drugs can be incorporated in the hydrophobic cores through hydrophobic

interaction or chemical conjugations. Copolymers with different characteristics have been investigated by adjusting the molecular weight of each block, chemical compositions and terminal functional groups. Thus, polymeric micelles with desirable biodistributions and drug release properties could be obtained by assembly of those copolymers.

Polymeric micelle particles should have appropriate sizes. First, the particles should be small enough to pass through the capillary vessels. On the other hand, polymer micelles should also be big enough to avoid excretion by the renal system. According to a study on renal filtration limits of proteins and water-soluble polymers, polymeric micelles with diameter in the range of several tens of nm will likely be able to avoid excretion by the kidneys.[8]

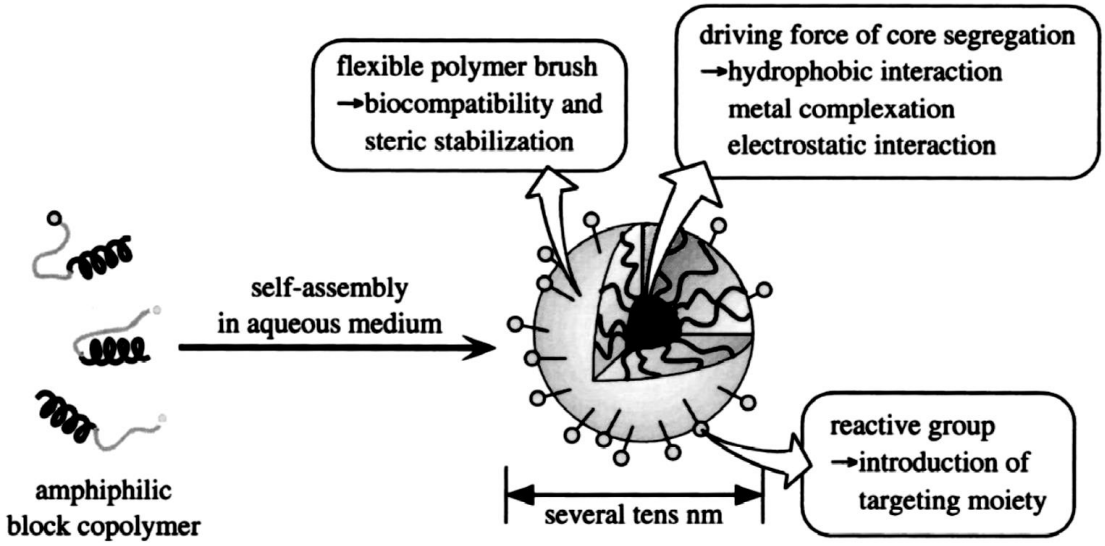

Figure 2.2.1.1. Configuration of polymeric micelles.[4]

2.2.2 Unique properties of PEO-containing copolymers

The reticuloendothelial system (RES) is an important part of the immune system. The RES consists of all phagocytic cells including monocytes and macrophages. It provides the function of clearing out any infection and old cell fragments from the body.[1] Avoiding RES uptake during the contact of biomaterials with the biological environment, which depends mostly on the hydrophilic shells, is one of the most important issues for bioapplicable polymeric micelles. Many hydrophilic polymers, including polyacrylamide, poly(hydroxyethyl methacrylate), poly(*N*, *N*- dimethylacrylamide), poly(vinyl alcohol), poly(ethylene oxide) (PEO or PEG) and so on, have been used to modify the properties of biomaterials. Especially, PEO has been utilized most widely due to its unique characteristics.[14]

First of all, PEO has excellent solubility in water. In a wide temperature range from room temperature to slightly below 100 ℃, PEO can dissolve in water in any composition.[15] In the other words, PEO is miscible with water. PEO is also soluble in many organic solvents.[14] As an excellent solute, PEO has high surface mobility and the interfacial energy between PEO and water is very low. These attractive properties make PEO particularly effective at resisting protein adsorption.[6,16]

Another important advantage of using PEO as a shell-forming block is the low toxicity. PEO is FDA-approved for parenteral administration.[1] It was reported that 10% PEO solution (M_w=4000 g/mol) could be administered intravenously to rats, guinea pigs, rabbits, and monkeys up to 16 g/kg without any noticeable toxicity.[1,17]

2.2.3 PEO-polyester copolymers

Polyesters are widely used and studied as an important class of biodegradable polymers, including poly(lactic acid), poly(glycolic acid), poly(ε-caprolactone) and their copolymers.[18,19] These polymers can be non-specifically biodegraded into non-harmful small molecules in aqueous media.

Allen et al. have explored the possibility of using micelles formed from polycaprolactone-*b*-poly(ethylene oxide) (PCL-*b*-PEO) as a carrier for FK506 (Tacrolimus),[20] which is the most important drug used for decreasing rejection caused by transplantation of liver,[21] kidney,[22] heart[23] and others. This drug was loaded into PCL_{20}-*b*-PEO_{44} physically by simply mixing, then dialyzing against water. The final loading efficiency was 21%.

The release rates of FK506 incorporated into the micelles relative to FK506 alone were measured by a dialysis method *in vitro*.[20] More than 50% of the drug was released from the complexes in the first 12 hours, and the number increased to 70% in the first 24 hours. In contrast, the drug without polymeric carriers was released completely in 4 hours (figure 2.2.3.1). Incorporation in the core-shell structures resulted in the drug being released over 6 days, but only 30% of the drug was released in the last five days.

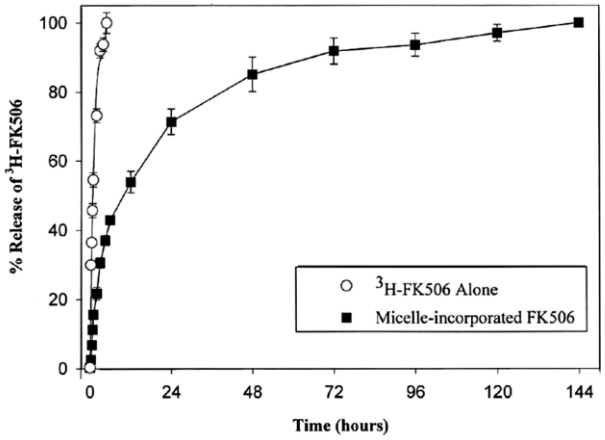

Figure 2.2.3.1. The in vitro release rates of ^{3}H-FK506 alone and PCL_{20}-*b*-PEO_{44} micelle-incorporated-3H-FK506.[20]

The micelle containing FK506 was radio-labeled and injected intravenously into male Sprague-Dawley rats for biodistribution measurements (Figure 2.2.3.2).[20] The biodistribution of micelles containing FK506 was significantly different from that of FK506 alone. The most attractive difference was that the micelles containing FK506 accumulated in the brain with higher concentration than FK506 alone.[20,24]

a

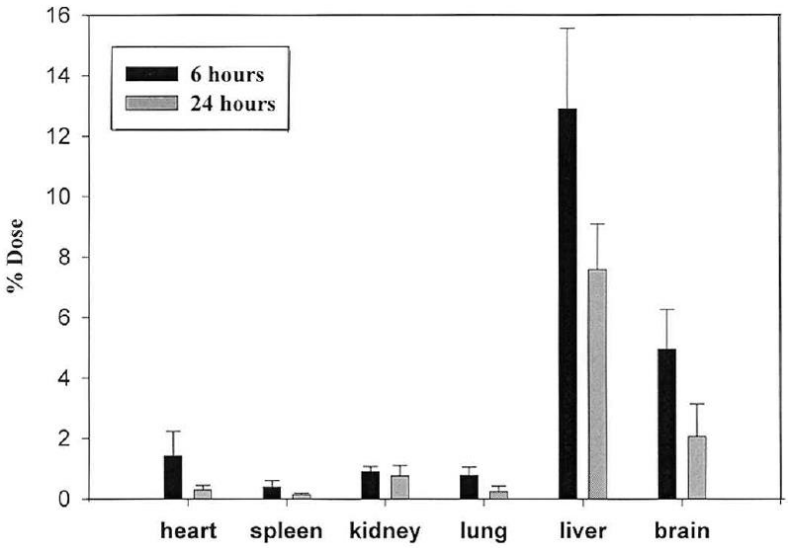

b

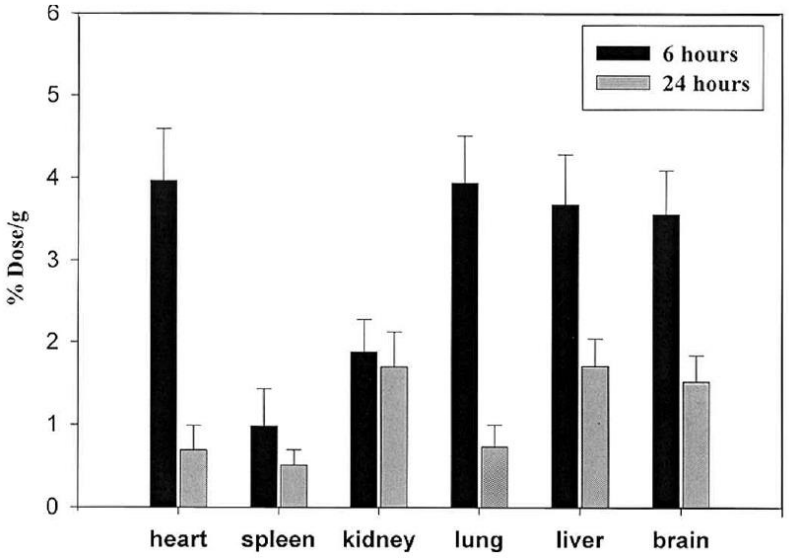

Figure 2.2.3.2. a. The biodistribution of radiolabeled micelle incorporated FK506 (in terms of % of total dose). **b.** The biodistribution of radiolabeled micelle incorporated FK506 (in terms of total dose/g tissue).[20]

Other than physical entrapment of the drug, which is described in the above-mentioned example, the PEO-polyester copolymers have also been chemically conjugated with drugs. Yoo et al. developed a doxorubicin delivery system using poly(DL-lactic-*co*-glycolic acid)-*b*-poly(ethylene oxide) (P(DLLA-*co*-GA)-*b*-PEO) to connect doxorubicin chemically.[25] In this work, PEO was used as the initiator to polymerize DL-lactide and

glycolide. Doxorubicin was connected to the copolymer through the terminal hydroxyl groups on the PDLLA-*co*-GA chain ends (Figure 2.2.3.3).

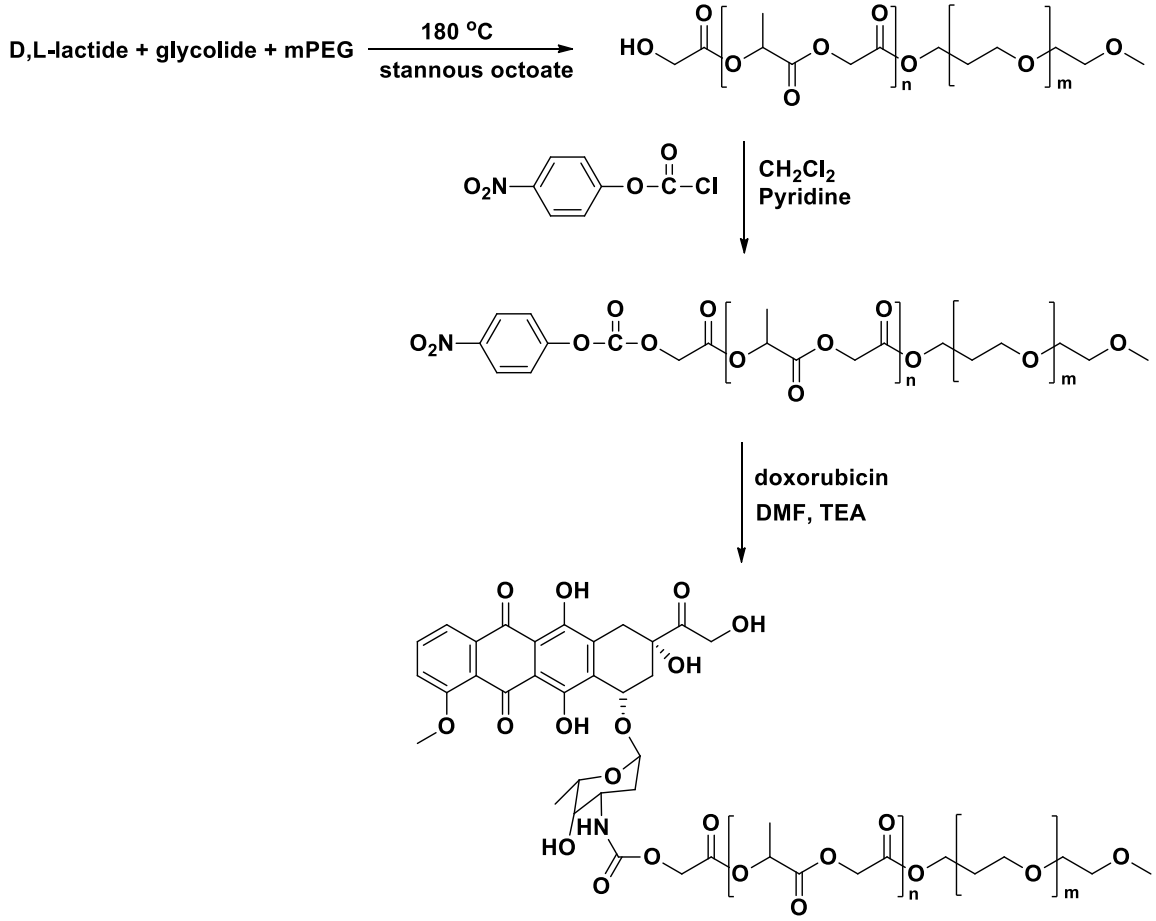

Figure 2.2.3.3. Illustration of synthesis of DOX-P(DLLA-co-GA)-b-PEO conjugate.[25]

Several physical characteristics were measured to investigate the difference between chemically and physically loaded doxorubicin-polymer complexes.[26] Covalent bonds are much stronger than intermolecular attractions such as van der Waals forces and hydrogen bonds, on which physical loading depends. Since chemical bonds lead to quantitative conjugation, the loading efficiency of this approach should be significantly higher than

physical loading, and this was confirmed by the experimental results (Table 2.2.3.1). In addition, a sustainable release of doxorubicin was extended from 3 days to 2 weeks (Figure 2.2.3.4).

Table 2.2.3.1. Effective diameters and loading efficiency of doxorubicin polymeric micelles.[26]

Doxorubicin loading	Effective diameter (nm)	Theoretical loading (w/w, %)	Actual loading (w/w, %)	Loading efficiency (%)
Physically entrapped (PLGA-PEG)	58.21 ±6.21	2.20	0.51 ±0.07	23.18 ±3.18
Conjugated (DOX-PLGA-PEG)	61.48 ±7.17	2.20	2.18 ±0.04	99.09 ±1.81

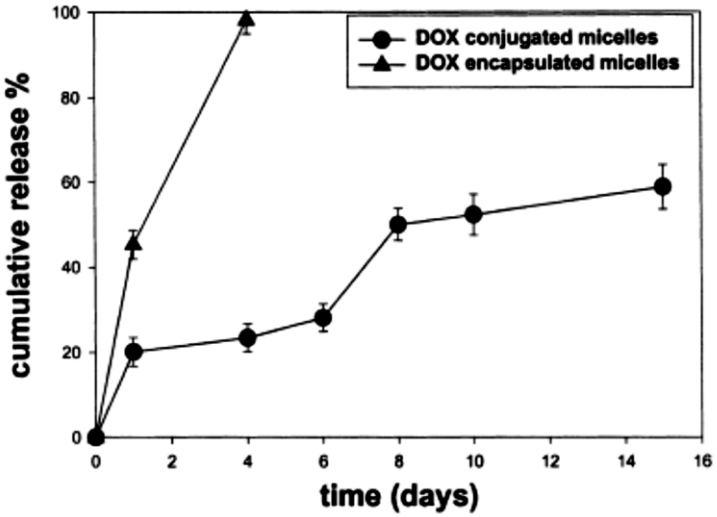

Figure 8. Release profiles of doxorubicin from polymeric micelles.[26]

2.2.4 PEO-PPO-PEO copolymers

Triblock copolymers based on poly(ethylene oxide-*b*-propylene oxide-*b*-ethylene oxide) (PEO-*b*-PPO-*b*-PEO) (the BASF tradename is Pluronics®) are well established, and they have been studied extensively as excipients in drug formulations.[27-48] At present, a wide range of molecular weights of Pluronics® are commercially available. Above the

critical micelle concentration (CMC), PEO-*b*-PPO-*b*-PEO can form spherical micelles in aqueous solution by self-assembly, with PEO blocks forming the shells and PPO blocks forming the core. Drugs that have poor solubilities in water might be loaded into the hydrophobic cores of PEO-*b*-PPO-*b*-PEO micelles and be stabilized by the PEO shells. This attractive feature makes PEO-*b*-PPO-*b*-PEO a potential drug delivery vehicle. Another important advantage of Pluronics® as a drug carrier is their ability to inhibit multidrug resistance (MDR) in cancer cells,[49,50] which can significantly decrease the efficacy of many drugs in tumor therapy. MDR is often caused by P-glycoprotein (P-gp), a transmembrane glycoprotein with a molecular weight of 170 kDa which acts as an ATP-dependent drug efflux pump.[49] It results in a lower accumulation and retention of drugs in tumor cells. Many studies on the inhibition of efflux action of P-gp by PEO-*b*-PPO-*b*-PEO copolymers have been reported.[28,29,31-33,37-41,43] For instance, Pluronic® P85 showed notable capacity for increasing the cytotoxicity of drugs against MDR cells by as much as 1,000 times while only a slight increase of cytotoxicity was observed against sensitive cells.[50]

A nanocapsule that encapsulated iodinated poppy seed oil (lipiodol), which has been widely used as a contrast agent, was synthesized by Bae et al. utilizing an emulsification/solvent evaporation method.[51] A PEO-*b*-PPO-*b*-PEO copolymer was activated by reaction with *p*-nitrophenyl chloroformate so that the terminal groups could be subsequently reacted with amino groups. In methylene chloride, the activated PEO-*b*-PPO-*b*-PEO was mixed with the lipiodol.[52] Then the mixture was added to an aqueous solution containing amine-functionalized six-arm-branched PEO and sonicated to form an

emulsion. The lipiodol-encapsulating nanocapsules were obtained after evaporation of the solvent. This synthesis is illustrated in Figure 2.2.4.1.

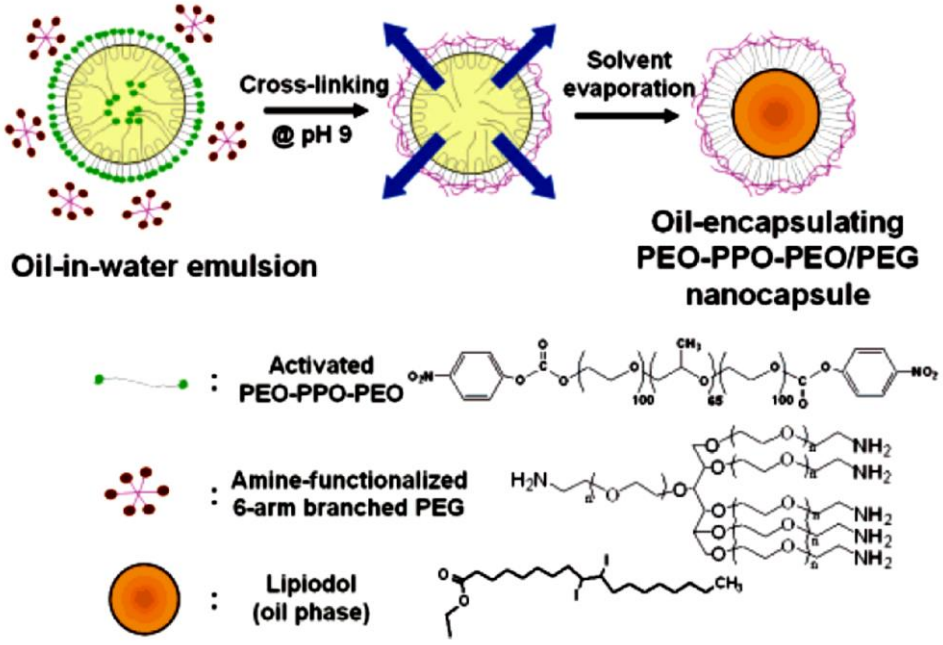

Figure 2.2.4.1. Illustration of synthesis of lipiodol-encapsulating nanocapsules.[51]

Paclitaxel, which is a widely used chemotherapeutic water-insoluble drug, was loaded into the nanocapsules by solubilizing it in the lipiodol/PEO-*b*-PPO-*b*-PEO mixture. The diameter, loading efficiency and loading content of nanocapsules with and without lipiodol were determined (Table 2.2.4.1).[51]

Table 2.2.4.1. Particle size, paclitaxel loading efficiency and loading content of nanocapsules with or without Lipiodol.[51]

Samples	Particle size (nm)	Loading efficiency (%)	Loading content (wt %)	Loading amount in Lipiodol (mg/mL)
w/ LP	115.8 ±15.2	46.5 ±9.5	0.80 ±0.04	25.8 ±5.2
w/o LP	102.7 ±9.5	12.8 ±1.9	0.18 ±0.01	NA

The release profile was measured in a buffer solution at pH 7.2 and physiological temperature[51] (Figure 2.2.4.2 A). Continuous release from the nanocapsules containing the lipiodol was detected with up to ~80% of the paclitaxel being released over 30 days. By contrast, about 90% of the paclitaxel was released within 5 days from the nanocapsules without lipiodol. The significant improvement of release rate indicated the potential of using this polymeric micelle as a carrier for hydrophobic drugs.

Cytotoxicities of different potential paclitaxel drug delivery systems were investigated (Figure 2.2.4.2 B).[51] The clinically available formulation of paclitaxel (Taxol) exhibited a high level of cytotoxicity above 1 μg/mL while the lipiodol nanocapsules did not. Folate-conjugated lipiodol nanocapsules showed even more cytotoxicity than the other two. Considering that folic acid is known to be effecting at achieving tumor-selective targeting, this result suggested that folate-conjugated LP nanocapsules can selectively restrain the proliferation of tumor cells.

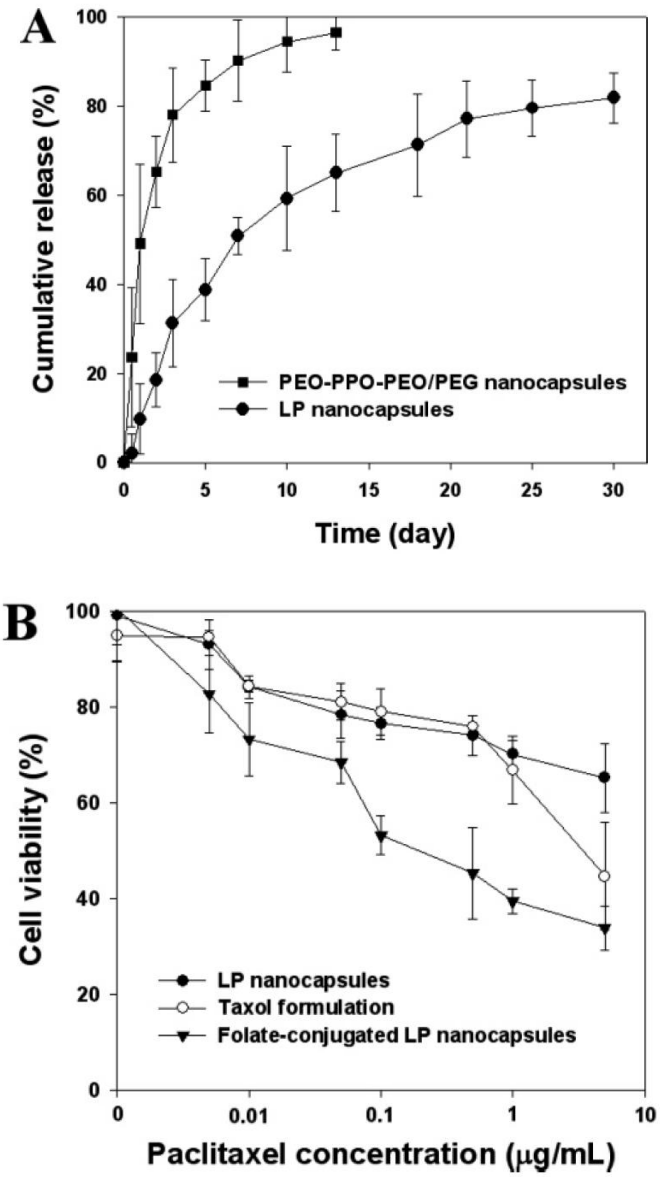

Figure 2.2.4.2. (A) Release profile of paclitaxel from nanocapsules w/ or w/o lipiodol. (B) Cytotoxicities of different formulations of paclitaxel.[51]

Pluronic® P85-*b*-poly(acrylic acid) (PEO-*b*-PPO-*b*-PEO-*b*-PAA) copolymers have been reported as potential carriers for doxorubicin as well.[53] In a phosphate buffer solution with pH 7.2, doxorubicin was loaded into this copolymer by electrostatic interaction between the electronegative PAA segments and electropositive doxorubicin molecules. As expected, pH influenced the release rate of doxorubicin from this copolymer due to

protonation of acrylates at low pH (Figure 2.2.4.3). A faster release of doxorubicin was determined at pH 5.0 than that at pH 7.2.

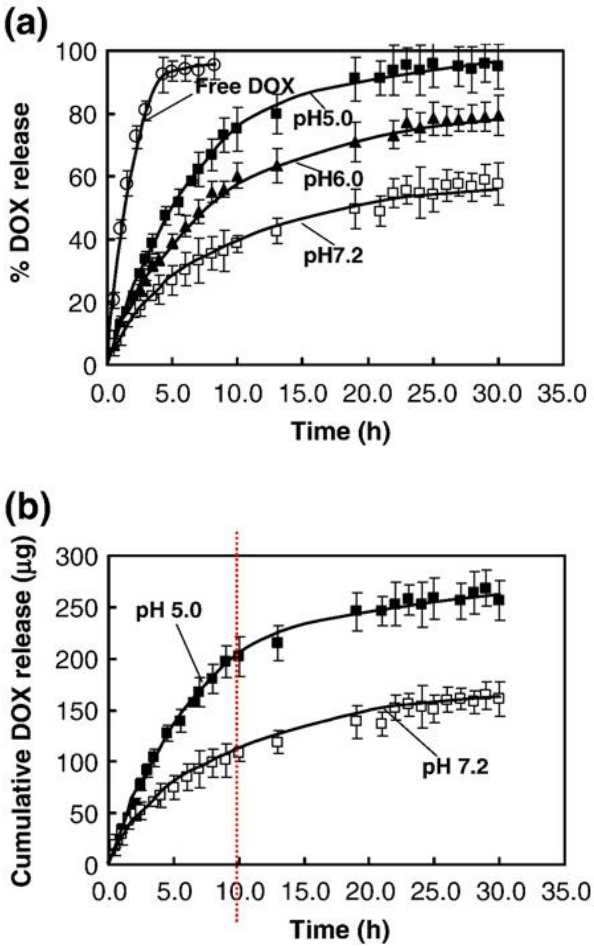

Figure 2.2.4.3. Illustration of pH-dependent release of doxorubicin from a P85-*b*-PAA copolymer.[53]

It was reported that the CMCs of Pluronics® could be lowered by crosslinking the outside shells.[54] In a characteristic procedure, the terminal hydroxyl groups of the PEO segments were oxidized to aldehydes, then polymers were crosslinked by reaction of the aldehyde groups with diamine compounds. Three diamines were investigated: 2,2'-(ethylenedioxy)bis(ethylamine) (EDBEA), 1,4-diaminobutane (DAB) and 1,2-diaminoethane (DAE). DAB was found to be the most efficient of the three for

crosslinking. It was suggested that EDBEA was too long, causing some aldehyde groups to remain unreacted, and that DAE was too short to connect the adjacent aldehyde groups (Figure 2.2.4.4). After crosslinking, the CMC of L121 was lowered from 5×10^{-3} to 5×10^{-4} wt%. With the lower CMC, the micelles were more stable in the plasma.

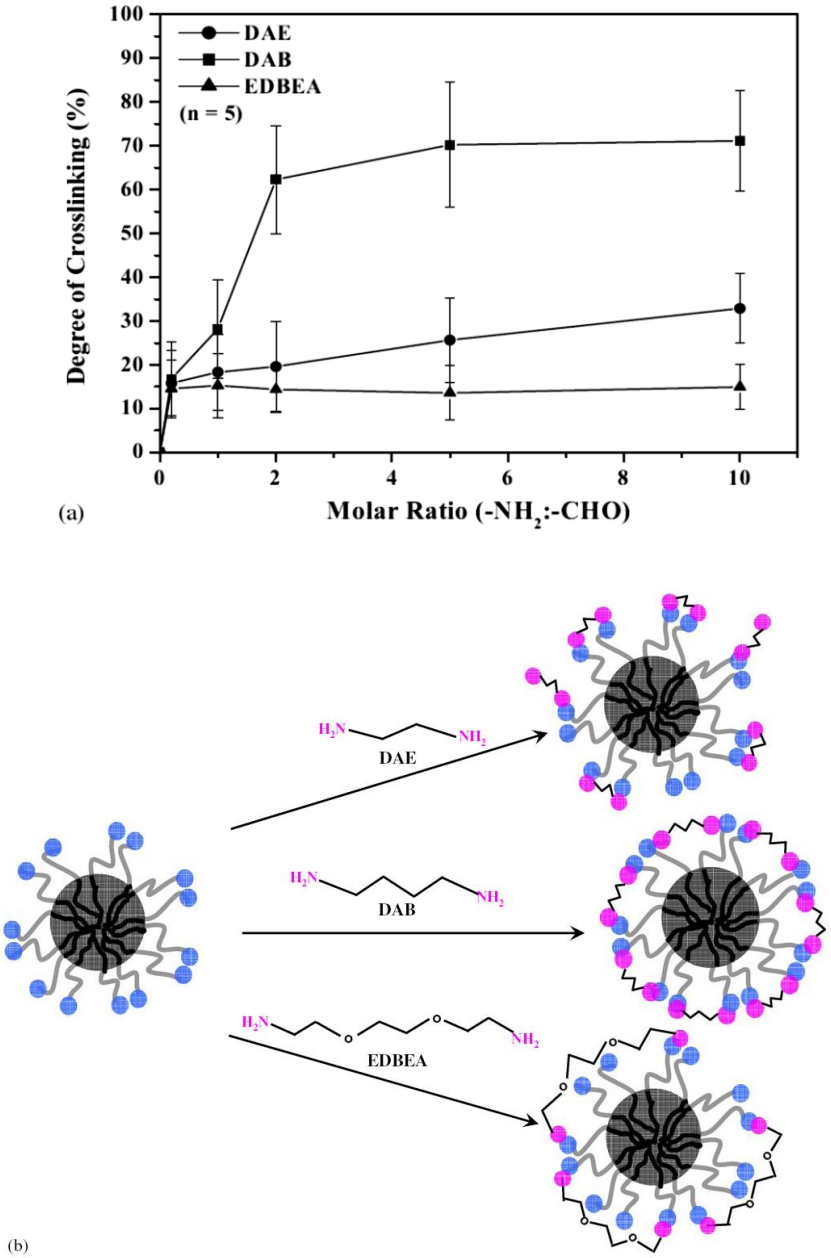

Figure 2.2.4.4. (A) Crosslinking degrees of DAE, DAB and EDBEA. (B) Schematic illustration of crosslinking.[54]

2.2.5 PEO-poly(amino acid) copolymers

Proteins, which are unique sequences of poly(amino acid)s, are one of the most important compositions of living species. Poly(amino acid)s also have excellent potential in drug delivery systems, especially copolymers based on PEO-*b*-poly(amino acid). An attractive feature of PEO-*b*-poly(amino acid)s is that functional groups, e.g., carboxyl groups, introduced by the poly(amino acid) blocks can be used to conjugate drugs chemically. These conjugates can accumulate at tumor sites as a result of the EPR effect. Then, the conjugates can cleave through nonspecific hydrolysis or enzymatic activity. This method can greatly reduce the harm to healthy cells and increase selectivities for tumor cells.

Doxorubicin-conjugated PEO-*b*-poly(α, β-aspartic acid) was synthesized in efforts to effectively target cytotoxic agent to solid tumors.[55] The synthesis procedure was developed by Kataoka et al. (Figure 2.2.5.1).[56] First, an α-methyl-ω-amino PEO was utilized as a macroinitiator for the polymerization of β-benzyl *N*-carboxy-L-aspartate anhydride followed by hydrolysis of the benzyl groups. Doxorubicin was connected to the copolymer through a condensation reaction of the glycosidic amino group with the pendent carboxyl groups on the poly(α, β-aspartic acid) blocks in the presence of 1-ethyl-3-[3-(dimethylamino)propyl]-carbodiimide and triethylamine. Up to 50% of the side carboxyl groups were conjugated to doxorubicin.

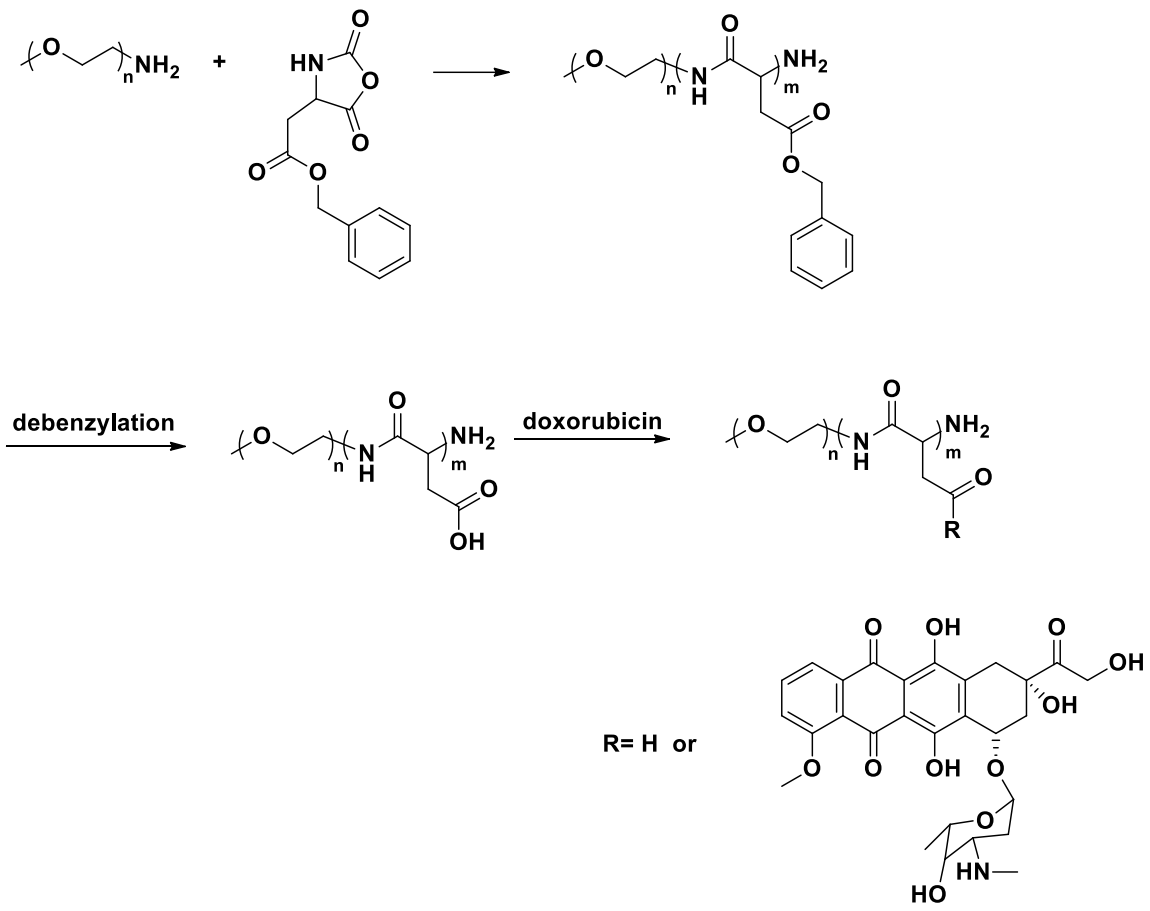

Figure 2.2.5.1. Schematic illustration of synthesis of DOX-conjugated PEO-P(Asp).[56]

In addition, the hydrophobicity of the poly(α, β-aspartic acid) block was enhanced due to the conjugation with doxorubicin, extra doxorubicun molecules could be entrapped in the hydrophobic cores of the copolymers by physical interactions.[4] A prolonged circulation of doxorubicin in the blood was successfully promoted by conjugation with the PEO-*b*-poly(α, β-aspartic acid) copolymer.

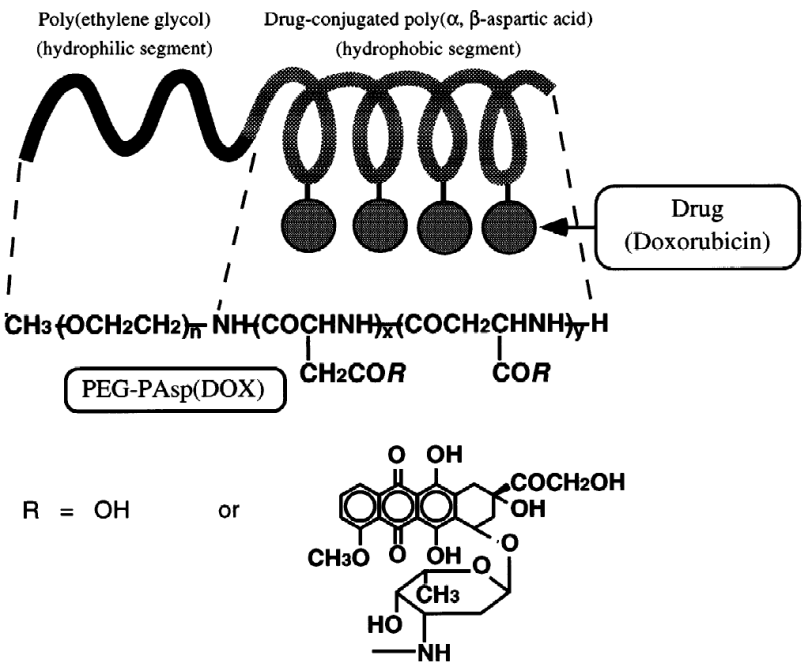

Figure 2.2.5.2. Structure of PEO-b-poly(α, β-aspartic acid)/DOX complex.[4]

2.3 Stimuli-sensitive copolymers

2.3.1 Multifunctional copolyethers based on tailor-made epoxides

In the past few years, "smart" polymeric micelles in terms of their responses to various environmental stimuli, including pH, temperature, ionic strength, magnetic or electric fields, or ultrasound, have been investigated for potential use in drug delivery.[57-59] By tuning functional groups on the amphiphilic copolymers, the abilities of "smart" polymeric micelles to target specific tissues can be adjusted.[60-63] Recently, a series of multifunctional PEO oligomers with pendent reactive groups distributed along the PEO backbones were reported.[64-69] The functional groups were introduced by anionic ring-opening copolymerization of functional epoxides with ethylene oxide.

Epoxides with pendent carbon-carbon double bonds are of great interests because they provide an outstanding platform to synthesize polyethers with a wide variety of

functionalities via thiol-ene coupling reaction. Polyethers based on a commercially available epoxide, allyl glycidyl ether (AGE), has been investigated as a potential material for drug delivery, gene transfection and proton-exchange membranes. Frey et al. reported a serious of random copolymers of EO and AGE with different comonomer molar percentages in the range from 0-100 %.[65,67] A critical challenge of the anionic ring-opening polymerization of AGE is the isomerization of allyl ether to propenyl ether (Scheme 2.3.1.1). It was reported that the degree of isomerization could be reduced to less than 10 % by lowering the reaction temperature to 40 °C. The obtained molecular weights were consistently above the theoretical values and this was attributed to the poor solubility of the cesium alkoxide initiator. However, P(EO-*co*-AGE) copolymers were utilized as a platform to synthesize multiple amino acid-PEOs. PEOs with side cysteine or L-glutathione moieties were synthesized via thiol-ene reaction of allyl side groups with *N*-acetyl-L-cysteine methyl ester or L-glutathione respectively. In order to avoid crosslink of the allyl groups, twenty molar excess of thiols were employed.

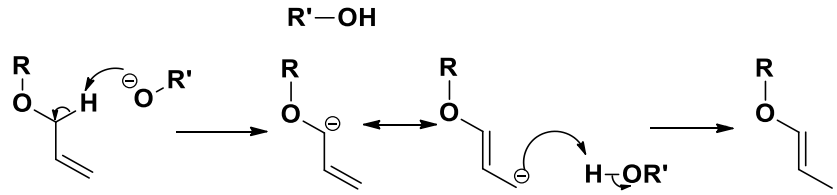

Scheme 2.3.1.1. Isomerization of allyl group to propenyl group in the presence of strong base.

Another interesting application of PAGEs is to make a covalently bonded drug conjugation. A diblock PEO-b-PAGE was investigated by Hruby et al. as a carrier for doxorubicin (Scheme 2.3.1.2).[70] Pendent ester groups were introduced onto the polymer via thiol-ene reaction of the side allyl groups with methyl mercaptoacetate. Subsequently,

the methyl ester groups were converted to hydrazides by reacting with 100 molar excess of hydrazine hydrate to prevent the formation of diacylhydrazine crosslink. Doxorubicin was covalently bound with the polymer via a pH-sensitive hydrazine bond. The hydrazine bond is stable under neutral conditions and labile under slightly acidic conditions as in most tumor tissues, thus resulted in a reduction of the side effects.

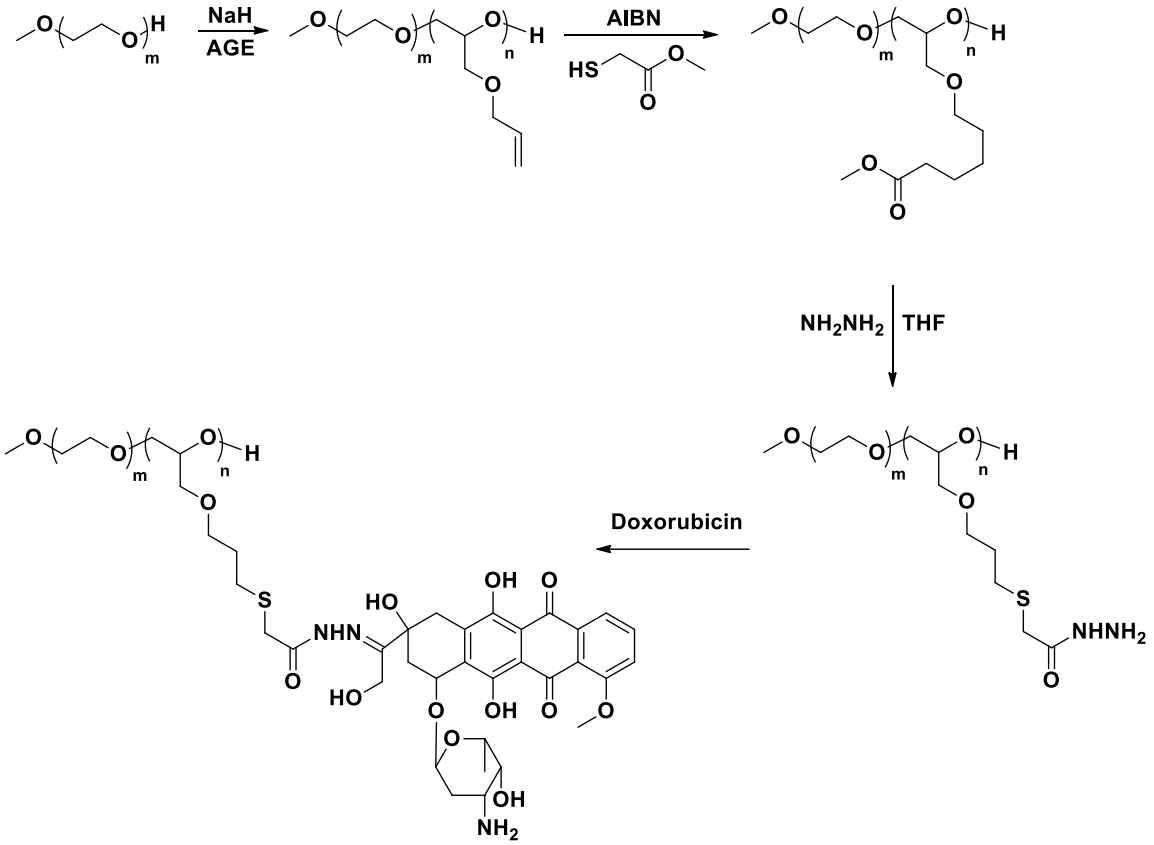

Scheme 2.3.1.2. Synthesis of polyether-doxorubicin conjugation.[70]

Due to the side reactions encountered with AGE, a novel epoxide ethoxy vinyl glycidyl ether (EVGE) was utilized as a comonomer for the polymerization of EO to synthesize multifunctional PEOs.[66] The pendent vinyl ether groups on these copolymers were post-reacted with benzyl mercaptan as a model molecule via thiol-ene reactions. Acetal-

formation was demonstrated as another type of post-polymerization modification by reaction of the vinyl ether groups with benzyl alcohol catalyzed by *p*-toluenesulfonic acid (Scheme 2.3.1.3). Both modifications were quantitative.

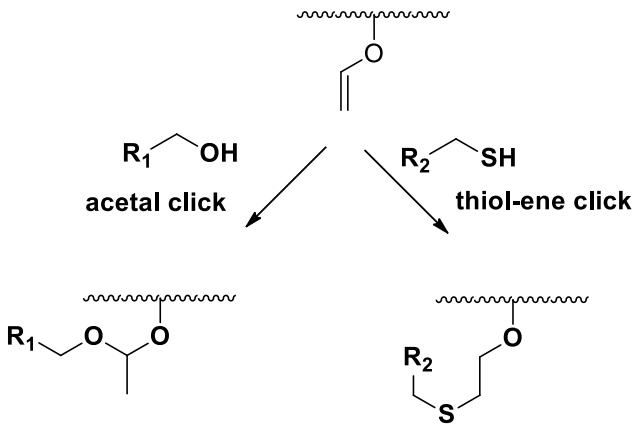

Scheme 2.3.1.3. Two types of post-polymerization modifications of vinyl ether groups: (1) acetal-formation with alcohols and (2) thiol-ene addition with thiols.[66]

Multi-aminofunctional PEO oligomers were also synthesized through copolymerization of EO with *N*,*N*-diallyl glycidyl amine (DAGA) (Scheme 2.3.1.4).[69] A protected catechol 2,2-dimethyl-1,3-benzodioxole-5-propanol was utilized as a initiator for the anionic ring-opening polymerization. The terminal catechol groups and pendent amines were deprotected by a single-step hydrolysis in 1 M HCl solution at rt. The obtained catechol groups were coated onto the surface of manganese oxide (MnO) nanoparticles to make T_1 MRI contrast agent. A fluorescent dye fluoresceine isothiocyanate (FITC) was conjugated with the nanoparticles by reaction with the amino groups to provide optical visibility of the nanoparticles in cells.

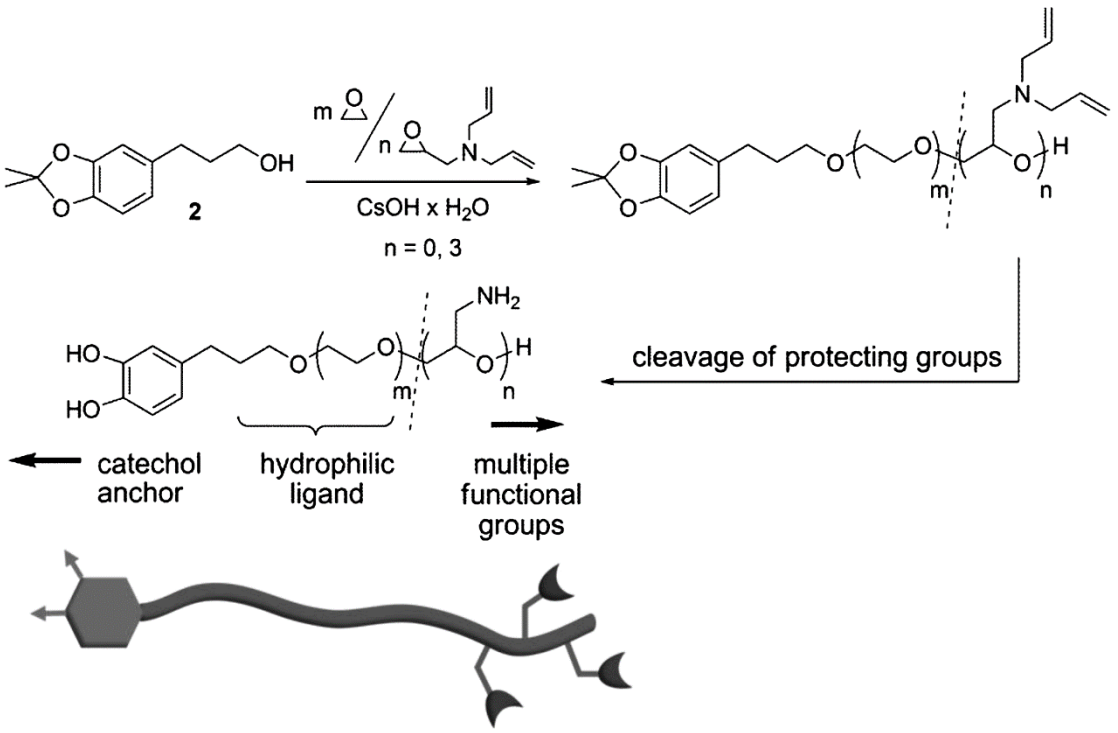

Scheme 2.3.1.4. Synthesis of catechol-P(EO-*co*-glycidyl amine).[69]

2.3.2 Thermosensitive polymers

Unlike many compounds that have better solubilities at higher temperature, certain polymers become less soluble in aqueous solution by increasing the temperature. This kind of polymer shows sharp transitions in solution at certain temperatures which are called the lower critical solution temperature (LCST).[71-82] In a thermodynamic viewpoint, the dissolution enthalpies ΔH of these polymers are negative which conduces dissolution. Whereas, the dissolution entropies ΔS are negative and this disfavors dissolution. Therefore, the dissolution free energy (ΔH-$T\Delta S$) is negative at temperature below the LCST and become positive by increasing temperature above the LCST. The hydrogen-bonding capabilities of these polymers are their characteristic properties because hydrogen

bonds between polymeric chains and the solvent molecules make dissolution enthalpies ΔH and entropies ΔS both negative.[71]

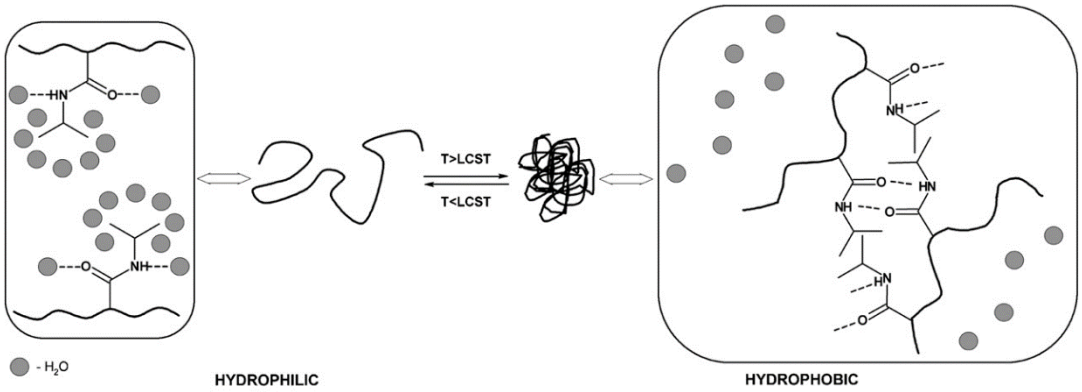

Figure 2.3.2.1. Schematic illustration of temperature-sensitive dissolution of PNIPAAM.[71]

One of the most studied thermosensitive polymer, poly(*N*-isopropyl acrylamide) (PNIPAAM), has a LCST at ~32 ℃ in aqueous solution.[71,83-95] It was reported that copolymerizing NIPAM with more or less hydrophilic units could change the LCST (Figure 2.3.2.3).[71,96-98] Generally, hydrophilic comonomers bring a higher LCST. In contrast, hydrophobic ones make the LCSTs lower. The effect of ionizable comonomers (containing carboxylic acid or amino groups) in the polymers based on PNIPAAM has also been studied. It was reported that LCSTs of these ionizable copolymers were affected by multiple factors: (1) hydrophobicities of the comonomers; (2) pH values of the solutions; (3) molar percentages of the comonomers.[98] Some other poly(*N*-substituted acrylamide), including poly(*N*,*N*-diethyl acrylamide) (PNDEAM), poly(*N*-ethyl acrylamide) (PNEAM) and their copolymers also exhibit LCSTs (Figure 2.3.2.2).[99]

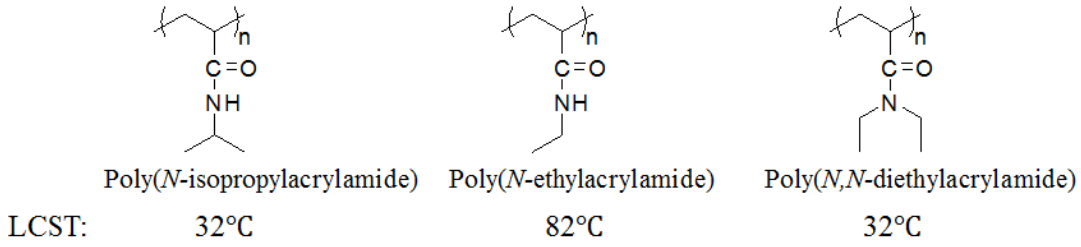

Figure 2.3.2.2. LCSTs of poly(*N*-substituted acrylamide)s.[99]

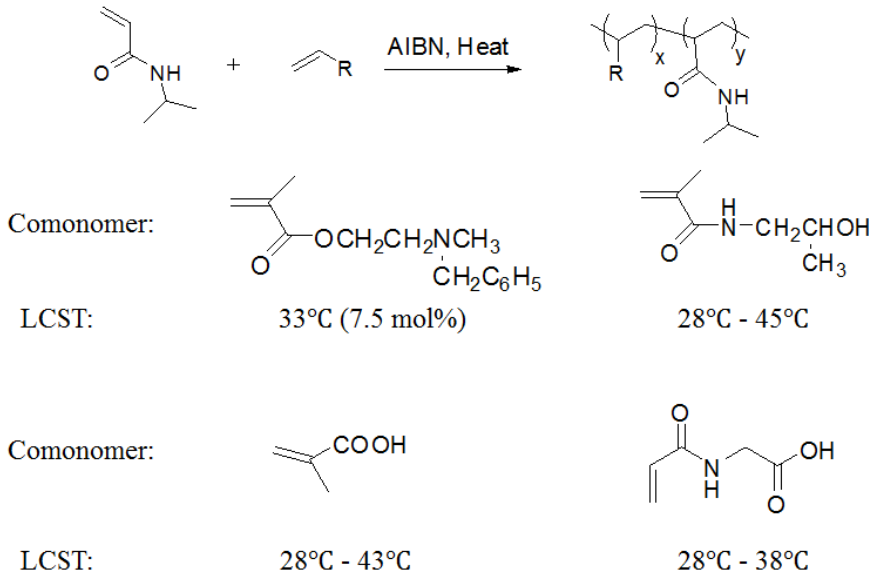

Figure 2.3.2.3. LCSTs of PNIPAAM copolymers.[71,96-98]

Recently, great efforts were made on developing drug delivery agents based on thermosensitive polymers.[100-104] Two different delivery systems have been studied: (1) above the LCSTs, micelles are built with thermosensitive polymers as the hydrophobic cores; (2) Below the LCSTs, thermosensitive polymers constitute the hydrophilic shells.[105]

This brings on the possibility of thermal control of drug delivery. Slight change of body temperature around the LCST could stimulate a burst release.[105]

The micelles comprised with thermosensitive blocks as the shell-forming segments and hydrophobic cores can be loaded with water insoluble drugs below the LCST. The hydrophilic shells help the micelles dispersed well in aqueous phase and prevent interaction between the inner cores with biocomponents. By local heating, the shells become hydrophobic and the micelles can be adsorbed by cell membrane via hydrophobic interaction (Figure 2.3.2.4). Thus, accumulation of the therapeutic agents at specific sites, such as tumor tissues, can be achieved.

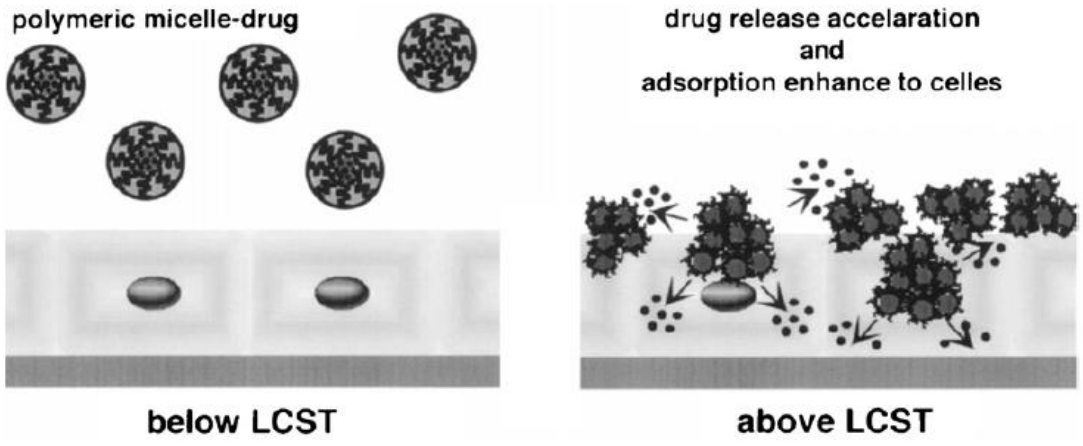

Figure 2.3.2.4. Schematic illustration of thermosensitive drug release from micelles with PNIPAAM as the shell-forming segments.[105]

Zhang et al. prepared thermosensitive micelles containing a diblock PNIPAAM-*b*-poly(methyl methacrylate) (PMMA) copolymer and an anti-inflammation drug prednisone acetate.[101] The PNIPAAM block was the shell-forming component and provided dispersibility at temperature below the LCST of PNIPAAM. The hydrophobic PMMA block incorporated with prednisone acetate and formed the inner core. The micelles were

colloidally stable and the drug release rate from the micelles was found to be relatively slow at 24-27 ℃. When the temperature was increased to 38-40 ℃, the shell-forming PNIPAAM block became hydrophobic and collapsed, and this led to a tremendous faster drug release (Figure 2.3.2.5).

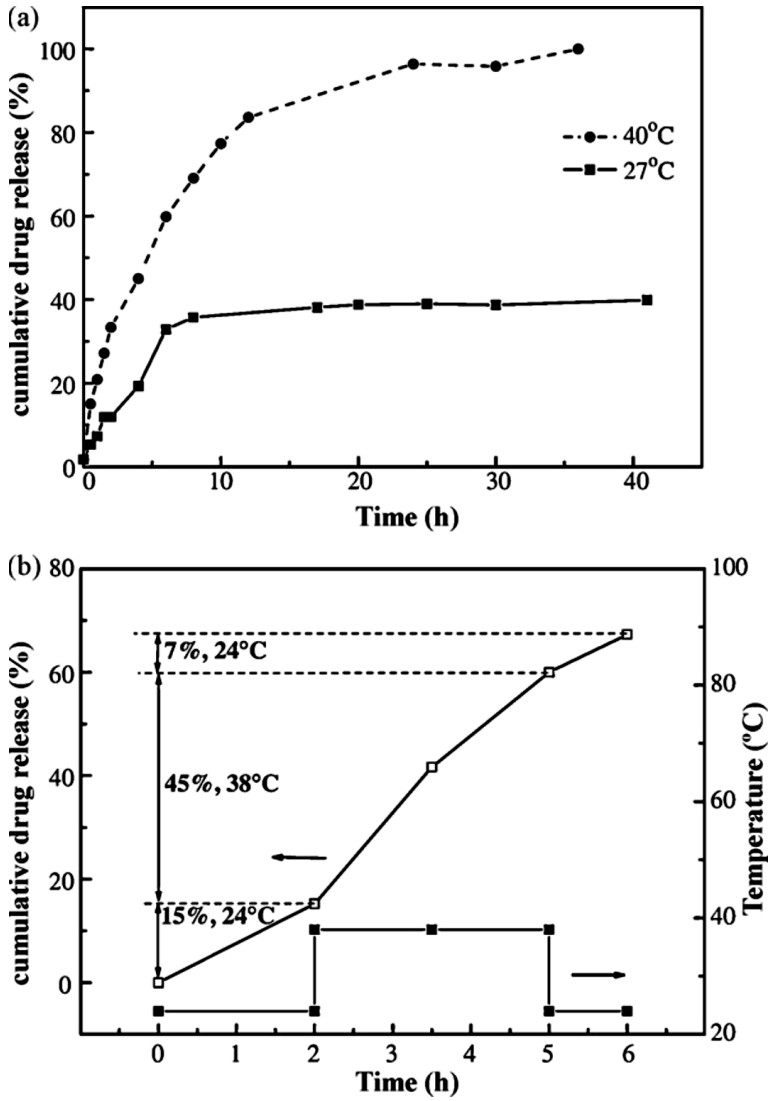

Figure 2.3.2.5. Comparison of release rates of prednisone acetate from PNIPAAM-*b*-PMMA micelles at temperatures below and above the LCST of PNIPAAM.[101]

A thermosensitive polymer with a LCST at ~ 37 °C was desirable for precise thermo-control of drug release in human body. Neradovic and coworkers reported that incorporation of 20 mol% of 2-hydroxypropyl methacrylamide (HPMAM) in the PNIPAAM block increased the LCST to ~37 °C.[106] An ester of HPMAM (HPMAM-lactide) was copolymerized with NIPAAM in the presence of AIBN to prepare P(NIPAAM-*co*-HPMAM-lactide) random copolymers. Diblock PEO-*b*-P(NIPAAM-*co*-HPMAM-lactide) copolymers were synthesized using 4,4'-azobis-(cyanopentanoic acid) substituted methoxyl-PEO (PEO_2-ABCPA) as a macroinitiator. The lactide was then removed by hydrolysis to obtain P(NIPAAM-*co*-HPMAM-lactide) and PEO-*b*-P(NIPAAM-*co*-HPMAM). The LCSTs of random and block copolymers with a series of comonomer contents were determine by static light scattering (Figure 2.3.2.6). It was found that the relatively hydrophobic HPMAM-lactide comonomer decreased the LCSTs of both random and block copolymers, and the hydrophilic HPMAM comonomer increased the LCSTs.

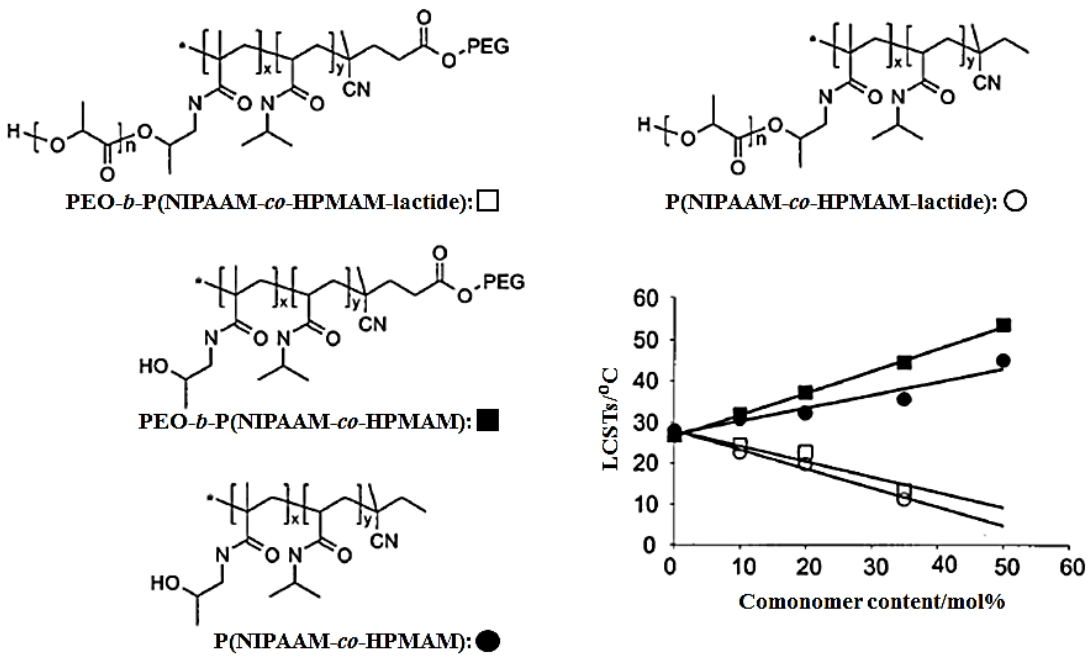

Figure 2.3.2.6. Structures and LCSTs of PNIPAAM and PHPMAM copolymers.[106]

Since the LCST of PNIPAAM is greatly affected by the hydrophobicities of comonomers as mentioned above, a pH-sensitive polymer can be prepared by incorporation of ionizable comonomers into the PNIPAAM polymers. Yang et al. reported an amphiphilic P(NIPAAM-*co*-*N*,*N*-dimethylacrylamide-*co*-10-undecenoic acid) (P(NIPAAM-*co*-DMAAM-*co*-UA)) copolymer.[102] The UA comonomer was pH-sensitive, and thus the LCST of this copolymer could be changed by adjusting the environmental pH. At pH 7.4, the LCST was above body temperature, and the doxorubicin-loaded micelles were stable under nominal physiological condition. The LCST became lower than body temperature in slightly acidic medium (pH 6.6), and a burst drug release was triggered (Figure 2.3.2.7). Therefore, accumulation of drugs in acidic tumor tissues could be achieved.

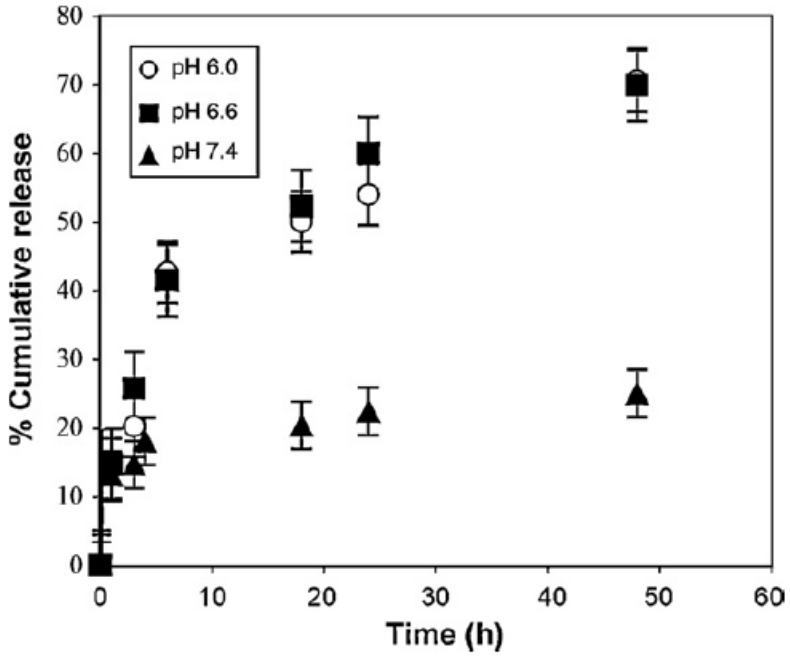

Figure 2.3.2.7. pH-sensitive release of doxorubicin from P(NIPAAM-*co*-DMAAM-*co*-UA) micelles at 37 °C.[102]

2.4 References:

(1) Adams, M. L.; Lavasanifar, A.; Kwon, G. S., Amphiphilic block copolymers for drug delivery *J. Pharm. Sci.* **2003**, *92*, 1343.

(2) Duncan, R., The dawning era of polymer therapeutics *Nat. Rev. Drug Discov.* **2003**, *2*, 347.

(3) Jagur-Grodzinski, J., Biomedical application of functional polymers *React. Funct. Polym.* **1999**, *39*, 99.

(4) Kataoka, K.; Harada, A.; Nagasaki, Y., Block copolymer micelles for drug delivery: design, characterization and biological significance *Adv. Drug Deliver. Rev.* **2001**, *47*, 113.

(5) Kataoka, K.; Harada, A.; Nagasaki, Y., Block copolymer micelles for drug delivery: Design, characterization and biological significance *Adv. Drug Deliver. Rev.* **2012**, *64*, 37.

(6) Lee, J. H.; Lee, H. B.; Andrade, J. D., Blood Compatibility of Polyethylene Oxide Surfaces *Prog. Polym. Sci.* **1995**, *20*, 1043.

(7) Lukyanov, A. N.; Torchilin, V. P., Micelles from lipid derivatives of water-soluble polymers as delivery systems for poorly soluble drugs *Adv. Drug Deliver. Rev.* **2004**, *56*, 1273.

(8) Moghimi, S. M.; Hunter, A. C.; Murray, J. C., Long-circulating and target-specific nanoparticles: Theory to practice *Pharmacol. Rev.* **2001**, *53*, 283.

(9) Torchilin, V. P., Structure and design of polymeric surfactant-based drug delivery systems *J. Control Release* **2001**, *73*, 137.
(10) Grodzinski, J., Biomedical application of functional polymers *Reactive & Functional Polymers* **1999**, *39*, 99.
(11) Maeda, H., The enhanced permeability and retention (EPR) effect in tumor vasculature: the key role of tumor-selective macromolecular drug targeting *Adv. Enzyme Reg.* **2001**, *41*, 189.
(12) Greish, K., Enhanced permeability and retention of macromolecular drugs in solid tumors: A royal gate for targeted anticancer nanomedicines *J. Drug Target* **2007**, *15*, 457.
(13) Maeda, H., *Adv. Enzyme Reg.* **2001**, *41*, 189.
(14) Zhang, F.; Kang, E. T.; Neoh, K. G.; Huang, W., Modification of gold surface by grafting of poly(ethylene glycol) for reduction in protein adsorption and platelet adhesion *J. Biomat. Sci-Polym. Edition* **2001**, *12*, 515.
(15) *Poly(ethylene oxide)*; Bailey, F. E.; Koleske, J. Y., Eds.; Academic Press: New York, 1976.
(16) Wang, P.; Tan, K. L.; Kang, E. T., Surface modification of poly(tetrafluoroethylene) films via grafting of poly(ethylene glycol) for reduction in protein adsorption *J. Biomat. Sci-Polym. Edition* **2000**, *11*, 169.
(17) *Safety of poly(ethylene glycol) and poly(ethylene glycol) derivatives*; Working, P. K.; Newman, M. S.; Johnson, J.; Cornacoff, J. B., Eds.; American Chemical Society: Washington DC, 1997.
(18) Peppas, L. B., Recent advances on the use of biodegradable microparticles and nanoparticles in controlled drug delivery *Int. J. Pham.* **1995**, *116*, 1.
(19) Gan, Z.; Jim, T. F.; Li, M.; Yuer, Z.; Wang, S.; Wu, C., Enzymatic Biodegradation of Poly(ethylene oxide-b- -caprolactone) Diblock Copolymer and Its Potential Biomedical Applications *Macromolecules* **1999**, *32*, 590.
(20) Allen, C.; Eisenberg, A.; Mrsic, J.; Maysinger, D., PCL-b-PEO micelles as a delivery vehicle for FK506: Assessment of a functional recovery of crushed peripheral nerve *Drug Deliv.* **2000**, *7*, 139.
(21) Lucey, M. R.; Abdelmalek, M. F.; Gagliardi, R.; Granger, D.; Holt, C.; Kam, I.; Klintmalm, G.; Langnas, A.; Shetty, K.; Tzakis, A.; Woodle, E. S., A comparison of tacrolimus and cyclosporine in liver transplantation: Effects on renal function and cardiovascular risk status *Am. J. Transplant* **2005**, *5*, 1111.
(22) Vincenti, F.; Study, T. K. T., Tacrolimus (FK 506) in kidney transplantation: Five-year survival results of the US multicenter, randomized, comparative trial *Transplant P.* **2001**, *33*, 1019.
(23) Crespo-Leiro, M. G., Tacrolimus in heart transplantation *Transplant P.* **2003**, *35*, 1981.
(24) Yura, H.; Yoshimura, N.; Hamashima, T.; Akamatsu, K.; Nishikawa, M.; Takakura, Y.; Hashida, M., Synthesis and pharmacokinetics of a novel macromolecular prodrug of Tacrolimus (FK506), FK506–dextran conjugate *J. Controlled Release* **1999**, *57*, 87.

(25) Yoo, H. S.; Park, T. G., Biodegradable polymeric micelles composed of doxorubicin conjugated PLGA–PEG block copolymer *J. Controlled Release* **2001**, *70*, 63.
(26) Yoo, H. S.; Park, T. G., Biodegradable polymeric micelles composed of doxorubicin conjugated PLGA-PEG block copolymer *J. Controlled Release* **2001**, *70*, 63.
(27) Batrakova, E. V.; Kelly, D. L.; Li, S.; Li, Y. L.; Yang, Z. H.; Xiao, L.; Alakhova, D. Y.; Sherman, S.; Alakhov, V. Y.; Kabanov, A. V., Alteration of genomic responses to doxorubicin and prevention of MDR in breast cancer cells by a polymer excipient: Pluronic P85 *Mol. Pharmaceut.* **2006**, *3*, 113.
(28) Batrakova, E. V.; Li, S.; Alakhov, V. Y.; Elmquist, W. F.; Miller, D. W.; Kabanov, A. V., Sensitization of cells overexpressing multidrug-resistant proteins by Pluronic P85 *Pharmaceut. Res.* **2003**, *20*, 1581.
(29) Batrakova, E. V.; Li, S.; Alakhov, V. Y.; Miller, D. W.; Kabanov, A. V., Optimal structure requirements for pluronic block copolymers in modifying P-glycoprotein drug efflux transporter activity in bovine brain microvessel endothelial cells *J. Pharmacol. Exp. Ther.* **2003**, *304*, 845.
(30) Batrakova, E. V.; Li, S.; Li, Y. L.; Alakhov, V. Y.; Elmquist, W. F.; Kabanov, A. V., Distribution kinetics of a micelle-forming block copolymer Pluronic P85 *J. Control Release* **2004**, *100*, 389.
(31) Batrakova, E. V.; Li, S.; Li, Y. L.; Alakhov, V. Y.; Kabanov, A. V., Effect of pluronic p85 on ATPase activity of drug efflux transporters *Pharmaceut. Res.* **2004**, *21*, 2226.
(32) Batrakova, E. V.; Zhang, Y.; Li, Y. L.; Li, S.; Vinogradov, S. V.; Persidsky, Y.; Alakhov, V. Y.; Miller, D. W.; Kabanov, A. V., Effects of pluronic p85 on GLUT1 and MCT1 transporters in the blood-brain barrier *Pharmaceut. Res.* **2004**, *21*, 1993.
(33) Belenkov, A. I.; Alakhov, V. Y.; Kabanov, A. V.; Vinogradov, S. V.; Panasci, L. C.; Monia, B. P.; Chow, T. Y. K., Polyethyleneimine grafted with pluronic P85 enhances Ku86 antisense delivery and the ionizing radiation treatment efficacy in vivo *Gene. Ther.* **2004**, *11*, 1665.
(34) Bronich, T. K.; Bontha, S.; Shlyakhtenko, L. S.; Bromberg, L.; Hatton, T. A.; Kabanov, A. V., Template-assisted synthesis of nanogels from Pluronic-modified poly(acrylic acid) *J. Drug Target* **2006**, *14*, 357.
(35) Gebhart, C. L.; Sriadibhatla, S.; Vinogradov, S.; Lemieux, P.; Alakhov, V.; Kabanov, A. V., Design and formulation of polyplexes based on pluronic-polyethyleneimine conjugates for gene transfer *Bioconjugate Chem.* **2002**, *13*, 937.
(36) Kabanov, A. V.; Alakhov, V. Y., Pluronic (R) block copolymers in drug delivery: From micellar nanocontainers to biological response modifiers *Crit. Rev. Ther. Drug* **2002**, *19*, 1.
(37) Kabanov, A. V.; Batrakova, E. V.; Alakhov, V. Y., Pluronic((R)) block copolymers for overcoming drug resistance in cancer *Adv. Drug Deliver Rev.* **2002**, *54*, 759.

(38) Kabanov, A. V.; Batrakova, E. V.; Alakhov, V. Y., Pluronic (R) block copolymers as novel polymer therapeutics for drug and gene delivery *J. Control Release* **2002**, *82*, 189.
(39) Kabanov, A. V.; Batrakova, E. V.; Alakhov, V. Y., An essential relationship between ATP depletion and chemosensitizing activity of Pluronic((R)) block copolymers *J. Control Release* **2003**, *91*, 75.
(40) Kabanov, A. V.; Batrakova, E. V.; Miller, D. W., Pluronic((R)) block copolymers as modulators of drug efflux transporter activity in the blood-brain barrier *Adv. Drug Deliver Rev.* **2003**, *55*, 151.
(41) Kabanov, A. V.; Lemieux, P.; Vinogradov, S.; Alakhov, V., Pluronic((R)) block copolymers: novel functional molecules for gene therapy *Adv. Drug Deliver Rev.* **2002**, *54*, 223.
(42) Kabanov, A. V.; Sriadibhatla, S.; Yang, Z. H.; Alakhov, V. Y., Effect of pluronic block copolymers on gene expression. *Abstr. Pap. Am. Chem. S.* **2004**, *228*, U388.
(43) Minko, T.; Batrakova, E. V.; Li, S.; Li, Y. L.; Pakunlu, R. I.; Alakhov, V. Y.; Kabanov, A. V., Pluronic block copolymers alter apoptotic signal transduction of doxorubicin in drug-resistant cancer cells *J. Control Release* **2005**, *105*, 269.
(44) Ochietti, B.; Guerin, N.; Vinogradov, S. V.; St-Pierre, Y.; Lemieux, P.; Kabanov, A. V.; Alakhov, V. Y., Altered organ accumulation of oligonucleotides using polyethyleneimine grafted with poly(ethylene oxide) or pluronic as carriers *J. Drug Target* **2002**, *10*, 113.
(45) Ochietti, B.; Lemieux, P.; Kabanov, A. V.; Vinogradov, S.; St-Pierre, Y.; Alakhov, V., Inducing neutrophil recruitment in the liver of ICAM-1-deficient mice using polyethyleneimine grafted with pluronic P123 as an organ-specific carrier for transgenic ICAM-1 *Gene. Ther.* **2002**, *9*, 939.
(46) Oh, K. T.; Bronich, T. K.; Kabanov, A. V., Micellar formulations for drug delivery based on mixtures of hydrophobic and hydrophilic Pluronic((R)) block copolymers *J. Control Release* **2004**, *94*, 411.
(47) Price, T. O.; Farr, S. A.; Yi, X.; Vinogradov, S.; Batrakova, E.; Banks, W. A.; Kabanov, A. V., Transport across the Blood-Brain Barrier of Pluronic Leptin *J Pharmacol. Exp. Ther.* **2010**, *333*, 253.
(48) Yi, X. A.; Zimmerman, M. C.; Yang, R. F.; Tong, J.; Vinogradov, S.; Kabanov, A. V., Pluronic-modified superoxide dismutase 1 attenuates angiotensin II-induced increase in intracellular superoxide in neurons *Free Radical Bio. Med.* **2010**, *49*, 548.
(49) Alakhov, V. Y.; Moskaleva, E. Y.; Batrakova, E. V.; Kabanov, A. V., Hypersensitization of multidrug resistant human ovarian carcinoma cells by pluronic P85 block copolymer *Bioconjugate Chem.* **1996**, *7*, 209.
(50) Venne, A.; Li, S. M.; Mandeville, R.; Kabanov, A.; Alakhov, V., Hypersensitizing effect of pluronic L61 on cytotoxic activity, transport, and subcellular distribution of doxorubicin in multiple drug-resistant cells *Cancer Res.* **1996**, *56*, 3626.
(51) Bae, K. H.; Lee, Y.; Park, T. G., Oil-encapsulating PEO-PPO-PEO/PEG shell cross-linked nanocapsules for target-specific delivery of paclitaxel *Biomacromolecules* **2007**, *8*, 650.

(52) Schortinghuis, J.; Pijpe, J.; Spijkervet, F. K. L.; Vissink, A., Retention of lipiodol after parotid gland sialography *Int. J. Oral Max. Surg.* **2009**, *38*, 346.
(53) Tian, Y.; Bromberg, L.; Lin, S. N.; Hatton, T. A.; Tam, K. C., Complexation and release of doxorubicin from its complexes with pluronic P85-b-poly(acrylic acid) block copolymers *J. Controlled Release* **2007**, *121*, 137.
(54) Yang, T. F.; Chen, C. N.; Chen, M. C.; Lai, C. H.; Liang, H. F.; Sung, H. W., Shell-crosslinked Pluronic L121 micelles as a drug delivery vehicle *Biomaterials* **2007**, *28*, 725.
(55) Yokoyama, M.; Fukushima, S.; Uehara, R.; Okamoto, K.; Kataoka, K.; Sakurai, Y.; Okano, T., Characterization of physical entrapment and chemical conjugation of adriamycin in polymeric micelles and their design for in vivo delivery to a solid tumor *J. Controlled Release* **1998**, *50*, 79.
(56) Yokoyama, M.; Kwon, G. S.; Okano, T.; Sakurai, Y.; Seto, T.; Kataoka, K., Preparation of Micelle-Forming Polymer-Drug conjugate *Bioconjugate Chem.* **1992**, *3*, 295.
(57) Larson, N.; Ghandehari, H., Polymeric Conjugates for Drug Delivery *Chem. Mater.* **2012**, *24*, 840.
(58) Nishiyama, N. B., Y.; Miyata, K.; Fukushima, S.; Kataoka, K., *Drug Discovery Today: Technologies* **2005**, *2*, 21.
(59) Torchilin, V., Multifunctional and stimuli-sensitive pharmaceutical nanocarriers *Eur. J. Pharm. Biopharm.* **2009**, *71*, 431.
(60) Bae, Y. H.; Park, K., Targeted drug delivery to tumors: Myths, reality and possibility *J. Controlled Release* **2011**, *153*, 198.
(61) Danhier, F.; Feron, O.; Preat, V., To exploit the tumor microenvironment: Passive and active tumor targeting of nanocarriers for anti-cancer drug delivery *J. Controlled Release* **2010**, *148*, 135.
(62) Bae, Y.; Jang, W. D.; Nishiyama, N.; Fukushima, S.; Kataoka, K., Multifunctional polymeric micelles with folate-mediated cancer cell targeting and pH-triggered drug releasing properties for active intracellular drug delivery *Mol. Biosyst.* **2005**, *1*, 242.
(63) Bae, Y.; Nishiyama, N.; Fukushima, S.; Koyama, H.; Yasuhiro, M.; Kataoka, K., Preparation and biological characterization of polymeric micelle drug carriers with intracellular pH-triggered drug release property: Tumor permeability, controlled subcellular drug distribution, and enhanced in vivo antitumor efficacy *Bioconjugate Chem.* **2005**, *16*, 122.
(64) Mangold, C.; Wurm, F.; Frey, H., Functional PEG-based polymers with reactive groups via anionic ROP of tailor-made epoxides *Polym. Chem.-Uk* **2012**, *3*, 1714.
(65) Mangold, C.; Obermeier, B.; Wurm, F.; Frey, H., From an Epoxide Monomer Toolkit to Functional PEG Copolymers With Adjustable LCST Behavior *Macromol. Rapid. Comm.* **2011**, *32*, 1930.
(66) Mangold, C.; Dingels, C.; Obermeier, B.; Frey, H.; Wurm, F., PEG-based Multifunctional Polyethers with Highly Reactive Vinyl-Ether Side Chains for Click-Type Functionalization *Macromolecules* **2011**, *44*, 6326.

(67) Obermeier, B.; Frey, H., Poly(ethylene glycol-co-allyl glycidyl ether)s: A PEG-Based Modular Synthetic Platform for Multiple Bioconjugation *Bioconjugate Chem.* **2011**, *22*, 436.
(68) Mangold, C.; Wurm, F.; Obermeier, B.; Frey, H., "Functional Poly(ethylene glycol)": PEG-Based Random Copolymers with 1,2-Diol Side Chains and Terminal Amino Functionality *Macromolecules* **2010**, *43*, 8511.
(69) Wilms, V. S.; Bauer, H.; Tonhauser, C.; Schilmann, A. M.; Muller, M. C.; Tremel, W.; Frey, H., Catechol-Initiated Polyethers: Multifunctional Hydrophilic Ligands for PEGylation and Functionalization of Metal Oxide Nanoparticles *Biomacromolecules* **2013**, *14*, 193.
(70) Hruby, M.; Konak, C.; Ulbrich, K., Polymeric micellar pH-sensitive drug delivery system for doxorubicin *J. Controlled Release* **2005**, *103*, 137.
(71) Dimitrov, I.; Trzebicka, B.; Muller, A. H. E.; Dworak, A.; Tsvetanov, C. B., Thermosensitive water-soluble copolymers with doubly responsive reversibly interacting entities *Prog. Polym. Sci.* **2007**, *32*, 1275.
(72) Kokufuta, E., Novel Applications for Stimulus-Sensitive Polymer Gels in the Preparation of Functional Immobilized Biocatalysts *Adv. Polym. Sci.* **1993**, *110*, 157.
(73) Okano, T., Molecular Design of Temperature-Responsive Polymers as Intelligent Materials *Adv. Polym. Sci.* **1993**, *110*, 179.
(74) Gehrke, S. H., Synthesis, Equilibrium Swelling, Kinetics, Permeability and Applications of Environmentally Responsive Gels *Adv. Polym. Sci.* **1993**, *110*, 81.
(75) Saito, S.; Konno, M.; Inomata, H., Volume Phase-Transition of N-Alkylacrylamide Gels *Adv. Polym. Sci.* **1993**, *109*, 207.
(76) Lowe, J. S.; Chowdhry, B. Z.; Parsonage, J. R.; Snowden, M. J., The preparation and physico-chemical properties of poly(N-ethylacrylamide) microgels *Polymer* **1998**, *39*, 1207.
(77) Bae, Y. H.; Okano, T.; Hsu, R.; Kim, S. W., Thermosensitive Polymers as on-Off Switches for Drug Release *Makromol. Chem.-Rapid* **1987**, *8*, 481.
(78) Chen, G. H.; Hoffman, A. S., Preparation and Properties of Thermoreversible, Phase-Separating Enzyme-Oligo(N-Isopropylacrylamide) Conjugates *Bioconjugate Chem.* **1993**, *4*, 509.
(79) Stayton, P. S.; Shimoboji, T.; Long, C.; Chilkoti, A.; Chen, G. H.; Harris, J. M.; Hoffman, A. S., Control of Protein-Ligand Recognition Using a Stimuli-Responsive Polymer *Nature* **1995**, *378*, 472.
(80) Chen, G. H.; Hoffman, A. S., A New Temperature-Responsive and Ph-Responsive Copolymer for Possible Use in Protein Conjugation *Macromol. Chem. Physic* **1995**, *196*, 1251.
(81) Chen, G. H.; Hoffman, A. S., Temperature-Induced Phase-Transition Behaviors of Random Vs Graft-Copolymers of N-Isopropylacrylamide and Acrylic-Acid *Macromol. Rapid Comm.* **1995**, *16*, 175.
(82) Chen, G. H.; Hoffman, A. S., Graft-Copolymers That Exhibit Temperature-Induced Phase-Transitions over a Wide-Range of Ph *Nature* **1995**, *373*, 49.

(83) Fujishige, S., Intrinsic Viscosity-Molecular Weight Relationships for Poly(N-Isopropylacrylamide) Solutions *Polym. J.* **1987**, *19*, 297.
(84) Fujishige, S.; Kubota, K.; Ando, I., Phase-Transition of Aqueous-Solutions of Poly(N-Isopropylacrylamide) and Poly(N-Isopropylmethacrylamide) *J. Phys. Chem.-Us* **1989**, *93*, 3311.
(85) Kubota, K.; Fujishige, S.; Ando, I., Single-Chain Transition of Poly(N-Isopropylacrylamide) in Water *J. Phys. Chem.-Us* **1990**, *94*, 5154.
(86) Kubota, K.; Hamano, K.; Kuwahara, N.; Fujishige, S.; Ando, I., Characterization of Poly(N-Isopropylmethacrylamide) in Water *Polym. J.* **1990**, *22*, 1051.
(87) Kubota, K.; Fujishige, S.; Ando, I., Solution Properties of Poly(N-Isopropylacrylamide) in Water *Polym. J.* **1990**, *22*, 15.
(88) Irie, M., Stimuli-Responsive Poly(N-Isopropylacrylamide) - Photoinduced and Chemical-Induced Phase-Transitions *Adv. Polym. Sci.* **1993**, *110*, 49.
(89) Schild, H. G.; Tirrell, D. A., Microcalorimetric Detection of Lower Critical Solution Temperatures in Aqueous Polymer-Solutions *J. Phys. Chem.-Us* **1990**, *94*, 4352.
(90) Cho, C. S.; Jung, J. H.; Sung, Y. K.; Lee, Y. M., Effect of Polymeric Surfactants on the Cloud Point of Poly(N-Isopropylacrylamide) *Macromol. Rapid Comm.* **1994**, *15*, 727.
(91) Zeng, F.; Tong, Z.; Feng, H. Q., Nmr investigation of phase separation in poly(N-isopropyl acrylamide)/water solutions *Polymer* **1997**, *38*, 5539.
(92) Zeng, F.; Tong, Z.; Yang, X. Z., Differences in vibrational spectra of poly(N-isopropyl acrylamide) from water solution before and after phase separation *Eur. Polym. J.* **1997**, *33*, 1553.
(93) Boutris, C.; Chatzi, E. G.; Kiparissides, C., Characterization of the LCST behaviour of aqueous poly(N-isopropylacrylamide) solutions by thermal and cloud point techniques *Polymer* **1997**, *38*, 2567.
(94) Huglin, M. B.; Liu, Y.; Velada, J. L., Thermoreversible swelling behaviour of hydrogels based on N-isopropylacrylamide with acidic comonomers *Polymer* **1997**, *38*, 5785.
(95) Liu, Y.; Mao, R. S.; Huglin, M. B.; Holmes, P. A., Network parameters and scaling behaviour of chemically crosslinked hydrogels of poly[(N,N-dimethylacrylamide)-co-(methyl methacrylate)] *Macromol. Chem. Physic.* **1997**, *198*, 1885.
(96) Bokias, G.; Hourdet, D.; Iliopoulos, I., Positively charged amphiphilic polymers based on poly(N-isopropylacrylamide): Phase behavior and shear-induced thickening in aqueous solution *Macromolecules* **2000**, *33*, 2929.
(97) Hahn, M.; Gornitz, E.; Dautzenberg, H., Synthesis and properties of ionically modified polymers with LCST behavior *Macromolecules* **1998**, *31*, 5616.
(98) Salgado-Rodriguez, R.; Licea-Claverie, A.; Arndt, K. F., Random copolymers of N-isopropylacrylamide and methacrylic acid monomers with hydrophobic spacers: pH-tunable temperature sensitive materials *Eur. Polym. J.* **2004**, *40*, 1931.

(99) Liu, H. Y.; Zhu, X. X., Lower critical solution temperatures of N-substituted acrylamide copolymers in aqueous solutions *Polymer* **1999**, *40*, 6985.
(100) Cammas, S.; Suzuki, K.; Sone, C.; Sakurai, Y.; Kataoka, K.; Okano, T., Thermo-responsive polymer nanoparticles with a core-shell micelle structure as site-specific drug carriers *J. Controlled Release* **1997**, *48*, 157.
(101) Wei, H.; Zhang, X. Z.; Zhou, Y.; Cheng, S. X.; Zhuo, R. X., Self-assembled thermoresponsive micelles of poly(N-isopropylacrylamide-b-methyl methacrylate) *Biomaterials* **2006**, *27*, 2028.
(102) Soppimath, K. S.; Tan, D. C. W.; Yang, Y. Y., pH-triggered thermally responsive polymer core-shell nanoparticles for drug delivery *Adv. Mater.* **2005**, *17*, 318.
(103) Schild, H. G., Poly (N-Isopropylacrylamide) - Experiment, Theory and Application *Prog. Polym. Sci.* **1992**, *17*, 163.
(104) Zhang, X. Z.; Zhuo, R. X., Dynamic properties of temperature-sensitive poly(N-isopropylacrylamide) gel cross-linked through siloxane linkage *Langmuir* **2001**, *17*, 12.
(105) Wei, H.; Cheng, S.; Zhang, X.; Zhuo, R., Thermo-sensitive polymeric micelles based on poly(N-isopropylacrylamide) as drug carriers *Prog. Polym. Sci.* **2009**, *34*, 893.
(106) Neradovic, D.; van Nostrum, C. F.; Hennink, W. E., Thermoresponsive polymeric micelles with controlled instability based on hydrolytically sensitive N-isopropylacrylamide copolymers *Macromolecules* **2001**, *34*, 7589.

Chapter 3. Design and Synthesis of Functional Amphiphilic Copolyethers

Most of the work described in this chapter was performed by the author of this dissertation. He was responsible for the synthesis and characterization of the monomers and polymers. Ran Liu aided in the preparation of several polymers and dynamic light scattering analysis. Dr. Sharavanan Balasubramaniam of the Dr. Richey M. Davis' group prepared and characterized the drug-containing nanoparticles.

3.1 Introduction

Amphiphilic copolymer micelles have been investigated as components of drug delivery vehicles for decades due to their capability of loading poorly soluble drugs and enhancing their biocompatibility.[1-8] Another attractive property of drug-loaded polymeric micelles is that their sizes lead to longer circulation times in the blood stream and at least some selectivity in targeting tumors via the enhanced permeability and retention (EPR) effect. This is due to the greater vascular permeability and immature lymph drainage system in solid tumor tissues.[9-11] In the past few years, "smart" polymeric micelles that respond to various environmental stimuli, including pH, temperature, ionic strength, magnetic or electric fields, or ultrasound, have been investigated for potential use in drug delivery.[12-14] By tuning functional groups on the amphiphilic copolymers, the abilities of "smart" polymeric micelles to target specific tissues can be adjusted.[15-18] Poly(ethylene oxide) (PEO) is broadly used as a shell-forming block on drug-loaded micelles[8,19-24] due to its excellent solubility in aqueous media,[8,23,25] low toxicity,[5,26] and resistance to protein adsorption. PEO shells can also provide steric stabilization of the micelles so that they disperse well in water.

Aliphatic copolyethers, which are usually prepared by ring-opening polymerization of epoxide-containing monomers, are of great interest in the biomedical area. The commercially available triblock copolyethers based on poly(ethylene oxide-*b*-propylene oxide-*b*-ethylene oxide) (PEO-*b*-PPO-*b*-PEO) (the BASF tradename is *Pluronics*) have been utilized to deliver water-insoluble drugs including doxorubicin[27] and paclitaxel[28]. Our group has previously reported the synthesis of PEO and diblock copolyethers (PEO-*b*-PPO) functionalized with terminal groups, including ammonium, carboxylic acid and phosphonate.[29-31] Some of those functional copolyethers were coated onto iron oxide nanoparticles to make well-dispersed MRI contrast agents.[31-35] Heterobifunctional triblock copolyethers with one terminal amino group and one terminal hydroxyl group were also prepared by our group and conjugated to an antioxidant enzyme, Cu/Zn superoxide dismutase (SOD1).[36]

Frey et al. reported a series of multifunctional PEO oligomers with pendent reactive groups distributed along the PEO backbones.[37-42] Those oligomers were synthesized via random anionic copolymerization of ethylene oxide (EO) with functional epoxide monomers including allyl glycidyl ether[38,40] and ethoxy vinyl glycidyl ether.[38,39,42] Due to side reactions encountered with allyl glycidyl ether, the copolymerizations with ethoxy vinyl glycidyl ether were considered superior. The pendent vinyl ether groups on these copolymers were post-reacted with a variety of functional thiols via free radical thiol-ene reactions. Multi-aminofunctional PEO oligomers were also synthesized through copolymerization of EO with *N*,*N*-dibenzyl glycidyl amine[38] and *N*,*N*-diallyl glycidyl amine.[42]

This paper describes the synthesis and characterization of a series of amphiphilic block copolyethers based on PEO and poly(1,2-butylene oxide) that incorporate pendent vinyl ethers or vinyl silanes at the interface between the blocks, and alternatively, within the hydrophobic blocks. The vinyl groups were functionalized after polymerization to provide sites for crosslinking or for appending targeting agents. These materials form crosslinkable micelles in aqueous media that are of interest for drug delivery vehicles and bio-imaging agents.

3.2 Experimental

3.2.1 Materials

Azobisisobutyronitrile (AIBN, 98%), acetic acid (99.8%), epichlorohydrin (≥99%), ethylene glycol vinyl ether (97%), 1,2-butylene oxide (BO) (99%), tetrabutylammonium bromide (≥99%), methoxy-poly(ethylene oxide) (mPEO) (Mn = 5000 $g \cdot mol^{-1}$), mercaptoacetic acid (≥98%), isopropanol (anhydrous 99.5%), cysteamine, boc-cysteamine (97%), vinylmagnesium bromide (1.0 M), sodium iodide (99.5%), ammonium chloride (≥99.5%), hexamethylphosphoramide (≥99%) were purchased from Aldrich and used as received. Mercaptoethylamine hydrochloride (≥98%), 18-crown-6 (99%), potassium hydride (30 wt.% in mineral oil), potassium hydroxide (1.0 N), trifluoroacetic acid (99%), sodium bicarbonate (99%) were purchased from Alfa Aesar and used as received. Dichloromethane (99.9%), sodium hydroxide and magnesium sulfate were purchased from Fisher Scientific and used as received. 3-Chloropropyldimethylchlorosilane was purchased from Gelest and used as received. *N*,*N*-Dimethylformamide (99.9%), spectra/por® dialysis membrane (MWCO: 1000, wet in 0.05% sodium azide) were purchased from Spectrum Chemical MFG Corp.

3.2.2 Characterization

^{1}H NMR spectral analyses were performed on a Bruker TopSpin 500 NMR operating at 500 MHz. Size exclusion chromatography (SEC) analyses were performed using a stationary phase consisting of three Waters polystyrene/divinylbenzene Styragel HT 5, 4, and 2 columns. Inhibitor free THF was used as the mobile phase and filtered with a 0.2 μm PTFE filter prior to use. An isocratic pump (Agilent 1260 infinitiy, Agilent Technologies, USA) with an online degasser (Agilent 1260), autosampler and column oven was used for mobile phase delivery and sample injection. A system of multiple detectors connected in series and maintained at 30 °C was used for the analysis. A multi-angle laser light scattering (MALS) detector (DAWN-HELEOS II, Wyatt Technology Corporation, USA), operating at a wavelength of 658 nm and a refractive index detector operating at a wavelength of 658nm (Optilab rEX, Wyatt Technology Corporation, USA) provided online results of the polymer SEC. The system was corrected for interdetector delay, band broadening, and the MALS signals were normalized using a 21,720 g/mole polystyrene standard. Data acquisition and analysis was completed using Astra 6 software from Wyatt Technology Corporation.

Dynamic light scattering (DLS) measurements were performed using a Zetasizer NanoZS particle analyzer (Malvern Instruments Ltd., Malvern, U. K.) equipped with a 4 mW solid-state He-Ne laser (λ = 633 nm) at a scattering angle of 173°. The average translational diffusion coefficient (D_t) was extracted from a single exponential (cumulants) fit of the correlation curve and the intensity-average hydrodynamic diameter (D_I) was determined through the Stokes-Einstein equation: $D_I = k_B T/(3\pi\eta D_t)$, where k_B is the Boltzmann constant, T is the absolute temperature and η, the solvent viscosity. The reported

intensity-weighted hydrodynamic diameters were averaged from five measurements. The critical micellar concentrations (*cmc*) of the copolymers in a 1:10 (v/v) THF-water mixture were determined by measuring the scattering intensities of a range of copolymer concentrations (0.001 – 10 mg mL^{-1}) by dynamic light scattering at 25°C. The inflection point on a graph of the mean count rate (kilocounts per second) as a function of copolymer concentration was taken as the *cmc*.

The drug loadings analysis and the saturation concentration of ritonavir in a 1:10 THF-water (v/v) mixture were determined by a reversed-phase high performance liquid chromatography (Agilent 1200 HPLC system). The chromatographic separation was performed with a ZORBAX Eclipse XDB-C18 column (4.5 × 150 mm, 5.0 μm pore size) maintained at 30°C. Ritonavir was detected by UV detection at a wavelength of 240 nm. The mobile phase consisted of 40/60 acetonitrile/potassium phosphate buffer (0.05 M, pH 5.65) at a flow rate of 1.5 mL min^{-1}. The total run time and the sample injection volume were 20 min and 5 μL, respectively. In order to measure the drug content in nanoparticles, lyophilized samples were suspended in acetonitrile at a concentration of 1 mg mL^{-1} and sonicated for 15 min. The solutions were filtered with a 0.2 μm nylon filter, and analyzed by HPLC in triplicate. The drug concentrations were determined by comparison to a standard curve for RTV. The drug loading and encapsulation efficiency were calculated as follows:

$$Drug\ loading\ (wt\%) = \frac{mass\ of\ RTV\ encapsulated}{total\ mass\ of\ nanoparticles} \times 100 \quad (0.1)$$

$$Encapsulation\ efficiency\ (\%) = \frac{experimental\ RTV\ loading}{targeted\ RTV\ loading} \times 100 \quad (0.2)$$

For measuring the saturation concentration, an excess amount of RTV was added to the THF-water mixture and stirred at 25°C for 72 h. The mixture was centrifuged at 13,000 rpm (16,060 × *g*) for 15 min in an accuSpin® Micro centrifuge (Fisher Scientific). The supernatant was passed through a 0.2 μm Nylon syringe filter before analysis.

3.2.3 Synthesis of Ethoxy Vinyl Glycidyl Ether (EVGE)

EVGE was prepared utilizing a modified procedure originally developed by Frey et al.[39] Sodium hydroxide (90 g, 2.3 mol) was dissolved in DI water (90 mL) in a 500-mL three-neck round-bottom flask equipped with a mechanical stirrer. Toluene (150 mL), ethylene glycol vinyl ether (10 g, 0.11 mol) and tetrabutylammonium bromide (3.5 g, 0.011 mol) were added to the solution and the mixture was cooled with an ice bath. The mixture was stirred and became very viscous. Epichlorohydrin (27 mL, 32 g, 0.34 mol) was added dropwise through a dropping funnel over 4 h at 0 ℃. The reaction was warmed to RT and reacted for another 20 hours. The reaction mixture became less viscous over this time. The mixture was transferred to a separatory funnel and the aqueous phase was removed. The organic phase was washed with DI water (4 × 150 mL) until a neutral aqueous phase was collected. Toluene and the excess of epichlorohydrin were removed under vacuum and the yellow residue was distilled at 100 °C, 5 Torr, yielding a colorless liquid (14 g, 78%).

3.2.4 Polymerization of Ethoxy Vinyl Glycidyl Ether

An exemplary procedure for the synthesis of a diblock mPEG (M_n=5,000 g mol^{-1})-*b*-PEVGE (M_n=1,300 g mol^{-1}) is provided. A 5,000 M_n mPEG (5.0 g, 1.0 mmol) was added to a 60-mL pressure tube equipped with a stir bar and dried under vacuum at 70 ℃ for 12 h, then cooled to RT. 18-Crown-6 ether (0.26 g, 1.0 mmol) was added and dried under

vacuum at RT for 0.5 h. Potassium hydride/mineral oil suspension (80 mg, 0.6 mmol) was added and dried under vacuum at RT for 0.5 h. The mixture was reacted at 70 ℃ with a slow nitrogen purge for 12 h, then a vacuum was applied to remove any residual H_2. EVGE (1.5 mL, 1.5 g) was syringed into the pressure tube and the mixture was stirred at 70 ℃. Small aliquots (~0.05 g) of the mixture were removed at known time intervals during the reaction to monitor the progress of the polymerization. The samples were dried under vacuum at 70 ℃ for 30 min to remove any unreacted EVGE and they were characterized via ^{1}H-NMR. Once the polymerization was complete (4 h), the reaction was cooled to RT and diluted with dichloromethane (100 mL). Acetic acid (0.06 g, 1.0 mmol) was added to neutralize the alkoxide. The organic phase was washed with sodium hydroxide solution (0.005 mol/L, 100 mL) followed by DI water (3 × 100 mL). The organic solution was concentrated under vacuum, then the polymer was precipitated in cold diethyl ether and dried under vacuum at RT yielding a waxy solid (5.1 g, 78%). The polymerization was also conducted in the absence of 18-crown-6 ether for comparison.

3.2.5 Synthesis of a Tapered mPEG-b-P(EVGE-co-BO) Copolymer

A tapered mPEG-*b*-P(EVGE-*co*-BO) copolymer was synthesized via copolymerization of EVGE and 1,2-BO. A 5,000 M_n mPEG (3.0 g, 0.60 mmol) was added to a 60-mL pressure tube equipped with a stir bar and dried under vacuum at 70 ℃ for 12 h, then cooled to RT. 18-Crown-6 ether (0.13 g, 0.50 mmol) was added and dried under vacuum at RT for 0.5 h. Potassium hydride/mineral oil suspension (51 mg, 0.38 mmol) was added and dried under vacuum at RT for 0.5 h. The mixture was heated at 70 ℃ with a slow nitrogen purge for 12 h, then a vacuum was applied to remove H_2. EVGE (0.8 mL, 0.8 g) and 1,2-BO (9 mL, 7.5 g) were syringed into the pressure tube and the mixture was stirred

at 70 ℃. Small aliquots (~0.05 g) of the mixture were removed at known time intervals during the reaction to study the polymerization rate and assess the microstructure of the copolymers. The samples were dried under vacuum at 70 ℃ for 30 min to remove any unreacted monomers and characterized via ^{1}H-NMR. Once the polymerization was complete (~4 h), the reaction was cooled to RT and diluted with dichloromethane (180 mL). Acetic acid (0.08 g, 1.3 mmol) was added to neutralize the alkoxide. The organic phase was washed with sodium hydroxide solution (0.005 mol/L, 200 mL) followed by DI water (3 × 200 mL). Dichloromethane was removed under vacuum yielding a waxy solid (10.3 g, 91%).

3.2.6 Synthesis of a Triblock mPEG-b-PEVGE-b-PBO Copolymer

A triblock mPEG-*b*-PEVGE-*b*-PBO copolymer was synthesized by adding EVGE and BO sequentially. A 5,000 M_n mPEG (6.7 g, 1.3 mmol), 18-crown-6 ether (0.30 g, 1.1 mmol) and potassium hydride/mineral oil suspension (108 mg, 0.81 mmol) were added using the protocol described above. EVGE (1.2 mL, 1.2 g, 8.3 mmol) was syringed into the pressure tube and the mixture was stirred at 70 ℃. After 12 h, BO (16 mL, 13 g, 0.18 mol) was added and the mixture was stirred at 70 ℃ for another 24 h. The reaction was cooled to RT and diluted with dichloromethane (200 mL). Acetic acid (0.08 g, 1.3 mmol) was added to neutralize the alkoxide. The organic phase was washed with sodium hydroxide solution (0.005 mol/L, 100 mL) followed by DI water (3 × 100 mL). Dichloromethane was removed under vacuum yielding a waxy solid (20 g, 96%).

3.2.7 Functionalization of pendent vinyl ether groups with mercaptoacetic acid

A mPEG-*b*-P(EVGE-*co*-BO) copolymer with pendent carboxylic acids was obtained via ene-thiol addition of mercaptoacetic acid across the vinyl ethers. In a characteristic

procedure, a 6,800 g mol^{-1} (by ^{1}H NMR) mPEG-*b*-P(EVGE-*co*-BO) (1.0 g, 0.15 mmol, 0.88 meq of vinyl ethers), mercaptoacetic acid (0.40 g, 4.3 mmol), and AIBN (0.07 g, 0.42 mmol) were dissolved in deoxygenated DMF (6 mL) in a 100-mL round-bottom flask equipped with a stir bar. The reaction was conducted at 70 ℃ for 24 h with stirring, then the mixture was cooled to RT. DI water (50 mL) was added to the flask, and the mixture was dialyzed against DI water (4 L) for 3 days. The solution was lyophilized yielding a white solid (1.1 g).

The amount of pendent acids was determined by acid-base titration of the product in isopropanol. A sample of the copolymer (55 mg) was dissolved in 5 mL of isopropanol by sonication. A 1.0 M potassium hydroxide solution was added to the polymer solution to adjust the pH to ~16 where all acids were deprotonated. The solution was stirred and titrated with a 0.05 M HCl/isopropanol solution, added through an automatic pipet. Asymmetric potential and pH values were measured with a Thermo Orion 3 Star pH meter.

3.2.8 Functionalization of pendent vinyl ether groups with BOC-cysteamine

A mPEG-*b*-P(EVGE-*co*-BO) copolymer with pendent amines was obtained via ene-thiol addition of *boc*-cysteamine across the vinyl ethers followed by removal of the *boc* groups. In a characteristic procedure, a 6,800 g mol^{-1} (by ^{1}H NMR) mPEG-*b*-P(EVGE-*co*-BO) (1.0 g, 0.15 mmol, 0.88 meq vinyl groups), *boc*-cysteamine (1.1 g, 6.2 mmol), and AIBN (0.07 g, 0.4 mmol) were dissolved in deoxygenated toluene (5 mL) in a 100-mL round-bottom flask equipped with a stir bar. The reaction was conducted at 70 ℃ for 18 h with stirring, then the mixture was cooled to RT. THF (5 mL) was added to the flask, and the mixture was dialyzed against THF (500 mL X 3) using benzoylated dialysis tubing (MWCO 2,000 g mol^{-1}) for 24 h. THF was removed under vacuum yielding a waxy solid (0.85 g, 74 %).

The pendent *boc* groups were removed by dissolving the *boc*-cysteamine-functional copolymer (0.85 g, 0.65 meq *boc* groups) in 5 mL of dichloromethane. Trifluoroacetic acid (5 mL, 0.07 mol) was added and the reaction was stirred at RT for 24 h. Triethylamine (9 mL, 0.13 mol) was added followed by dilution with THF (5 mL) and the mixture was dialyzed against 4 L X 5 of DI water through a cellulose acetate membrane (MWCO 1,000 g mol^{-1}) for 48 h. The amino-functional polymer was recovered by freeze-drying. The amount of pendent amines was determined by acid-base titrations of the products in isopropanol using the procedure described above.

3.2.9 Synthesis of vinyl dimethyl silyl propyl glycidyl ether (VSiGE)

3-Hydroxydimethylvinylsilane was synthesized utilizing a modified procedure from our previous report.[29,31] 3-Chloropropyldimethylchlorosilane (20.0 g, 0.12 mol) was added into a dry 500-mL round-bottom flask with a magnetic stir bar. The flask was cooled with an ice bath. A 1.0 M vinylmagnesium bromide/THF solution (240 mL, 0.24 mol) was slowly added in 30 min. The mixture was stirred at RT for 24 h and then diluted with 200 mL of dichloromethane. Saturated aqueous ammonium chloride solution (150 mL) was slowly added and the mixture was transferred to a separatory funnel to remove the aqueous layer. The organic layer was further washed with saturated sodium chloride solution (3 × 150 mL) and dried with anhydrous manganese sulfate. Dichloromethane was removed on a rotary evaporator yielding a yellow liquid. The product was distilled at 100 ℃ under reduced pressure yielding a colorless liquid (15.2 g, 80%).

3-Chloropropyldimethylvinylsilane (14.4 g, 0.089 mol) and sodium iodide (26.1 g, 0.17 mol) were dissolved in 120 mL of acetone in a 250-mL round-bottom flask equipped with a magnetic stir bar and a condenser. The mixture was stirred under reflux for 24 h and the

acetone was rota-evaporated. Dichloromethane (100 mL) was added and the mixture was vacuum filtered to remove the salt. Dichloromethane was rota-evaporated and the product was distilled under vacuum at 100 ℃ yielding 3-iodopropyldimethylvinylsilane (19.5 g, 86%).

3-Iodopropyldimethylvinylsilane (18.9 g, 0.074 mol), sodium bicarbonate (9.4 g, 0.11 mol), DI water (14 mL) and hexamethylphosphoramide (50 mL) were added into a 250-mL round-bottom flask with a stir bar. The mixture was stirred at 100 ℃ for 24 h and then cooled to RT and diluted with 30 mL of DI water. The aqueous layer was extracted with diethyl ether (3 × 100 mL) and the organic layer was washed with DI water (3 × 200 mL). Diethyl ether was rota-evaporated and the product was distilled under vacuum at 100 ℃ yielding 3-iodopropyldimethylvinylsilane (7.5 g, 65%).

Vinyl dimethyl silyl propyl glycidyl ether (VSiGE) was prepared utilizing a modified procedure originally developed by Frey et al.[39] Sodium hydroxide (18 g, 0.45 mol) was dissolved in DI water (18 mL) in a 250-mL three-neck round-bottom flask equipped with a mechanical stirrer. Toluene (30 mL), 3-hydroxydimethylvinylsilane (2 g, 14 mmol) and tetrabutylammonium bromide (0.46 g, 1.4 mmol) were added to the solution and cooled with an ice bath. The mixture was stirred vigorously and became very viscous. Epichlorohydrin (3.8 g, 41 mmol) was diluted with 5 mL of toluene and added into the flask dropwise through a dropping funnel within 4 hours. The reaction was conducted at RT for another 20 hours and became less viscous. The mixture was transferred to a separatory funnel and the aqueous phase was removed. The organic phase was washed with DI water (4 × 50 mL) until a neutral aqueous phase was collected. Toluene and the excess

of epichlorohydrin were removed under vacuum and the yellow residue was distilled at 100 °C, 2 Torr, yielding a colorless liquid (1.78 g, 64%).

3.2.10 Synthesis of a tapered mPEG-b-poly[VSiGE-co-(1,2-BO)] copolymer

A tapered mPEG-*b*-poly[VSiGE-*co*-(1,2-BO)] copolymer was synthesized by copolymerization of VSiGE with 1,2-BO. A 5,000 M_n mPEO (2.0 g, 0.4 mmol), 18-crown-6 ether (0.10 g, 0.38 mmol) and a potassium hydride/mineral oil suspension (32 mg, 0.24 mmol) were added using the protocol described above. VSiGE (0.33 g, 1.6 mmol) and 1,2-BO (2.9 mL, 2.4 g, 33 mmol) was syringed into the pressure tube and the mixture was stirred at 70 ℃. Small aliquots (~0.05 g) of the mixture were removed at known time intervals during the reaction to monitor the progress of the polymerization. The reaction was cooled to RT after 4 h when 74% of the 1,2-BO was reacted. The polymer was isolated and purified as described above yielding a solid copolymer (3.82 g, 81%).

3.2.11 Functionalization of pendent vinyl silane groups with cysteamine hydrochloride

A mPEG-*b*-poly[VSiGE-*co*-(1,2-BO)] copolymer with pendent amines was obtained via ene-thiol addition of cysteamine hydrochloride across the vinyl silanes. A 10,000 g mol^{-1} (by ^{1}H NMR) mPEG-*b*-poly[VSiGE-*co*-(1,2-BO)] (1.9 g, 0.19 mmol, 0.65 meq of vinyl silanes), cysteramine hydrochloride (0.43 g, 3.8 mmol), and AIBN (0.23 g, 1.3 mmol) were dissolved in a mixed 1:2 v:v toluene:DMF solvent (10 mL) in a 100-mL round-bottom flask equipped with a stir bar. The mixture was purged with nitrogen for 2 h and the reaction was conducted at 80 ℃ for 18 h with stirring, then the mixture was cooled to RT. Toluene was removed under vacuum. DI Water (50 mL) was added to the flask, and the mixture was dialyzed against DI water (4 L) through a cellulose acetate membrane

(MWCO 1,000 g mol^{-1}) for 2 days. The solution was lyophilized for 3 days yielding a white solid (1.7 g, 89%).

3.2.12 Synthesis of poly(butylene oxide) homopolymer

A benzyl-PBO (M_n: 2,000 g mol^{-1}) was synthesized via anionic ring-opening polymerization of 1,2-BO. A potassium naphthalide solution was prepared by charging naphthalene (14.1 g, 0.11 mol) into a 250-mL, flame-dried, round-bottom flask equipped with a glass stir bar. Dry THF (100 mL) was syringed into the flask to dissolve the naphthalene. Potassium metal (3.96 g, 0.10 mol) was added to the solution followed by a N_2 purge for 30 min. The solution was stirred overnight and titrated with 1 N HCl to determine the molarity of the potassium naphthalide solution (0.95 M). 18-Crown-6 ether (2.6 g, 10 mmol) was added to a 60-mL pressure tube equipped with a stir bar and dried under vacuum at RT for 0.5 h. Benzyl alcohol (1.08 g, 10 mmol) was added and dried under vacuum at RT for 0.5 h followed by addition of potassium naphthalide solution (10 mL, 9.5 mmol). 1,2-BO (24 mL, 20 g) was syringed into the pressure tube and the mixture was stirred at 70 ℃ for 12 h. The reaction was cooled to RT and diluted with dichloromethane (150 mL). Acetic acid (0.60 mL, 10 mmol) was added to neutralize the alkoxide. The organic phase was washed with DI water (3 × 100 mL). The obtained organic solution was dried under vacuum at 70 ℃ yielding a liquid (19.4 g, 99%).

3.2.13 Critical aggregation concentrations measurements

The critical micellar concentrations of the copolymers in aqueous dispersions were measured at 25 ℃ using a Zetasizer Nano-ZS particle analyzer (Malvern Instruments Ltd., Worcestershire, U. K.) equipped with a 4 mW He-Ne laser (λ = 633 nm) with backscattering detection (scattering angle = 173 °). The scattering intensities (in kilocounts

per second) over a range of copolymer concentrations (0.001-10 mg mL^{-1}) were recorded using a constant attenuator setting of 10. The photon count rates for each concentration were averaged from three measurements. The inflection point on a graph of the mean count rate (kilocounts per second) as a function of copolymer concentration was taken as the *cmc*.

3.2.14 Preparation of block copolymer-stabilized ritonavir nanoparticles

A representative procedure for preparing RTV-polyether nanoparticles containing 20 wt% RTV is as follows. Ritonavir (14.3 mg) was dissolved in THF (3.9 mL) containing PEO(5k)-*b*-PBO(9k) (42.9 mg) and PBO(2k) (14.3 mg). A four-jet multi-inlet vortex mixer design based on one previously reported was used to form the nanoparticles.[43] The THF solution was filtered with a 0.2 μm Nylon syringe filter, and fed into the multi-inlet vortex mixer at 9.99 mL min^{-1} using a computer-controlled syringe pump (New Era Pump Systems, Farmingdale, New York) along with three streams of de-ionized water at 33.3 mL min^{-1}, controlled by a PHD 4000 programmable syringe pump (Harvard Apparatus, Holliston, Massachusetts), yielding a final liquid phase composition of 1:10 (v/v) THF/water. After the nanoparticle suspension was formed in the mixer, it was dialyzed to remove THF against de-ionized water (4000 mL) for 24 h using a Spectra/Por dialysis bag (1,000 MWCO, Spectrum Laboratories, Inc.) with four changes of dialysate. The dialyzed suspension was freeze-dried for 72 h (0.021 mBar, -52 °C) and stored as a solid product.

3.3 Results and discussion

3.3.1 Synthesis of epoxy-functional monomers

Heterobifunctional monomers with one of the two functional groups being polymerizable are desirable to prepare polymers with pendent functional groups. A series of amphiphilic block copolymers have been prepared by anionic ring-opening

polymerizations utilizing poly(ethylene oxide) oligomers with one potassium alkoxide endgroup to initiate copolymerization of functional epoxides with 1,2-butylene oxide. Two functional epoxide monomers, one with a vinyl ether pendent group (EVGE) and the other with a vinylsilyl pendent substituent (VSiGE), were synthesized and incorporated into these copolymers through polymerization of the epoxy moieties. The pendent vinyl ether or vinylsilyl groups were also functionalized after the polymerizations with amines or carboxylic acids to provide crosslinkable sites. In terms of potential applications, our objective was to synthesize materials that would form amphiphilic micelles in aqueous solutions so that they can be loaded with relatively hydrophobic drugs, then the cores of those micelles can be crosslinked after the drugs are incorporated to mediate their release rates. While crosslinked micellar drug delivery vehicles have been developed previously wherein the micelles have been crosslinked prior to drug loading, there have been problems with that approach in obtaining efficient drug incorporation.

Substituted epoxide monomers can be synthesized by peroxide-catalyzed epoxidation of alkenes, conversion of alkenes to vicinal halohydrins followed by elimination and cyclization with base, or by base-promoted reaction of epichlorohydrin with alcohols. EVGE and VSiGE were synthesized in heterogeneous phase transfer reactions of epichlorohydrin with ethylene glycol vinyl ether or 3-hydroxydimethylvinylsilane respectively (Schemes 3.3.1.1 and 3.1.1.2). An excess of epichlorohydrin was added slowly to a cold toluene-water mixture to avoid generating heat rapidly. Tetra-n-butylammonium bromide was utilized as a phase transfer catalyst. The formation of tetra-n-butylammonium alkoxide resulted in a very viscous mixture and the viscosity decreased as the alkoxide was

consumed. The products were purified by distillation under reduced pressure and the structures were verified by ^{1}H NMR (Figures 3.3.1.1 and 3.1.1.2).

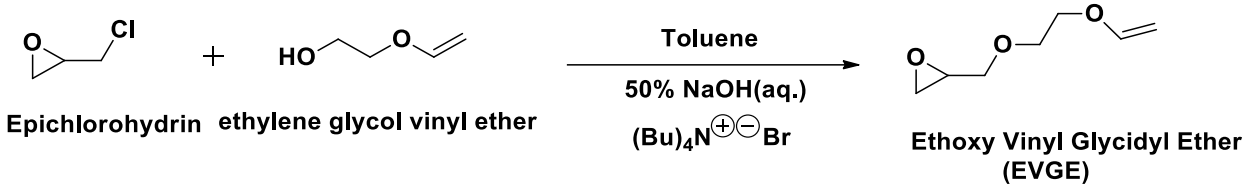

Scheme 3.3.1.1. Synthesis of ethoxy vinyl glycidyl ether monomer.

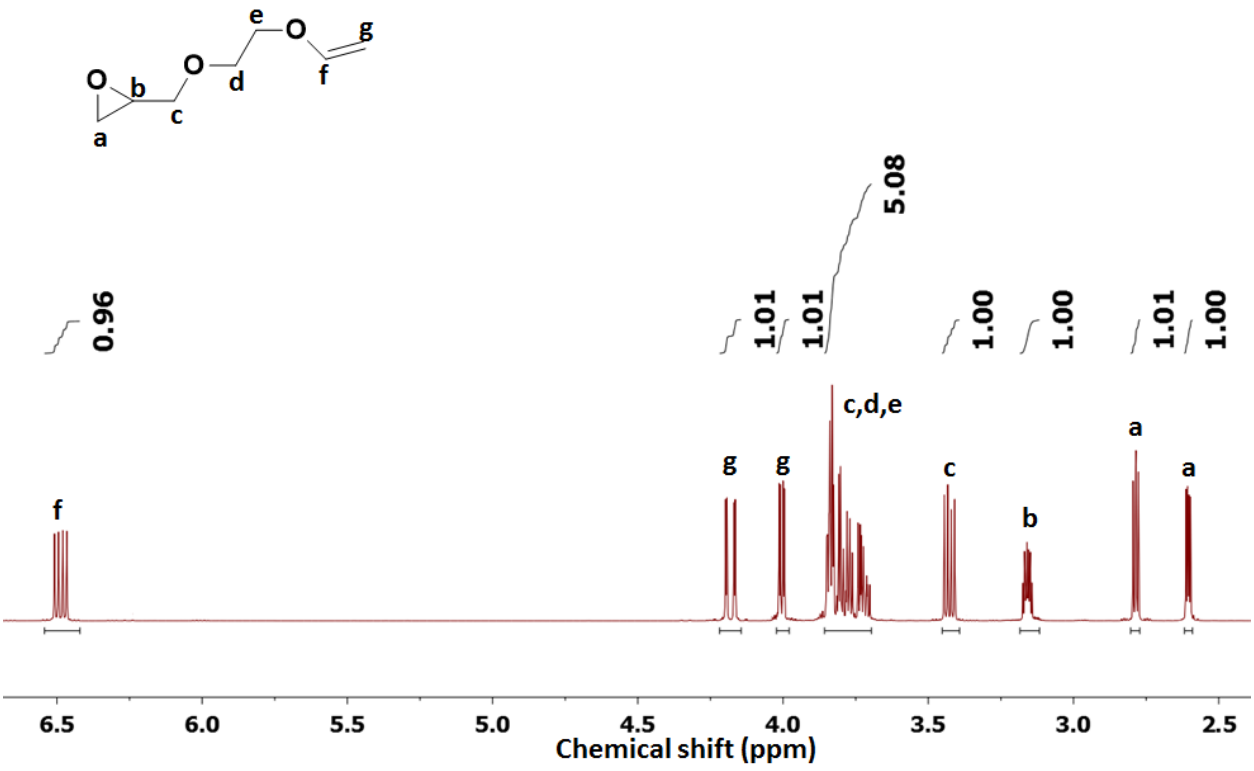

Figure 3.3.1.1. ^{1}H NMR spectrum of ethoxy vinyl glycidyl ether monomer.

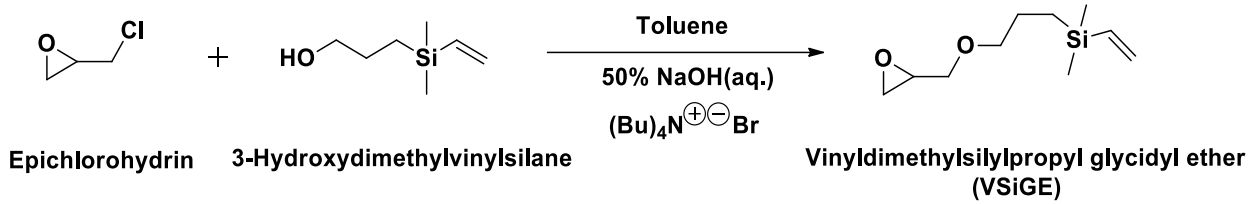

Scheme 3.3.1.2. Synthesis of vinyldimethylsilylpropyl glycidyl ether monomer.

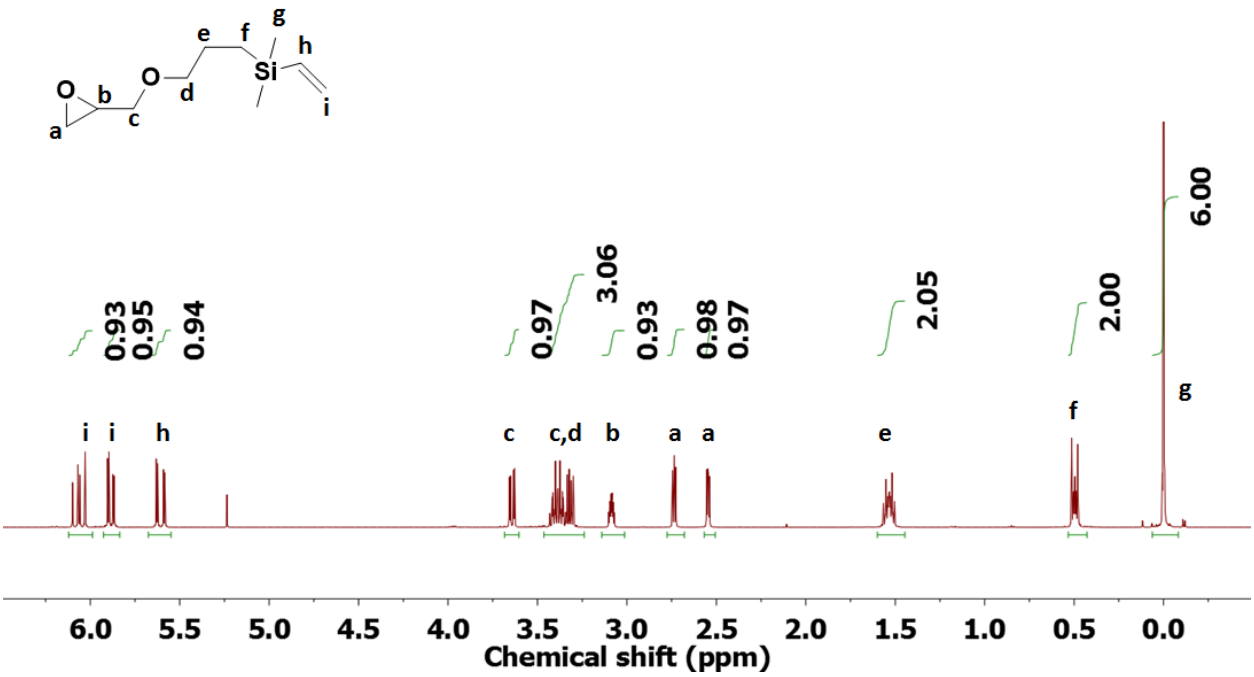

Figure 3.3.1.2. ^{1}H NMR spectrum of vinyldimethylsilylpropyl glycidyl ether monomer.

3.3.2 Synthesis of copolyethers with pendent vinyl ethers

mPEG was utilized as a macroinitiator for anionic ring-opening polymerizations of the epoxide monomers. Melt polymerizations of EVGE (1.5 g of monomer with 5 g of a 5000 g/mole mPEG and 0.6 of the stoichiometric amount of potassium hydride) were compared at 70 ℃, with and without a stoichiometric concentration of 18-crown-6 ether. The

polymerization was complete within 4 hours in the presence of the 18-crown-6 ether, while it required more than three days to complete in the absence of the crown ether. It has been reported that 18-crown-6 ether provides an octahedral cavity for chelating metal ions[44] and reduces association of the alkoxide polymer ends with the counterions.[45] Thus, the increased reaction rate of EVGE is attributed to free alkoxide propagating species.

Copolymerization is an important strategy to synthesize polymeric materials with multifunctional groups with properties that are tunable between those of the respective homopolymers.[39-41,46] EVGE and BO were copolymerized via anionic ring-opening polymerization initiated by mPEG in the presence of the crown ether (Scheme 3.3.2.1). Copolyethers with two types of microstructures of the functional repeating units were prepared. In one case, the EVGE and BO were polymerized sequentially, while in the other, the two monomers were polymerized together.

The microstructures of copolymers prepared with varying ratios of EVGE and BO were monitored throughout the polymerization by isolating polymer samples and characterizing their compositions by ^{1}H NMR (Figure 3.3.2.1). The rate of incorporation of EVGE into the copolymers was faster than that of BO (Figure 3.3.2.2). The rates of polymerization of monosubstituted epoxides are affected by both steric hindrance and electronegativities of the substituents.[47-49] It has been reported that the reactivity of BO is slightly lower than that of propylene oxide, while styrene oxide is much less reactive due to the bulky phenyl substituent on the epoxide ring.[48] Since EVGE and BO both have a linear substituent, steric factors would not be expected to cause significant rate differences. The fact that EVGE is more reactive than BO can be largely attributed to differences in electronegativities. ^{1}H NMR chemical shifts of the methylene and methine groups in the epoxide rings were

investigated to probe the relative electronegativities of the substituents. The chemical shifts of the methine groups were 3.16 ppm in EVGE and 2.87 ppm in BO respectively. The chemical shifts of the methylene groups were 2.60 and 2.79 ppm in EVGE and 2.46 and 2.71 ppm in BO respectively. The higher chemical shifts of the methine and methylene groups in EVGE suggests that the substituent on EVGE was more electronegative than the pendent ethyl on BO.

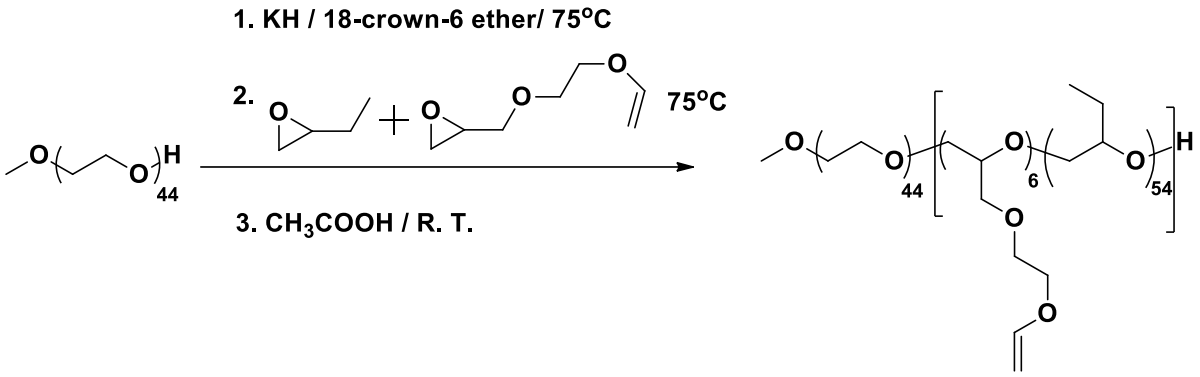

Scheme 3.3.2.1. Synthesis of a tapered 2k mPEG-*b*-P(0.9k EVGE-co-3.9k BO) copolymer.

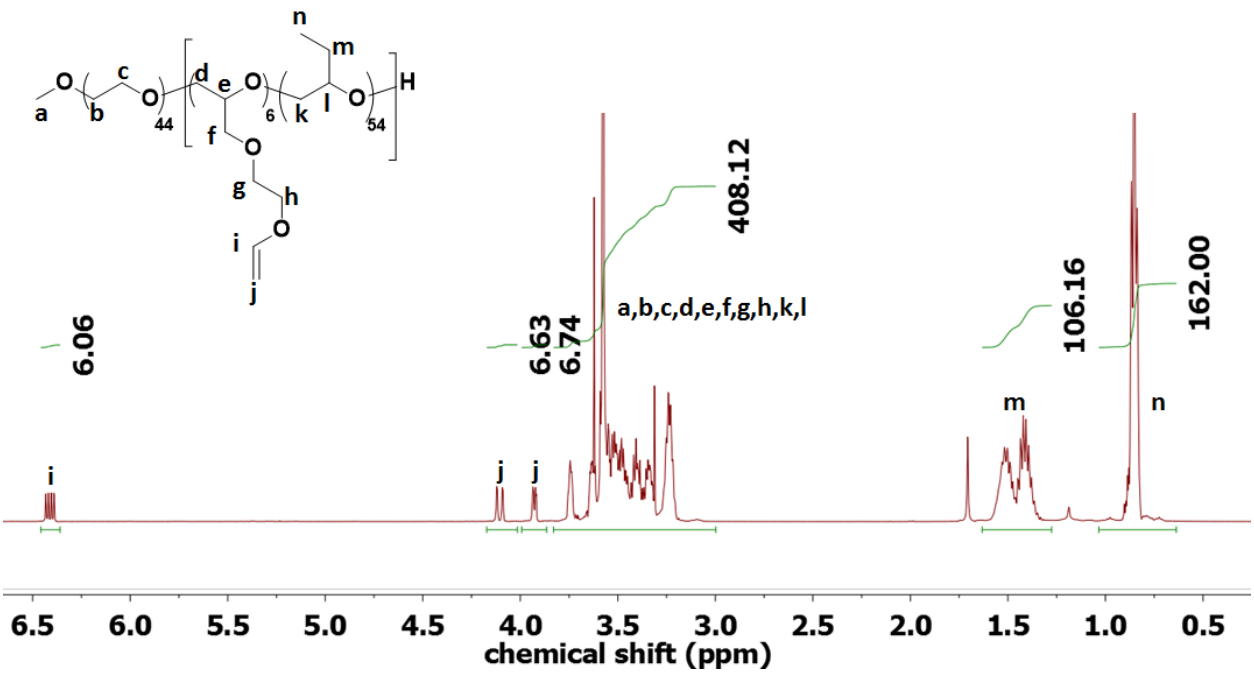

Figure 3.3.2.1. [1]H NMR of a tapered 2k mPEG-*b*-P(0.9k EVGE-co-3.9 BO) copolymer.

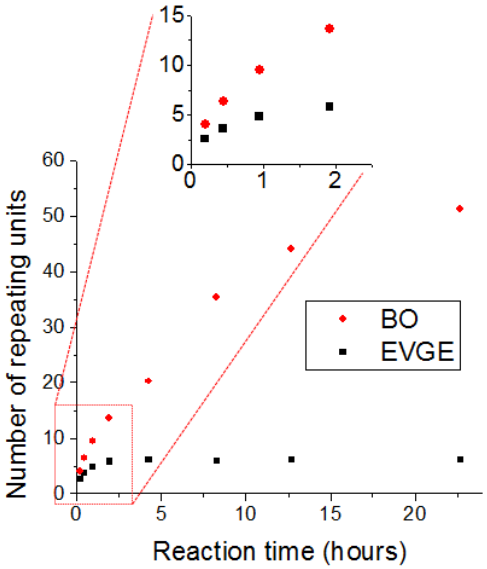

Figure 3.3.2.2. Monomer conversions during copolymerization of EVGE with BO.

The kinetic studies showed that EVGE was consumed early during copolymerization with BO. Thus, this produced an interesting tapered structure in the hydrophobic block, in which the density of the EVGE repeating units was high near the PEO macroinitiator and a long sequence of a BO block formed the terminal section of the chain. The copolymers with all the functional groups at the interface between the hydrophilic PEO blocks and the hydrophobic PBO blocks were prepared via adding EVGE and BO sequentially. The molecular weight distributions obtained from size exclusion chromatography (SEC) measurements were below 1.1 (Figure 3.3.2.3 and Table 3.3.2.1). The difference between total M_n from ^{1}H NMR and SEC increases as the M_n increases.

Table 3.3.2.1. Molecular weights of functional copolyethers.

Block lengths of polymers by ^{1}H NMR (kDa)	M_n by ^{1}H NMR (kDa)	M_n by SEC (kDa)	M_w by SEC (kDa)	PDI
Tapered 2K PEO-P(0.9K EVGE-co-3.9K BO)	6.8	8.3	8.8	1.07
Triblock 5k PEO-0.76k PEVGE-9.4k PBO	15.2	10.8	11.5	1.06
Tapered 5K PEO-P(1.2K EVGE-co-12K BO)	18.2	13.0	13.4	1.03
Tapered 5K PEO-P(0.68K VSiGE-co-4.4K BO)	10.1	8.8	9.3	1.06

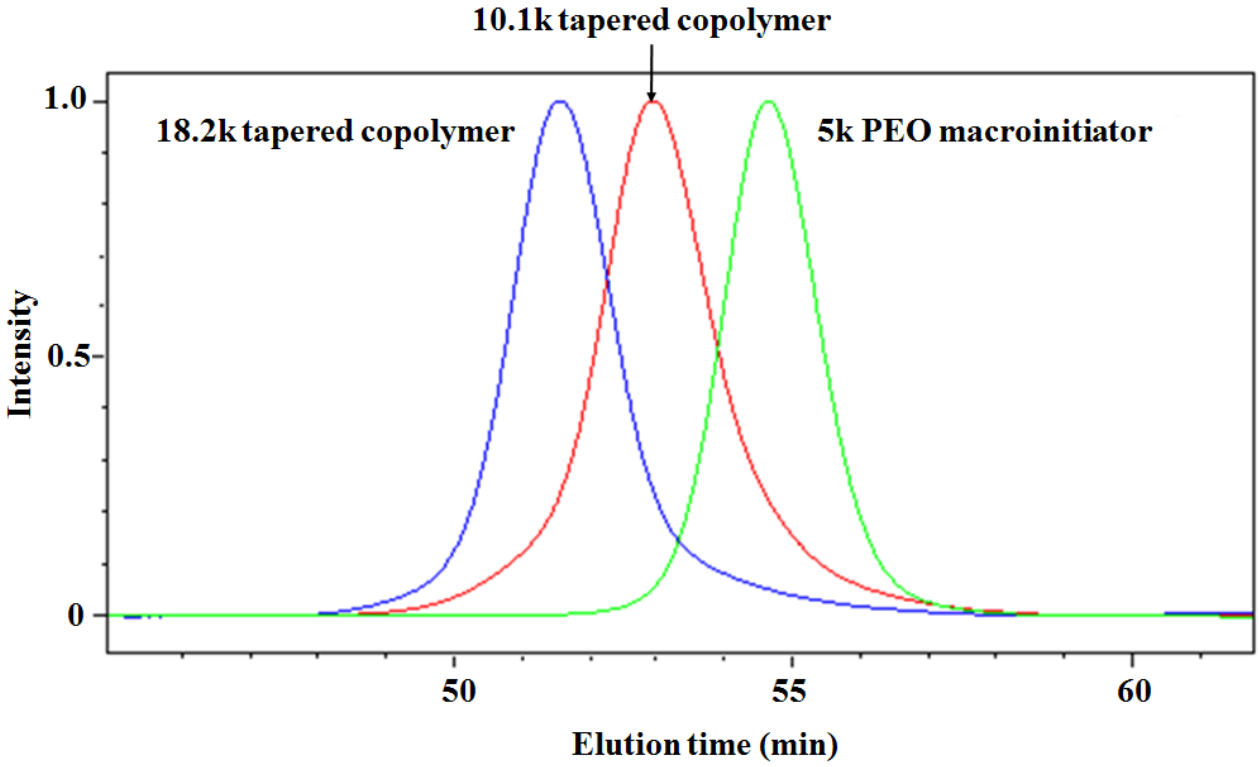

Figure 3.3.2.3. Representative SEC chromatograms of copolyethers.

3.3.3 Functionalization of copolyethers with pendent vinyl ethers

Thiol-ene reactions, which are highly efficient reactions of thiols with reactive carbon-carbon double bonds, were reported in the early 1900s.[29,50,51] These reactions have been intensively investigated and employed for post-polymerization modifications due to their desirable features including high yields, fast reaction rates, mild reaction conditions and insensitivity to oxygen and water.[31,50,52-55] A variety of ene functional groups have been evaluated and ranked according to their relative reactivity and vinyl ethers are one of the most reactive enes.[50,53] In addition, it is noteworthy that vinyl ethers do not undergo radical homopolymerization.[39,50,53,56] This avoids many of the side reactions in thiol-ene reactions that plague such reactions with allyl and acrylate analogues. In the present research,

carboxylic acids were introduced onto the copolymer via a thiol-ene reaction of the vinyl ethers with mercaptoacetic acid (Scheme 3.3.3.1). Conversion of the vinyl groups to two methylene groups was confirmed by appearance of the resonance at 2.77 ppm in the ^{1}H NMR spectrum, which corresponded to the methylene group next the sulfur atom, as well as complete disappearance of the resonances of the vinyl protons at 3.95, 4.12 and 6.42 ppm (Figure 3.3.3.1).

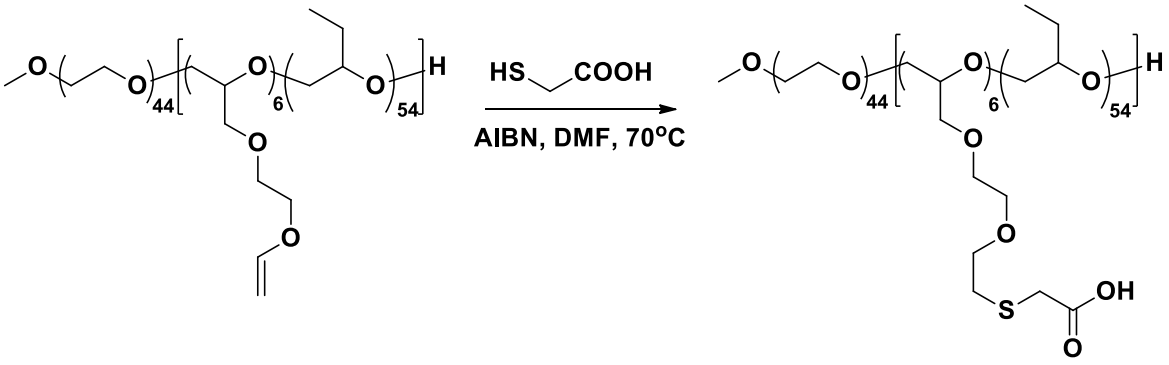

Scheme 3.3.3.1. Thiol-ene addition of mercaptoacetic acid to a tapered 2k mPEG-*b*-P(0.9k EVGE-co-3.9k BO) copolymer.

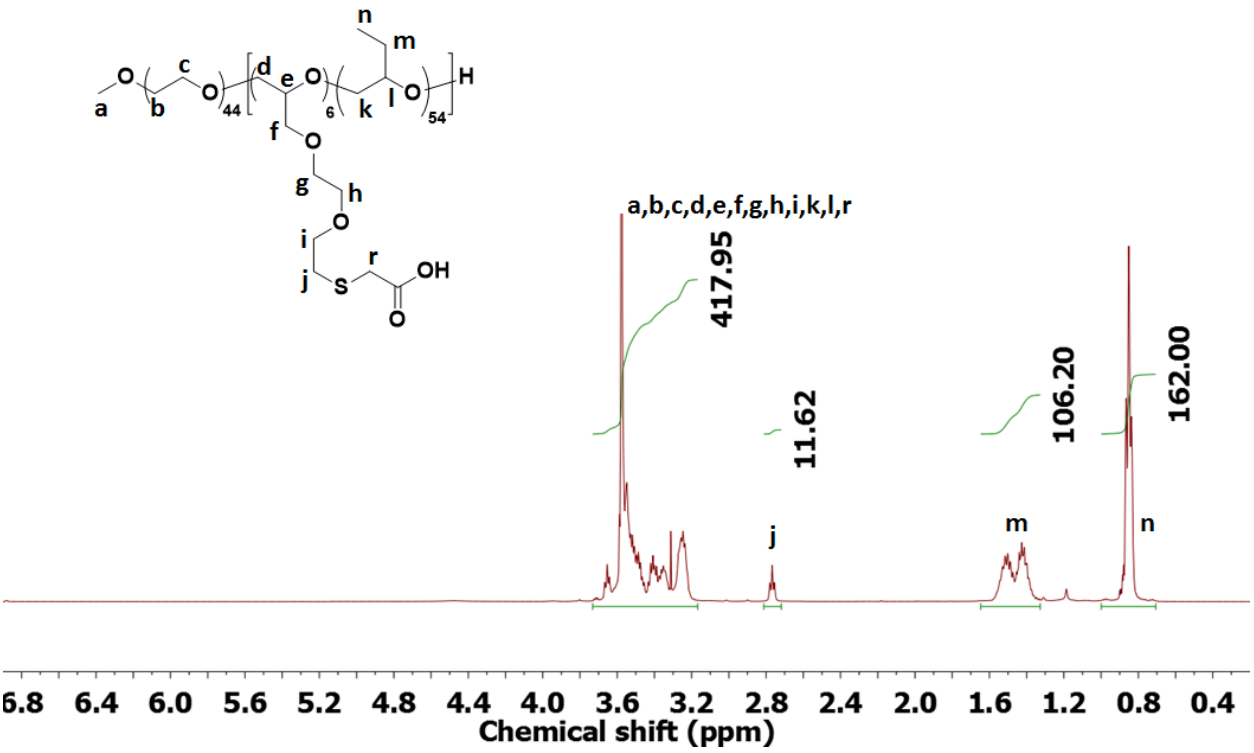

Figure 3.3.3.1. ^{1}H NMR of a carboxylic acid-functional tapered 2k mPEG-*b*-P(0.9k EVGE-co-3.9k BO) copolymer.

boc-Cysteamine was also added onto the pendent vinyl ethers (Scheme 3.3.3.2). Successful addition of *boc*-cysteamine was monitored by observing the disappearance of the vinyl groups and appearance of the methyl peaks at 1.35 ppm in the ^{1}H NMR spectra spectrum (Figure 3.3.3.2). Comparison of the integrations confirmed quantitative functionalization. The *boc* groups were removed in a TFA/dichloromethane 1:1 v:v mixture at room temperature (Scheme 3.3.3.3). Complete removal of the *boc* groups was confirmed by disappearance of the methyl peak at 1.35 ppm in ^{1}H NMR spectrum (Figure 3.3.3.3).

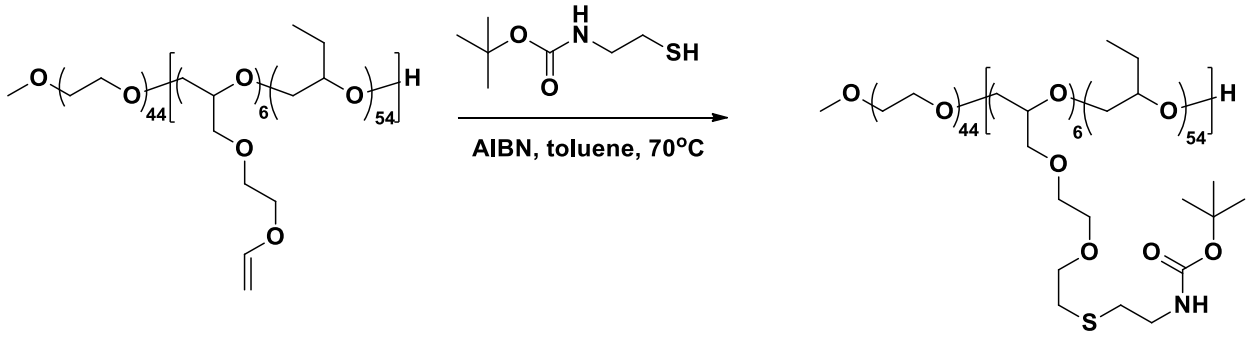

Scheme 3.3.3.2. Thiol-ene addition of *boc*-cysteamine to a tapered 2k mPEG-*b*-P(0.9k EVGE-co-3.9k BO) copolymer.

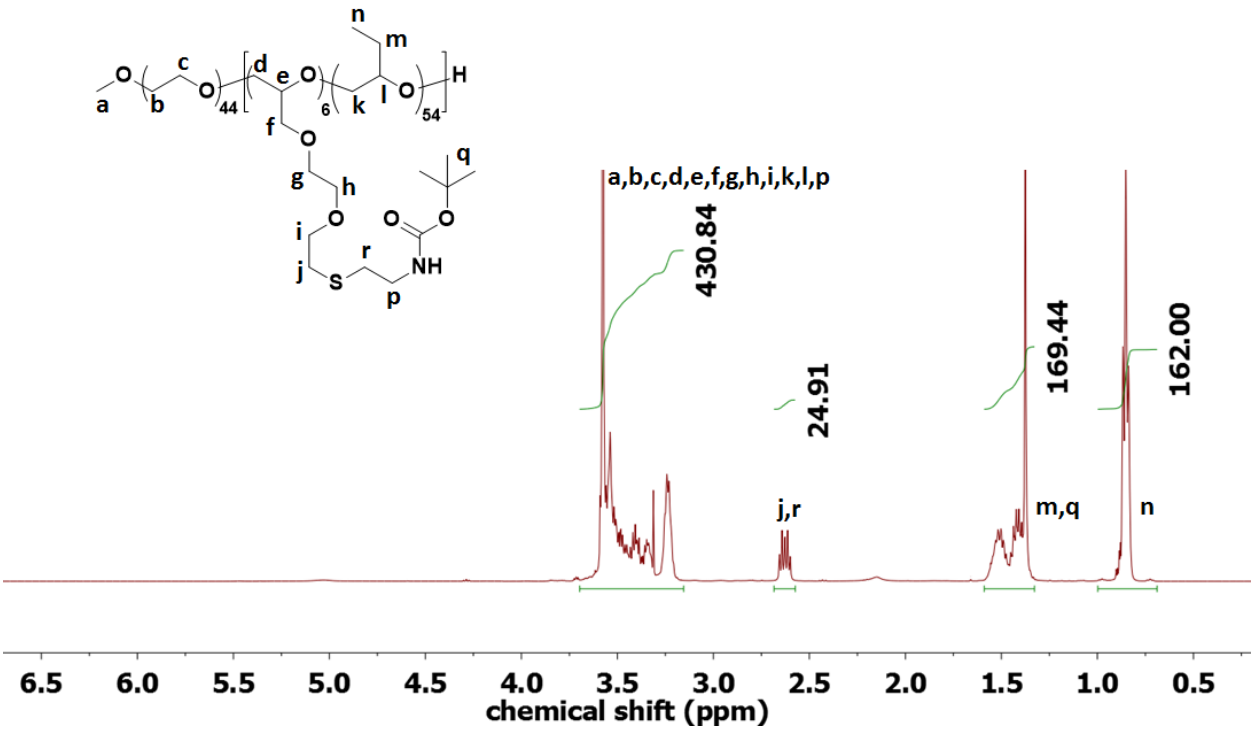

Figure 3.3.3.2. ^{1}H NMR of a *boc*-cysteamine-functional tapered 2k mPEG-*b*-P(0.9k EVGE-co-3.9k BO) copolymer.

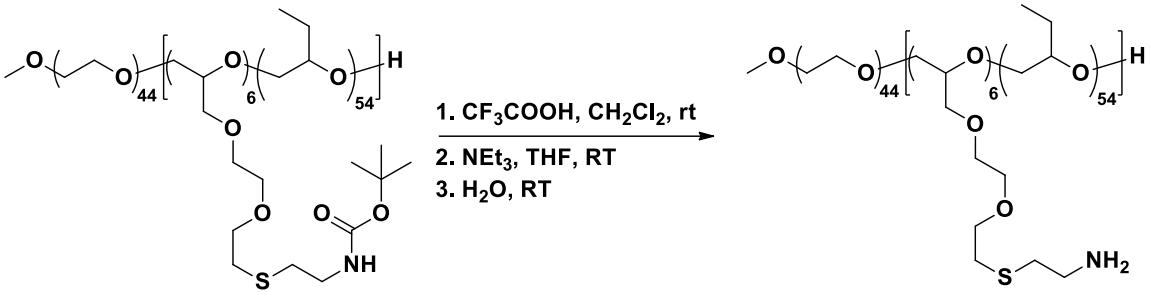

Scheme 3.3.3.3. Removal of *boc* group.

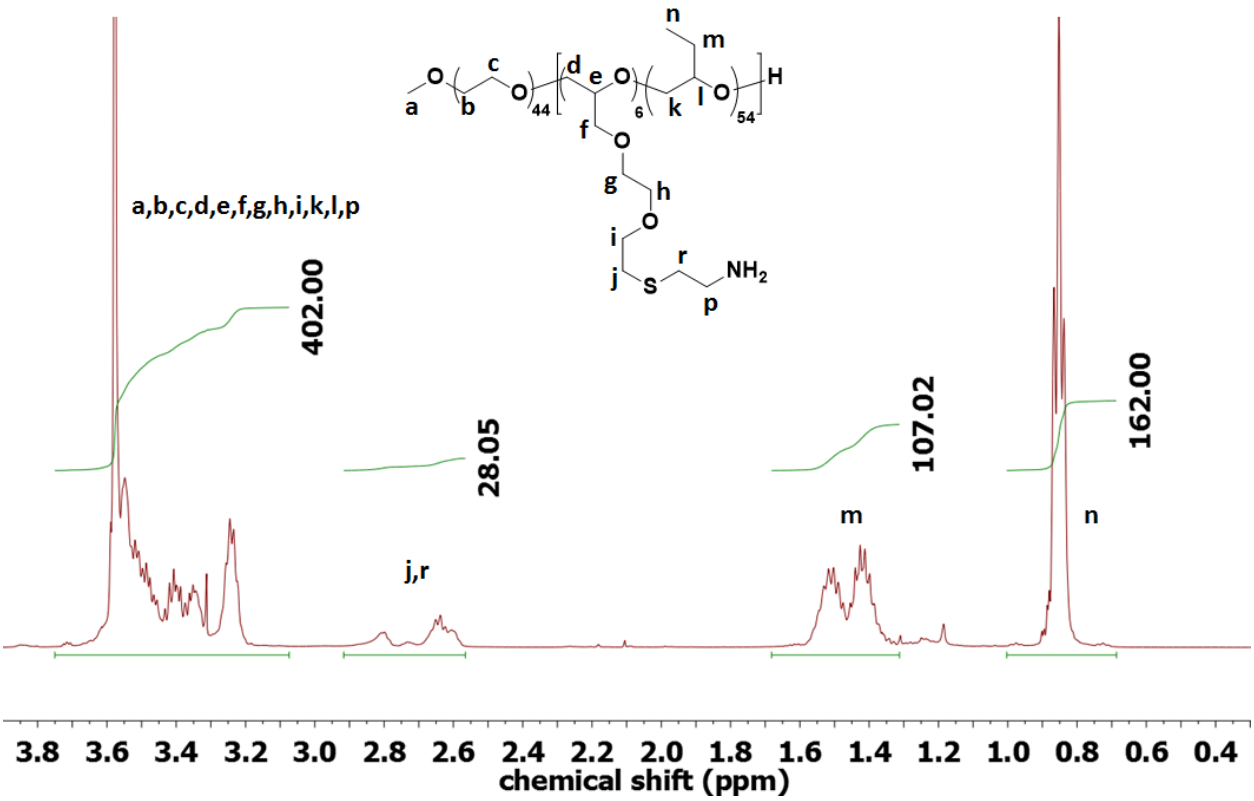

Figure 3.3.3.3. ^{1}H NMR spectrum confirmed successful removal of *boc* group.

The amounts of acids and amines on the copolymers were quantified by titration with HCl in isopropanol. Isopropanol was utilized as a solvent since some of these amphiphilic

copolymers formed micelles in water, and it was reasoned that micellar structures could complicate the titrations. A 1 M KOH solution was added to a solution of the polymer in isopropanol to adjust pH to ~16 to ensure that all of the amines or acids were deprotonated, then the solution was titrated with a HCl/isopropanol solution (Figure 3.3.3.4). Reaction of the excess potassium hydroxide with hydrochloric acid was complete at pH ~12. The inflection points at pH ~3 corresponded to titration of the pendent acids and the inflection points at pH ~4 corresponded to titration of the pendent amines. The volume of the added potassium hydroxide solution between the two inflection points was used to calculate the amount of acids or amines. In all cases, the functionalities measured by titration were in good agreement with the expected values for quantitative functionalization (Table 3.3.3.1).

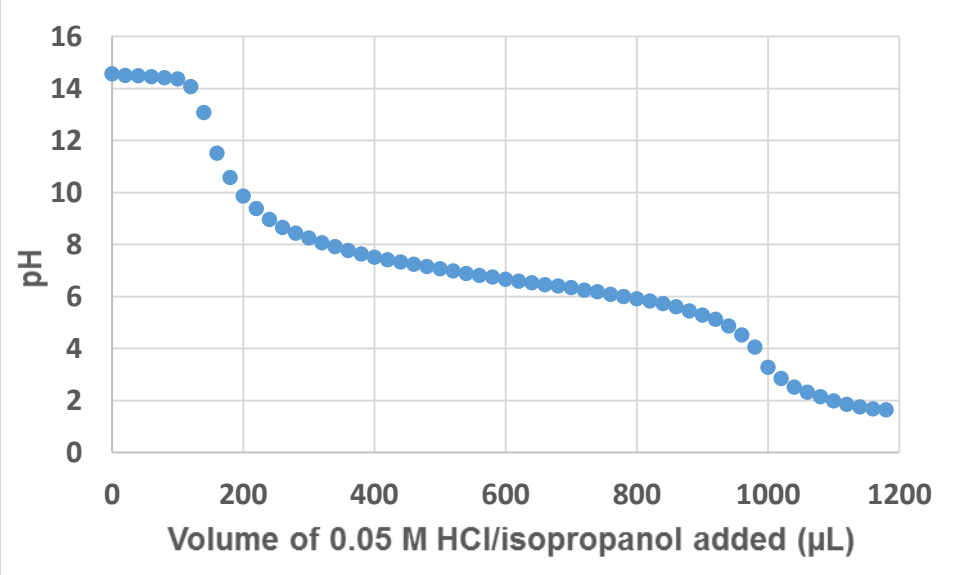

Figure 3.3.3.4. A representative titration curve of carboxylate-functional tapered 2k mPEG-*b*-P(0.9k EVGE-co-3.9k BO).

Table 3.3.3.1. Quantification of functional groups on the copolymers.

Polymers	Vinyl groups per chain	Obtained COOHs per chain	Obtained Amines per chain
Tapered 2K mPEG-P(0.9K EVGE-*co*-3.9K BO)	6.6	6.52 ±0.06	6.31 ±0.10
Triblock 5k mPEG-0.76k PEVGE-9.4k PBO	5.3	5.26 ±0.10	5.14 ±0.09
Tapered 5K mPEG-P(1.2K EVGE-*co*-12K BO)	8.8	8.48 ±0.14	8.45 ±0.33

We also attempted to add cysteamine hydrochloride onto the pendent vinyl ethers in DMF, but this was complicated by acid-catalyzed reaction of the vinyl ether bonds, as suggested by disappearance of the resonances at 3.95, 4.12 and 6.42 ppm in the ^{1}H NMR spectrum. Moreover, no amine was detected by titration. This was attributed to reaction of the pendent vinyl ethers with hydrochloric acid that dissociated from the cysteamine hydrochloride. To eliminate the effect of the hydrochloride, thiol-ene reactions of cysteamine with pendent vinyl ethers were also attempted in toluene and THF, but the reactions were very slow and inefficient. Li et al. reported that electron-withdrawing inductive effects in thiols significantly influenced reactivity of thiol-ene reactions.[63] The chemical shifts of the methylene groups next to the sulfur atom are 3.21 ppm in $HSCH_2COOH$ and 2.57 ppm in $HSCH_2CH_2NH_2$ respectively. Therefore, thiol-ene reaction of cysteamine was much slower than that of mercaptoacetic acid and it was considered impractical to utilize cysteamine to add amines onto the vinyl ethers.

3.3.4 Synthesis and functionalization of copolyethers with pendent vinyl silanes

Since vinyl ether groups are unstable in acid, alternative functional epoxides that permit thiol-ene addition without side reactions in acidic media are highly desirable. VSiGE is a new functional epoxide with a vinylsilane group that is stable in acid media.

Polymerization of VSiGE was carried out using the same procedure as for the polymerization of EVGE (Scheme 3.3.4.1). The PEO-*b*-PVSiGE copolymer was characterized by ^{1}H NMR to determine the chemical composition. The resonances at 3.4-3.8 ppm were assigned to all the methylene and methine groups next to oxygen atoms (Figure 3.3.4.1). The average degree of polymerization of the VSiGE was calculated by comparing the integral ratio of the peak at 0.47 ppm, which corresponded to the methylene group next to the silicon atom, to the peaks at 3.4-3.8 ppm. The tapered mPEG-*b*-P(VSiGE-*co*-BO) copolymer was synthesized via copolymerization of VSiGE and 1,2-BO (Scheme 3.3.4.2 and Figure 3.3.4.2).

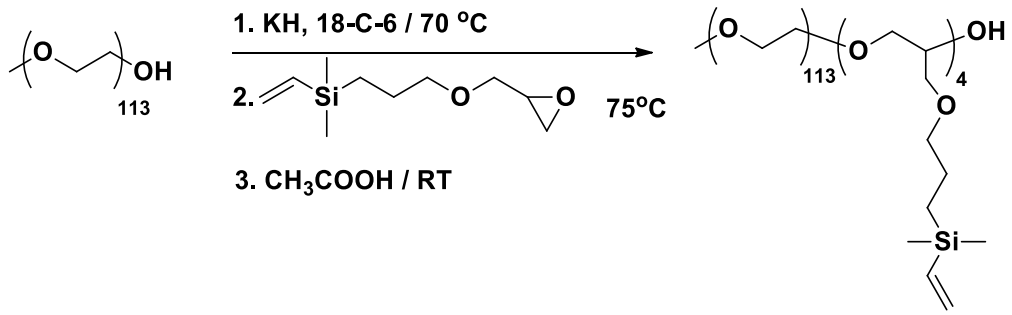

Scheme 3.3.4.1. Synthesis of a diblock 5k mPEG-*b*-0.8k PVSiGE copolymer.

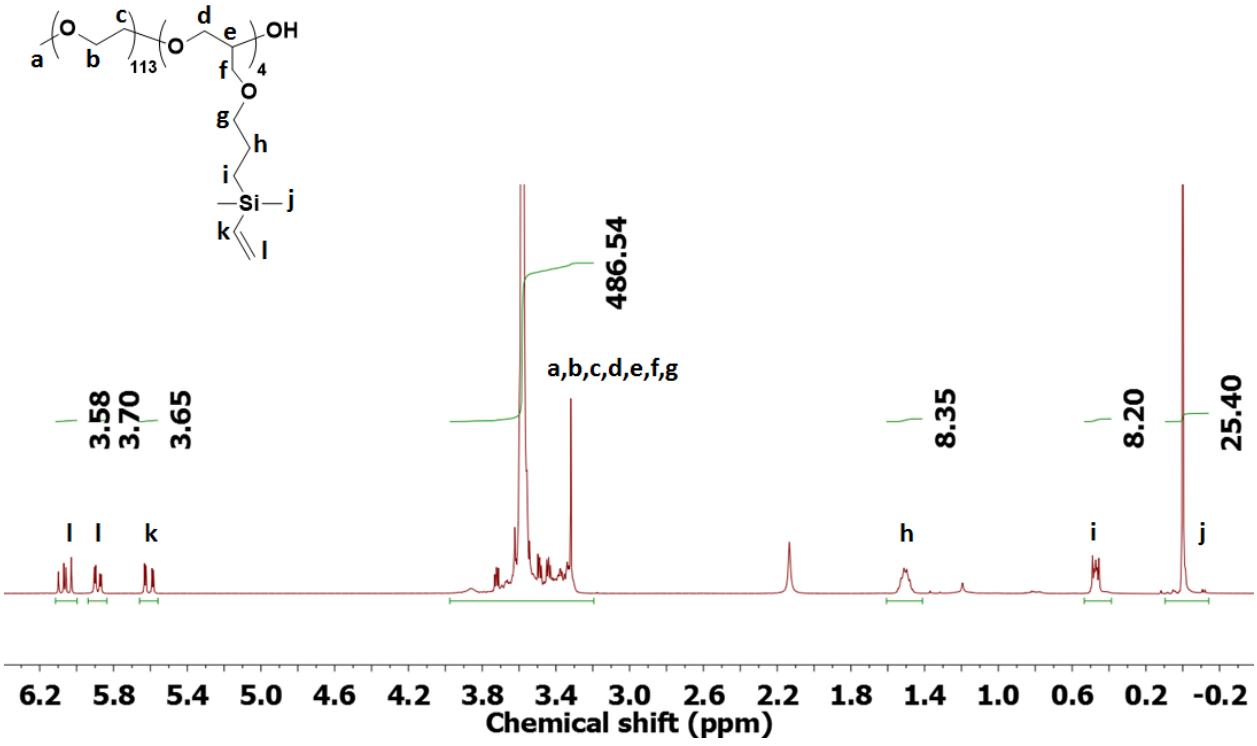

Figure 3.3.4.1. [1]H NMR of a diblock 5k mPEG-*b*-0.8k PVSiGE copolymer.

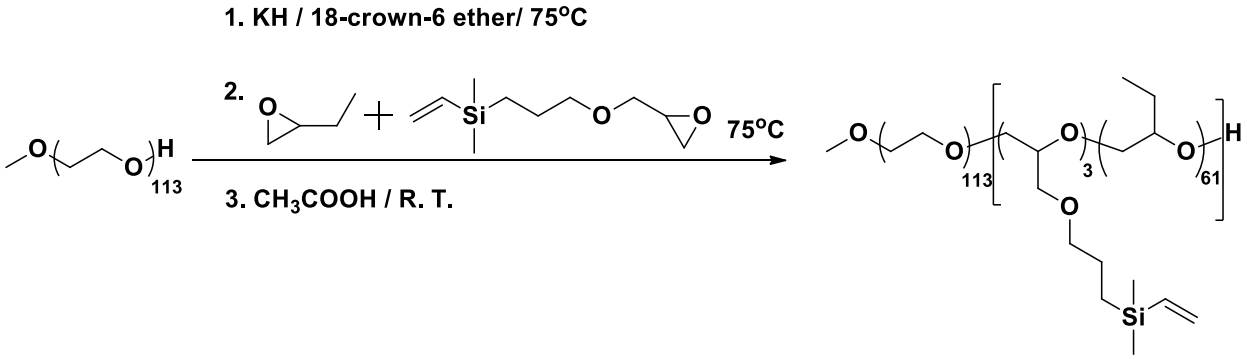

Scheme 3.3.4.2. Synthesis of a tapered 5k mPEG-*b*-P(0.7k EVGE-*co*-4.4k BO) copolymer.

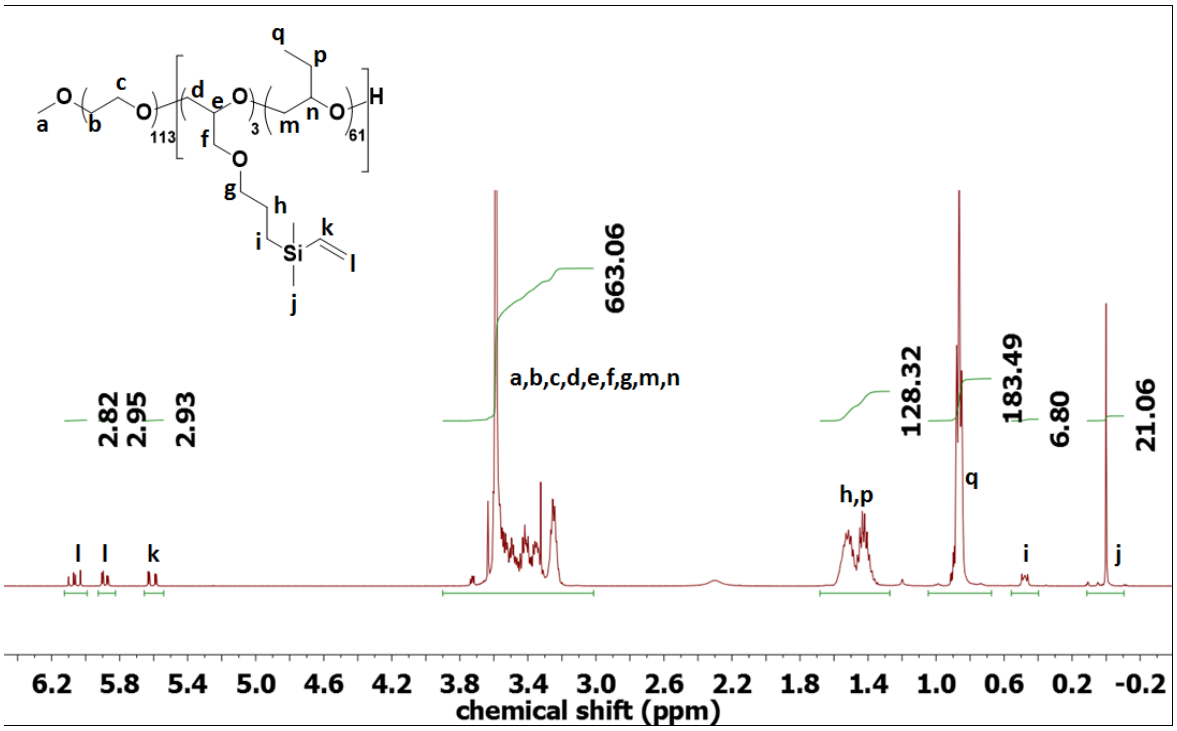

Figure 3.3.4.2. ^{1}H NMR spectrum of a tapered 5k mPEG-*b*-P(0.7k EVGE-*co*-4.4k BO) copolymer.

Amines were successfully introduced to the copolymer via thiol-ene reaction of the pendent vinylsilanes with cysteamine hydrochloride (Scheme 3.3.4.3). A mixed 1:2 v:v toluene:DMF solvent was utilized to solubilize both the relatively hydrophobic block of the copolymer and also the polar cysteamine hydrochloride salt. The reaction was monitored by observing complete disappearance of the vinyl groups and appearance of the methylene groups at 2.5-3.0 ppm in the ^{1}H NMR spectrum (Figure 3.3.4.3). The amount of amines on the copolymer was quantified by titration in isopropanol as described previously. Functionality of amines was found to be 3.1, which was close to the target 3.4.

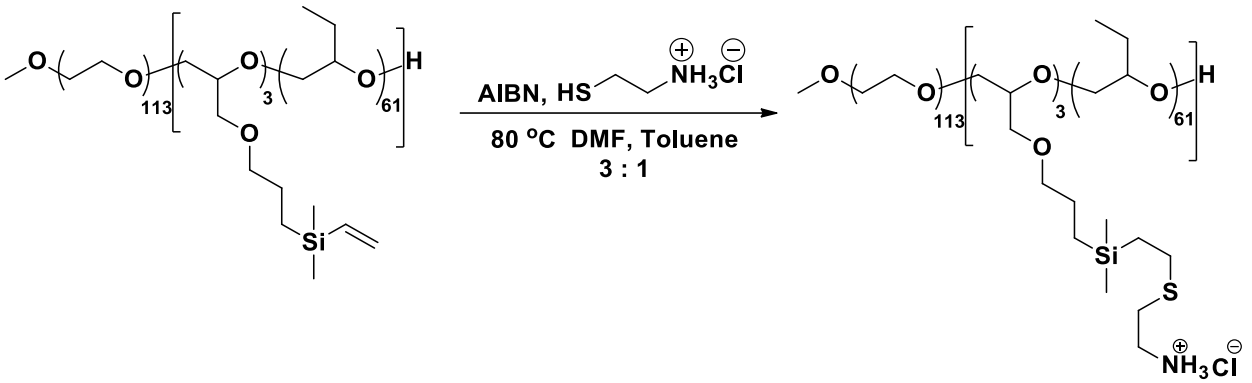

Scheme 3.3.4.3. Thiol-ene addition of cysteamine hydrochloride to a tapered 5k mPEG-*b*-P(0.7k EVGE-*co*-4.4k BO) copolymer.

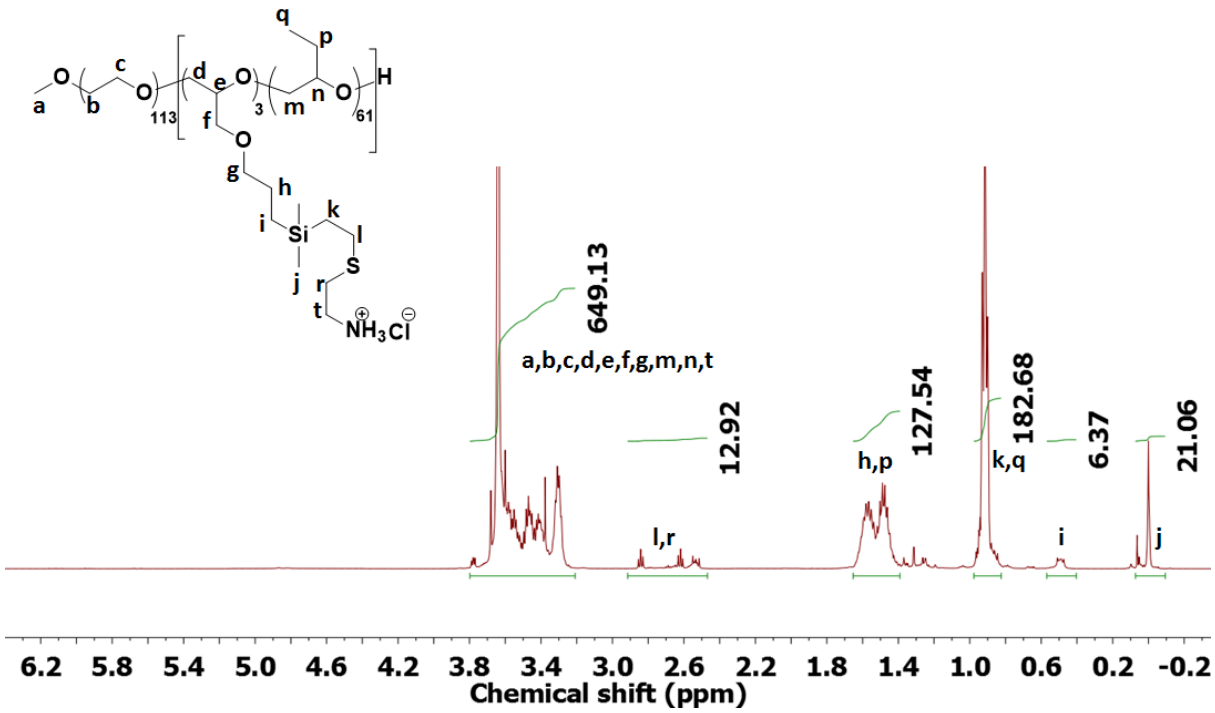

Figure 3.3.4.3. ^{1}H NMR spectrum of an amino-functional tapered 5k mPEG-*b*-P(0.7k EVGE-*co*-4.4k BO) copolymer.

3.3.5. Solution properties of functional copolyethers

The functional amphiphilic copolymers have great potential for loading drugs or metal oxide nanoparticles and forming colloidally stable complexes in aqueous media. The

pendent amines and acids make the micelles pH-sensitive and this was investigated by measurements of critical micellar concentrations (CMCs). The copolymers with pendent carboxylic acids or amines were dispersed in 0.01 M HCl solution or 0.01 M KOH solution with a series of concentrations. The CMC of each polymer was determined by measuring the intensity of scattered light by DLS (in kilocounts per second) as a function of polymer concentration. At concentrations below the CMC, the intensities were very low. When the CMC was reached, there was a sudden change in intensity due to the onset of the larger micelles (Table 3.3.5.1). The polymers with pendent acids had higher CMCs in KOH than in HCl solutions. This was attributed to the fact that the carboxylic acids were negatively charged in the KOH solutions and the hydrophobicity of the polymers was reduced. The CMCs of the amino-functional copolymers were higher in the HCl solutions since the amines were positively charged. In addition, the copolymer with a longer PBO block was less affected by pH than the one with a shorter PBO block. All CMCs of the functional copolyethers presented in this research were in the range of 0.005-0.5 mg/mL, which were greatly lower than the CMCs of some typical Pluronic triblock copolyethers[62] (in the range of 3-45 mg/mL, Table 3.3.5.2). The low CMCs promoted high colloidal stabilities of the polymeric micelles, which were of great interests as drug carriers.

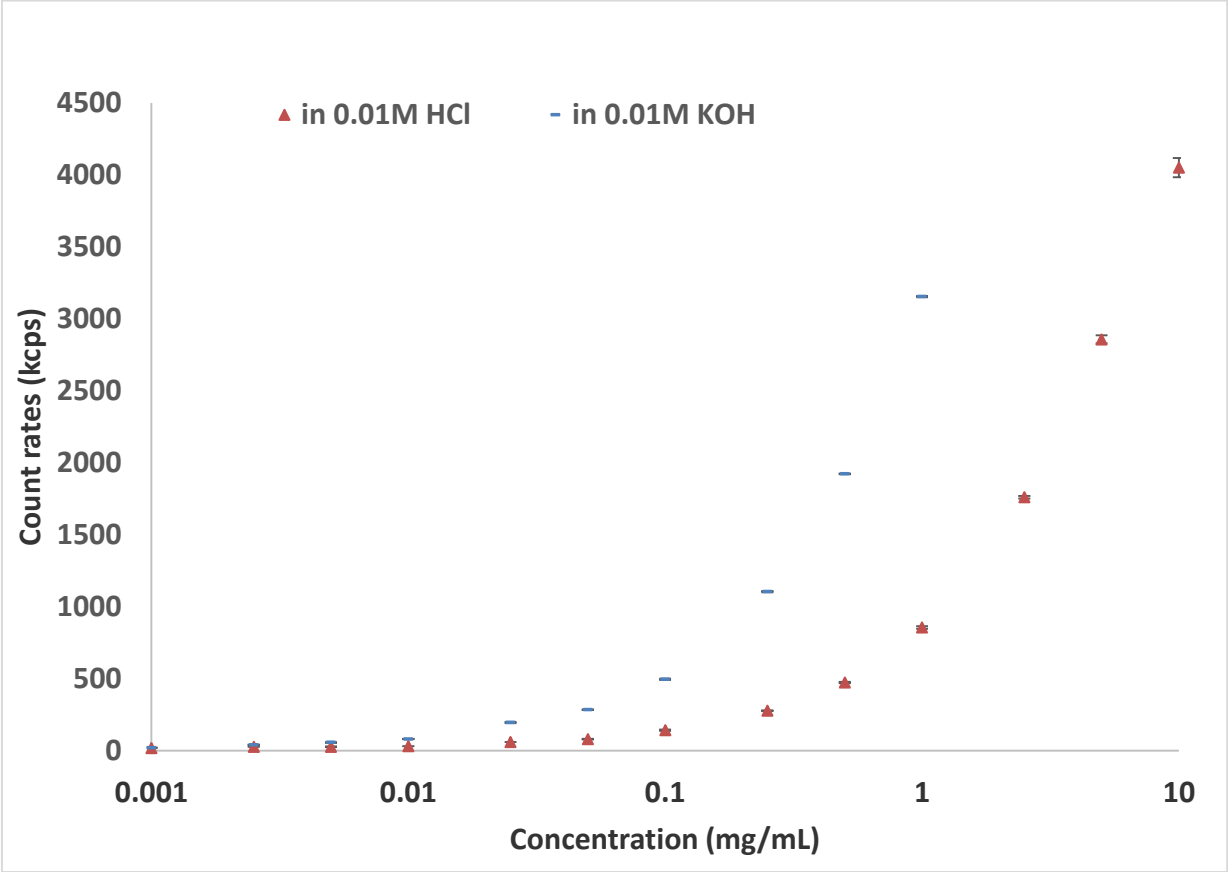

Figure 3.3.5.1. Count rates from DLS of an amino-functional tapered 2K mPEG-P(0.9K EVGE-*co*-3.9K BO) copolymer.

Table 3.3.5.1. CMC's of pH-sensitive functional copolyethers in HCl or KOH solutions at 25 °C.

Functional polymers	CMC in 0.01 M HCl (pH=2) (mg/mL)	CMC in 0.01 M KOH (pH=12) (mg/mL)
Vinyl-functional-tapered 2K mPEG-P(0.9K EVGE-*co*-3.9K BO)	0.025	0.025
Amino-functional-tapered 2K mPEG-P(0.9K EVGE-*co*-3.9K BO)	0.25	0.025
Carboxylate-functional-tapered 2K mPEG-P(0.9K EVGE-*co*-3.9K BO)	0.025	0.5
Vinyl-functional-tapered 5K mPEG-P(1.2K EVGE-*co*-12K BO)	0.005	0.005
Carboxylate-functional-tapered 5K mPEG-P(1.2K EVGE-*co*-12K BO)	0.005	0.025
Amino-functional-tapered 5K mPEG-P(1.2K EVGE-*co*-12K BO)	0.01	0.005

Table 3.3.5.2. CMC's of Pluronic® triblock copolyethers in water at 25 °C.[62]

Polymer	Structure	Total M.W.	CMC(mg/mL)
P84	EO_{19}-PO_{43}-EO_{19}	4,200	26
P85	EO_{26}-PO_{40}-EO_{26}	5,900	40
P104	EO_{27}-PO_{61}-EO_{27}	6,500	3
P105	EO_{37}-PO_{56}-EO_{37}	14,600	3
F108	EO_{132}-PO_{50}-EO_{132}	5,750	45
F127	EO_{100}-PO_{65}-EO_{100}	12,600	7

It was also found that the micelle diameters of structures formed by the uncharged polymers were significantly higher than the values of the charged ones (Table 3.3.5.3). The small sizes of the charged polymers were expected based on the molecular weights and

were consistent with a spherical micelle shape. This large apparent diameters of uncharged micelles led us to hypothesize that the structures have a cylindrical shape. Micelle shape depends on a property known as the packing parameter (v), which is a ratio of the tail area to the head area, $= \frac{area\ of\ tail}{area\ of\ head}$. The hydrophobic cores of the uncharged polymers, which formed the tail in the micelles, included the middle block of BO-EVGE and the end BO block. By contrast, the hydrophobic cores of the charged polymers (when the ionic groups are fully ionized) were smaller. The bulkiness of the tails increased the magnitude of the packing parameter, and thus changed the micellar shapes.

Table 3.3.5.3. Micellar diameters (intensity-average) measured in aqueous dispersions at 25°C.

Polymer	D_I in 0.01 M HCl (nm)	D_I in 0.01 M KOH (nm)
Vinyl-functional-tapered 2K mPEG-P(0.9K EVGE-*co*-3.9K BO)	125	133
Amino-functional-tapered 2K mPEG-P(0.9K EVGE-*co*-3.9K BO)	21	122
Carboxylate-functional-tapered 2K mPEG-P(0.9K EVGE-*co*-3.9K BO)	114	19

3.3.6 Preparation of block copolymer micelles containing ritonavir

There is a need for well-defined antiretroviral drug nanoparticles with good control over particle sizes and compositions, and relatively narrow size polydispersities. Prud'homme and co-workers have reported extensively on a scalable rapid precipitation technique using a multi-inlet vortex mixer to produce stable block copolymer nanoparticles containing drugs, imaging agents, peptides and targeting ligands.[43,57-60] In this method, an organic stream containing the drugs and a block copolymer dispersion stabilizer is rapidly combined with a miscible non-solvent (water) under highly supersaturated conditions. This

can yield nanoparticles in a continuous process that can kinetically trap the drugs and that have controlled compositions and sizes.

Well-defined nanoparticles comprised of ritonavir stabilized by an amphiphilic block copolymer comprised of poly(ethylene oxide)-b-poly(butylene oxide) were synthesized by this method. Ritonavir (RTV) (Figure 3.3.6.1), a protease inhibitor with extremely low aqueous solubility (1.3 μg mL^{-1} at pH 6.8 and 37 ℃),[61] was chosen as a model antiretroviral drug.

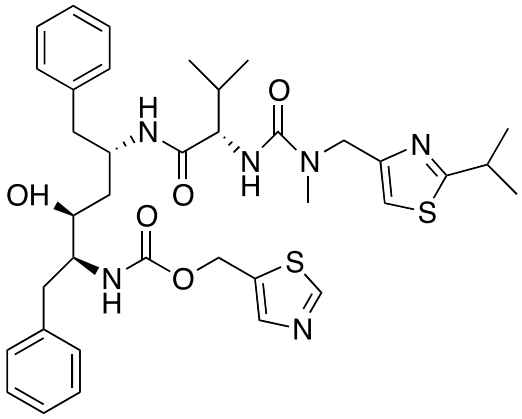

Figure 3.3.6.1. Molecular structure of ritonavir.

Nanoparticles with targeted ritonavir loadings of 10, 20, and 30 wt % were formulated by varying the initial drug concentrations in a THF solution containing the 2k PBO homopolymer (nucleating agent) and the diblock mPEG(5k)-*b*-PBO(9k) copolymer. The critical micellar concentrations (*cmc*) of the copolymers in a 1:10 (v/v) THF-water mixture were determined by measuring the scattering intensities of a range of copolymer concentrations (0.001 – 10 mg mL^{-1}) by dynamic light scattering at 25 ℃. The inflection point on a graph of the mean count rate (kilocounts per second) as a function of copolymer concentration was taken as the *cmc*. The copolymer concentration (10X higher than the *cmc* in a 1:10 (v/v) THF-water mixture) and the homopolymer:copolymer ratio (1:3, wt/wt)

were kept constant at each drug loading. Table 3.3.6.1 and Figure 3.3.6.2 show the intensity-weighted diameters, polydispersity indices, and the experimentally determined drug loadings for the nanoparticles stabilized with the polyether copolymers. The DLS data presented were measured on nanoparticle dispersions in a 1:10 (v/v) THF-water mixture immediately after formation by rapid precipitation. The error bars for sizes represent the standard deviation from five measurements. Monomodal size distributions with relatively low polydispersities (< 0.2) were obtained with all ritonavir loadings. Figure 3.3.6.2 shows drug loadings of the copolymer nanoparticles containing the ritonavir that were determined by HPLC. Near constant encapsulation efficiencies in the range of 75-80 % were achieved irrespective of the targeted drug loading.

Table 3.3.6.1 Hydrodynamic diameters and polydispersities of ritonavir nanoparticles stabilized with 5k PEO-*b*-9k PBO and 2k homoPBO in a 1:10 (v/v) THF-water mixture.

Targeted RTV loadings (wt %)	D_I (nm)	PDI
10	88 ± 4	0.15
20	86 ± 3	0.18
30	88 ± 6	0.19

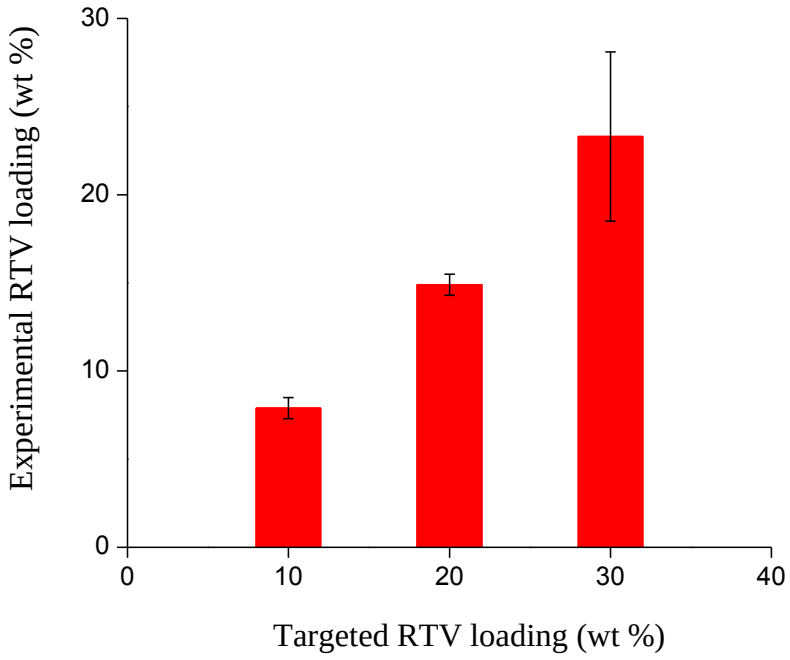

Figure 3.3.6.2 Drug loading of ritonavir nanoparticles stabilized with 5k PEO-b-9k PBO and 2k homoPBO at various targeted RTV loadings in the range of 10-30 wt %. Error bars represent standard deviations from three measurements.

Nanoparticles containing targeted ritonavir loadings of 0, 5, 10 and 20 wt % were formulated with the triblock 5k PEO-*b*-0.76k PEVGE-*b*-9.4k PBO copolymer utilizing the same procedure as mentioned above without a 2k homoPBO. Table 3.3.6.2 shows the intensity-weighted diameters and polydispersity indices for the nanoparticles stabilized with the polyether copolymers. Monomodal size distributions with relatively low polydispersities (< 0.2) were obtained with all ritonavir loadings. The experimentally determined drug loading was 7.3±1.2 wt% for the nanoparticles with 10 wt% targeted loading.

Table 3.3.6.2 Hydrodynamic diameters and polydispersities of ritonavir nanoparticles stabilized with 5k PEO-*b*-0.76k PEVGE-*b*-9.4k PBO.

Targeted RTV loadings (wt %)	D_I (nm)	PDI
0	94 ± 5	0.07
5	92 ± 6	0.09
10	95 ± 3	0.12
20	80 ± 6	0.14

3.4 Conclusions

Two heterobifunctional epoxides, one containing a vinyl ether group (EVGE) and the other with a vinylsilane (VSiGE), were prepared and utilized to synthesize amphiphilic multi-functional polyethers with PEO and PBO. Kinetic studies of the copolymerizations of functional epoxides with BO revealed an interesting tapered microstructure in the hydrophobic block, in which the density of the EVGE repeating units was high near the PEO macroinitiator and a long sequence of a BO block formed the terminal section of the chain.

Pendent amines and carboxylic acids were introduced onto the copolymers via thiol-ene reactions. The critical micelle concentrations of these functional amphiphilic copolyethers were pH-sensitive. These materials also form crosslinkable micelles in aqueous media that are of interest for drug delivery vehicles and bio-imaging agents. We prepared well-controlled nanoparticles containing ritonavir and the functional amphiphilic copolyethers with relatively low polydispersities (<0.2) utilizing a continuous rapid precipitation method. The drug loading efficiencies were in the range of 75-80%.

3.5 Acknowledgement

The authors gratefully acknowledge the financial support of the National Science Foundation for this research under contracts DMR-1263248 (REU) and DMR-1106182.

3.6 References

(1) Kataoka, K.; Harada, A.; Nagasaki, Y., Block copolymer micelles for drug delivery: design, characterization and biological significance *Adv. Drug Delivery Rev.* **2001**, *47*, 113.
(2) Kataoka, K.; Harada, A.; Nagasaki, Y., Block copolymer micelles for drug delivery: Design, characterization and biological significance *Adv. Drug Delivery Rev.* **2012**, *64*, 37.
(3) Lukyanov, A. N.; Torchilin, V. P., Micelles from lipid derivatives of water-soluble polymers as delivery systems for poorly soluble drugs *Adv. Drug Delivery Rev.* **2004**, *56*, 1273.
(4) Torchilin, V. P., Structure and design of polymeric surfactant-based drug delivery systems *J. Controlled Release* **2001**, *73*, 137.
(5) Adams, M. L.; Lavasanifar, A.; Kwon, G. S., Amphiphilic block copolymers for drug delivery *J. Pharm. Sci.* **2003**, *92*, 1343.
(6) Moghimi, S. M.; Hunter, A. C.; Murray, J. C., Long-circulating and target-specific nanoparticles: Theory to practice *Pharmacol. Rev.* **2001**, *53*, 283.
(7) Duncan, R., The dawning era of polymer therapeutics *Nat. Rev. Drug Discov.* **2003**, *2*, 347.
(8) Lee, J. H.; Lee, H. B.; Andrade, J. D., Blood Compatibility of Polyethylene Oxide Surfaces *Prog. Polym. Sci.* **1995**, *20*, 1043.
(9) Maeda, H., The enhanced permeability and retention (EPR) effect in tumor vasculature: The key role of tumor-selective macromolecular drug targeting *Adv. Enzyme. Regul.* **2001**, *41*, 189.
(10) Maeda, H., SMANCS and polymer-conjugated macromolecular drugs: advantages in cancer chemotherapy *Adv. Drug Delivery Rev.* **2001**, *46*, 169.
(11) Matsumura, Y.; Maeda, H., A New Concept for Macromolecular Therapeutics in Cancer-Chemotherapy - Mechanism of Tumoritropic Accumulation of Proteins and the Antitumor Agent Smancs *Cancer Res.* **1986**, *46*, 6387.
(12) Larson, N.; Ghandehari, H., Polymeric Conjugates for Drug Delivery *Chem. Mater.* **2012**, *24*, 840.
(13) Nishiyama, N. B., Y.; Miyata, K.; Fukushima, S.; Kataoka, K., *Drug Discovery Today: Technologies* **2005**, *2*, 21.
(14) Torchilin, V., Multifunctional and stimuli-sensitive pharmaceutical nanocarriers *Eur. J. Pharm. Biopharm.* **2009**, *71*, 431.
(15) Bae, Y. H.; Park, K., Targeted drug delivery to tumors: Myths, reality and possibility *J. Controlled Release* **2011**, *153*, 198.

(16) Danhier, F.; Feron, O.; Preat, V., To exploit the tumor microenvironment: Passive and active tumor targeting of nanocarriers for anti-cancer drug delivery *J. Controlled Release* **2010**, *148*, 135.
(17) Bae, Y.; Jang, W. D.; Nishiyama, N.; Fukushima, S.; Kataoka, K., Multifunctional polymeric micelles with folate-mediated cancer cell targeting and pH-triggered drug releasing properties for active intracellular drug delivery *Mol. Biosyst.* **2005**, *1*, 242.
(18) Bae, Y.; Nishiyama, N.; Fukushima, S.; Koyama, H.; Yasuhiro, M.; Kataoka, K., Preparation and biological characterization of polymeric micelle drug carriers with intracellular pH-triggered drug release property: Tumor permeability, controlled subcellular drug distribution, and enhanced in vivo antitumor efficacy *Bioconjugate Chem.* **2005**, *16*, 122.
(19) Zhang, F.; Kang, E. T.; Neoh, K. G.; Huang, W., Modification of gold surface by grafting of poly(ethylene glycol) for reduction in protein adsorption and platelet adhesion *J. Biomat. Sci.-Polym. E* **2001**, *12*, 515.
(20) Balamurugan, S.; Ista, L. K.; Yan, J.; Lopez, G. P.; Fick, J.; Himmelhaus, M.; Grunze, M., Reversible protein adsorption and bioadhesion on monolayers terminated with mixtures of oligo(ethylene glycol) and methyl groups *J. Am. Chem. Soc.* **2005**, *127*, 14548.
(21) Gref, R.; Luck, M.; Quellec, P.; Marchand, M.; Dellacherie, E.; Harnisch, S.; Blunk, T.; Muller, R. H., 'Stealth' corona-core nanoparticles surface modified by polyethylene glycol (PEG): influences of the corona (PEG chain length and surface density) and of the core composition on phagocytic uptake and plasma protein adsorption *Colloid Surface B* **2000**, *18*, 301.
(22) Chen, Y. J.; Kang, E. T.; Neoh, K. G.; Wang, P.; Tan, K. L., Surface modification of polyaniline film by grafting of poly(ethylene glycol) for reduction in protein adsorption and platelet adhesion *Synthetic Met.* **2000**, *110*, 47.
(23) Wang, P.; Tan, K. L.; Kang, E. T., Surface modification of poly(tetrafluoroethylene) films via grafting of poly(ethylene glycol) for reduction in protein adsorption *J. Biomat. Sci.-Polym. E* **2000**, *11*, 169.
(24) Trubetskoy, V. S.; Torchilin, V. P., Use of Polyoxyethylene-Lipid Conjugates as Long-Circulating Carriers for Delivery of Therapeutic and Diagnostic Agents *Adv. Drug Delivery Rev.* **1995**, *16*, 311.
(25) Bailey, F. E. K., J. Y., Eds. *Poly(ethylene oxide)*; Academic Press: New York, 1976.
(26) Working, P. K. N., M. S.; Johnson, J.; Cornacoff, J. B., Eds.; *Safety of poly(ethylene glycol) and poly(ethylene glycol) derivatives*; American Chemical Society: Washington DC, 1997.
(27) Tian, Y.; Bromberg, L.; Lin, S. N.; Hatton, T. A.; Tam, K. C., Complexation and release of doxorubicin from its complexes with pluronic P85-b-poly(acrylic acid) block copolymers *J. Controlled Release* **2007**, *121*, 137.
(28) Bae, K. H.; Lee, Y.; Park, T. G., Oil-encapsulating PEO-PPO-PEO/PEG shell cross-linked nanocapsules for target-specific delivery of paclitaxel *Biomacromolecules* **2007**, *8*, 650.

(29) Vadala, M. L.; Thompson, M. S.; Ashworth, M. A.; Lin, Y.; Vadala, T. P.; Ragheb, R.; Riffle, J. S., Heterobifunctional poly(ethylene oxide) oligomers containing carboxylic acids *Biomacromolecules* **2008**, *9*, 1035.
(30) Thompson, M. S.; Vadala, T. P.; Vadala, M. L.; Lin, Y.; Riffle, J. S., Synthesis and applications of heterobifunctional poly(ethylene oxide) oligomers *Polymer* **2008**, *49*, 345.
(31) Goff, J. D.; Huffstetler, P. P.; Miles, W. C.; Pothayee, N.; Reinholz, C. M.; Ball, S.; Davis, R. M.; Riffle, J. S., Novel Phosphonate-Functional Poly(ethylene oxide)-Magnetite Nanoparticles Form Stable Colloidal Dispersions in Phosphate-Buffered Saline *Chem. Mater.* **2009**, *21*, 4784.
(32) Carroll, M. R. J.; Huffstetler, P. P.; Miles, W. C.; Goff, J. D.; Davis, R. M.; Riffle, J. S.; House, M. J.; Woodward, R. C.; St Pierre, T. G., The effect of polymer coatings on proton transverse relaxivities of aqueous suspensions of magnetic nanoparticles *Nanotechnology* **2011**, *22*.
(33) Miles, W. C.; Goff, J. D.; Huffstetler, P. P.; Reinholz, C. M.; Pothayee, N.; Caba, B. L.; Boyd, J. S.; Davis, R. A.; Riffle, J. S., Synthesis and Colloidal Properties of Polyether-Magnetite Complexes in Water and Phosphate-Buffered Saline *Langmuir* **2009**, *25*, 803.
(34) Miles, W. C.; Huffstetler, P. P.; Goff, J. D.; Chen, A. Y.; Riffle, J. S.; Davis, R. M., Design of Stable Polyether-Magnetite Complexes in Aqueous Media: Effects of the Anchor Group, Molecular Weight, and Chain Density *Langmuir* **2011**, *27*, 5456.
(35) Pothayee, N.; Balasubramaniam, S.; Pothayee, N.; Jain, N.; Hu, N.; Lin, Y. N. A.; Davis, R. M.; Sriranganathan, N.; Koretsky, A. P.; Riffle, J. S., Magnetic nanoclusters with hydrophilic spacing for dual drug delivery and sensitive magnetic resonance imaging *J. Mater. Chem. B* **2013**, *1*, 1142.
(36) Tong, J. Y., X.; Kabanov, A. V.; Liang, J. and Riffle, J. S., Novel Superoxide Dismutase-Triblock Copolyether Conjugates for Enhanced Cellular Delivery *Polymer Preprints* **2011**, *52*, 301.
(37) Mangold, C.; Wurm, F.; Frey, H., Functional PEG-based polymers with reactive groups via anionic ROP of tailor-made epoxides *Polym. Chem.-Uk* **2012**, *3*, 1714.
(38) Mangold, C.; Obermeier, B.; Wurm, F.; Frey, H., From an Epoxide Monomer Toolkit to Functional PEG Copolymers With Adjustable LCST Behavior *Macromol. Rapid. Comm.* **2011**, *32*, 1930.
(39) Mangold, C.; Dingels, C.; Obermeier, B.; Frey, H.; Wurm, F., PEG-based Multifunctional Polyethers with Highly Reactive Vinyl-Ether Side Chains for Click-Type Functionalization *Macromolecules* **2011**, *44*, 6326.
(40) Obermeier, B.; Frey, H., Poly(ethylene glycol-co-allyl glycidyl ether)s: A PEG-Based Modular Synthetic Platform for Multiple Bioconjugation *Bioconjugate Chem.* **2011**, *22*, 436.
(41) Mangold, C.; Wurm, F.; Obermeier, B.; Frey, H., "Functional Poly(ethylene glycol)": PEG-Based Random Copolymers with 1,2-Diol Side Chains and Terminal Amino Functionality *Macromolecules* **2010**, *43*, 8511.
(42) Wilms, V. S.; Bauer, H.; Tonhauser, C.; Schilmann, A. M.; Muller, M. C.; Tremel, W.; Frey, H., Catechol-Initiated Polyethers: Multifunctional Hydrophilic

Ligands for PEGylation and Functionalization of Metal Oxide Nanoparticles *Biomacromolecules* **2013**, *14*, 193.
(43) Liu, Y.; Cheng, C. Y.; Prud'homme, R. K.; Fox, R. O., Mixing in a multi-inlet vortex mixer (MIVM) for flash nano-precipitation *Chemical Engineering Science* **2008**, *63*, 2829.
(44) Maskornick, M. J., The ability of crown ethers to increase the specific activity of potassium alkoxides in DMSO *Tetrahedron Lett.* **1972**, *13*, 1797.
(45) Stolarzewicz, A.; Grobelny, Z., New Aspects in the Anionic-Polymerization of Phenyl Glycidyl Ether *Makromol. Chem.* **1992**, *193*, 531.
(46) Lee, B. F.; Wolffs, M.; Delaney, K. T.; Sprafke, J. K.; Leibfarth, F. A.; Hawker, C. J.; Lynd, N. A., Reactivity Ratios and Mechanistic Insight for Anionic Ring-Opening Copolymerization of Epoxides *Macromolecules* **2012**, *45*, 3722.
(47) Price, C. C.; Carmelite, D. D., Reactions of Epoxides in Dimethyl Sulfoxide Catalyzed by Potassium t-Butoxide *J. Am. Chem. Soc.* **1966**, *88*, 4039.
(48) Stolarzewicz, A.; Neugebauer, D., Influence of substituent on the polymerization of oxiranes by potassium hydride *Macromol. Chem. Physi.c* **1999**, *200*, 2467.
(49) Brocas, A. L.; Mantzaridis, C.; Tunc, D.; Carlotti, S., Polyether synthesis: From activated or metal-free anionic ring-opening polymerization of epoxides to functionalization *Prog. Polym. Sci.* **2013**, *38*, 845.
(50) Hoyle, C. E.; Bowman, C. N., Thiol-Ene Click Chemistry *Angew. Chem. Int. Edit* **2010**, *49*, 1540.
(51) Posner, T., *Ber. Dtsch. Chem. Ges.* **1905**, *38*, 646.
(52) Lou, F. W.; Xu, J. M.; Liu, B. K.; Wu, Q.; Pan, Q.; Lin, X. F., Highly selective anti-Markovnikov addition of thiols to vinyl ethers under solvent- and catalyst-free conditions *Tetrahedron Lett.* **2007**, *48*, 8815.
(53) Cramer, N. B.; Reddy, S. K.; O'Brien, A. K.; Bowman, C. N., Thiol-ene photopolymerization mechanism and rate limiting step changes for various vinyl functional group chemistries *Macromolecules* **2003**, *36*, 7964.
(54) Kade, M. J.; Burke, D. J.; Hawker, C. J., The Power of Thiol-ene Chemistry *J. Polym. Sci. Pol. Chem.* **2010**, *48*, 743.
(55) Lowe, A. B., Thiol-ene "click" reactions and recent applications in polymer and materials synthesis *Polym. Chem.-Uk* **2010**, *1*, 17.
(56) Mishima, E.; Yamago, S., Controlled Alternating Copolymerization of (Meth)acrylates and Vinyl Ethers by Using Organoheteroatom-Mediated Living Radical Polymerization *Macromol. Rapid. Comm.* **2011**, *32*, 893.
(57) Johnson, B. K.; Prud'homme, R. K., Flash NanoPrecipitation of Organic Actives and Block Copolymers using a Confined Impinging Jets Mixer *Aust. J. Chem.* **2003**, *56*, 1021.
(58) Ungun, B.; Prud'homme, R. K.; Budijono, S. J.; Shan, J.; Lim, S. F.; Ju, Y.; Austin, R., Nanofabricated upconversion nanoparticles for photodynamic therapy *Opt. Express* **2009**, *17*, 80.
(59) Gindy, M. E.; Panagiotopoulos, A. Z.; Prud'homme, R. K., Composite Block Copolymer Stabilized Nanoparticles: Simultaneous Encapsulation of Organic Actives and Inorganic Nanostructures *Langmuir* **2008**, *24*, 83.

(60) D'Addio, S. M.; Prud'homme, R. K., Controlling drug nanoparticle formation by rapid precipitation *Adv. Drug Delivery Rev.* **2011**, *63*, 417.
(61) Ilevbare, G. A.; Liu, H.; Edgar, K. J.; Taylor, L. S., Understanding Polymer Properties Important for Crystal Growth Inhibition—Impact of Chemically Diverse Polymers on Solution Crystal Growth of Ritonavir *Crystal Growth & Design* **2012**, *12*, 3133.
(62) Alexandridis, P.; Holzwarth, J. F.; Hatton, T. A.Micellization of poly(ethylene oxide)-poly(propylene oxide)-poly(ethylene oxide) triblock copolymers in aqueous solutions: thermodynamics of copolymer association *Macromolecules* **1994,** *27*, 2414.
(63) Hong, M.; Liu, S-R.; Li, B-X. and Li, Y-S. Application of Thiol-ene Click Chemistry to Preparation of Functional Polyethylene with High Molecular Weight and High Polar Group Content: Influence of Thiol Structure and Vinyl Type on Reactivity *Polymer chemistry* **2012,** *50*, 2499.

Chapter 4. Poly(ethylene oxide)-*b*-poly(L-glutamic acid) Ionic-nonionic Block Copolymers and their Magnetic Complexes

Most of the work described in this chapter was performed by the author of this dissertation. He was solely responsible for the synthesis and characterization of the monomer, initiators, polymers, iron oxide nanoparticles and complexes. Dr. Sharavanan Balasubramaniam of the Dr. Richey M. Davis' group aided in the thermal analysis, SQuID analysis and transmission electron microscope imaging.

4.1 Introduction

Polypeptides have been widely investigated as biomaterials due to their biodegradable and biocompatible properties.[1-6] They are comprised of naturally occurring amino acids as repeating units, which are linked together by amide bonds rather than nondegradable C-C bonds. The pendent carboxylic acids on the poly(ethylene oxide)-b-poly(L-glutamic acid block copolymers discussed in this work are negatively charged throughout most of the physiological pH range and provide accessibility for guest molecules through electrostatic interactions and/or hydrogen bonds.[7]

Poly(L-glutamic acid) has been found to be nontoxic in C3H/Kam mice at a single dose of up to 800 mg/kg or multiple doses at an accumulated dose of 1.8 g/kg.[7-9] It degrades faster via enzymatic degradation than poly(L-aspartic acid) or poly(D-glutamic acid).[7,10] It has been observed that pH has a strong effect on the enzymatic degradation rate of of poly(L-glutamic acid).[7,11-13] This effect was attributed to a change from an α-helix conformation at pH<5 to a random coil structure at neutral pH.[7,14,15] In order to obtain

better biocompatibility and to disperse the polypeptide well in aqueous media, a nonionic poly(ethylene oxide) (PEO) block can be integrated with poly(L-glutamic acid).

Aminofunctional PEOs have been used as macroinitiators for polymerization of the *N*-carboxyanhydride (NCA) of γ-benzyl-L-glutamate yielding bi-, tri-, and star-block copolymers.[16-22] The benzyl groups can be removed by hydrolysis[23-27] or hydrogenolysis[28]. Poly(L-glutamic acid) and its derivatives have been utilized as polymeric carriers for chemotherapeutic drugs such as paclitaxel[8,9], camptothecin[29-31] and doxorubicin[32-34].

Our group has previously reported that iron oxide nanoparticles can be efficiently complexed with poly(ethylene oxide)-*b*-poly(acrylic acid) (PEO-*b*-PAA) through interactions between the anionic segment of the copolymer and the iron oxide surfaces.[35,36] These self-assembled magnetic block ionomer complexes (MBICs) were found to be potential carriers for gentamicin that has multiple cationic sites. These complexes are interesting due to their potential to be used as dual bio-imaging and therapeutic agents.

Considering that poly(L-glutamic acid) has similar side carboxylic acids as those on PAA, it was rationalized that MBICs could also be synthesized based on PEO-*b*-poly(L-glutamic acid) (PEO-*b*-PG). This is of interest due to the biocompatible and biodegradable nature of the poly(L-glutamic acid) component of the backbone. This chapter describes synthesis and characterization of well-defined PEO-*b*-PG copolymers and introduces their complexation with magnetic nanoparticles.

4.2 Experimental

4.2.1 Materials

3-Chloropropyldimethylchlorosilane was purchased from Gelest and used as received. Tetrahydrofuran (THF) was refluxed over sodium metal with benzophenone until the

solution reached a deep purple, fractionally distilled, and deoxygenated prior to use. Azoisobutyronitrile (AIBN, 98%), acetic acid (99.8%), benzyl alcohol (99.8%), ethylene oxide (EO, ≥99.5%), sodium iodide (≥99.5%), methanesulfonic acid (≥99.5%), iodomethane (99.5%), sodium hydroxide (1.0 N and 5.0 N in water), iron (III) acetylacetonate ($Fe(acac)_3$, ≥97.0%), L-glutamic acid (≥98.5%), *N*,*N*-dimethylformamide (DMF, 99.8%), hexamethylphosphoramide (99%), oleic acid (technical grade, 90%), allyl chloride (98%), dithiothreitol (98%), potassium persulfate (99%), sodium metabisulfite (98%) and vinylmagnesium bromide (1.0 N in THF) were purchased from Aldrich and used as received. Mercaptoethylamine hydrochloride (≥98%), Celite® (standard super-cel), and triphosgene (98%) were purchased from Alfa Aesar and used as received. Dichloromethane (HPLC grade), hexane (HPLC grade), acetone (HPLC grade), diethyl ether (99.8%), chloroform (99.98%), toluene (99.9%), methanol (HPLC grade), 2-propanol and magnesium sulfate (anhydrous) were purchased from Fisher Scientific and used as received. Ammonium chloride, sodium bicarbonate and hydrochloric acid (1.0 N in water) were purchased from J. T. Baker and used as received. A double metal cyanide (DMC) catalyst ($Zn_3[Co(CN)_6]_2$) was graciously donated by Bayer was dried at room temperature for 24 h under vacuum and diluted with distilled THF to yield a 4.1 mg mL^{-1} dispersion. Dialysis tubing was obtained from Spectra/Por. Phosphate buffered saline (PBS) was obtained from Mediatech Inc.

4.2.2 Characterization

^{1}H-NMR spectral analyses of compounds were performed using a Varian Unity 400 NMR or a Varian Inova 400 NMR operating at 399.97 MHz. An Alliance Waters 2690 Separations Module with a Viscotek T60A dual viscosity detector and laser refractometer

equipped with a Waters HR 0.5 + HR 2 + HR 3 + HR 4 styragel column set was used for size exclusion chromatography (SEC) analyses. SEC data were collected in chloroform and NMP containing 0.05 M LiBr at 30 or 50 ℃ respectively. Data were analyzed utilizing a Universal calibration constructed with polystyrene standards to obtain absolute molecular weights.

Thermogravimetric analyses (TGA) were carried out on the PEO-*b*-PG- iron oxide nanoparticles using a TA Instruments TGA Q500 to determine the fraction of each complex that was comprised of iron oxide. Each sample was first held at 110 ℃ for 10 min to drive off any excess moisture. The sample (10-15 mg) was then equilibrated at 100 ℃ and the temperature was ramped at 10 ℃ min^{-1} to a maximum of 700 ℃ in a nitrogen atmosphere. The mass remaining was recorded throughout the experiment. The mass remaining at 700 ℃ was taken as the fraction of iron oxide in the complexes. The experiments were conducted in triplicate.

DLS measurements were conducted with a Malvern Zetasizer NanoZS particle analyzer (Malvern Instruments Ltd) at a wavelength of 633 nm from a 4.0 mW, solid-state He-Ne laser at a scattering angle of 173 ° and at 25.0 ± 0.1 ˚C. Intensity, volume and number average diameters were calculated with the Zetasizer Nano 4.2 software utilizing an algorithm based upon Mie theory that transforms time-varying intensities to particle diameters. For DLS analysis, the dialyzed complexes were dispersed in DI water at a concentration of 0.1 mg mL^{-1}, and the dispersion was sonicated for 1 min in a 75T VWR Ultrasonicator (120 W, 45 kHz), then filtered through a 1.0 μm, Teflon™ filter directly into a polystyrene cuvette for analysis.

A 7T MPMS SQuID magnetometer (Quantum Design) was used to determine magnetic properties. Hysteresis loops were generated for the PEO-*b*-PG- iron oxide nanoparticles at 300 K. Inductively coupled plasma-atomic emission spectroscopy (ICP-AES) was performed with a SPECTRO ARCOS 165 ICP spectrometer (SPECTRO Analytical Instruments, Germany). The particles were digested to release free iron by reacting them with concentrated nitric acid at a concentration of 0.2 mg mL^{-1} for 5 days at 25 °C. They were diluted to 0.02 mg mL^{-1} with DI water prior to measurement.

4.2.3 Synthesis of 3-hydroxypropyldimethylvinylsilane (3-HPMVS).

3-Hydroxydimethylvinylsilane was synthesized utilizing a modified procedure from our laboratories.[37,38] 3-Chloropropyldimethylchlorosilane (20.0 g, 0.12 mol) was added into a dry 500-mL round-bottom flask with a magnetic stir bar. The flask was cooled with an ice bath. A 1.0 M vinylmagnesium bromide/THF solution (240 mL, 0.24 mol) was slowly added over 30 min. The mixture was stirred at RT for 24 h and then diluted with 200 mL of dichloromethane. Saturated aqueous ammonium chloride solution (150 mL) was slowly added and the mixture was transferred to a separatory funnel to remove the aqueous layer. The organic layer was further washed with saturated sodium chloride solution (3 × 150 mL) and dried with anhydrous magnesium sulfate. Dichloromethane was rotary-evaporated yielding a yellow liquid. The product was distilled at 85 ℃, 5 Torr, yielding a colorless liquid (15.2 g, 80%).

3-Chloropropyldimethylvinylsilane (14.4 g, 0.089 mol) and sodium iodide (26.1 g, 0.17 mol) were dissolved in 120 mL of acetone in a 250-mL round-bottom flask equipped with a magnetic stir bar and a condenser. The mixture was stirred under reflux for 24 h and the acetone was removed by rotary-evaporation. Dichloromethane (100 mL) was added and

the mixture was vacuum filtered to remove the salt. Dichloromethane was removed by rotary-evaporation and the product was distilled at 100 ℃, 5 Torr, yielding 3-iodopropyldimethylvinylsilane (19.5 g, 86%).

3-Iodopropyldimethylvinylsilane (18.9 g, 0.074 mol), sodium bicarbonate (9.4 g, 0.11 mol), DI water (14 mL) and hexamethylphosphoramide (50 mL) were added into a 250-mL round-bottom flask with a stir bar. The mixture was stirred at 100 ℃ for 24 h and then cooled to RT and diluted with 30 mL of DI water. The aqueous layer was extracted with diethyl ether (3 × 100 mL) and the organic layer was washed with DI water (3 × 200 mL). Diethyl ether was removed by rotary-evaporation and the product was distilled at 100 ℃, 5 Torr, yielding 3-hydroxypropyldimethylvinylsilane (7.5 g, 65%).

4.2.4 Synthesis of ammonium-PEO-CH_3.

An exemplary procedure for the polymerization of a 3,500 g mol^{-1} dimethylvinylsilyl-PEO-OH is provided. 3-HPMVS (0.69 g, 4.8 mmol) was syringed into a clean, flame-dried round-bottom flask, then 5 mL of THF and the double metal cyanide catalyst suspension (0.60 mL, 2.0 mg of the catalyst) was added via a syringe. The resulting initiator mixture was stirred for 24 h at room temperature. A 300-mL, high-pressure Series 4561 Parr reactor was utilized for the polymerization. EO (17 g, 0.39 mol) was distilled from a lecture bottle into the pressure reactor cooled with an isopropanol-dry ice bath, then the reactor was pressurized to 30 psi with ultrahigh purity nitrogen. The initiator solution was added to the Parr reactor via syringe, then the Parr reactor was heated to 105 °C. A temperature spike to 140 °C with a maximum pressure of 200 psi was noted, and this was followed by a gradual pressure decrease of 120 psi over 40 min. Once an equilibrium pressure was achieved the reactor was cooled to room temperature and its contents were diluted with

~200 mL of chloroform. The resulting solution was filtered through Celite® to remove the catalyst, then the polymer was precipitated by pouring it into cold diethyl ether. The product was collected by vacuum filtration and dried under vacuum at room temperature for 24 h.

Dimethylvinylsilyl-PEO-OH (14 g, 4 mmol) was dissolved in 45 mL of THF, then a NaH/THF suspension (5 mL, 4.8 mmol) was added. The mixture was stirred for 4 h at 60 °C, then iodomethane (0.36 mL, 5.8 mmol) was added by syringe at room temperature. The resulting solution was stirred for another 24 h at RT. The reaction mixture was diluted with 100 mL of chloroform and washed 3 times with DI H_2O. The solvent was removed by rotary evaporation and the product was dried under vacuum at 60 °C yielding a yellow solid (13.3 g, 95%).

Heterobifunctional PEO with a terminal ammonium group (ammonium-PEO-CH_3) was obtained via ene-thiol addition of mercaptoethylamine hydrochloride across the vinylsilane using a modified procedure from our previous reports.[37-39] In a characteristic procedure, a 3,500 g mol^{-1} dimethylvinylsilyl-PEO-CH_3 (3.5 g, 1.0 mmol), mercaptoethylamine hydrochloride (0.228 g, 2.0 mmol), and AIBN (0.082 g, 0.50 mmol) were dissolved in deoxygenated DMF (16 mL) in a 100-mL round-bottom flask equipped with a stir bar. The reaction was conducted at 70 °C for 24 h with stirring, then the reaction mixture was cooled to room temperature. DI water (100 mL) was added to the flask, and the mixture was transferred to a separatory funnel. Dichloromethane (200 mL) was added to the separatory funnel to extract the polymer from the water layer. The dichloromethane layer was washed with a 1 N solution of sodium bicarbonate (3X), followed by 3 washes with DI water. The dichloromethane solution was concentrated under vacuum, and the

ammonium-PEO-CH_3 was precipitated into cold diethyl ether and dried at 25 °C under vacuum for 12 h.

4.2.5 Synthesis of the N-carboxyanhydride (NCA) of γ-benzyl-L-glutamate

The *N*-carboxyanhydride (NCA) of γ-benzyl-L-glutamate was synthesized using a procedure adapted from the literature.[28] L-Glutamic acid (22 g, 0.15 mol) and benzyl alcohol (24 g, 0.22 mol) were dispersed in 22 mL of toluene and heated to 45 °C. Methanesulfonic acid (17 g, 0.18 mol) was added and the mixture was stirred at 45 °C for 3.5 h. The reaction mixture was stirred for another 5 h at 30 °C, then cooled and extracted with 44 mL of DI water. The solution was diluted with 66 mL of ethanol with adjustment of the pH to ~7 with sodium bicarbonate (20 g with 230 mL of water, 0.24 mol) to precipitate the compound. γ-Benzyl-L-glutamate was obtained by filtration and washed with 20 mL of ethanol (2X) and 30 mL of DI water (3X) (yield 13.9 g, 39%).

γ-Benzyl-L-glutamate (12.6 g, 53 mmol) and triphosgene (7.0 g, 24 mmol) were dried under 0.5 Torr at RT for 1 h, then dispersed in 140 mL of THF. The suspension was stirred for 2.5 h at 40 °C yielding a clear solution. The solution was concentrated to ~30 mL. Hexane (150 mL) was added to precipitate the NCA of γ-benzyl-L-glutamate. A white powder was collected by filtration and recrystallized 3 times with THF/hexane yielding a white powder (11.6 g, 83%).

4.2.6 Synthesis of poly(ethylene oxide)-b-poly(L-glutamic acid)

A 3,500 M_n amino-PEO-CH_3 (1.3 g, 0.37 mmol) was dried under vacuum at 60 °C for 12 h and dissolved in 50 mL of deoxygenated DMF. The NCA of γ-benzyl-L-glutamate (3.1 g, 12 mmol) was dried under vacuum at RT for 12 h and dissolved in 12 mL of DMF.

These two solutions were mixed and the reaction was stirred at RT for 60 h. Vacuum was applied every 12 h to remove any carbon dioxide. Diethyl ether (500 mL) was added to precipitate the poly(ethylene oxide)-*b*-poly(γ-benzyl-L-glutamate). The copolymer was collected by filtration (3.6 g, 90%).

Poly(ethylene oxide)-*b*-poly(γ-benzyl-L-glutamate) (3.6 g, 0.3 mmol) was dissolved in 50 mL of chloroform and cooled with an ice bath. NaOH (5 N, 6 mL, 30 mmol), DI water (8 mL), isopropanol (28 mL) and methanol (28 mL) were mixed and added to the copolymer solution. The reaction mixture was stirred for 10 h in the ice bath, then the copolymer was isolated by precipitation into 500 mL of cold diethyl ether. The copolymer was collected by filtration, then dissolved in DI water (100 mL) with adjustment of the pH to ~ 7 with 1 N HCl. The mixture was dialyzed against 4 L of DI water for 24 h in a 1,000 g mol^{-1} MWCO dialysis bag to remove NaCl and any residual benzyl alcohol. A white powder was obtained after freeze-drying (2.34 g, 89%).

4.2.7 Synthesis of magnetic iron oxide nanoparticles

The nanoparticles were prepared using a procedure adapted from Pinna et al.[35,36,38,40] $Fe(acac)_3$ (2.14 g, 8.4 mmol) and benzyl alcohol (45 mL, 0.43 mol) were charged to a 250-mL, three-neck, round-bottom flask equipped with a water condenser and placed in a Belmont metal bath with an overhead stirrer with thermostatic (±1 °C) control. The solution was dehydrated at 110 °C for 1 h under a N_2 stream. The temperature was increased in 25 °C increments and held at each step temperature for 1 h, until it reached the reflux temperature of benzyl alcohol at 205 °C, then the temperature was maintained for 40 h. The reaction was cooled to room temperature and the particles were collected by centrifugation (4000 rpm, 30 min). The iron oxide nanoparticles were washed 3 times with

acetone (100 mL each), then were dispersed in chloroform (20 mL) containing oleic acid (0.3 g). The solvent was removed under vacuum at room temperature, and the oleic acid-stabilized iron oxide nanoparticles were washed 3 times with acetone (50 mL each) to remove excess oleic acid. The particles were dried under vacuum overnight at room temperature and stored as a dispersion in chloroform at a concentration of 20 mg mL^{-1} prior to use.

4.2.8 Adsorption of poly(ethylene oxide)-b-poly(L-glutamic acid) onto iron oxide nanoparticles

A representative method for preparing a targeted composition of 67:33% by weight polymer to iron oxide complex is provided. Oleic acid-stabilized iron oxide nanoparticles (50.0 mg) prepared as described above were dispersed in chloroform (10 mL) and charged to a 50-mL round-bottom flask. Poly(ethylene oxide)-*b*-poly(L-glutamic acid) (100.0 mg) was dispersed in 1) chloroform or 2) DMSO and added dropwise to the dispersion. The mixture was sonicated in a VWR 75T sonicator for 4 h under N_2, and then stirred at RT for 20 h. The nanoparticles were precipitated in hexanes (200 mL). A permanent magnet was utilized to collect the iron oxide nanoparticles and free oleic acid was decanted with the supernatant. The complexes were dried under vacuum for 1 h at RT, then dispersed in DI water (20 mL) with adjustment of the pH to ~7 with 1 N NaOH and sonication for 30 min. The complexes were dialyzed against DI water (4 L) for 24 h using a 25,000 g mol^{-1} MWCO dialysis bag to remove free polymer. The dispersion was filtered through a 1.0 μm Teflon™ filter to remove any aggregates. A black-brown powder was obtained after freeze-drying.

4.2.9 Synthesis of a heterobifunctional ammonium-PEO-allyl

Heterobifunctional PEO oligomers with a terminal ammonium group (amino-PEO-OH) were obtained via ene-thiol addition of mercaptoethylamine hydrochloride across the vinylsilane endgroup. A 2,500 g mol^{-1} dimethylvinylsilyl-PEO-OH (7.0 g, 2.8 mmol), mercaptoethylamine hydrochloride (0.95 g, 8.3 mmol), and AIBN (0.34 g, 0.2.1 mmol) were dissolved in deoxygenated DMF (25 mL) in a 100-mL round-bottom flask equipped with a stir bar. The reaction was conducted at 70 °C for 24 h with stirring, then the reaction mixture was cooled to room temperature. DI water (100 mL) was added to the flask, and the mixture was transferred to a separatory funnel. Dichloromethane (200 mL) was added to the separatory funnel to extract the polymer from the water layer. The dichloromethane layer was washed with a 1 N solution of sodium bicarbonate (2×150 mL), followed by 3 washes with DI water. The dichloromethane was removed under vacuum at 60 °C yielding a solid (6.79 g, 97%).

Amino-PEO-OH (6.75 g, 2.6 mmol) was dissolved in 10 mL of THF followed by adding potassium naphthalate solution (2.23 mL, 2.41 mmol). Allyl chloride (0.4 mL, 5.2 mmol) was added into the mixture. The resulting solution was stirred for another 24 h at 50 °C. The reaction mixture was diluted with 100 mL of chloroform and washed 3 times with DI H_2O. The organic layer was dried under vacuum at 60 °C yielding a yellow solid (6.46 g, 96%).

4.2.10 Synthesis of allyl- and thiol-poly(ethylene oxide)-b-poly(L-glutamic acid) (allyl-PEO-PG and thiol-PEO-PG)

A 2,600 M_n amino-PEO-allyl (1.5 g, 0.58 mmol) was dried under vacuum at 60 °C for 12 h and dissolved in 530 mL of deoxygenated DMF. The NCA of γ-benzyl-L-glutamate

(3.55 g, 13 mmol) was dried under vacuum at RT for 12 h and dissolved in 10 mL of DMF. These two solutions were mixed and the reaction was stirred at RT for 3 days. Vacuum was applied every 12 h to remove any carbon dioxide. Diethyl ether (500 mL) was added to precipitate the poly(ethylene oxide)-*b*-poly(γ-benzyl-L-glutamate). The copolymer was collected by filtration (3.67 g, 83 %).

Allyl-poly(ethylene oxide)-*b*-poly(γ-benzyl-L-glutamate) (3.5 g, 0.49 mmol) was dissolved in 50 mL of chloroform and cooled with an ice bath. NaOH (5 N, 9.5 mL, 47.5 mmol), DI water (13 mL), isopropanol (45 mL) and methanol (45 mL) were mixed and added to the copolymer solution. The reaction mixture was stirred for 10 h with an ice bath and this was followed by precipitation of the copolymer into 500 mL of cold diethyl ether. The copolymer was collected by filtration and dissolved in DI water (100 mL) with adjustment of the pH to ~ 7 with 1 N HCl. The mixture was dialyzed against 4 L of DI water for 24 h in a 1,000 g mol^{-1} MWCO dialysis bag to remove NaCl and any residual benzyl alcohol. A white powder was obtained after freeze-drying (2.46 g, 96%).

Allyl-poly(ethylene oxide)-*b*-poly(L-glutamic acid) (0.114 g, 0.022 mmol), dithiothreitol (0.151 g, 0.98 mmol) and 4,4'-azobis(cyanovaleric acid) (0.0021 g, 0.0075 mmol) were dispersed in 1 mL of deoxygenated water. A 1N NaOH aqueous solution (0.4 mL, 0.4 mmol) was added to clarify the mixture. The solution was purged with nitrogen at 50 °C for 1 h. The reaction was conducted at 80 °C for 24 h with stirring, then the reaction mixture was cooled to RT. A 2N HCl solution (0.25 mL, 0.5 mmol) was added and this was followed by dialysis against 4 L of DI water for 32 h in a 3,000 g mol^{-1} MWCO dialysis bag to remove salts and any residual dithiothreitol. A white powder was obtained after freeze-drying (0.113 g, 99%).

4.2.11 Synthesis of diallyl- and dithiol-PEO.

A 2,000 M_n dihydroxyfunctional PEO (2.88 g, 2.88 meq of hydroxyl groups) was vacuum-dried at 60 °C for 1 h, then it was dissolved in 5 mL of THF. The solution was added to a round-bottom flask containing KH (0.122 g, 3.05 mmol), and the mixture was stirred for 2 h at 60 °C, then allyl chloride (0.70 mL, 8.6 mmol) was added by syringe. The resulting solution was stirred for another 36 h at 60 °C. The reaction mixture was diluted with 50 mL of chloroform and washed 3 times with DI H_2O. The solvent was removed by rotary evaporation and the product was dried under vacuum at 60 °C yielding a light yellow solid (2.59 g, 63%).

Diallyl-PEO (0.10 g, 0.05 mmol, 0.10 meq of allyl groups), dithiothreitol (1.4 g, 9.1 mmol), potassium persulfate (0.043 g, 0.16 mmol) and sodium metabifulfite (0.016 g, 0.084 mmol) were vacummed at room temperature for 1 h followed by adding 4 mL of deoxygenated water. The reaction was conducted at room temperature for 46 h with stirring, then the reaction mixture was dialyzed against 4 L × 2 of DI water for 24 h in a 1,000 g mol^{-1} MWCO dialysis bag to remove salts and any residual dithiothreitol. A white powder was obtained after freeze-drying (0.098 g, 98%).

4.2.12 Synthesis of magnetic clusters

Aqueous solutions of potassium persulfate (0.6 mg/mL), sodium metabifulfite (0.5 mg/mL), diallyl-PEO (1.3 mg/mL) and dithol-PEO (1.3 mg/mL) were used as stock solutions for the following synthesis. Two types of magnetic complexes, one containing 67 wt% of a 1:1 wt:wt mixture of allyl-PEO-PG and CH_3O-PEO-PG (allyl-magnetic complexes) and the other one containing 67 wt% of a 1:1 wt:wt mixture of thiol-PEO-PG and CH_3O-PEO-PG (thiol-magnetic complexes), were synthesized using the procedure

described above. Magnetic clusters were synthesized via three methods. First, allyl-magnetic complexes (20.5 mg total, 1.3×10^{-6} eq of allyl groups), dithiol-PEO (1 mL, 1.3 mg, 6.5×10^{-7} mol), potassium persulfate (0.3 mL, 0.18 mg of potassium persulfate, 6.6×10^{-7} mol) and sodium metabisulfite (0.12 mL, 0.06 mg, 3.2×10^{-7} mol) were mixed and purged with nitrogen for 4 h. The reaction was conducted at room temperature for 2 days with stirring, then the reaction mixture was dialyzed against 4 L of DI water for 24 h in a 25,000 g mol^{-1} MWCO dialysis bag to remove salts and any residual dithiol-PEO. A black-brown powder was obtained after freeze-drying (20.2 mg, 99%). Secondly, thiol-magnetic complexes (20.5 mg total, 1.3×10^{-6} eq of thiol groups), diallyl-PEO (1 mL, 1.3 mg, 6.5×10^{-7} mol), potassium persulfate (0.18 g, 6.5×10^{-7} mol) and sodium metabifulfite (0.06 g, 3.2×10^{-7} mol) were purged with nitrogen for 4 h. The reaction was conducted at room temperature for 2 days with stirring, then the reaction mixture was dialyzed against 4 L of DI water for 24 h in a 25,000 g mol^{-1} MWCO dialysis bag to remove salts and any residual diallyl-PEO. A black-brown powder was obtained after freeze-drying (20.1 mg, 98%). Third, thiol-magnetic complexes (18.4 mg, 1.2×10^{-6} eq of thiol groups), allyl-magnetic complexes (19.3 mg, 1.2×10^{-6} eq of allyl groups), potassium persulfate (0.16 g, 6.5×10^{-7} mol) and sodium metabifulfite (0.06 g, 3.2×10^{-7} mol) were mixed and purged with nitrogen for 4 h. The reaction was conducted at room temperature for 2 days with stirring, then the reaction mixture was dialyzed against 4 L of DI water for 24 h in a 25,000 g mol^{-1} MWCO dialysis bag to remove salts. A black-brown powder was obtained after freeze-drying (37.3 mg, 99%).

4.2.13 Measurements of transverse relaxivities

The proton transverse relaxation times (T_2) were measured on a Model mq-60 NMR Analyzer (Bruker Minispec) at a magnetic field strength of 1.4 T corresponding to a proton Larmor frequency of 60 MHz. T_2 was obtained from fitting a monoexponential decay curve to signal data generated by a Carr-Purcell-Meiboom-Gill (CPMG) spin-echo pulse sequence with an echo spacing of 0.5 ms and a repetition time of 5 s. Samples were filtered through a 1.0 μm Teflon™ filter and 500 μL were transferred into a 7.5 mm NMR tube and measurements were made at 37.5 °C after equilibration for 15 min. The transverse relaxivity (r_2) was calculated from the least-square fit of the relaxation rate ($1/T_2$) as a function of iron concentration. Fe concentrations were determined by ICP-AES as described previously.

4.3 Results and discussion

4.3.1 Synthesis of amino-functional PEO macroinitiators

Amino-functional PEO has been used as a macroinitiator for ring-opening of *N*-carboxyanhydrides (NCA) via nucleophilic acyl substitution to prepare block copolymers containing PEO and polypeptides.[26,27,41-45] To prepare a heterobifunctional PEO, 3-HPMVS was used as an initiator which allowed post polymerization functionalization (Scheme 4.3.1.1). Dimethylvinylsilyl-PEO-OH with number average molecular weights of 1,200 and 3,500 g/mol were synthesized and characterized by ^{1}H NMR and SEC. The number average molecular weights were calculated from the integral ratio of resonances corresponding to the methyl groups next to the silicon at 0.49 ppm relative to the repeat

units of ethylene oxide at 3.64 ppm (Figure 4.3.1.1). SEC analyses revealed monomodal distributions with molecular weights of 1,180 (PDI=1.12) and 3,030 (PDI=1.40).

The hydroxyl groups were deprotonated with sodium hydride and this was followed by reaction of the alkoxide with methyl iodide. ^{1}H NMR was used to monitor this reaction by noting the appearance of the peak at 3.36 ppm corresponding to the methoxy endgroups (Figure 4.3.1.2). Amino groups were introduced to the other end via thiol-ene addition. An excess of thiol groups was utilized to maximize the conversion of vinyl groups. The thiol-ene addition was monitored by ^{1}H NMR by noting the disappearance of vinyl protons at 5.62-6.20 ppm and the appearance of new peaks at 0.85, 2.53, 2.61 and 2.86 ppm corresponding to the terminal methylene groups (Figure 4.3.1.3).

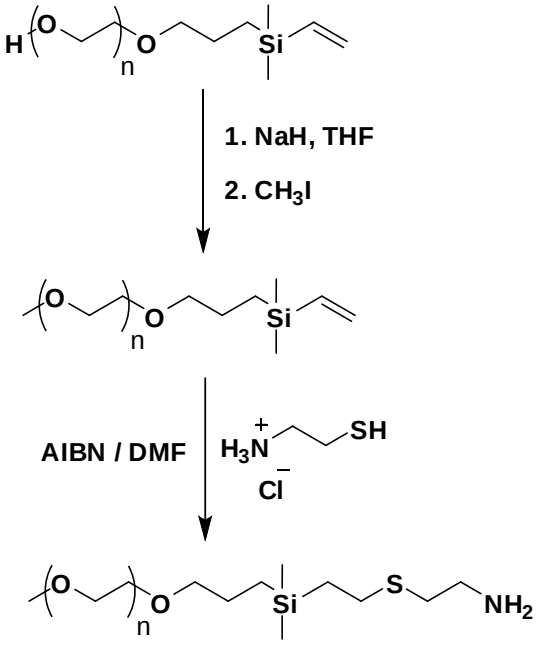

Scheme 4.3.1.1. Synthesis of an amino-PEO-OCH_3.

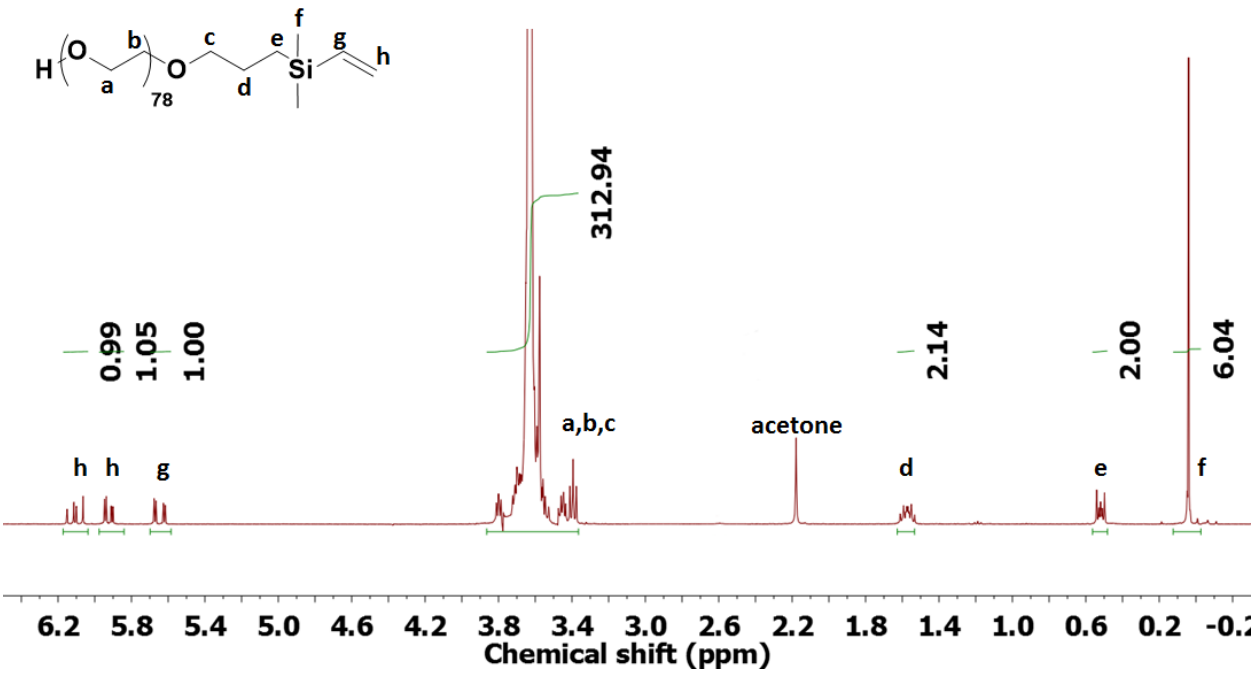

Figure 4.3.1.1. ^{1}H NMR of a 3.5k vinylsilane-PEO-OH.

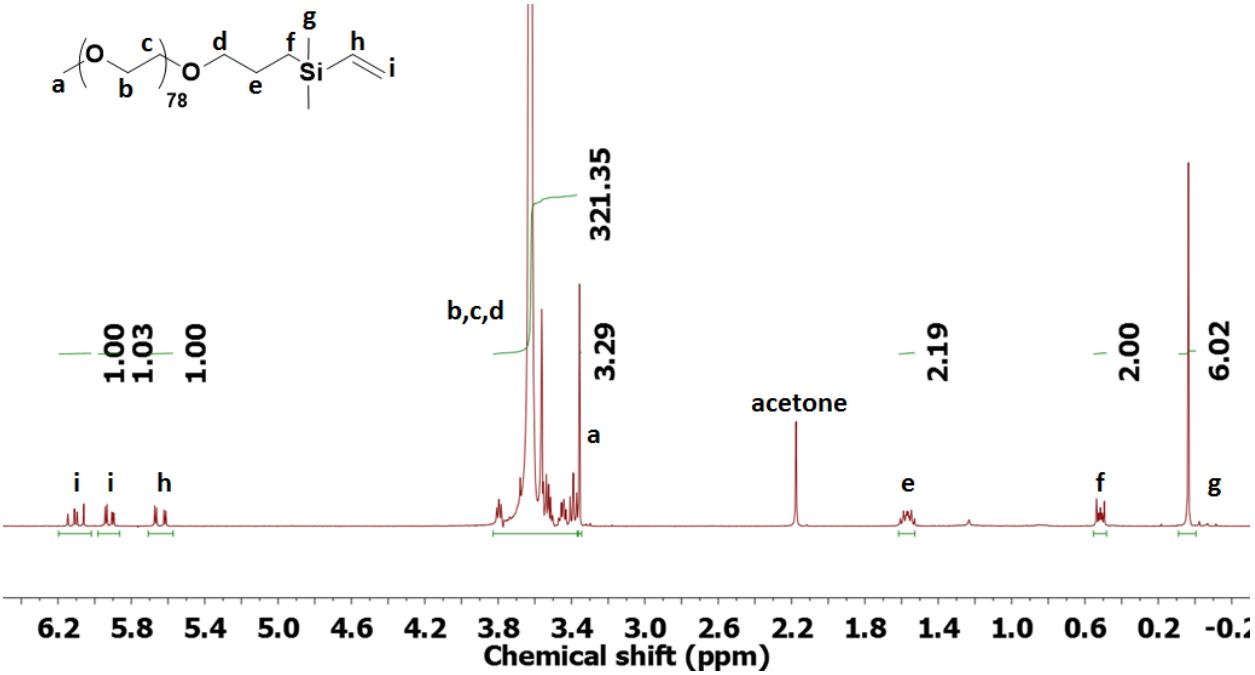

Figure 4.3.1.2. ^{1}H NMR of a 3.5k amino-PEO-OH.

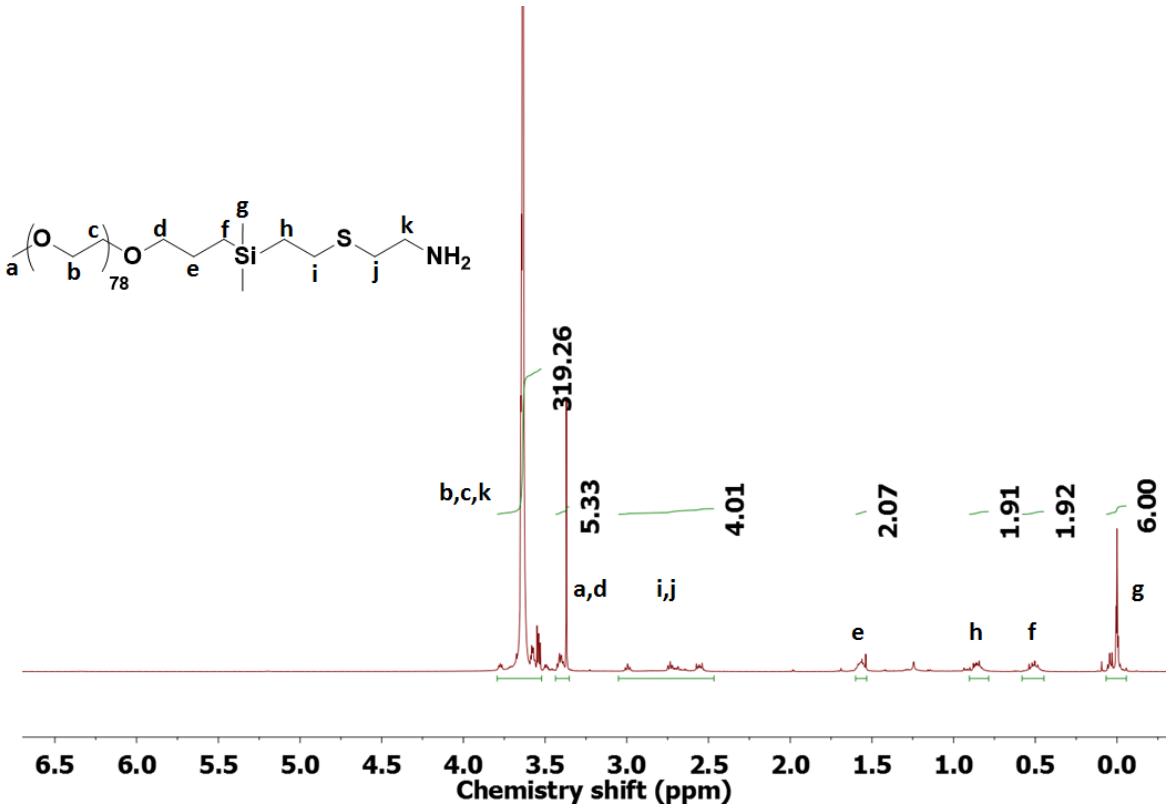

Figure 4.3.1.3. ^{1}H NMR of a 3.5k amino-PEO-OCH$_3$.

4.3.2 Synthesis of poly(ethylene oxide)-b-poly(L-glutamic acid)

In this study, the NCA of benzyl-L-glutamate was used as a monomer (Scheme 4.3.2.1). Benzyl-L-glutamate was prepared by reaction of L-glutamic acid with an excess of benzyl alcohol in the presence of 1.2 equivalents of methanesulfonic acid relative to L-glutamic acid. The product was recrystallized three times from hot water to enhance its purity (Figure 4.3.2.1). Dry benzyl-L-glutamate was dispersed in THF with triphosgene yielding a clear solution within two hours. The NCA of benzyl-L-glutamate was recrystallized three times from THF/hexane and its structure was verified by ^{1}H NMR (Figure 4.3.2.2). Melting

points of benzyl-L-glutamate and the NCA of benzyl-L-glutamate were determined to be 167-169 and 94-95 ℃ respectively, which were close to the literature values.[46,47]

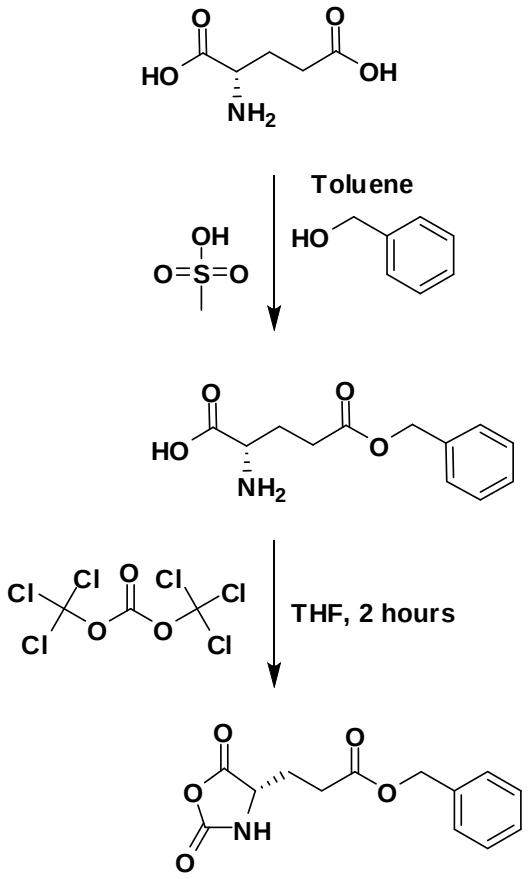

Scheme 4.3.2.1. Synthesis of an NCA of γ-benzyl-L-glutamate.

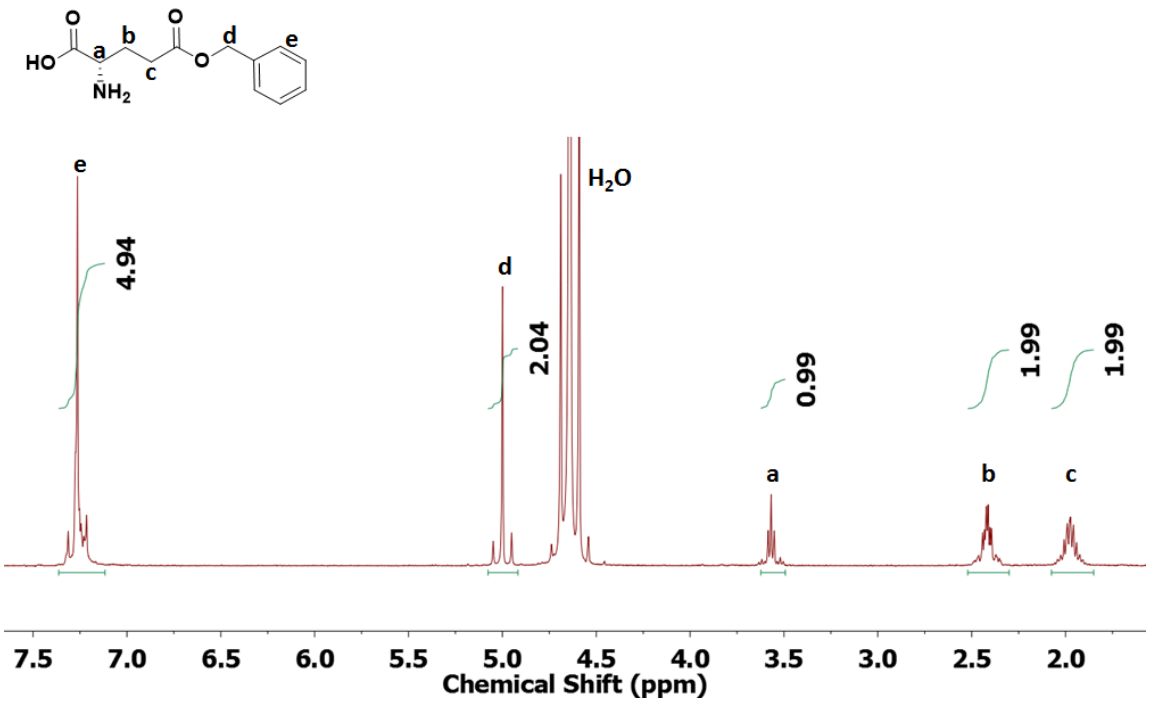

Figure 4.3.2.1. ^{1}H NMR of benzyl-L-glutamate.

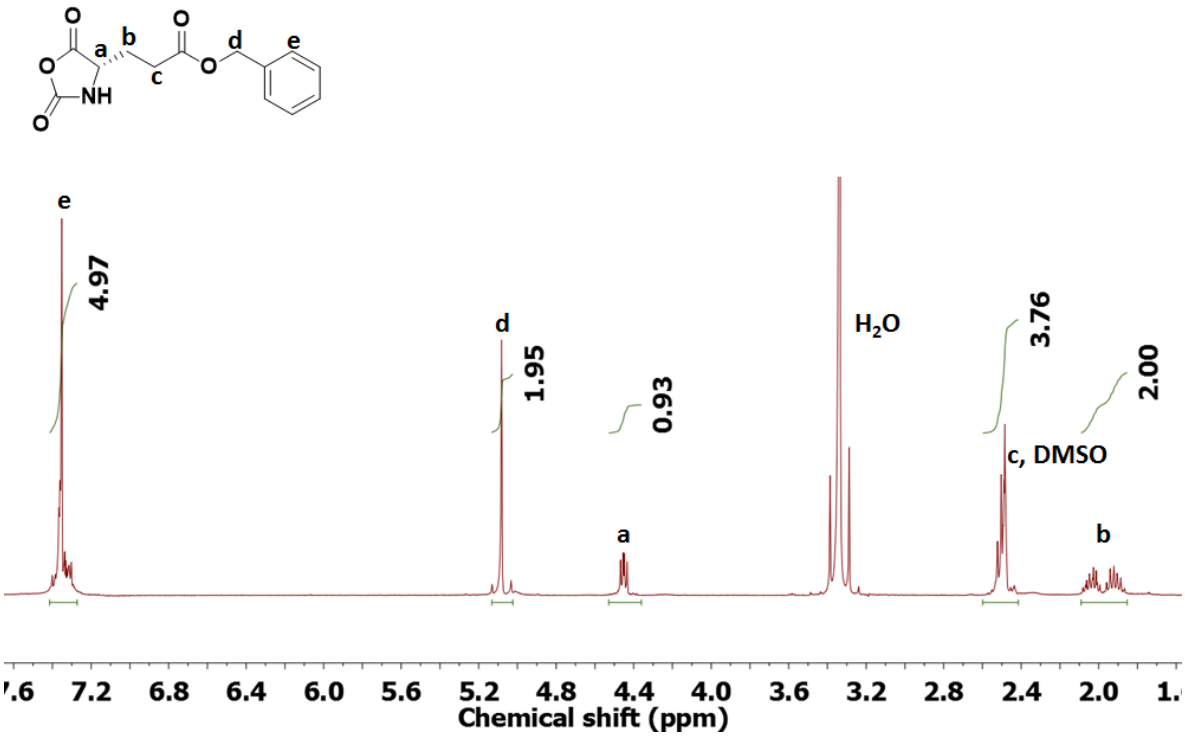

Figure 4.3.2.2. ^{1}H NMR spectrum of the NCA of γ-benzyl-L-glutamate in d_6-DMSO.

Polymerizations of the NCA of benzyl-L-glutamate were carried out at room temperature in DMF (Scheme 4.3.2.2). The carbon dioxide by-product from the polymerization was removed intermittently by applying vacuum twice a day to enhance monomer conversion. The PEO-*b*-poly(benzyl-L-glutamate) copolymers were characterized by ^{1}H NMR and SEC to determine the chemical compositions and molecular weights (Table 4.3.2.1). The resonance at 3.64 ppm was assigned to the EO repeat units and the peaks at 7.24, 5.03. 3.93 and 1.82-2.56 ppm were assigned to the benzyl-L-glutamate repeat units (Figure 4.3.2.3). Block lengths were calculated by comparing the integral ratio of the resonance corresponding to the phenyl group at 7.24 ppm and ethylene oxide at 3.64 ppm to the methylene group next to the silicon at 0.47 ppm. The results were

in good agreement with the targeted block lengths (Table 4.3.2.1). SEC traces were monomodal (Figure 4.3.2.5) and the polymers had narrow molecular weight distributions that are characteristic of controlled polymerizations.

The side carboxylic acids, which can provide accessibility for guest molecules through electrostatic interactions and/or hydrogen bonds, were obtained by hydrolysis of the benzyl-L-glutamate repeat units (Scheme 4.3.2.2). The benzyl groups were removed with a mild heterogeneous alkaline hydrolysis procedure to avoid cleavage of the backbone amide bonds. The products were acidified and characterized by ^{1}H NMR in d_6-DMSO (Figure 4.3.2.4). The extents of the hydrolyzed benzyl-L-glutamates were monitored by partial disappearance of the resonances at 7.24 and 5.03 ppm corresponding to the benzyl groups. The polymeric salts after hydrolysis were characterized by ^{1}H NMR in D_2O and by noting the disappearance of resonances at 7.24 or 5.03 ppm corresponding to the benzyl groups. The lack of benzyl resonances was attributed to poor solubility of the benzyl-L-glutamate units in D_2O.

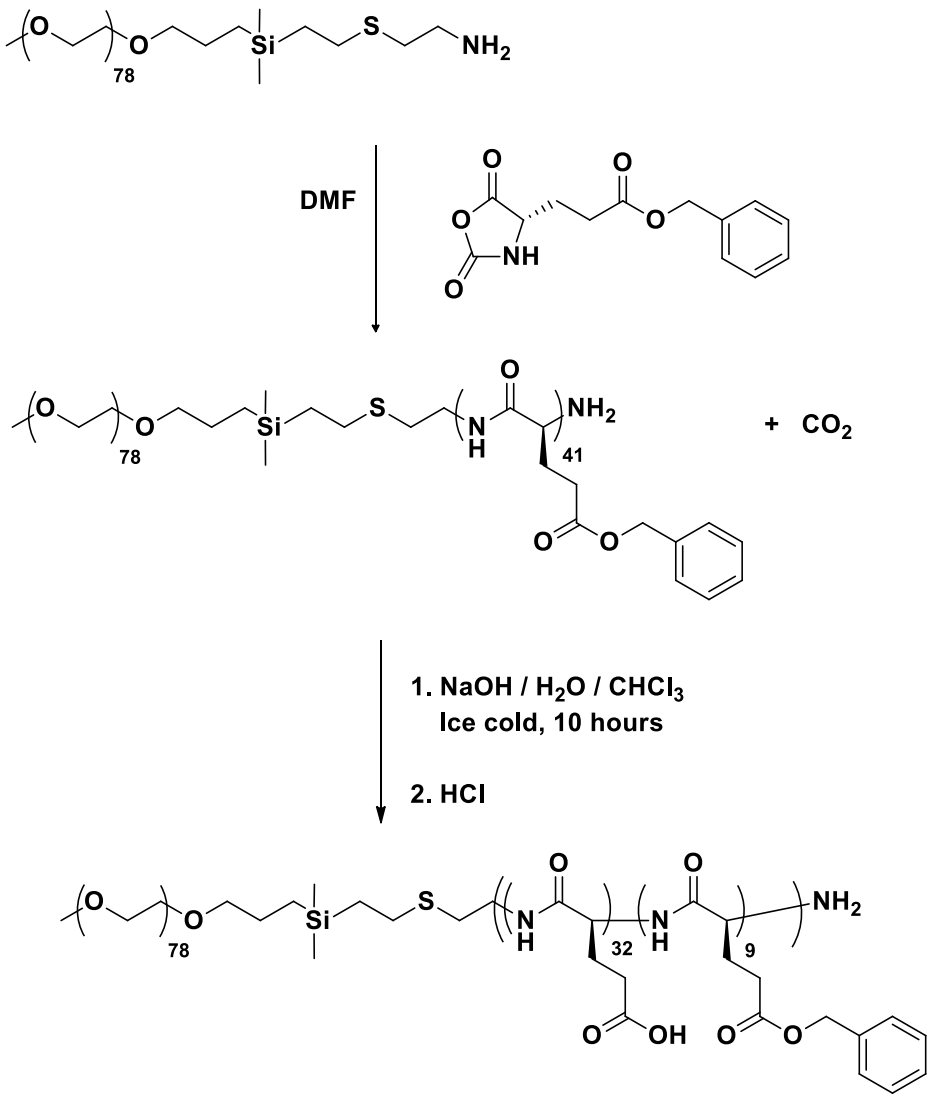

Scheme 4.3.2.2. Synthesis of a poly(ethylene oxide)-*b*-poly(L-glutamic acid).

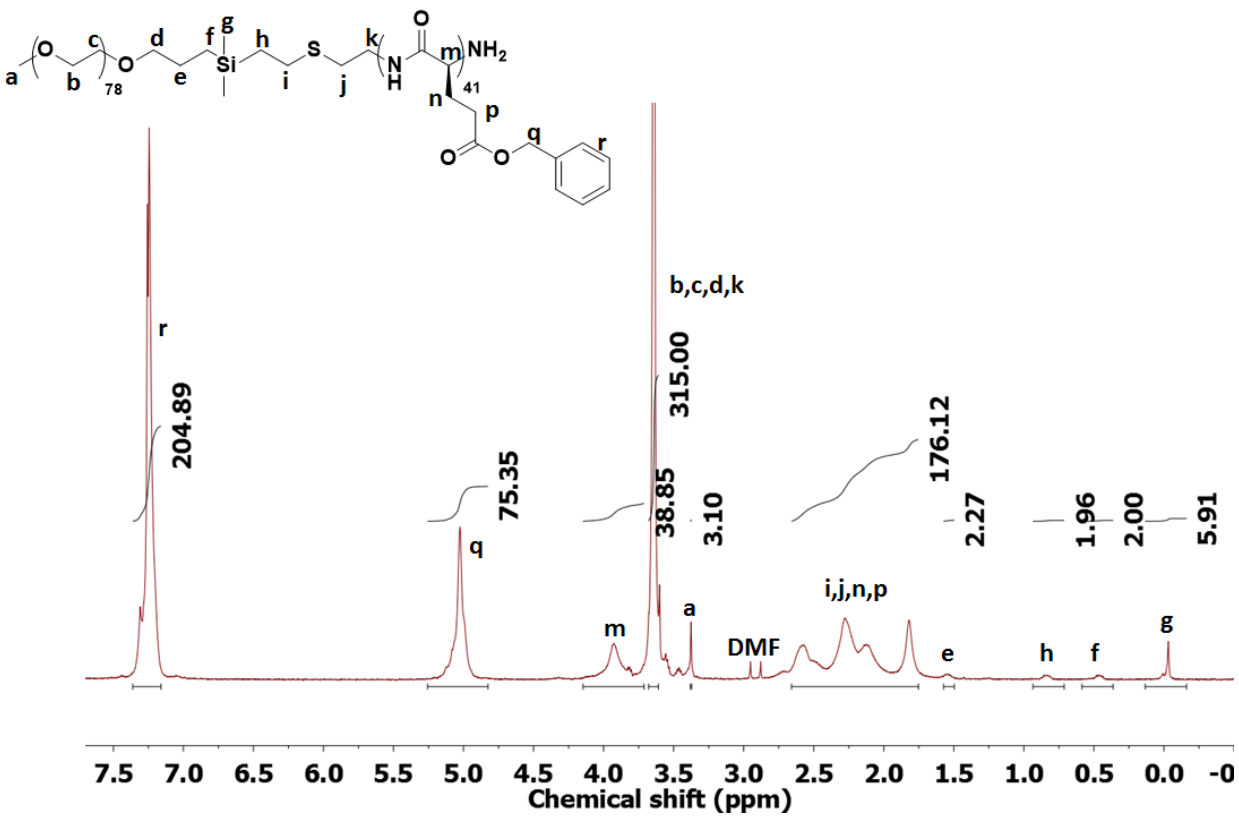

Figure 4.3.2.3. ^{1}H NMR spectrum of the PEO-*b*-poly(γ-benzyl-L-glutamate) in d_6-DMSO.

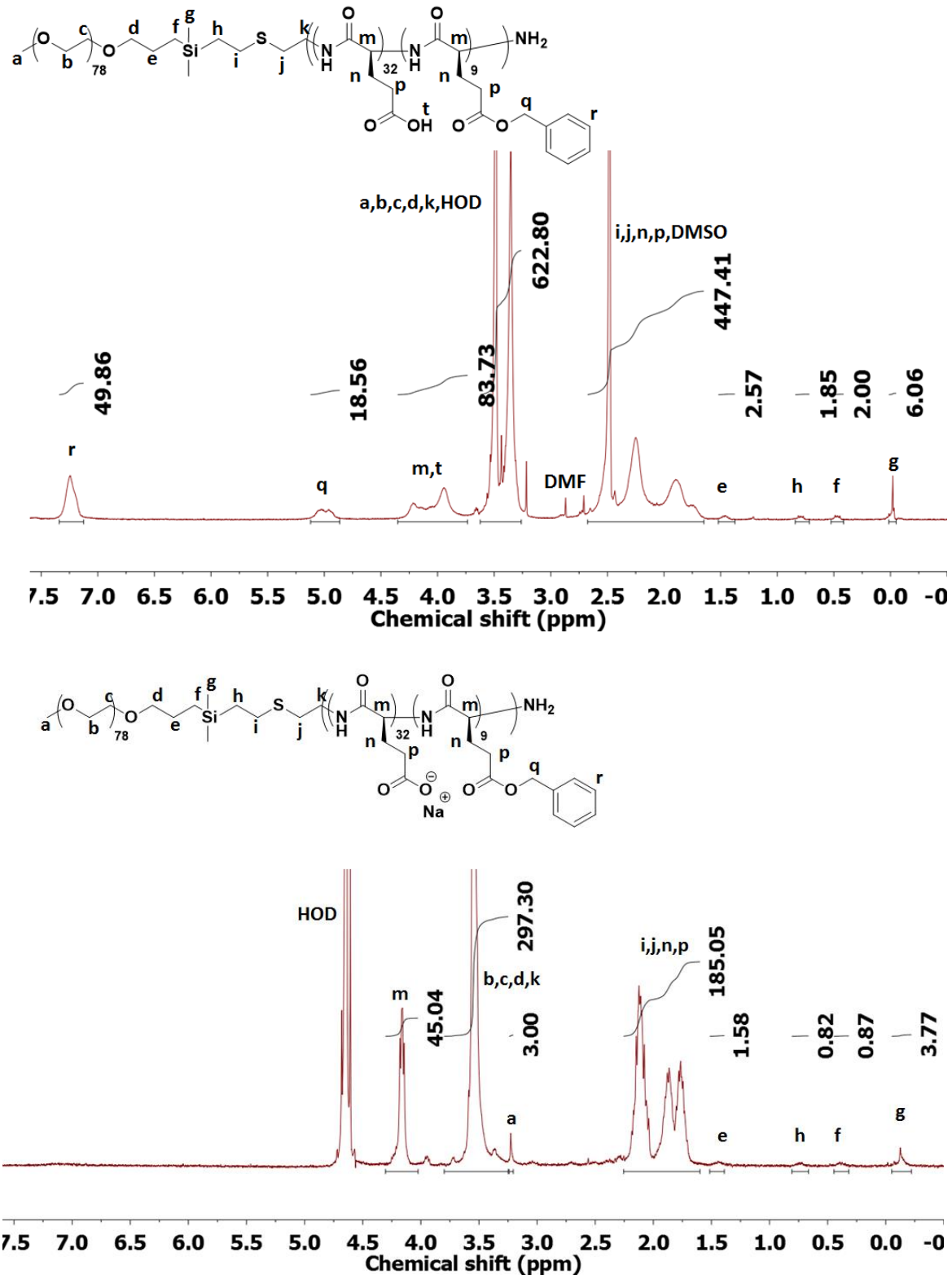

Figure 4.3.2.4. ^{1}H NMR spectra of a PEO-*b*-poly(L-glutamic acid) in d_6-DMSO (acid form, top) and in D_2O (salt form, bottom).

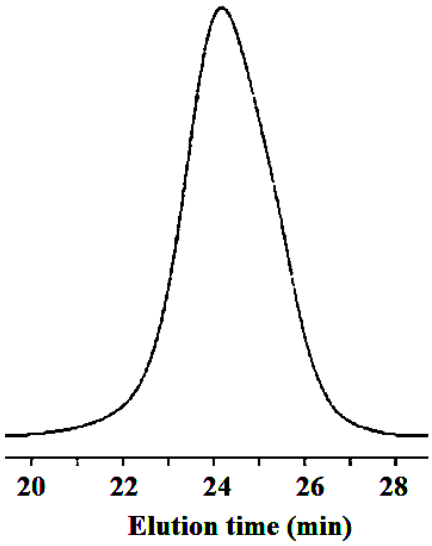

Figure 4.3.2.5. SEC trace of a 3.5 K PEO-*b*-10.9 K poly(γ-benzyl-L-glutamate).

Table 4.3.2.1. Molecular weights of the PEO-*b*-poly(γ-benzyl-L-glutamate)s.

Target block length	Block length (NMR)	Target total M_n g/mol^{-1}	M_n (NMR) g/mol^{-1}	M_n (SEC) g/mol^{-1}	PDI
1,500-6,200	1,200-7,800	7,700	9,000	7,200	1.12
3,500-7,800	3,500-7,400	11,300	10,900	12,400	1.11
3,500-8,500	3,500-8,600	12,000	12,100	14,500	1.18

4.3.3 Synthesis of diallyl- and dithiol-functional PEO

Diallyl- and dithiol-functional PEO oligomers were synthesized and used as crosslinking components in the preparation of magnetic clusters (Scheme 4.3.3.1). A dihydroxy-functional PEO with a number average molecular weight of 2,000 g/mol was deprotonated with sodium hydride and the dialkoxide was reacted with allyl chloride to produce allyloxy endgroups. ^{1}H NMR was used to monitor the reaction by noting the appearance of peaks at 4.0, 5.2 and 5.9 ppm corresponding to the allyloxy endgroups (Figure 4.3.3.1). Thiol groups were introduced to the ends via thiol-ene addition. Ten times excess of dithiothreitol

was utilized to avoid chain coupling. This reaction was conducted at room temperature with sodium metabisulfite and potassium persulfate as the redox free radical resource. The thiol-ene addition was monitored by ^{1}H NMR by noting the disappearance of allyl protons on allyl chloride at 4.0, 5.2 and 5.9 ppm and new peaks at 1.8, 2.6, 2.8 and 3.8 ppm corresponding to terminal groups on the oligomers (Figure 4.3.3.2).

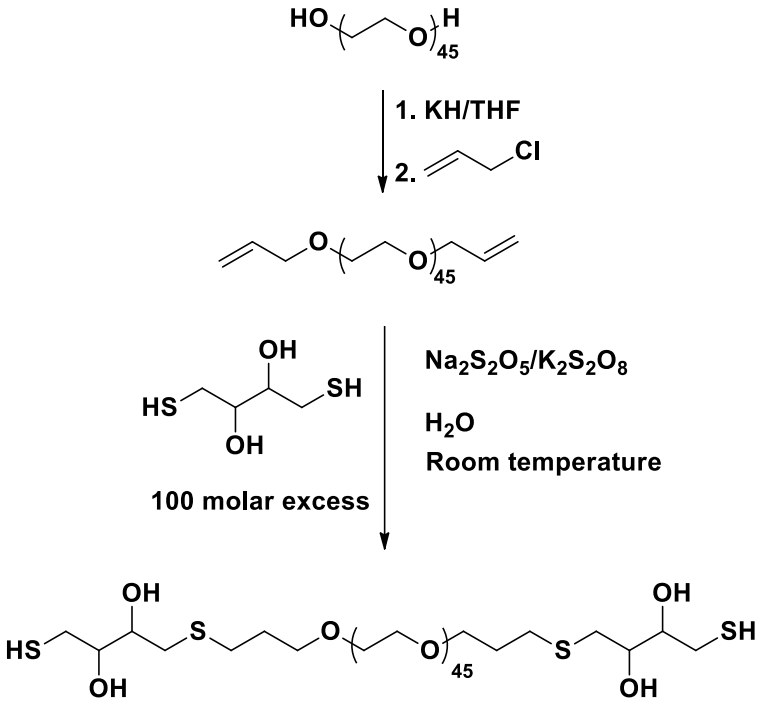

Scheme 4.3.3.1. Synthesis of dially-PEO and dithiol-PEO.

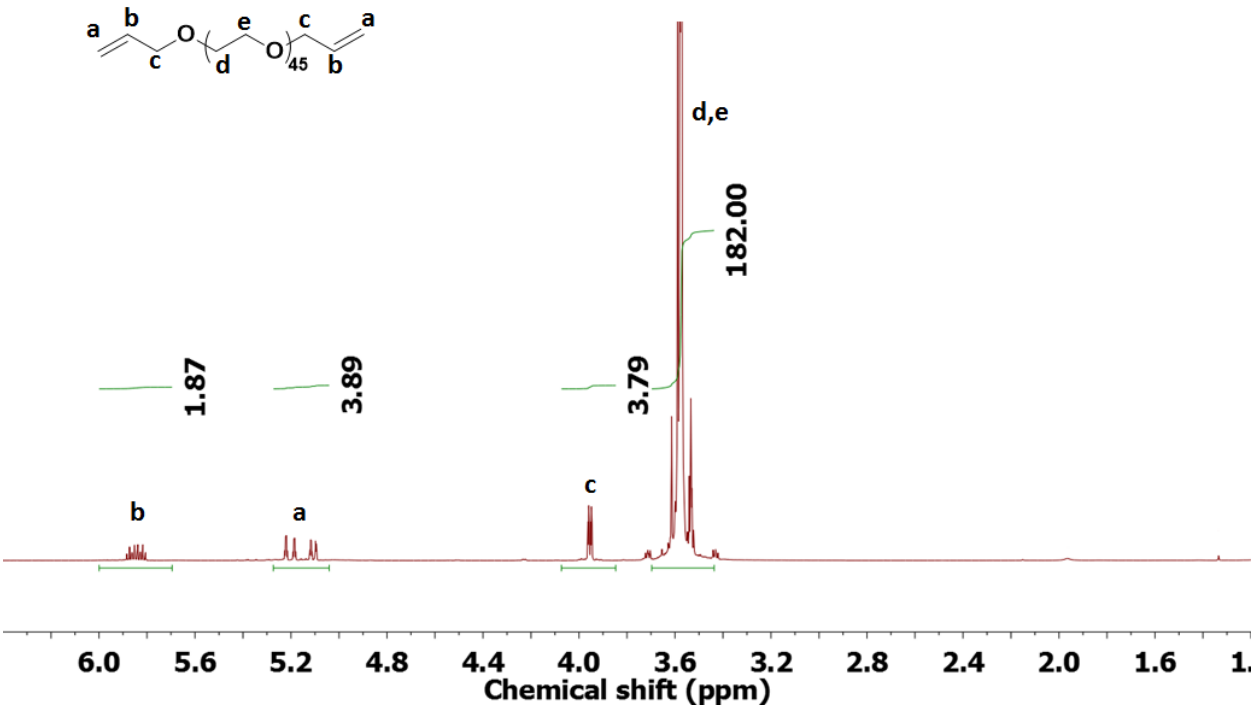

Figure 4.3.3.1. ^{1}H NMR of a 2k diallyl-PEO.

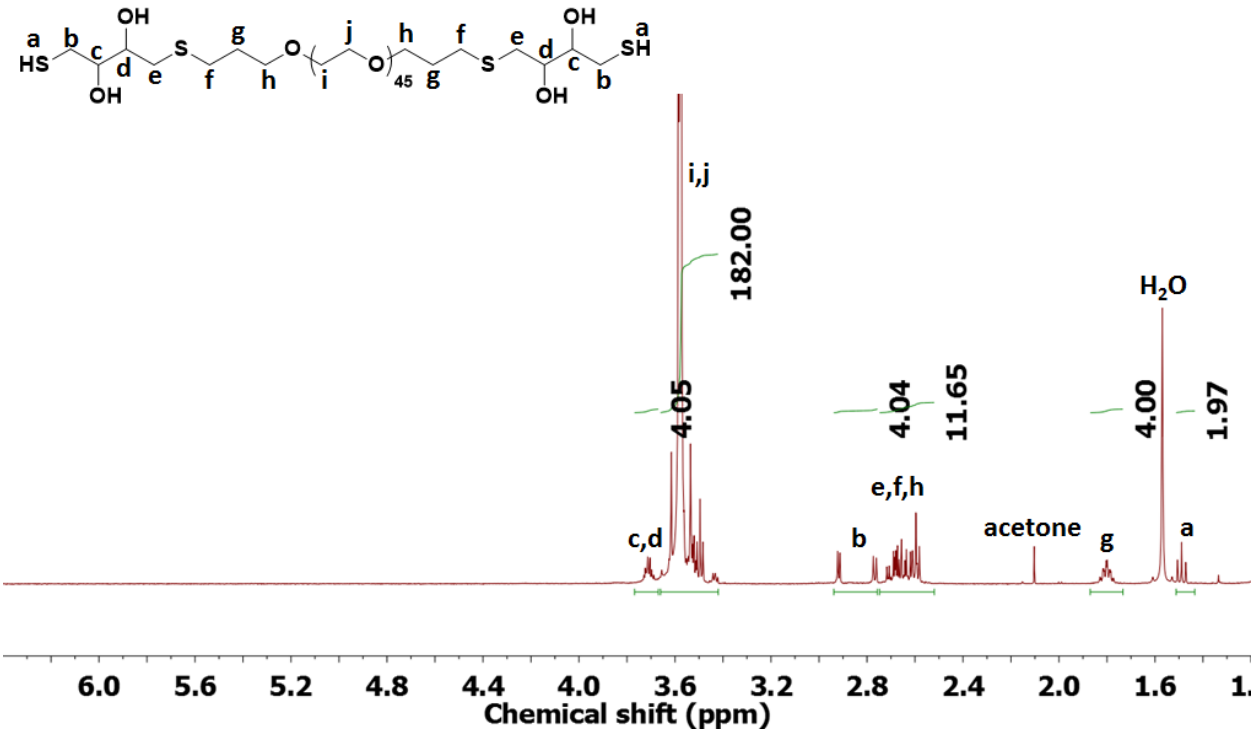

Figure 4.3.3.2. ^{1}H NMR of a 2k dithiol-PEO.

4.3.4 Synthesis of allyl- and thiol-poly(ethylene oxide)-b-poly(L-glutamic acid)

Allyl- and thiol groups were introduced to the PEO ends of PEO-b-poly(L-glutamic acid) block copolymers (Scheme 4.3.4.1). The hydroxyl groups on amino-PEO-OH were deprotonated with sodium hydride and the alkoxide was reacted with allyl chloride. ^{1}H NMR was used to monitor this reaction by noting the appearance of peaks at 5.2 and 5.9 ppm corresponding to the allyl endgroups (Figure 4.3.4.1).

Amino-PEO-allyl was used as a macroinitiator to synthesize allyl-PEO-*b*-poly(L-glutamic acid) by initiating the NCA with the terminal amine. Polymerization of the NCA and subsequent removal of the benzyl esters were carried out using the same procedures as described for preparing methoxy-poly(ethylene oxide)-*b*-poly(L-glutamic acid) (Figures 4.3.4.2 and 4.3.4.3). Thiol groups were then introduced to the PEO end via thiol-ene

addition. As described previously, an excess of thiol groups were utilized to avoid chain coupling. The thiol-ene addition was monitored by ^{1}H NMR by observing disappearance of the allyl protons at 5.9 ppm (Figure 4.3.4.4).

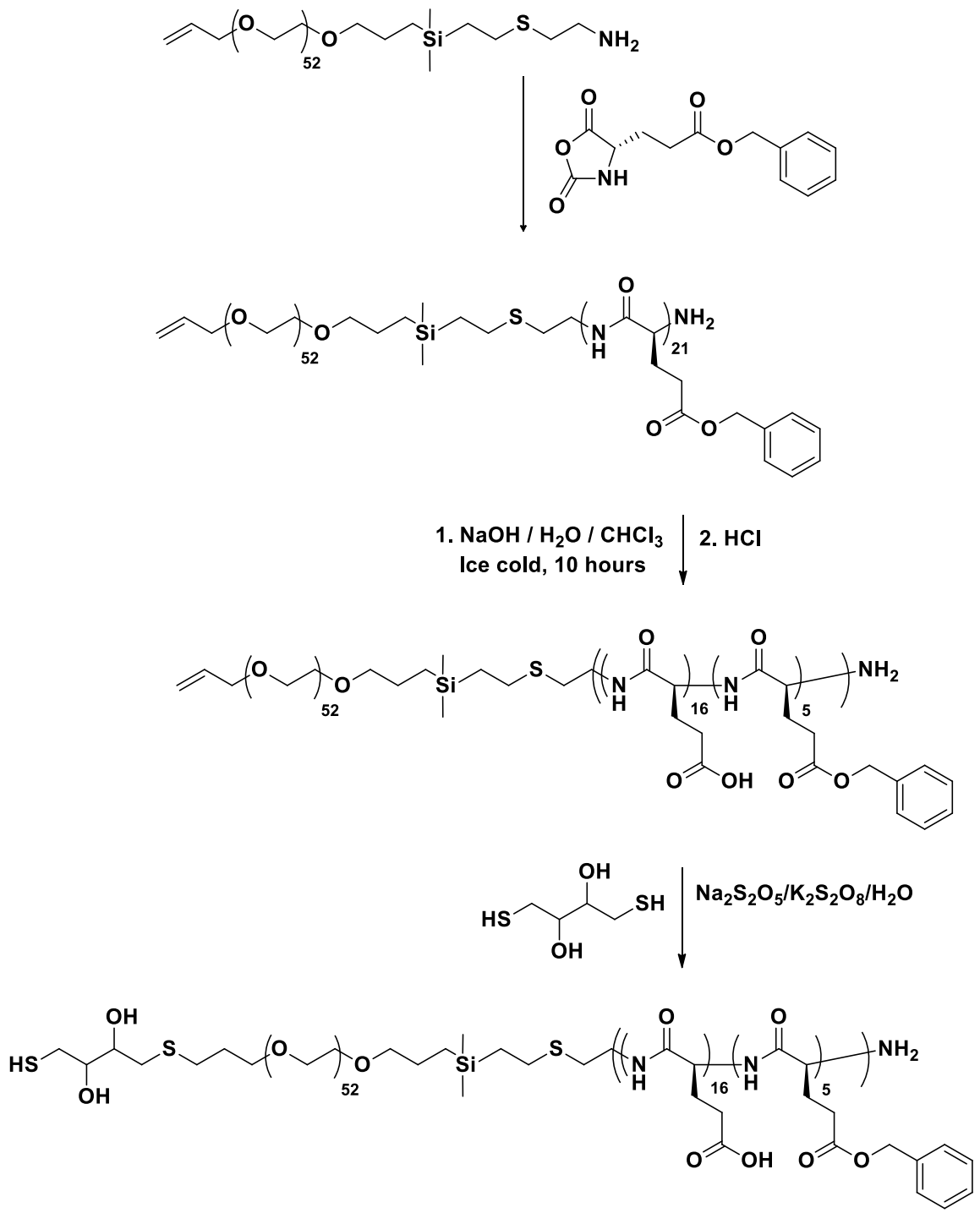

Scheme 4.3.4.1. Synthesis of an allyl-poly(ethylene oxide)-*b*-poly(L-glutamic acid) and a thiol-poly(ethylene oxide)-*b*-poly(L-glutamic acid).

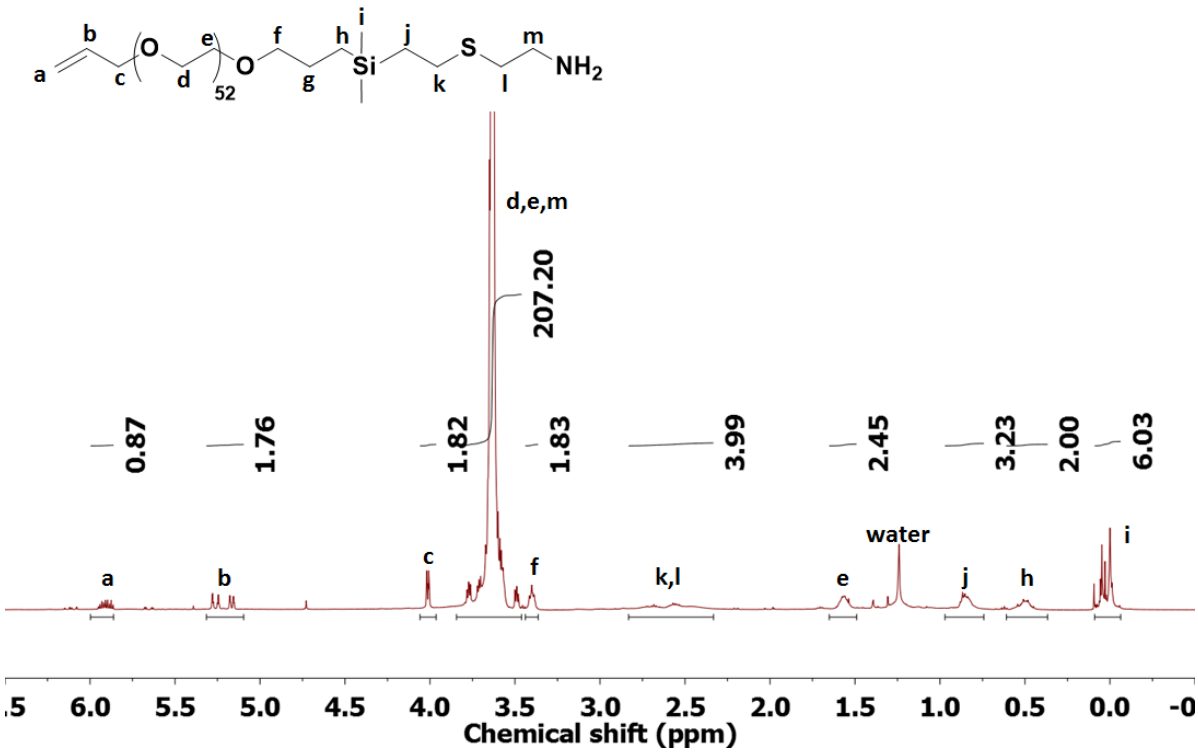

Figure 4.3.4.1. ^{1}H NMR of a 2.5k amino-PEO-allyl.

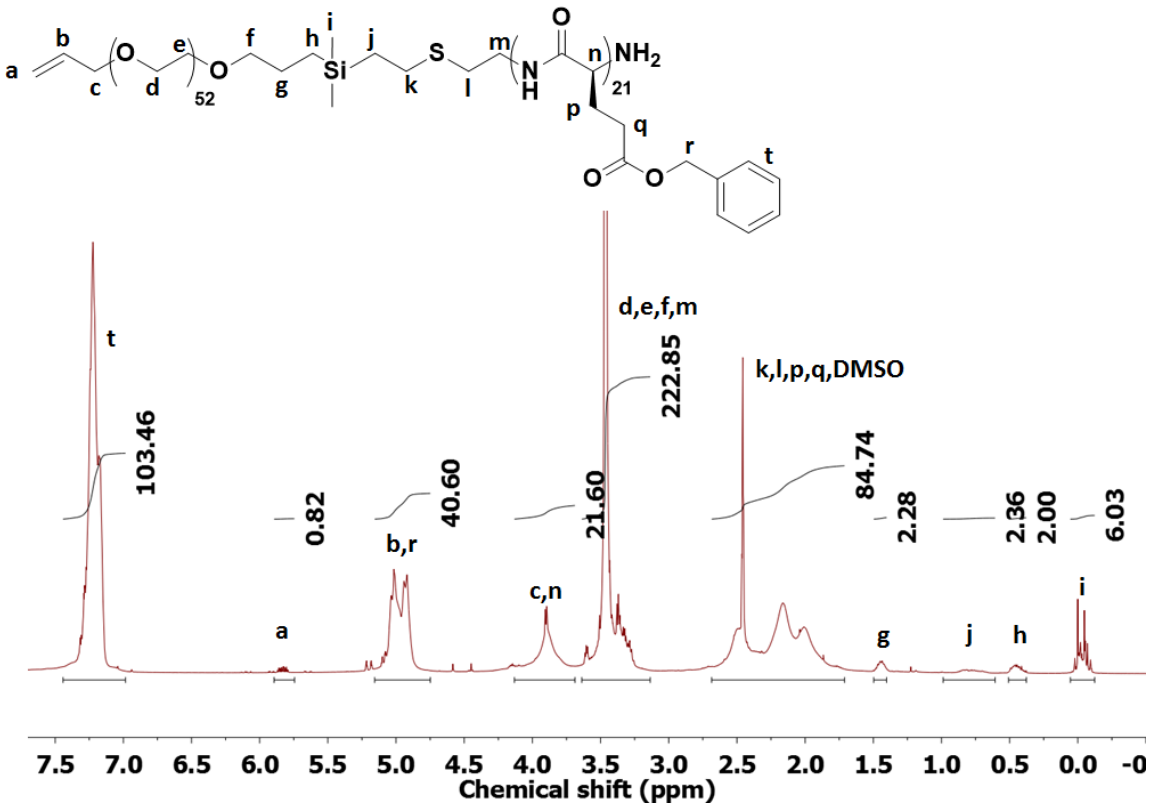

Figure 4.3.4.2. ^{1}H NMR spectrum of an allyl-PEO-*b*-poly(γ-benzyl-L-glutamate) in d_6-DMSO.

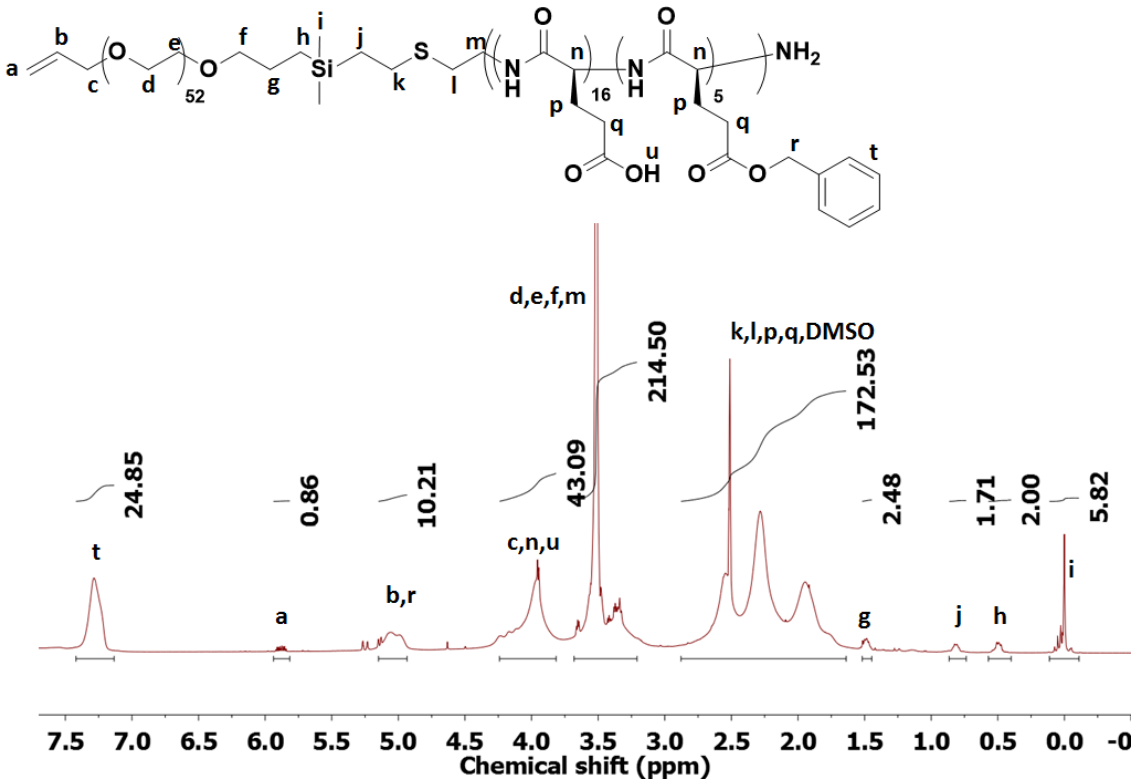

Figure 4.3.4.3. ^{1}H NMR spectra of an allyl-PEO-*b*-poly(L-glutamic acid) in d_6-DMSO.

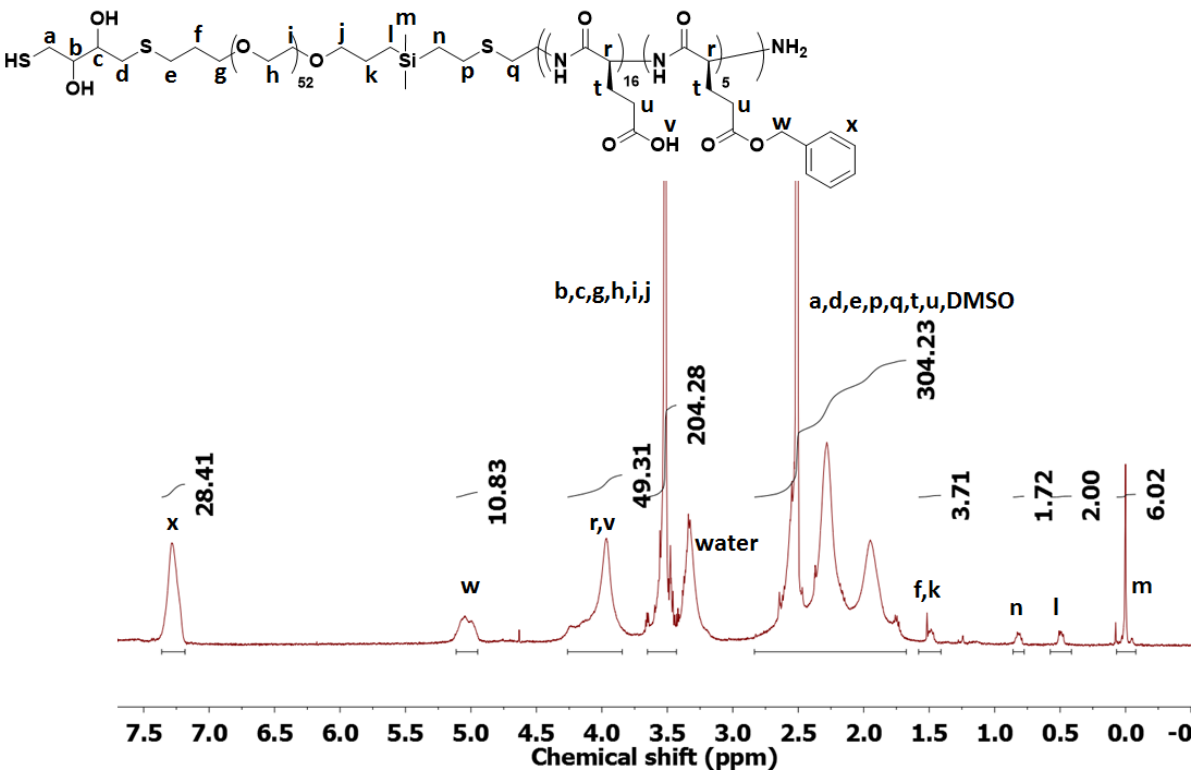

Figure 4.3.4.4. ^{1}H NMR of a thiol-poly(ethylene oxide)-*b*-poly(L-glutamic acid).

4.3.5 Adsorption of poly(ethylene oxide)-b-poly(L-glutamic acid) onto iron oxide nanoparticles

A variety of polymers and small molecules have been reported as coatings for iron oxide nanoparticles to provide colloidally stable dispersions in aqueous media.[10,11,16,18,20,21] In this study, poly(ethylene oxide)-*b*-poly(L-glutamic acid) (EO_{79}-BLG_{41}) was utilized as a biodegradable stabilizer and adsorbed onto oleic acid-coated iron oxide nanoparticles via ligand adsorption from 1) chloroform and 2) from a mixed 1:1 v:v chloroform:DMSO solvent (Scheme 4.3.5.1). After adsorption, the complexes were precipitated in hexane to remove oleic acid and dialyzed against water to remove any unbound polymers.

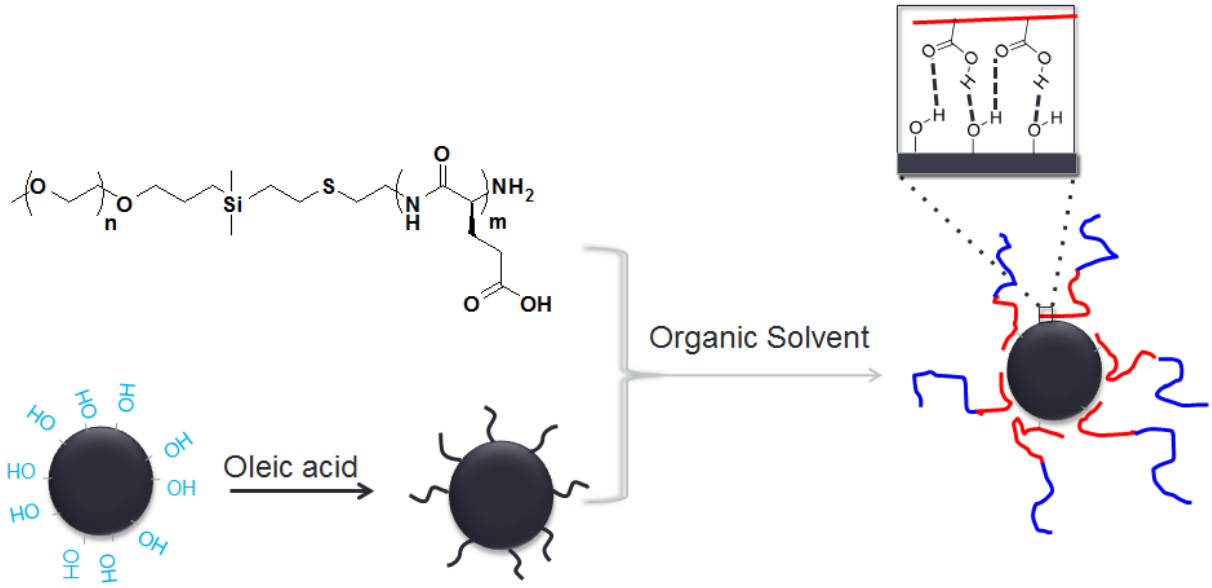

Scheme 4.3.5.1. Synthesis of magnetic block ionomer complexes.

The compositions of the complexes determined by TGA were close to the targets (Table 4.3.5.1). The intensity average hydrodynamic diameters of the nanoparticles were measured by DLS (Table 4.3.5.1). Intensity weighted diameters are reported due to their sensitivity to the presence of aggregates (since they scale with radii to the 6th power).[38] The average hydrodynamic size of the complex made from the mixed solvent was smaller than that prepared from chloroform. This was attributed to better solubility of the poly(L-glutamic acid) block in the mixed solvent. Thus, adsorption from the mixed solvent was considered a superior method. Based on our previous work, it appeared that phosphate salts from PBS could displace carboxylate anchor groups if they were only present as endgroups.[38,48,49] In this work, the stability of the glutamate anchor groups in binding to the iron oxide surface was evaluated in PBS containing 0.14 M NaCl. Dispersions of the complexes prepared from the mixed solvent system were stable in PBS for up to 1 week

(Figure 4.3.5.1). This was attributed to cooperative binding that was obtained due to the polymeric nature of the poly(L-glutamate) block.

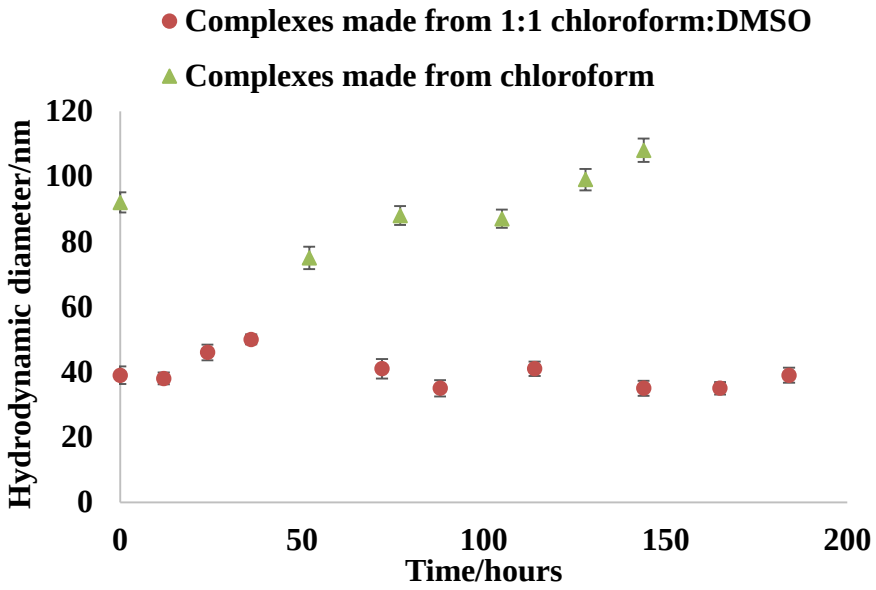

Figure 4.3.5.2. Colloidal stability in phosphate buffered saline of iron oxide-PEO-*b*-poly(L-glutamic acid) complexes made in organic solvents.

PEO-*b*-poly(L-glutamic acid) was also coated onto the iron oxide nanoparticles from water with adjustment of the pH to 9 to provide a clear dispersion. The complex prepared in the aqueous dispersion contained 57 wt % of polymer, which was significantly lower than the targeted 67 wt %. Moreover, this complex precipitated within one hour of exposure to PBS (Figure 4.3.5.2). The low polymer composition and instability of the complex were attributed to electrostatic repulsion between the poly(L-glutamate) block and the iron oxide surface, which were both negatively charged in water at pH 9. Thus, once again the method for preparing these complexes from the mixed chloroform/DMSO solution was considered superior.

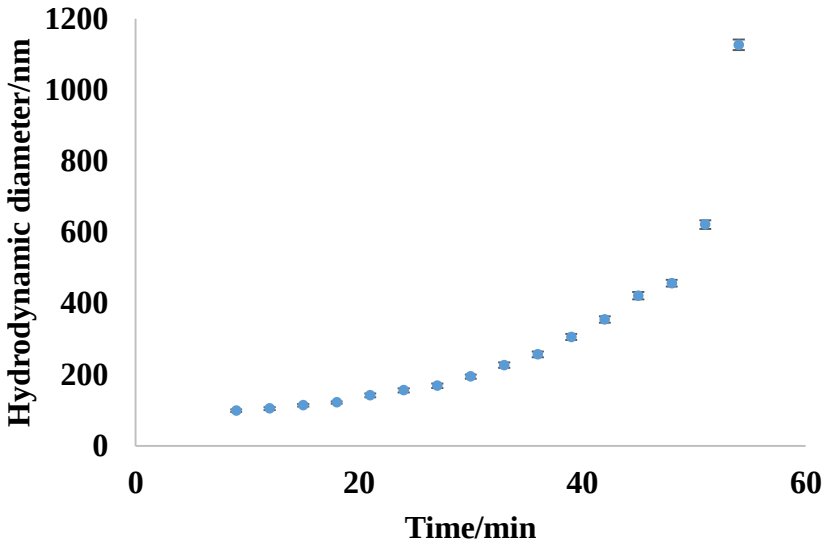

Figure 4.3.5.2. Colloidal instability in phosphate buffered saline of the iron oxide-PEO-*b*-poly(L-glutamic acid) complexes made in water at pH 9.

Table 4.3.5.1. Properties of the iron oxide/PEO-*b*-PG complexes.

Solvent system	Target wt% of polymer	Obtained wt% of polymer	Size (D_I/nm)	PDI
Water (pH=9)	67%	52%	83	0.15
Chloroform	67%	70%	81	0.12
Chloroform/DMSO	67%	65%	40	0.25

A TEM image of the non-crosslinked particles that were prepared in the mixed chloroform/DMSO solvent (Figure 4.3.5.3) showed that they dispersed well in aqueous media. The average diameter of the single particles obtained from a log-normal fit to the measured particle sizes was 7.38 ± 0.26 nm.

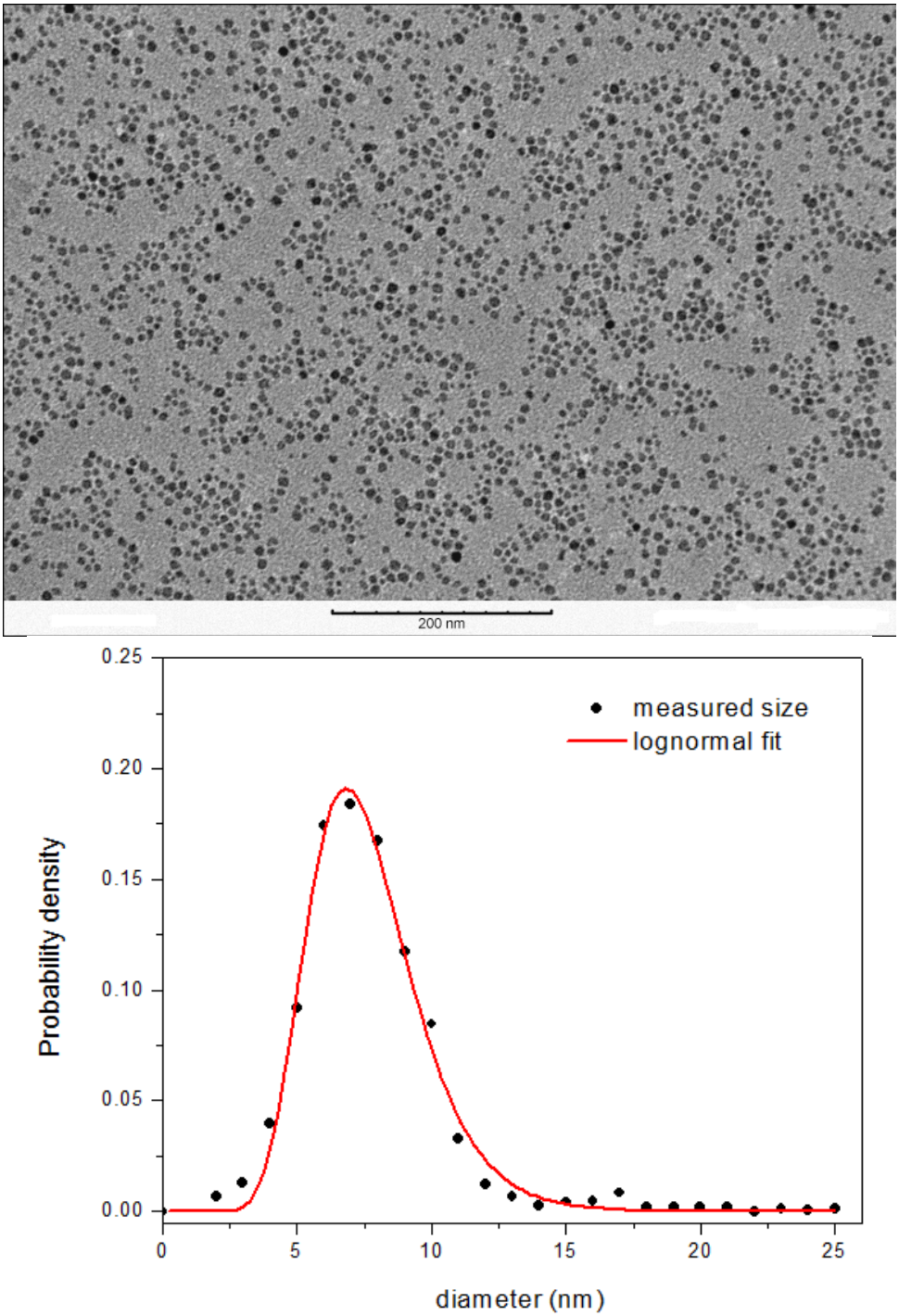

Figure 4.3.5.3. TEM of magnetic single particles made from the mixed chloroform/DMSO solvents and size analysis from a lognormal fit.

4.3.6 Synthesis of magnetic clusters.

Allyl- and thiol-functional poly(ethylene oxide)-*b*-poly(L-glutamic acid) were also coated onto the iron oxide nanoparticles through ligand adsorption from a mixed 1:1 v:v chloroform:DMSO solvent to form primarily single particles with functional groups on the outer PEO ends. Clusters were formed from these complexes by 1) crosslinking the allyl-tipped single particles with dithiol-PEO (Cluster 1), 2) crosslinking the thiol-tipped single particles with diallyl-PEO (Cluster 2) and 3) crosslinking two of the functional single particles with each other (Cluster 3). A 1:1 ratio of allyl to thiol groups was utilized in each case. The intensity average hydrodynamic diameters of the particles increased significantly after crosslinking (Table 4.3.7.1), which confirmed the formation of clusters. Cluster 1 had smaller size (D_I=67 nm) than cluster 2 (D_I=104 nm) due to the radical initiated polymerization of the outer allyl groups on each allyl-tipped single particle. Cluster 3 had the largest average size (D_I=165 nm), and this was attributed to the existence of iron oxide in both allyl- and thiol-crosslink species as well as the reduction of undesirable intra-particle crosslink by avoiding the use of bifunctional PEOs. Thus, crosslinking two of the functional single particles with each other was considered the superior method. TEM image of crosslinked particles (Figure 4.3.6.1) also confirmed the formation of clusters. The clusters were stable in PBS for up to 1 week (Figure 4.3.6.2).

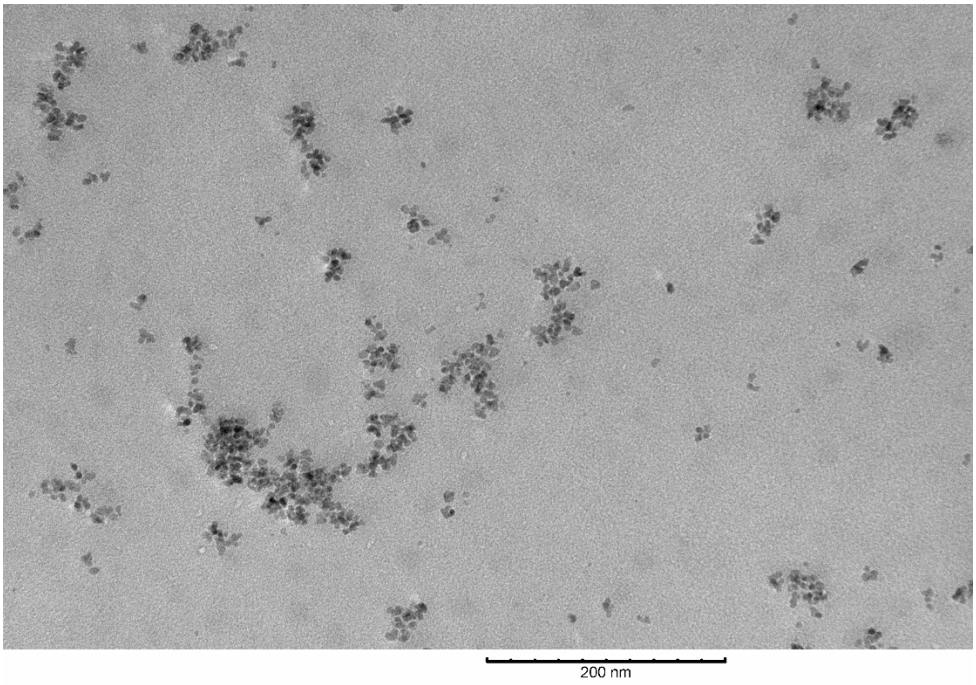

Figure 4.3.6.1. TEM of magnetic clusters 3.

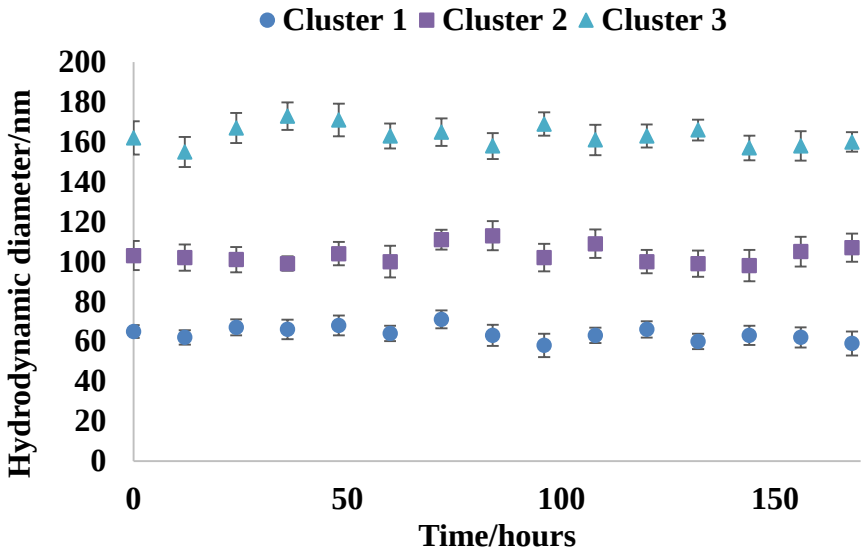

Figure 4.3.6.2. Colloidal stability in phosphate buffered saline at 25 ºC of magnetic clusters.

4.3.7 Magnetic Properties of iron oxide/PEO-b-poly(L-glutamic acid) complexes

The magnetic properties of the oleic acid-coated iron oxide nanoparticles were characterized via SQuID analysis. Hysteresis loops revealed that the complexes were superparamagnetic at 300 K with a saturation magnetization of 50 emu g^{-1} (Figure 4.3.7.1). The composition of the oleic acid-coated iron oxide nanoparticles determined by TGA was 79 wt % of iron oxide, and this corresponded to a saturation magnetization of ~64 emu g^{-1} of iron oxide. This value corresponded to ~88 emu g^{-1} of Fe and was consistent with the values reported for Fe_3O_4 nanoparticles with similar size.[50]

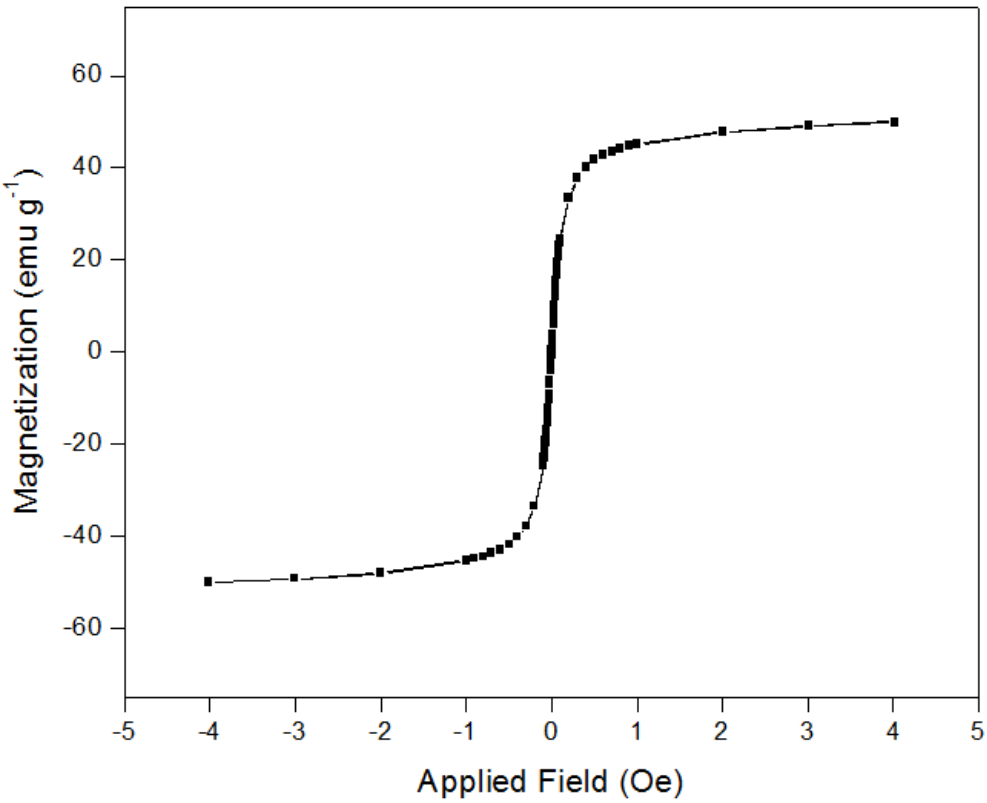

Figure 4.3.7.1. Hysteresis loop of oleic acid-coated iron oxide nanoparticles at 300K.

There is great interest in development of superparamagnetic iron oxide nanoparticles as MRI contrast agents. Localized field gradients generated by these particles in applied

magnetic fields result in rapid dephasing of the proton spins, thus increasing transverse relaxivities (r_2).[51,52] The complexes (without functional PEO tips) made from the mixed chloroform/DMSO solvent (D_I=40 nm) and those made in chloroform (D_I=81 nm) had transverse relaxivities of 43 and 64 s^{-1}(mM Fe)$^{-1}$ respectively (Figure 4.3.7.2). Faster transverse NMR relaxivities of the complex made from chloroform also suggested its larger size according to a recent finding by our group that controlled aggregation led to considerably shorter T_2 relaxation times (higher r_2 relaxivities).[35,36,53] Transverse relaxivities of the allyl-tipped single particles and their clusters were measured under the same condition as well. The allyl-tipped single particles had a transverse relaxivity (44 s^{-1}(mM Fe)$^{-1}$) close to the non-functional single particles (43 s^{-1}(mM Fe)$^{-1}$) as expected since their intensity average diameters were close (38 and 40 nm respectively). The clusters had r_2 relaxivities increasing from 72 to 243 and 368 (s-mM Fe)$^{-1}$ as the sizes increased from 67 to 104 and 165 nm. This result was in agreement with a recent report by Pothayee *et al.* that relaxivities of magnetic particles were related to their sizes.[35,36]

It was also found that the relaxivities of the clusters were affected by the hydrophilicities of the inner spaces. The magnetic clusters reported by Pothayee *et al.*[35,36] were synthesized from ~7 nm iron oxide nanoparticles (similar to the iron oxide used in this research) coated with amino-3.5K poly(ethylene oxide)-*b*-6.8K poly(acrylic acid) (PEO-*b*-PAA) diblock copolymers and crosslinked with a poly(ethylene oxide) diacrylate (Mn=700). The clusters coated with PEO-*b*-PAA had r_2s of 410 s^{-1} mM Fe^{-1} (D_I=143 nm) and 604 s^{-1} mM Fe^{-1} (D_I=181 nm), which were higher than the cluster 3 (DI=165 nm, r2=368 s^{-1} mM Fe^{-1}) in this research. This was attributed to the greater amount of the anionic groups (94 acrylic acids) per chain on the PEO-*b*-PAA copolymer than those (16 glutamic acids) on the PEO-

b-PG copolymer. The anionic groups made the intra-clusters spaces more accessible to water molecules and resulted in higher r_2s. Another set of magnetic clusters were synthesized by Balasubramaniam *et al.* with similar iron oxide cores (~7 nm) with a poly(ethylene oxide)-b-poly(D,L-lactide) diblock copolymer. These clusters had hydrophobic inner structures that led to lower r_2s. For example, particles with hydrophobic-cores and an intensity-average diameter of 147 nm had an r_2 of 202 s^{-1} mM Fe^{-1}.

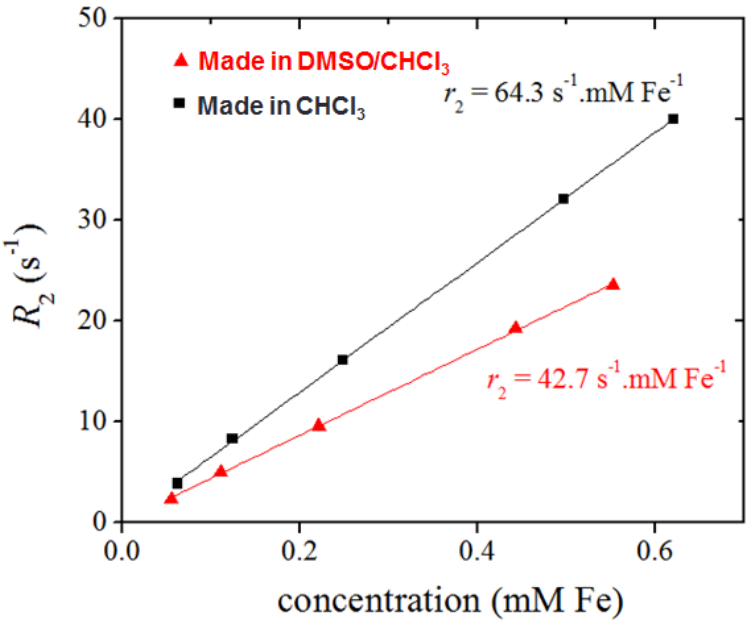

Figure 4.3.7.2. Transverse relaxivities of the single iron oxide-PEO-*b*-poly(L-glutamic acid) complexes made from the mixed solvent (D_I=40 nm) and from chloroform (D_I=81 nm).

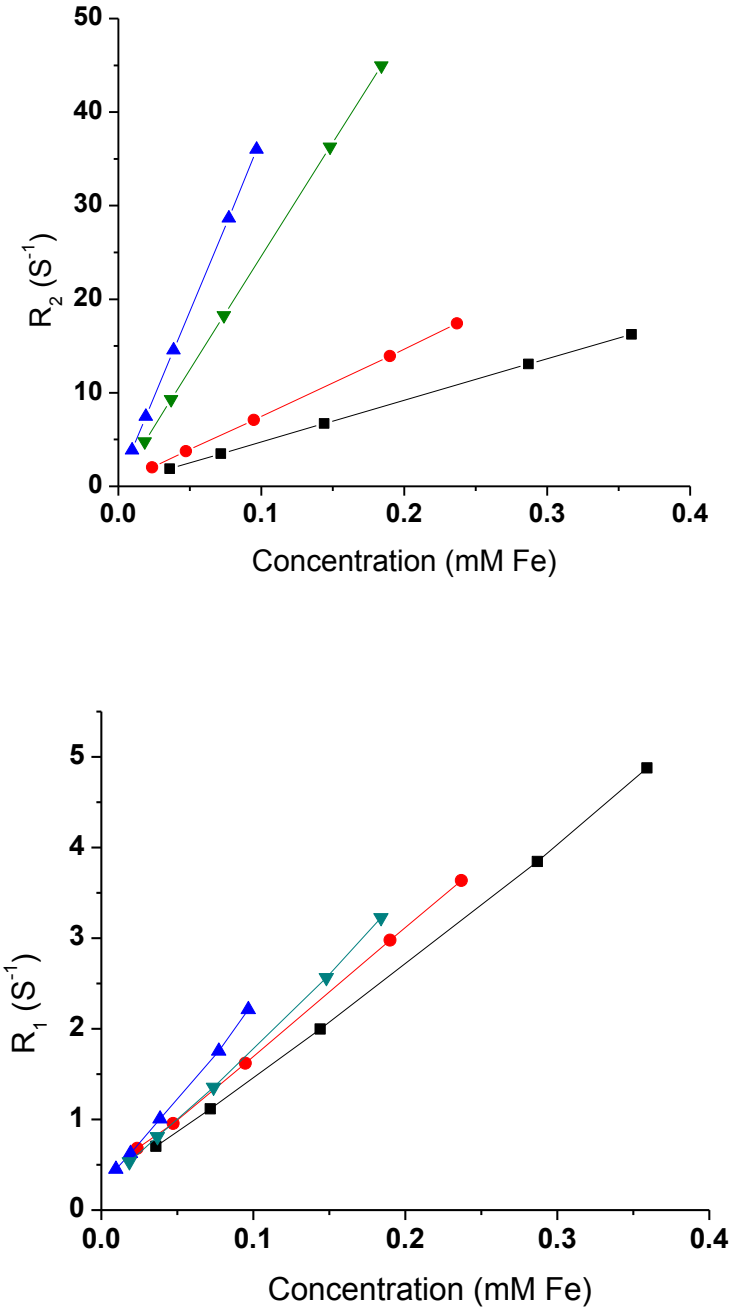

Figure 4.3.7.3. Transverse relaxivities (top) and longitudinal relaxivities (bottom) of the iron oxide-PEO-*b*-poly(L-glutamic acid) clusters.

Table 4.3.7.1. Sizes, transverse relaxivities and longitudinal relaxivities of the iron oxide-PEO-*b*-poly(L-glutamic acid) complexes.

Sample	Obtained wt% of polymer	D_I (nm)	PDI	r_2 (s^{-1} mM Fe^{-1})	r_1 (s^{-1} mM Fe^{-1})
Single Particles	65%	38	0.18	44	13
Clusters 1	66%	67	0.26	72	14
Clusters 2	65%	104	0.17	243	16
Clusters 3	67%	165	0.18	368	20

4.4 Conclusions

Diblock copolymers of PEO-*b*-poly(L-glutamic acid) were synthesized and coated on iron oxide nanoparticles via ligand adsorption in a chloroform/DMSO mixed organic solvent, thus yielding biodegradable magnetic block ionomer complexes. Dispersions of these complexes in media simulating physiological conditions were colloidally stable for up to a week.

Allyl- and thiol-poly(ethylene oxide)-*b*-poly(L-glutamic acid) were also synthesized and coated onto the iron oxide nanoparticles. Biodegradable magnetic clusters were prepared by three methods and crosslinking two of the functional single particles with each other was determined to be the best one. The clusters were determined to have higher relaxivities than the single particles and have great potential as an MRI contrast agent.

4.5 Acknowledgements

The authors are grateful for the financial support from NSF under contract DMR 0805179.

4.6 References

(1) Deming, T. J. *Adv. Drug Delivery Rev.* 2002, *54*, 1145.

(2) Dos Santos, S.; Chandravarkar, A.; Mandal, B.; Mimna, R.; Murat, K.; Saucede, L.; Camus, M.; Tuchscherer, G.; Mutter, M. *Biopolymers* 2005, *80*, 568.

(3) Dos Santos, S.; Chandravarkar, A.; Mandal, B.; Mimna, R.; Murat, K.; Saucede, L.; Tella, P.; Tuchscherer, G.; Mutter, M. *J. Am. Chem. Soc.* 2005, *127*, 11888.

(4) Lu, H.; Cheng, J. J. *J. Am. Chem. Soc.* 2007, *129*, 14114.

(5) Mart, R. J.; Osborne, R. D.; Stevens, M. M.; Ulijn, R. V. *Soft Matter.* 2006, *2*, 822.

(6) Wang, X. Y.; Kim, H. J.; Wong, C.; Vepari, C.; Matsumoto, A.; Kaplan, D. L. *Mater. Today* 2006, *9*, 44.

(7) Li, C. *Adv. Drug Delivery Rev.* 2002, *54*, 695.

(8) Li, C.; Price, J. E.; Milas, L.; Hunter, N. R.; Ke, S.; Yu, D. F.; Charnsangavej, C.; Wallace, S. *Clin. Cancer Res.* 1999, *5*, 891.

(9) Li, C.; Yu, D. F.; Newman, R. A.; Cabral, F.; Stephens, L. C.; Hunter, N.; Milas, L.; Wallace, S. *Cancer Res.* 1998, *58*, 2404.

(10) Harris, L. A.; Goff, J. D.; Carmichael, A. Y.; Riffle, J. S.; Harburn, J. J.; St Pierre, T. G.; Saunders, M. *Chem. Mater.* 2003, *15*, 1367.

(11) Fahlvik, A. K.; Holtz, E.; Schroder, U.; Klaveness, J. *Invest. Radiol.* 1990, *25*, 793.

(12) Miller, W. G. *J. Am. Chem. Soc.* 1964, *86*, 3913.

(13) Pytela, J.; Kotva, R.; Metalova, M.; Rypacek, F. *Int. J. Biol. Macromol.* 1990, *12*, 241.

(14) Dolnik, V.; Novotny, M.; Chmelik, J. *Biopolymers* 1993, *33*, 1299.

(15) Tsutsumi, A.; Perly, B.; Forchioni, A.; Chachaty, C. *Macromolecules* 1978, *11*, 977.

(16) Horak, D.; Babic, M.; Jendelova, P.; Herynek, V.; Trchova, M.; Pientka, Z.; Pollert, E.; Hajek, M.; Sykova, E. *Bioconjugate Chem.* 2007, *18*, 635.

(17) Cho, C. S.; Nah, J. W.; Jeong, Y. I.; Cheon, J. B.; Asayama, S.; Ise, H.; Akaike, T. *Polymer* 1999, *40*, 6769.

(18) Lutz, J. F.; Stiller, S.; Hoth, A.; Kaufner, L.; Pison, U.; Cartier, R. *Biomacromolecules* 2006, *7*, 3132.

(19) Cho, C. S.; Kim, S. W.; Komoto, T. *Makromol. Chem.* 1990, *191*, 981.

(20) Pothayee, N.; Pothayee, N.; Jain, N.; Hu, N.; Balasubramaniam, S.; Johnson, L. M.; Davis, R. M.; Sriranganathan, N.; Riffle, J. S. *Chem. Mater.* 2012.

(21) Pothayee, N.; Balasubramaniam, S.; Davis, R. M.; Riffle, J. S.; Carroll, M. R. J.; Woodward, R. C.; Pierre, T. G. S. *Polymer* 2011, *52*, 1356.

(22) Cho, C. S.; Jeong, Y. I.; Kim, S. H.; Nah, J. W.; Kubota, M.; Komoto, T. *Polymer* 2000, *41*, 5185.

(23) Tanaka, M.; Mori, A.; Imanishi, Y.; Bamford, C. H. *Int. J. Biol. Macromol.* 1985, *7*, 173.

(24) Tansey, W.; Ke, S.; Cao, X. Y.; Pasuelo, M. J.; Wallace, S.; Li, C. *J. Controlled Release* 2004, *94*, 39.

(25) Yang, Z. Q.; Zhang, Y. H.; Markland, P.; Yang, V. C. *J. Biomed. Mater. Res.* 2002, *62*, 14.

(26) Yokoyama, M.; Miyauchi, M.; Yamada, N.; Okano, T.; Sakurai, Y.; Kataoka, K.; Inoue, S. *Cancer Res.* 1990, *50*, 1693.

(27) Cabral, H.; Nishiyama, N.; Okazaki, S.; Koyama, H.; Kataoka, K. *J. Controlled Release* 2005, *101*, 223.

(28) Menahem, T.; Pravda, M.; Mastai, Y. *Chirality* 2009, *21*, 862.

(29) Zou, Y. Y.; Wu, Q. P.; Tansey, W.; Chow, D.; Hung, M. C.; Vej, C. C.; Wallace, S.; Li, C. *Int. J. Oncol.* 2001, *18*, 331.

(30) Singer, J. W.; De Vries, P.; Bhatt, R.; Tulinsky, J.; Klein, P.; Li, C.; Milas, L.; Lewis, R. A.; Wallace, S. *Ann. Ny. Acad. Sci.* 2000, *922*, 136.

(31) Singer, J. W.; Bhatt, R.; Tulinsky, J.; Buhler, K. R.; Heasley, E.; Klein, P.; de Vries, P. *J. Controlled Release* 2001, *74*, 243.

(32) Hoes, C. J. T.; Grootoonk, J.; Duncan, R.; Hume, I. C.; Bhakoo, M.; Bouma, J. M. W.; Feijen, J. *J. Controlled Release* 1993, *23*, 37.

(33) Hoes, C. J. T.; Vanheeswijk, W. A. R.; Degrooth, B.; Mud, J.; Greve, J.; Feijen, J. *Pharm. Weekblad* 1985, *7*, 26.

(34) Zunino, F.; Pratesi, G.; Micheloni, A. *J. Controlled Release* 1989, *10*, 65.

(35) Pothayee, N.; Pothayee, N.; Jain, N.; Hu, N.; Balasubramaniam, S.; Johnson, L. M.; Davis, R. M.; Sriranganathan, N.; Riffle, J. S. *Chem. Mater.* 2012, *24*, 2056.

(36) Pothayee, N.; Balasubramaniam, S.; Pothayee, N.; Jain, N.; Hu, N.; Lin, Y. N. A.; Davis, R. M.; Sriranganathan, N.; Koretsky, A. P.; Riffle, J. S. *J. Mater. Chem. B* 2013, *1*, 1142.

(37) Vadala, M. L.; Thompson, M. S.; Ashworth, M. A.; Lin, Y.; Vadala, T. P.; Ragheb, R.; Riffle, J. S. *Biomacromolecules* 2008, *9*, 1035.

(38) Goff, J. D.; Huffstetler, P. P.; Miles, W. C.; Pothayee, N.; Reinholz, C. M.; Ball, S.; Davis, R. M.; Riffle, J. S. *Chem. Mater.* 2009, *21*, 4784.

(39) Thompson, M. S.; Vadala, T. P.; Vadala, M. L.; Lin, Y.; Riffle, J. S. *Polymer* 2008, *49*, 345.

(40) Pinna, N.; Grancharov, S.; Beato, P.; Bonville, P.; Antonietti, M.; Niederberger, M. *Chem. Mater.* 2005, *17*, 3044.

(41) Wang, L. Y.; Wang, S. G.; Bei, J. Z. *Polym. Advan. Technol.* 2004, *15*, 617.

(42) Deming, T. J. *Adv. Polym. Sci.* 2006, *202*, 1.

(43) Yokoyama, M.; Kwon, G. S.; Okano, T.; Sakurai, Y.; Seto, T.; Kataoka, K. *Bioconjugate Chem.* 1992, *3*, 295.

(44) Osada, K.; Christie, R. J.; Kataoka, K. *J. R. Soc. Interface* 2009, *6*, S325.

(45) Nishiyama, N.; Yokoyama, M.; Aoyagi, T.; Okano, T.; Sakurai, Y.; Kataoka, K. *Langmuir* 1999, *15*, 377.

(46) Daly, W. H.; Poche, D. *Tetrahedron Lett.* 1988, *29*, 5859.

(47) Blout, E. R.; Karlson, R. H. *J. Am. Chem. Soc.* 1956, *78*, 941.

(48) Miles, W. C.; Goff, J. D.; Huffstetler, P. P.; Reinholz, C. M.; Pothayee, N.; Caba, B. L.; Boyd, J. S.; Davis, R. A.; Riffle, J. S. *Langmuir* 2009, *25*, 803.

(49) Miles, W. C.; Huffstetler, P. P.; Goff, J. D.; Chen, A. Y.; Riffle, J. S.; Davis, R. M. *Langmuir* 2011, *27*, 5456.

(50) Jun, Y. W.; Huh, Y. M.; Choi, J. S.; Lee, J. H.; Song, H. T.; Kim, S.; Yoon, S.; Kim, K. S.; Shin, J. S.; Suh, J. S.; Cheon, J. *J. Am. Chem. Soc.* 2005, *127*, 5732.

(51) Josephson, L.; Lewis, J.; Jacobs, P.; Hahn, P. F.; Stark, D. D. *Magn. Reson. Imaging* 1988, *6*, 647.

(52) Jung, C. W.; Jacobs, P. *Magn. Reson. Imaging* 1995, *13*, 661.

(53) Carroll, M. R. J.; Huffstetler, P. P.; Miles, W. C.; Goff, J. D.; Davis, R. M.; Riffle, J. S.; House, M. J.; Woodward, R. C.; St Pierre, T. G. *Nanotechnology* 2011, *22*.

Chapter 5. Synthesis and Characterization of Heterobifunctional Triblock Copolyethers

Most of the work described in this chapter was performed by the author of this dissertation. He was solely responsible for the synthesis and characterization of the initiators and polymers. Drs. Xiang Yi and Jing Tong of the Dr. Alexander V. Kabanov's group prepared and characterized the polymer-superoxide dismutase conjugates.

5.1 Introduction

Amphiphilic copolyethers, particularly triblock copolyethers based on poly(ethylene oxide-*b*-propylene oxide-*b*-ethylene oxide) (PEO-*b*-PPO-*b*-PEO) (the BASF tradename is Pluronics®) are well established, and they have been studied extensively as excipients in drug formulations.[1-20] At present, a wide range of molecular weights of Pluronics® are commercially available. Above the critical micelle concentration (CMC), PEO-*b*-PPO-*b*-PEO can form spherical micelles in aqueous solution by self-assembly, with PEO blocks forming the shells and PPO blocks forming the cores. Drugs that have poor solubility in water can potentially be loaded into the hydrophobic cores of PEO-*b*-PPO-*b*-PEO micelles and dispersions of the materials can be stabilized by the PEO shells. This attractive feature makes PEO-*b*-PPO-*b*-PEO copolymers potential drug delivery vehicles. Another important advantage of select Pluronics® as a drug carrier is their ability to inhibit multidrug resistance (MDR) in cancer cells,[21,22] which can significantly decrease the efficacy of many drugs in tumor therapy. MDR is often caused by P-glycoprotein (P-gp), a transmembrane glycoprotein with a molecular weight of 170 kDa which acts as an ATP-dependent drug efflux pump.[21] It results in lower accumulation and retention of drugs in tumor cells. Many studies on the inhibition of efflux action of P-gp by PEO-*b*-PPO-*b*-PEO copolymers have

been reported.[12,13,15-17,23] For instance, Pluronic P85 showed notable capacity for increasing the cytotoxicity of drugs against MDR cells by as much as 1,000 times while only a slight increase of cytotoxicity was observed against sensitive cells.[22]

One major problem in commercial development of therapeutic proteins is their poor transport across cellular membranes and biological barriers such as the blood-brain barrier (BBB). One solution to this problem is to modify proteins with amphiphilic block copolymers such as PEO-*b*-PPO-*b*-PEO, Pluronics®.[1,2,24,25] Kabanov et al. reported that the lengths of both the hydrophobic (PPO) and hydrophilic (PEO) blocks of Pluronics® are important for cellular binding/uptake of such protein-polyether conjugates.[1] However, it isn't possible to independently tune the two PEO block lengths with commercial Pluronics® since a difunctional PPO macroinitator is utilized to grow both PEO blocks simultaneously (HO-EO_n-*b*-PO_m-*b*-EO_n-OH). Another challenge in traditional synthesis of polyethers is to introduce functional groups that allow for post-polymerization functionalization for specific applications. In this study, a series of heterobifunctional asymmetric amino-EO_{n1}-*b*-PO_m-*b*-EO_{n2}-OH block copolymers (APs) with different molecular weights of each block were synthesized and the amino terminal group was conjugated to an antioxidant enzyme, Cu/Zn superoxide dismutase (SOD1). The conjugates were characterized and their cellular uptake was investigated. The three blocks in these polymers are hypothesized to have different functions.

5.2 Experimental

5.2.1 Materials

Tetrahydrofuran (THF, Optima Grade, EMD Chemicals, 99.5%) was refluxed over sodium metal with benzophenone until the solution reached a deep purple, fractionally

distilled, and deoxygenated just prior to use. Acetone, azobisisobutyronitrile (AIBN), ethylene oxide (EO, 99.5+%), 2-mercaptoethylamine hydrochloride, potassium (98%), propylene oxide (PO, ≥99%), sodium iodide (>98%) and 1.0 M vinyl magnesium bromide were purchased from Aldrich and used as received. 3-Chloropropyldimethylchlorosilane and 3-chloropropyltrichlorosilane (Gelest) were used as received. Chloroform, dichloromethane, diethyl ether, methanol, magnesium sulfate, and sodium bicarbonate (Fisher Scientific) were used as received. Ethanol (200 proof) was obtained from Decon Laboratories and used as received. Toluene (Fisher Scientific) was stirred over CaH_2, fractionally distilled, then deoxygenated with N_2 for 30 minutes prior to use. Naphthalene (Aldrich, 99%) was sublimed prior to use. Glacial acetic acid (Aldrich) was diluted with distilled THF to yield a 2.5 M solution. N,N-Dimethylformamide (DMF, EMD Chemicals) was dried over CaH_2, fractionally distilled under vacuum and stored under nitrogen at 25 ℃. A double-metal catalyst, ($Zn_3[Co(CN)_6]_2$) graciously donated by Bayer, was dried at room temperature for 24 h under vacuum and diluted with distilled THF to yield a 4.1 mg mL^{-1} dispersion.

5.2.2 Instrumentation

Spectroscopic analyses of the block copolymers were performed using a Varian Inova 400 NMR and a Varian Unity 400 NMR. Size exclusion chromatography (SEC) in chloroform was conducted with an Alliance Waters 2690 Separations Module with a Viscotek T60A dual viscosity detector and laser refractometer equipped with a Waters HR 0.5 + HR 2 + HR 3 + HR 4 styragel column set at 30 ℃. A Universal calibration was utilized to obtain absolute molecular weights.

5.2.3 Synthesis of 3-hydroxypropyldimethylvinylsilane (3-HPMVS)

3-Hydroxydimethylvinylsilane was synthesized utilizing a modified procedure from our previous work.[26,27] 3-Chloropropyldimethylchlorosilane (20.0 g, 0.12 mol) was added into a dry 500-mL round-bottom flask with a magnetic stir bar. The flask was cooled with an ice bath. A 1.0 M vinylmagnesium bromide/THF solution (240 mL, 0.24 mol) was slowly added over 30 min. The mixture was stirred at RT for 24 h and then diluted with 200 mL of dichloromethane. Saturated aqueous ammonium chloride solution (150 mL) was slowly added and the mixture was transferred to a separatory funnel to remove the aqueous layer. The organic layer was further washed with saturated sodium chloride solution (3 × 150 mL) and dried with anhydrous magnesium sulfate. Dichloromethane was rotary-evaporated yielding a yellow liquid. The product was distilled at 85 ℃, 5 Torr, yielding a colorless liquid (15.2 g, 80%).

3-Chloropropyldimethylvinylsilane (14.4 g, 0.089 mol) and sodium iodide (26.1 g, 0.17 mol) were dissolved in 120 mL of acetone in a 250-mL round-bottom flask equipped with a magnetic stir bar and a condenser. The mixture was stirred under reflux for 24 h and the acetone was removed by rotary evaporation. Dichloromethane (100 mL) was added and the mixture was vacuum filtered to remove the salt. Dichloromethane was rotary-evaporated and the product was distilled under vacuum at 100 ℃, 5 Torr, yielding 3-iodopropyldimethylvinylsilane (19.5 g, 86%).

3-Iodopropyldimethylvinylsilane (18.9 g, 0.074 mol), sodium bicarbonate (9.4 g, 0.11 mol), DI water (14 mL) and hexamethylphosphoramide (50 mL) were added into a 250-mL round-bottom flask with a stir bar. The mixture was stirred at 100 ℃ for 24 h and then cooled to RT and diluted with 30 mL of DI water. The aqueous layer was extracted with diethyl ether (3 × 100 mL) and the organic layer was washed with DI water (3 × 200 mL).

Diethyl ether was removed by rotary evaporation and the product was distilled under vacuum at 100 ℃, 5 Torr, yielding 3-hydroxypropyldimethylvinylsilane (7.5 g, 65%).

5.2.4 Synthesis of dimethylvinylsilylpropyl-PEO-PPO-PEO-OH

An exemplary procedure for synthesis of a 2,700 g mol^{-1} dimethylvinylsilyl-PEO is provided. 3-Hydroxypropyldimethylvinylsilane (1.31 g, 9.1 mmol) was syringed into a flame-dried round-bottom flask followed by adding a double metal cyanide catalyst/THF suspension (0.65 mL, 2.9 mg of the catalyst). The mixture was stirred at RT for 24 h to adsorb the initiator onto the heterogeneous catalyst. A 300-mL, high-pressure Series 4561 Parr reactor was utilized for the polymerization. EO (25 g, 0.57 mol) was distilled from a lecture bottle into the pressure reactor cooled with an isopropanol-dry ice bath, then the Parr reactor was charged with 30 psi of ultrahigh purity nitrogen gas. The initiator solution was added to the Parr reactor via syringe and heated to 115 °C with stirring. A maximum pressure (~400 psi) and exotherm temperature (~165 °C) were noted followed by a gradual pressure decrease to ~82 psi. Once an equilibrium pressure was achieved (~3 h), the reactor was cooled to RT and the contents were diluted with ~100 mL of dichloromethane. The solution was filtered through Celite® twice to remove the double metal catalyst. The filtrate was concentrated to ~30 mL followed by precipitation of the polymer in diethyl ether cooled with isopropanol-dry ice bath. The product was dried under vacuum at RT yielding a white solid (19.5 g, 75%).

A 2,700 g mol^{-1} dimethylvinylsilyl-PEO homopolymer (10.5 g, 3.9 mol) was utilized as a macroinitiator for synthesis of a diblock dimethylvinylsilyl-PEO-PPO copolymer. The homopolymer was added to a 250-mL round-bottom flask and dried under vacuum at 60 °C overnight, then 30 mL of THF were added to dissolve the macroinitiator. A double

metal cyanide catalyst/THF suspension (1.4 mL, 5.5 mg of the catalyst) was added to the flask and the mixture was stirred for a day at RT. Ultrahigh purity nitrogen gas (20 psi) was charged to a clean and dry 300-mL, high-pressure Series 4561 Parr reactor followed by addition of PO (9.2 mL, 7.7 g, 0.11 mol). The macroinitiator suspension was added to the Parr reactor and heated to 115 °C with stirring. A maximum pressure (~140 psi) and exotherm temperature (166 °C) were noted followed by a gradual pressure decrease to ~90 psi. Once an equilibrium pressure was achieved (~5 h), the reactor was cooled to RT and the contents were diluted with ~200 mL of chloroform. The solution was filtered through Celite® twice to remove the metal catalyst. The filtrate was concentrated to ~30 mL, then the solution was precipitated by adding it into diethyl ether cooled with isopropanol-dry ice bath. The product was dried under vacuum at RT yielding a white solid (17.5 g, 96%).

A triblock dimethylvinylsilyl-PEO-PPO-PEO copolymer was synthesized by anionic ring-opening polymerization of EO initiated by a diblock dimethylvinylsilyl-PEO-PPO copolymer. A potassium naphthalide solution was prepared. Naphthalene (4.2 g, 33 mmol) was sublimed and added into a 250-mL, flame-dried, round-bottom flask equipped with a glass stir bar. Dry THF (27 mL) was syringed into the flask to dissolve the naphthalene. Potassium metal (1.23 g, 0.32 mol) was sliced and added to the flask under nitrogen and the mixture was stirred at RT overnight yielding a dark green solution. The solution was titrated in triplicate with 1 M HCl solution using bromothymol blue in methanol as an indicator. The concentration of potassium naphthalene was 1.04±0.03 M. A dimethylvinylsilyl-PEO-PPO (M_n = 4,700 g mol^{-1}, 17.4 g, 3.7 mmol) was dried under vacuum at 60 °C for 24 hours, and then dissolved in THF (40 mL). A potassium naphthalide solution (3.6 mL, 1.7 mmol) was added to the polymer solution to deprotonate the terminal

hydroxyl group. EO (4.5 g, 0.10 mol) was distilled from a lecture bottle into a 300-mL, high-pressure Series 4561 Parr cooled with an isopropanol-dry ice bath. The macroinitiator solution was added to the reactor via syringe and stirred for 24 hours at RT. Acetic acid (5 mL of a 0.93 M solution in THF, 4.6 mmol) was added to the pressure reactor via syringe to terminate the polymerization. The pressure reactor was purged with N_2 for 1 h, then the contents were transferred to a 250-mL round-bottom flask. THF was removed by rotary evaporation and the product was dissolved in 200 mL of dichloromethane. The product was washed with DI water (3 X 150 mL). The organic layer was rotary-evaporated to remove most of the dichloromethane and the polymer was dried under vacuum at 60 °C for 24 h (17.6 g, 80%).

5.2.5. Ammonium functionalization of dimethylvinylsilylpropyl-PEO-PPO-PEO-OH

A triblock monoammonium-PEO-PPO-PEO copolymer was obtained via ene-thiol addition of cysteamine hydrochloride across the terminal vinyl group. In a characteristic procedure, a 5,200 g mol^{-1} dimethylvinylsilylpropyl-PEO-PPO-PEO-OH (15 g, 2.9 mmol), cysteamine hydrochloride (0.66 g, 5.8 mmol), and AIBN (0.09g, 0.55 mmol) were dissolved in DMF (100 mL) in a 250-mL round-bottom flask equipped with a stir bar. The solution was purged with ultrahigh purity nitrogen gas at RT for 20 min. The reaction was conducted at 80 ℃ for 24 h with stirring, then the mixture was cooled to RT. The mixture was diluted with dichloromethane (100 mL). The organic layer was washed with a saturated sodium bicarbonate aqueous solution (3×100 mL) followed by washing with DI water (2×100 mL). Dichloromethane was removed by rotary-evaporation and the product was dried under vacuum at 60 ℃ overnight yielding a waxy solid (11.9 g, 79%).

5.2.6. Synthesis and characterization of SOD1-polymer conjugates

The monoamino-functional asymmetric block polymers and monoaminofunctional Pluronic® P85 were conjugated to SOD1. Each polymer (10 mg) was mixed with a 20-fold molar excess of disuccinimidyl suberate (DSS) in 0.9 mL of DMF. The mixture was supplemented with 0.1 mL of sodium borate buffer (0.1 M, pH 8.0) and incubated for 30 min at 25 ℃. Excess DSS was removed by gel filtration on a Sephadex LH-20 column (2.5 x 20 cm) in anhydrous CH_2Cl_2 and the solvent was removed *in vacuo*. The activated polymer was dissolved in 1 mL of 20% aq. ethanol and mixed with 2 mg of SOD1 (moles of polymer to SOD1 was 20:1) in 0.5 mL of sodium borate (0.1 M, pH 8.0). The mixture was incubated overnight at 4 ℃. The conjugates were purified on a Tosoh Bioscience TSKgel G3000SW (7.8 mm x 30 cm) column in 0.1 M Na_3PO_4/0.2 M NaCl (pH 7.4) containing 5% methanol (elution rate: 1 mL/min, detection at 220 nm). The fractions containing the conjugates were desalted and lyophilized.

The products were analyzed by electrophoresis (SDS-PAGE) and mass spectrometry to characterize their compositions and sizes. A 2,4,6-trinitrobenzenesulfonic acid (TNBS) assay was utilized to determine the degree of modification. Ten microliters of SOD1-polymer conjugate solutions (protein concentration 0.1-0.6 mg/mL) were mixed with 10 μL of TNBS solution (1.7 mM) in 80 μL of sodium borate buffer (0.1 M, pH 9.5) and incubated at 37 ℃ for 2 h. The absorbance was measured at 405 nm using the microplate reader. The degree of modification (average number of amino groups modified) was calculated according to the equation:

$$S\ (modification\ degree) = 11\ \times \frac{A_{native}/C_{native} - A_{modified}/C_{modified}}{A_{native}/C_{native}}$$

where A_{native} and $A_{modified}$ were the absorbences and C_{native} and $C_{modified}$ were the concentrations of native and modified SOD1, respectively. The total number of primary amino groups in SOD1 is 11.

Enzymatic activity of the conjugates was measured using a pyrogallol auto-oxidation assay. Pyrogallol autoxidation in the presence of $O_2^{\bullet-}$ occurs rapidly at pH < 9.5 and yields a chromophore that absorbs at 420 nm. SOD1 catalyzes the dismutation of $O_2^{\bullet-}$ and thus inhibits pyrogallol autoxidation. As such, the enzymatic activity of SOD1 or SOD1–polymer conjugates can be determined in a kinetic assay by measuring the absorbance of oxidized pyrogallol in the presence of various amounts of enzyme. Briefly, 20 μl of 0.0002 to 200 μg/mL of SOD1 or SOD1–polymer conjugate samples in distilled water was mixed with 20 μL of a fresh solution of pyrogallol (0.5 mg/mL) in distilled water and then supplemented with Tris–HCl buffer (0.1 M, pH 8) containing 1 mM pentetic acid to a final volume of 200 μL. In control experiments, mixtures of distilled water without enzyme and/or without pyrogallol were utilized. The reaction mixtures were added to 96-well plates in triplicate and the rates of autoxidation were measured immediately as slopes by recording increases in absorbance at 420 nm up to 10 min in the microplate reader SpectraMax M5. The data were interpreted as the inhibition rate (%) using the equation $[(S_1-S_S)/(S_1-S_2)]\times100\%$, where S_1 is the slope for enzyme-free water with pyrogallol, S_2 is the slope for enzyme-free water without pyrogallol, and S_S is the slope of the sample with pyrogallol. The residual activity of modified SOD1 was expressed on a percentage basis of unmodified enzyme.

5.2.7 Cellular uptake of SOD1-polymer conjugates

MDCK cells (from ATCC, CCL-34) were seeded in 24-well plates at a density of 50,000 cells/well in Dulbecco's Modified Eagle Medium (DMEM) supplemented with 1% penicillin/streptomycin and 10% fetal bovine serum. Cells were cultured for two days to reach 80~90% confluence. For uptake experiments, the cells were treated with SOD1 or SOD1-polymer conjugates at 100 μg/mL for 24 h in serum-free conditions, washed 3X with cold phosphate-buffered saline (PBS) and then collected by treating with 0.05% trypsin. Cell pellets were lysed by sonication and total cellular protein was measured using a MicroBCA assay. Cell lysates (50 uL) were used for ELISA to determine the concentration of cellular SOD1. Unmodified SOD1 or SOD1 conjugates at concentrations from 0.1 to 50 ng/mL were used as calibration standards. Data were interpreted as cellular SOD1 concentration normalized by cell protein content. Statistical analysis was performed using one-way ANOVA (LSD multiple comparisons). A minimum *p* value of 0.05 was regarded as the significance level.

5.3 Results and discussion

5.3.1 Synthesis of 3-hydroxypropyldimethylvinylsilane (3-HPMVS)

To prepare a heterobifunctional polyether, 3-hydroxypropyldimethylvinylsilane was synthesized and utilized as an initiator (Scheme 5.3.1.1), in which the vinyl group allowed post-polymerization functionalization. 3-Chloropropyldimethylvinylsilane was synthesized by a Grignard reaction of 3-chloropropyldimethylchlorosilane with vinylmagnesium bromide. ^{1}H NMR was utilized to confirm the conversion of chlorine next to the silicon to a vinyl group by observing the appearance of resonances at 5.7-6.2 ppm (Figure 5.3.1.1). The other chlorine was stable against the Grignard reagent according to

the integration of vinyl group. The remaining chlorine was substituted by iodine to make a better leaving group for hydrolysis. This substitution reaction was conducted in acetone since the sodium chloride by-product is not soluble in acetone and thus, the equilibrium is moved toward the iodide product. The substitution was monitored by the resonance corresponding to the methylene next to the halide, which shifted from 3.50 to 3.18 ppm (Figure 5.3.1.2). The iodide was then hydrolyzed yielding 3-hydroxypropyldimethylvinylsilane. This conversion was confirmed by the shift of the terminal methylene peak from 3.18 to 3.54 ppm (Figure 5.3.1.3).

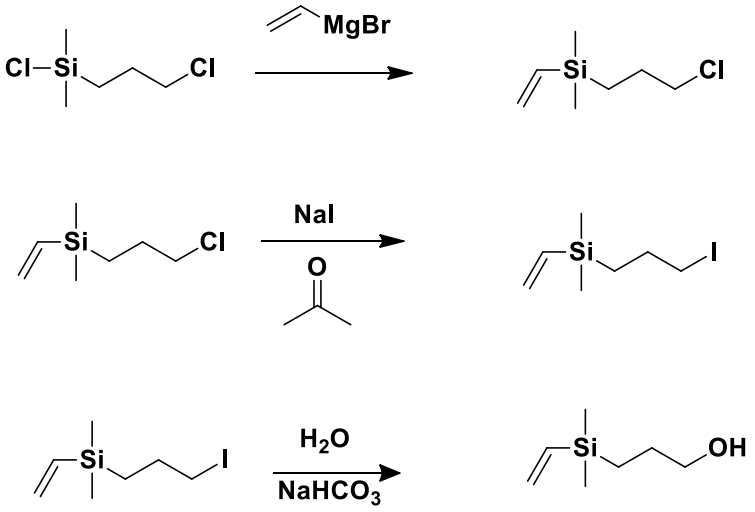

Scheme 5.3.1.1. Synthesis of 3-hydroxypropyldimethylvinylsilane (3-HPMVS).

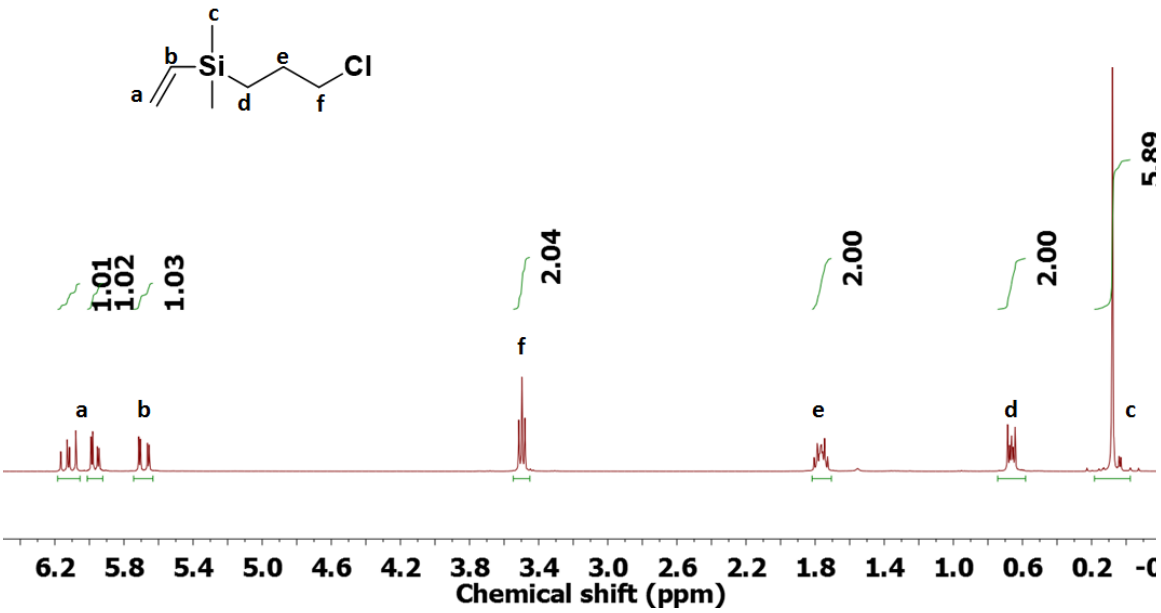

Figure 5.3.1.1. ^{1}H NMR spectrum of 3-chloropropyldimethylvinylsilane.

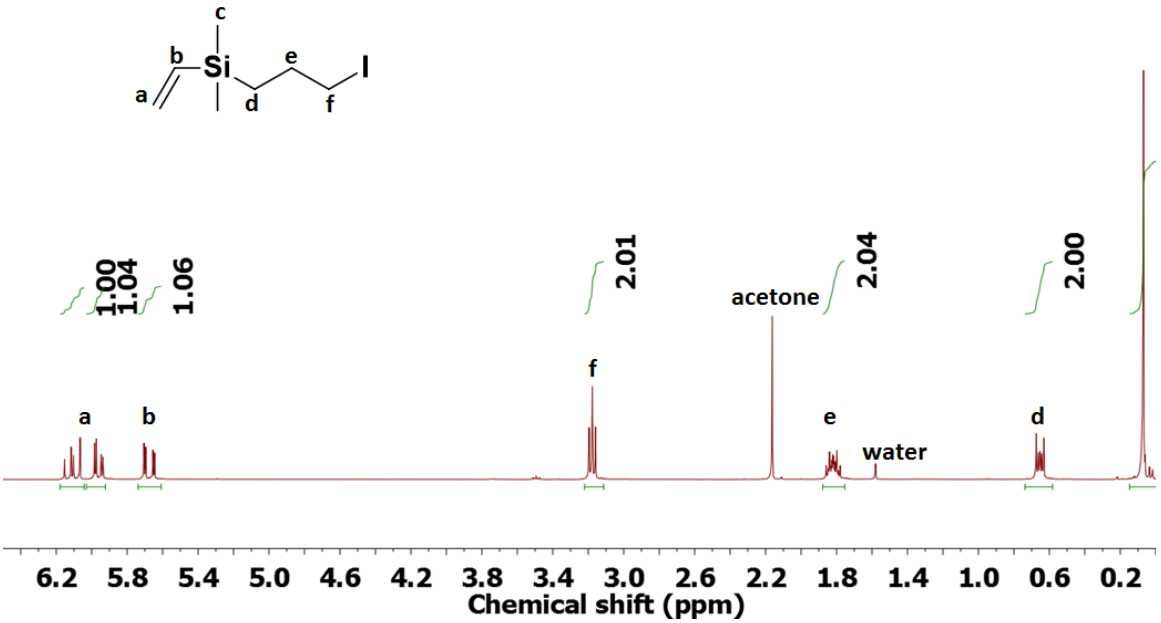

Figure 5.3.1.2. ^{1}H NMR spectrum of 3-iodopropyldimethylvinylsilane.

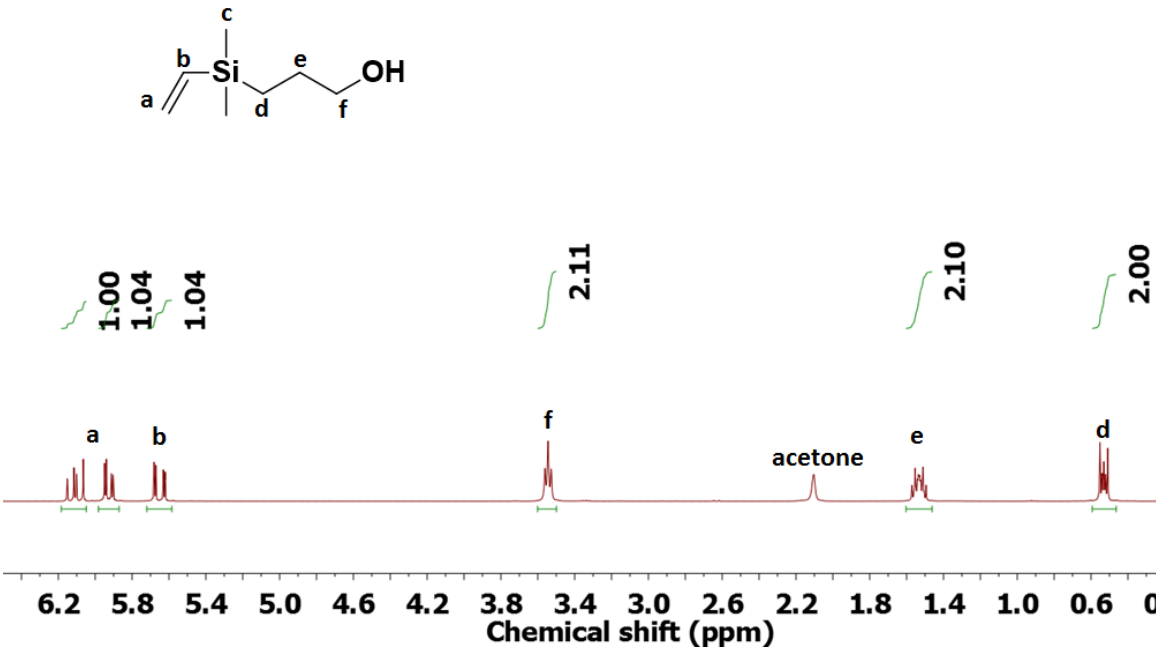

Figure 5.3.1.3. ^{1}H NMR spectrum of 3-hydroxypropyldimethylvinylsilane.

5.3.2 Synthesis and characterization of asymmetric triblock copolymers

A method for preparing H_2N-PEO-PPO-PEO-OH copolymers wherein the block lengths of the PEO and PPO segments were varied independently was developed. The triblock copolymers were synthesized through sequential monomer additions in three steps. The first two blocks were polymerized with a $Zn_3[Co(CN)_6]_2$ coordination catalyst and this avoided the common side reactions that occur in base-catalyzed polymerization of PO (Schemes 5.3.2.1 and 5.3.2.2). The third block (PEO) had to be polymerized with base to afford good molecular weight distributions of the terminal low molecular weight PEO segment (Scheme 5.3.2.3).

The average degrees of polymerization of EO in the first PEO blocks were calculated by comparing the integral ratio of the peak at 0.47 ppm, which corresponded to the methylene group next to the silicon atom, to the peaks at 3.4-3.8 ppm corresponding to the EO repeating units (Figure 5.3.2.1). The average molecular weights of the second PPO blocks were determined by comparing the integral ratio of the peak at 0.47 ppm, which corresponded to the methylene group next to the silicon atom, to the peaks at 1.1 ppm corresponding to the methyl groups in PO repeating units (Figure 5.3.2.2).

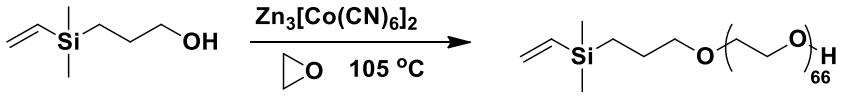

Scheme 5.3.2.1. Synthesis of a 2.7k vinyl-PEO-OH.

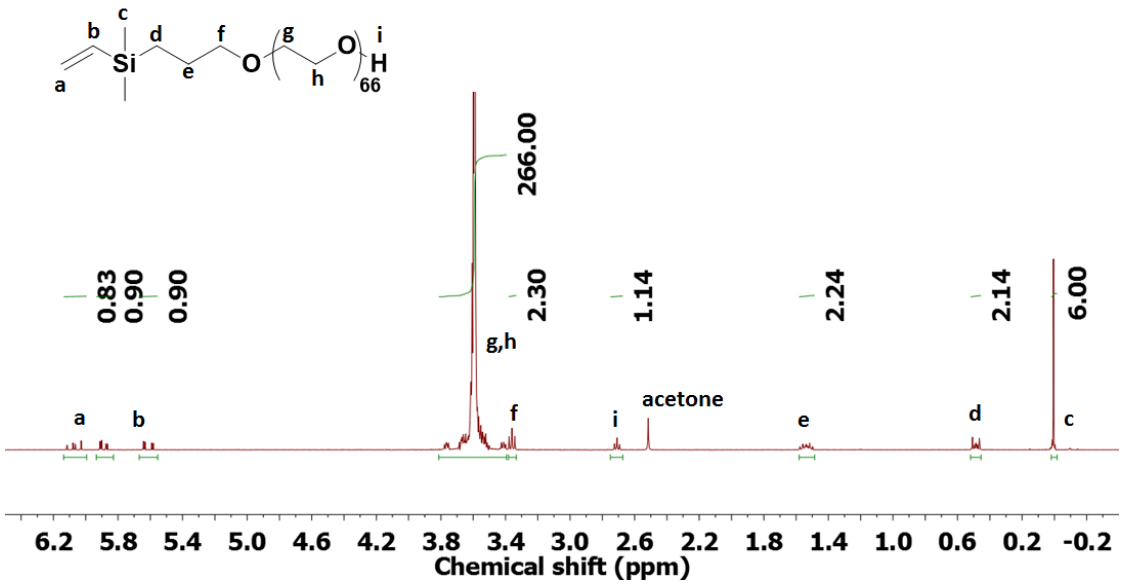

Figure 5.3.2.1. ^{1}H NMR of a 2.7k vinyl-PEO-OH.

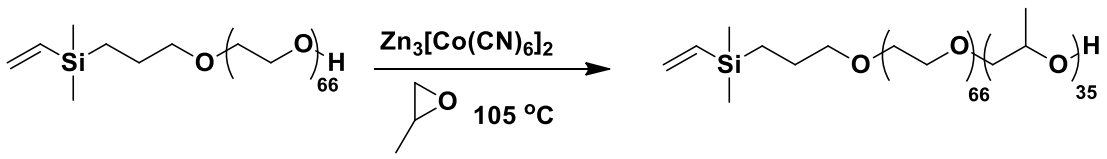

Scheme 5.3.2.2. Synthesis of a vinyl-2.7k PEO-2.0k PPO-OH.

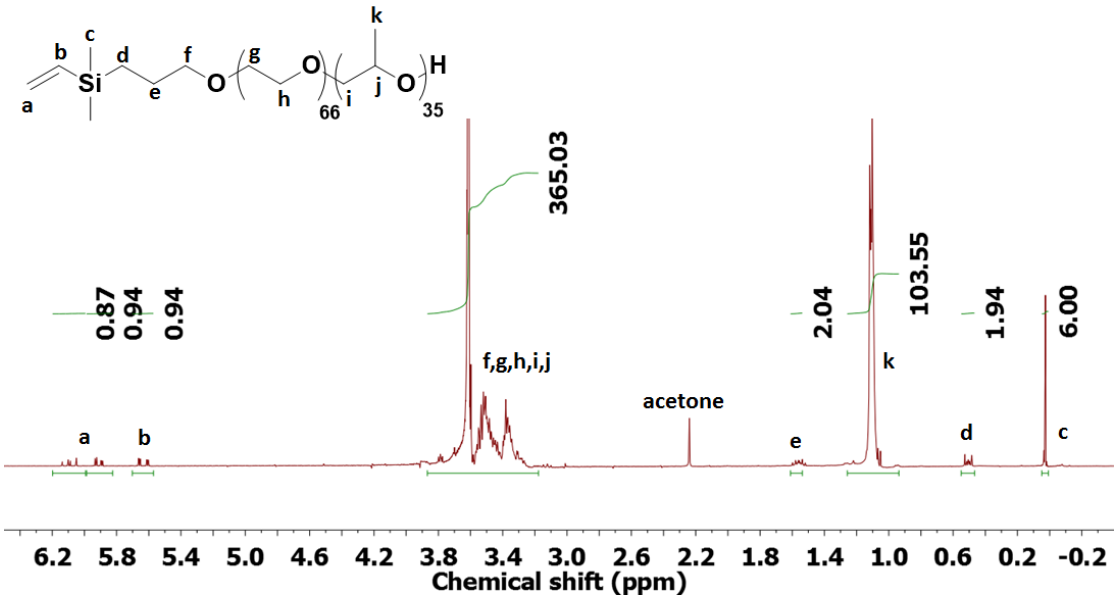

Figure 5.3.2.2. ^{1}H NMR of a vinyl-2.7k PEO-2.0k PPO-OH.

The third PEO block was prepared via ring-opening polymerization of EO using a diblock dimethylvinylsilylpropyl-PEO-PPO-OH copolymer as an initiator (5.3.2.3). In this stage, secondary –OH groups in the terminal PO units are converted to primary -OH groups in the EO units. It is well known that the reaction of an activated secondary alcohol with EO is slower than the reaction of an analogous activated primary alcohol with EO, thus making propagation of EO faster than the crossover reaction from the PO block to the first EO addition. Coordination of a zinc ion on the heterogeneous double metal cyanide may also affect the relative rates of this crossover reaction versus EO propagation. The effects

of these relative rates need to be minimized to obtain better control over the molecular weight distribution of the third block. We investigated both the use of the coordination catalyst and also an anionic initiator to understand how the molecular weight distributions were affected, and found that anionic polymerization of the short PEO terminal block was the superior approach. The block length of the third (PEO) block was calculated by the increased integral number of the resonances at 3.2-3.8 ppm relative to the PO unit resonances (Figure 5.3.2.3).

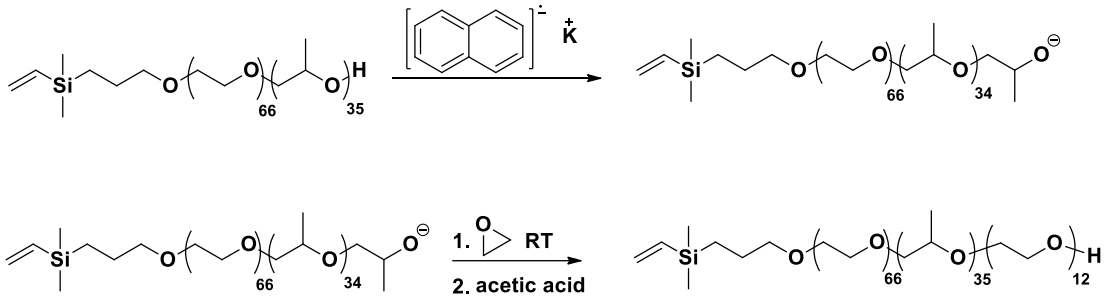

Scheme 5.3.2.3. Synthesis of a vinyl-2.7k PEO-2.0k PPO-0.5k PEO-OH.

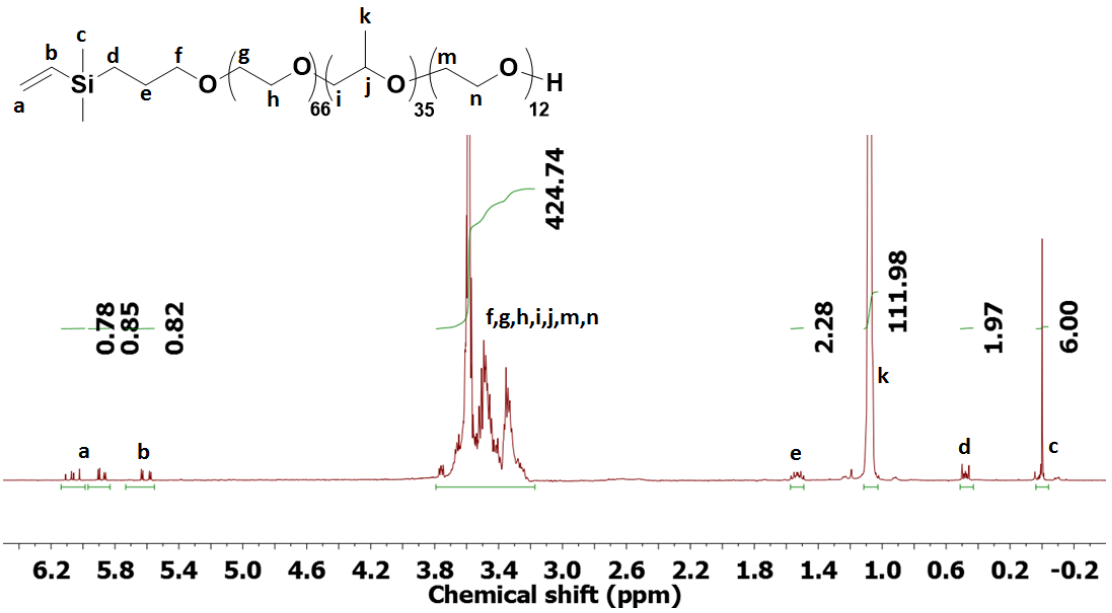

Figure 5.3.2.3. ^{1}H NMR spectrum of a vinyl-2.7k PEO-2.0k PPO-0.5k PEO-OH.

To determine the extent of conversion of terminal PO units to EO units with the short terminal blocks, the triblock copolymers were reacted with trifluoroacetic anhydride (Scheme 5.3.2.4). ^{19}F NMR spectra of the polymeric trifluoroacetate esters were compared with a homopolymer of propylene oxide that had exclusively secondary alcohol endgroups and a commercial P85 triblock copolymer ester (Figure 5.3.2.4 and Table 5.3.2.1). The secondary esters had a lower ^{19}F chemical shift relative to the primary esters due to the extra electron-donating methyl group in the poly(propylene oxide) repeating unit. Moreover, the secondary ester had two peaks in the ^{19}F NMR spectrum and this was attributed to the chiral center next to the ester bond.

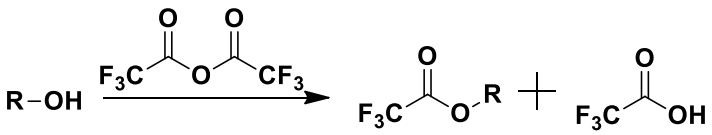

Scheme 5.3.2.4. A representative reaction of a polyether with trifluoroacetic anhydride.

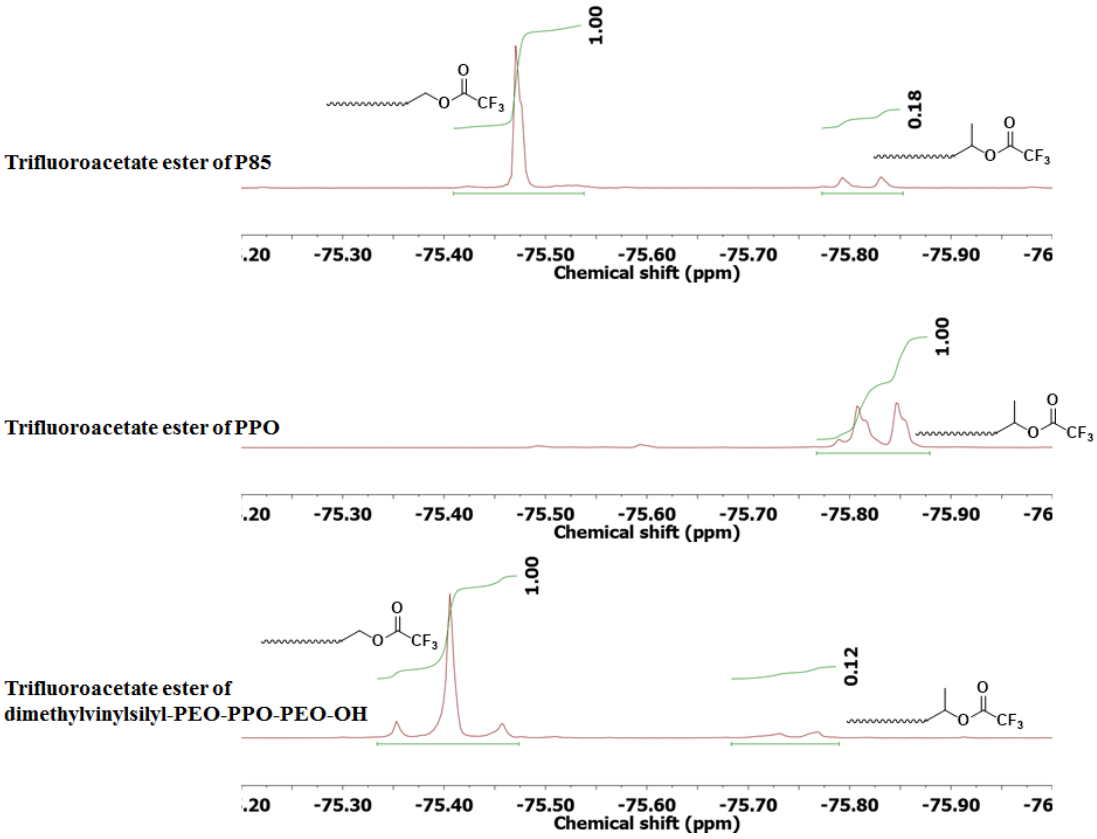

Figure 5.3.2.4. ^{19}F NMR spectra of polyether trifluoroacetate esters.

Table 5.3.2.1. Characterization of asymmetric triblock copolyethers.

Targeted MW (g/mol) NH_2-PEO-PPO-PEO-OH	^{1}H-NMR Mn (g/mol) NH_2-PEO-PPO-PEO-OH	^{1}H-NMR total Mn (g/mol)	SEC total Mn (g/mol)	PDI By GPC	Extent of primary OH end groups
1,000-2,000-500	1,074-1,716-279	3,069	2973*	1.05	89%
2,500-2,000-500	2,609-1,991-471	5,071	4,233*	1.18	90%
2,500-3,500-1,500	2,733-3,731-1,326	7,790	5,150*	1.43	94%
2,500-3,500-2,600	2,733-3,596-2,591	8,920	6,536*	1.05	100%

*The difference between total M_n from ^{1}H-NMR and SEC increases as the M_n increases.

5.3.3 Synthesis of triblock amino-PEO-PPO-PEO-OH copolymers

Thiol-ene reactions, which are highly efficient reactions of thiols with reactive carbon-carbon double bonds, were reported in the early 1900s.[26,28,29] These reactions have been intensively investigated and employed for post-polymerization modifications due to their desirable features including high yield, fast reaction rates, mild reaction conditions and insensitivity to oxygen and water.[27,28,30-33] It is noteworthy that the vinylsilyl group does not undergo radical homopolymerization.[23,28,31,34] This avoids many of the side reactions in thiol-ene reactions that plague such reactions with allyl and acrylate analogues. In the present research, terminal amines were introduced onto the copolymers via a thiol-ene reaction of the terminal vinylsilyl groups with cysteamine hydrochloride (Scheme 5.3.3.1). The reaction was monitored by observing complete disappearance of the vinyl groups at 5.6-6.2 ppm and appearance of the methylene groups at 0.8 and 2.5-3.0 ppm in the ^{1}H NMR spectrum (Figure 5.3.3.1). The appearance of the extra peak at ~0 ppm was attributed to the existence of both Markovnikov and anti-Markovnikov addition.

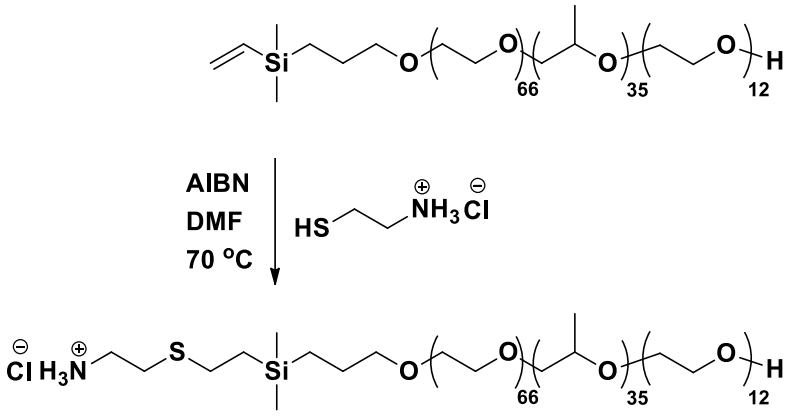

Scheme 5.3.3.1. A thiol-ene reaction of a vinyl-2.9k PEO-2.5k PPO-0.5k PEO-OH with cysteamine hydrochloride.

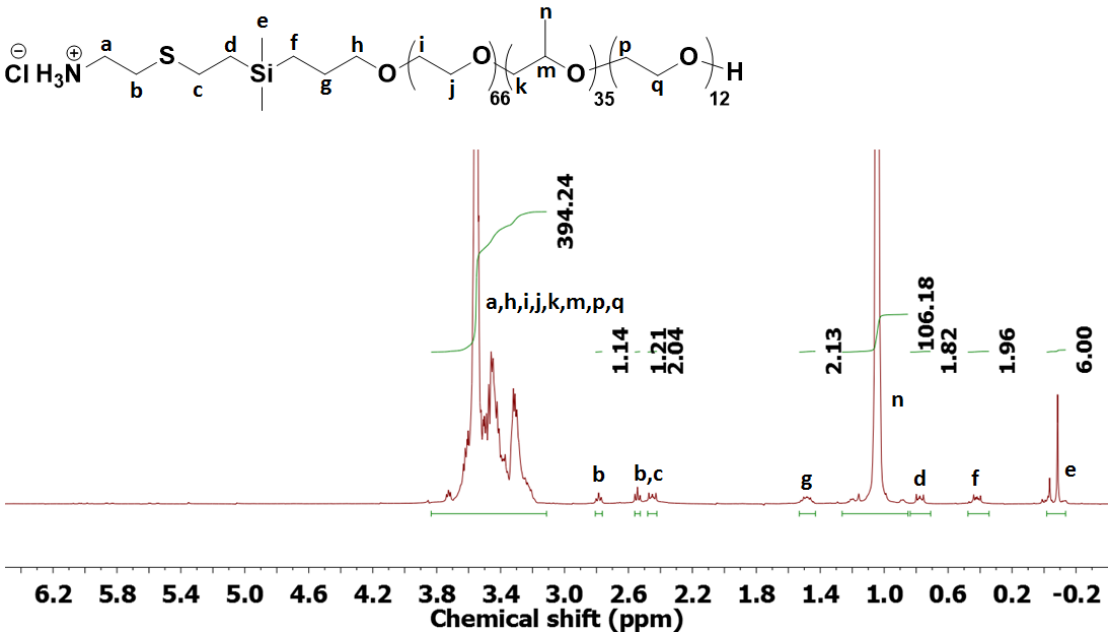

Figure 5.3.3.1. ^{1}H NMR spectrum of an amino-2.9k PEO-2.5k PPO-0.5k PEO-OH.

5.3.4 Synthesis and characterization of SOD1-polymer conjugates

As shown in Scheme 5.3.4.1**,** triblock amino-PEO-*b*-PPO-*b*-PEO-OH copolyethers were reacted with an excess of disuccinimidyl suberate (DSS) to form amide bonds with the terminal amine on the initiator end of the first PEO block. This generated activated N-hydroxysuccinimide (NHS) esters on one end of the copolyethers. After removing the excess DSS, the activated polymeric ester groups were conjugated with primary amines on SOD1. The conjugates were purified to remove excess free polymers and any non-conjugated SOD1. Six SOD1-polymer conjugates, including SOD1-Pluronic® P85 and SOD1-AP1 to AP5 (Table 5.3.4.1) were investigated. The presence of protein smears were observed by sodium dodecyl sulfate-polyacrylamide gel electrophoresis (SDS-PAGE) for all the SOD1-polymer conjugates, confirming conjugation of the polymers with SOD1 (Figure 5.3.4.1A). As observed with SOD1-AP2 as an example, mass spectra suggested

that the conjugates contained a mixture of proteins modified by several polymer chains (labeled by arrows) (Figure 5.3.4.1B).

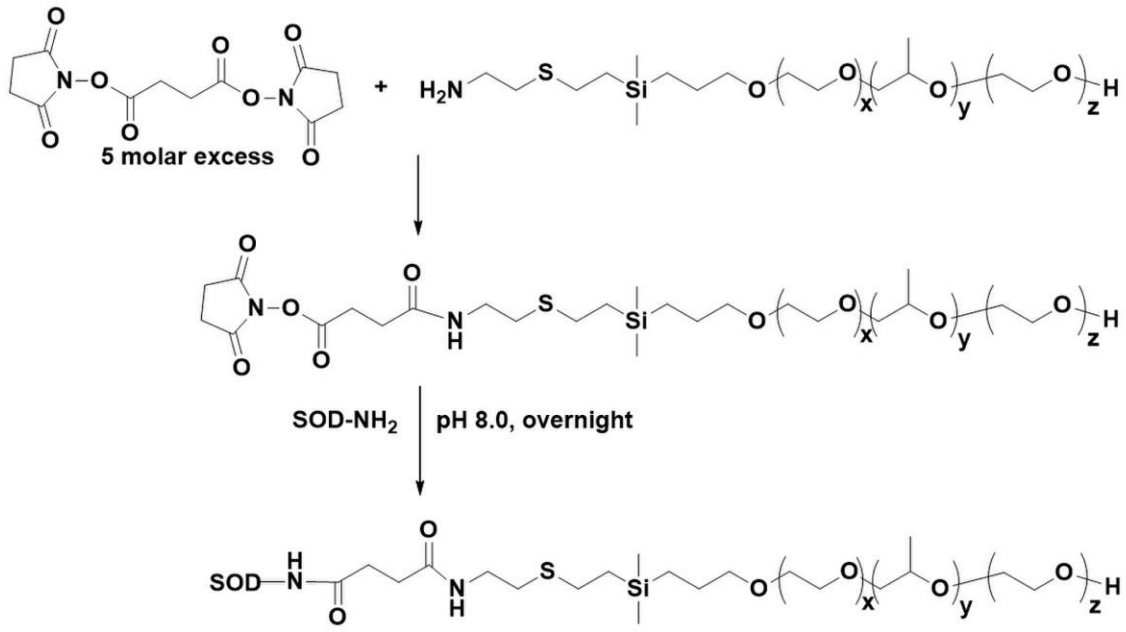

Scheme 5.3.4.1 Synthesis of SOD-polyether conjugates.

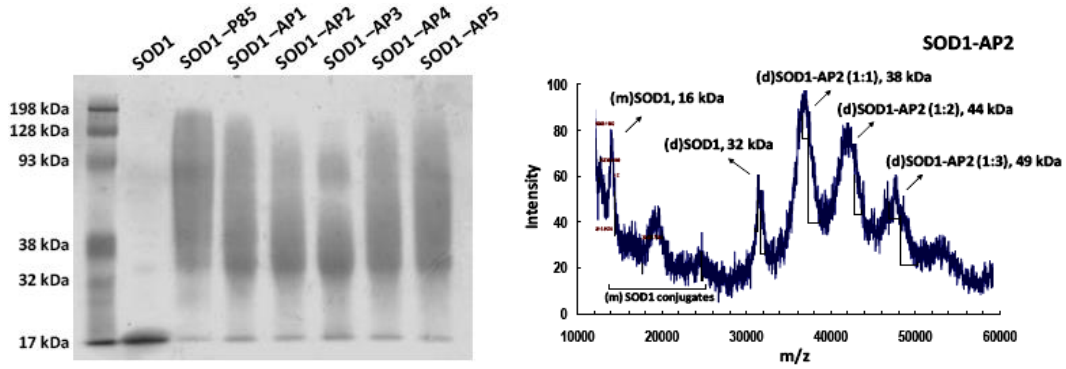

Figure 5.3.4.1 (A) SDS-PAGE of SOD1 and SOD1-polymer conjugates (left) and (B) a mass spectrum of SOD1-AP2 conjugates (right).

The average numbers of polymers attached to each SOD1 enzyme was 8-10 for all the conjugates, as determined by titration of residual amines on the protein with TNBS

(Scheme 5.3.4.2 and Table 5.3.4.1). Less than 10% of the native SOD1 enzymatic activity was retained with these conjugates, as measured by the pyrogallol assay. SOD1-P85 conjugates with lower modification degrees were made with DSS or dithio-bis(succinimidyl propionate) (DSP) as the linker. The loss of enzyme activity was attributed to heavy polymer modification (Table 5.3.4.2).

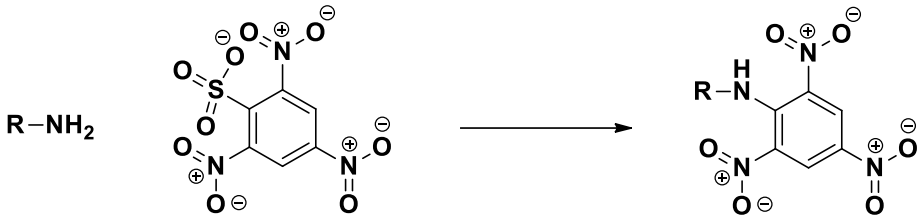

Scheme 5.3.4.2 Reaction of primary amine with 2,4,6-trinitrobenzenesulfonic acid (TNBS).

Table 5.3.4.1. Characteristics of SOD1-polymer conjugates.

Conjugates	Polymer Structure	Modification Degree[a]	Residual Activities (%)[b]
SOD-PEO	EO_{114}	>10	N/A
SOD-P85	EO_{26}-PO_{40}-EO_{26}	9.9	5.87
SOD-AP1	NH_2-EO_{45}-PO_{60}-EO_{34}	8.9	5.13
SOD-AP2	NH_2-EO_{61}-PO_{34}-EO_{11}	9.5	8.20
SOD-AP3	NH_2-EO_{23}-PO_{34}-EO_8	8.9	4.34
SOD-AP4	NH_2-EO_{62}-PO_{63}-EO_{29}	8.1	5.21
SOD-AP5	NH_2-EO_{62}-PO_{63}-EO_{58}	8.6	5.21

[a] Average number of polymer chains per SOD1 as determined by TNBS titration of residual amino groups.

[b] Residual activity was determined by the pyrogallol autoxidation kinetic assay and calculated based on the percentage of activity of the native SOD1.

Table 5.3.4.2. Residual activities of SOD1-polymer conjugates with various degrees of modification.

Polymer	Linker	Polymer:SOD1 molar ratio	Modification Degree	Residual Activity (%)
P85	DSP	5	1.26	62
P85	DSP	10	2.92	57
P85	DSP	30	4.11	44
P85	DSP	60	7.99	NN
P85	DSS	5	3.9	38
P85	DSS	10	5.41	27
P85	DSS	30	7.44	25

5.3.5 Cellular uptake of SOD1-polymer conjugates

After 24 hours of incubation with the cells, all of the SOD1-polymer conjugates and SOD1-PEO exhibited significant cellular uptake compared to unmodified SOD1 ($p<0.05$) (Figure 5.3.5.1), but the uptake for SOD1-P85 was higher than for the others ($p<0.05$). This suggests that some of these polymers have potential for enhancing cellular delivery of proteins.

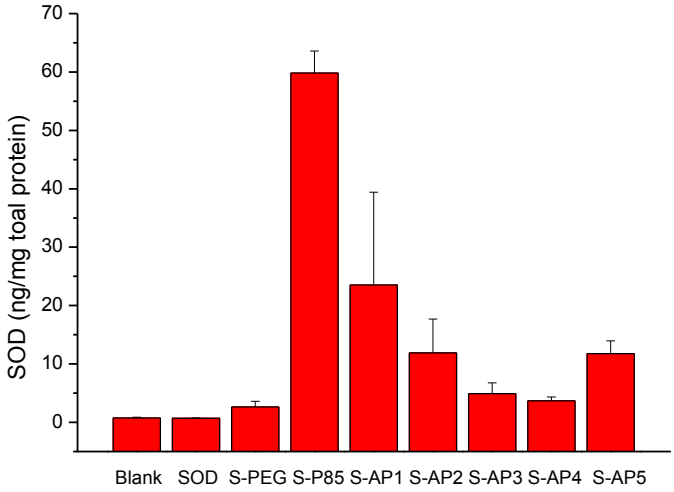

Figure 5.3.5.1. Cellular uptake of SOD1 and SOD1-polymer conjugates.

5.4 Conclusions

A series of asymmetric amphiphilic PEO-PPO-PEO copolyethers with different block lengths were synthesized and characterized. Amino groups were introduced to one end of the copolyether for conjugating with the protein. The copolyethers were conjugated to SOD1 through reaction with NHS-functional coupling agents. It was established that the conjugation method resulted in heavy enzyme modification (8-10 polymers per enzyme) but highly reduced enzymatic activities. The low enzymatic activities were attributed to the large amount of polymers that were bound to the enzyme. All of the conjugates exhibited enhanced cellular uptake compared to unmodified SOD1, with SOD1-P85 having the highest uptake.

5.5 References

(1) Yi, X.; Batrakova, E.; Banks, W. A.; Vinogradov, S.; Kabanov, A. V., Protein conjugation with amphiphilic block copolymers for enhanced cellular delivery *Bioconjugate Chem.* **2008**, *19*, 1071.

(2) Yi, X. A.; Zimmerman, M. C.; Yang, R. F.; Tong, J.; Vinogradov, S.; Kabanov, A. V., Pluronic-modified superoxide dismutase 1 attenuates angiotensin II-induced increase in intracellular superoxide in neurons *Free Radical Bio. Med.* **2010**, *49*, 548.

(3) Kabanov, A. V.; Batrakova, E. V.; Alakhov, V. Y., Pluronic((R)) block copolymers for overcoming drug resistance in cancer *Adv. Drug Delivery Rev.* **2002**, *54*, 759.

(4) Gebhart, C. L.; Sriadibhatla, S.; Vinogradov, S.; Lemieux, P.; Alakhov, V.; Kabanov, A. V., Design and formulation of polyplexes based on pluronic-polyethyleneimine conjugates for gene transfer *Bioconjugate Chem.* **2002**, *13*, 937.

(5) Kabanov, A. V.; Batrakova, E. V.; Alakhov, V. Y., Pluronic (R) block copolymers as novel polymer therapeutics for drug and gene delivery *J. Controlled Release* **2002**, *82*, 189.

(6) Ochietti, B.; Lemieux, P.; Kabanov, A. V.; Vinogradov, S.; St-Pierre, Y.; Alakhov, V., Inducing neutrophil recruitment in the liver of ICAM-1-deficient mice using polyethyleneimine grafted with pluronic P123 as an organ-specific carrier for transgenic ICAM-1 *Gene. Ther.* **2002**, *9*, 939.

(7) Ochietti, B.; Guerin, N.; Vinogradov, S. V.; St-Pierre, Y.; Lemieux, P.; Kabanov, A. V.; Alakhov, V. Y., Altered organ accumulation of oligonucleotides using polyethyleneimine grafted with poly(ethylene oxide) or pluronic as carriers *J. Drug Target* **2002**, *10*, 113.

(8) Kabanov, A. V.; Lemieux, P.; Vinogradov, S.; Alakhov, V., Pluronic((R)) block copolymers: novel functional molecules for gene therapy *Adv. Drug Delivery Rev.* **2002**, *54*, 223.

(9) Kabanov, A. V.; Alakhov, V. Y., Pluronic (R) block copolymers in drug delivery: From micellar nanocontainers to biological response modifiers *Crit. Rev. Ther. Drug* **2002**, *19*, 1.

(10) Batrakova, E. V.; Li, S.; Alakhov, V. Y.; Elmquist, W. F.; Miller, D. W.; Kabanov, A. V., Sensitization of cells overexpressing multidrug-resistant proteins by Pluronic P85 *Pharmaceut. Res.* **2003**, *20*, 1581.

(11) Kabanov, A. V.; Batrakova, E. V.; Alakhov, V. Y., An essential relationship between ATP depletion and chemosensitizing activity of Pluronic((R)) block copolymers *J. Controlled Release* **2003**, *91*, 75.

(12) Batrakova, E. V.; Li, S.; Alakhov, V. Y.; Miller, D. W.; Kabanov, A. V., Optimal structure requirements for pluronic block copolymers in modifying P-glycoprotein drug efflux transporter activity in bovine brain microvessel endothelial cells *J. Pharmacol. Exp. Ther.* **2003**, *304*, 845.

(13) Kabanov, A. V.; Batrakova, E. V.; Miller, D. W., Pluronic((R)) block copolymers as modulators of drug efflux transporter activity in the blood-brain barrier *Adv. Drug Delivery Rev.* **2003**, *55*, 151.

(14) Batrakova, E. V.; Li, S.; Li, Y. L.; Alakhov, V. Y.; Elmquist, W. F.; Kabanov, A. V., Distribution kinetics of a micelle-forming block copolymer Pluronic P85 *J. Controlled Release* **2004**, *100*, 389.
(15) Batrakova, E. V.; Li, S.; Li, Y. L.; Alakhov, V. Y.; Kabanov, A. V., Effect of pluronic p85 on ATPase activity of drug efflux transporters *Pharmaceut. Res.* **2004**, *21*, 2226.
(16) Batrakova, E. V.; Zhang, Y.; Li, Y. L.; Li, S.; Vinogradov, S. V.; Persidsky, Y.; Alakhov, V. Y.; Miller, D. W.; Kabanov, A. V., Effects of pluronic p85 on GLUT1 and MCT1 transporters in the blood-brain barrier *Pharmaceut. Res.* **2004**, *21*, 1993.
(17) Belenkov, A. I.; Alakhov, V. Y.; Kabanov, A. V.; Vinogradov, S. V.; Panasci, L. C.; Monia, B. P.; Chow, T. Y. K., Polyethyleneimine grafted with pluronic P85 enhances Ku86 antisense delivery and the ionizing radiation treatment efficacy in vivo *Gene. Ther.* **2004**, *11*, 1665.
(18) Kabanov, A. V.; Sriadibhatla, S.; Yang, Z. H.; Alakhov, V. Y., Effect of pluronic block copolymers on gene expression. *Abstr. Pap. Am. Chem. S.* **2004**, *228*, U388.
(19) Oh, K. T.; Bronich, T. K.; Kabanov, A. V., Micellar formulations for drug delivery based on mixtures of hydrophobic and hydrophilic Pluronic((R)) block copolymers *J. Controlled Release* **2004**, *94*, 411.
(20) Minko, T.; Batrakova, E. V.; Li, S.; Li, Y. L.; Pakunlu, R. I.; Alakhov, V. Y.; Kabanov, A. V., Pluronic block copolymers alter apoptotic signal transduction of doxorubicin in drug-resistant cancer cells *J. Controlled Release* **2005**, *105*, 269.
(21) Alakhov, V. Y.; Moskaleva, E. Y.; Batrakova, E. V.; Kabanov, A. V., Hypersensitization of multidrug resistant human ovarian carcinoma cells by pluronic P85 block copolymer *Bioconjugate Chem.* **1996**, *7*, 209.
(22) Venne, A.; Li, S. M.; Mandeville, R.; Kabanov, A.; Alakhov, V., Hypersensitizing effect of pluronic L61 on cytotoxic activity, transport, and subcellular distribution of doxorubicin in multiple drug-resistant cells *Cancer Res.* **1996**, *56*, 3626.
(23) Mangold, C.; Dingels, C.; Obermeier, B.; Frey, H.; Wurm, F., PEG-based Multifunctional Polyethers with Highly Reactive Vinyl-Ether Side Chains for Click-Type Functionalization *Macromolecules* **2011**, *44*, 6326.
(24) Batrakova, E. V.; Vinogradov, S. V.; Robinson, S. M.; Niehoff, M. L.; Banks, W. A.; Kabanov, A. V., Polypeptide point modifications with fatty acid and amphiphilic block copolymers for enhanced brain delivery *Bioconjugate Chem.* **2005**, *16*, 793.
(25) Price, T. O.; Farr, S. A.; Yi, X.; Vinogradov, S.; Batrakova, E.; Banks, W. A.; Kabanov, A. V., Transport across the Blood-Brain Barrier of Pluronic Leptin *J Pharmacol. Exp. Ther.* **2010**, *333*, 253.
(26) Vadala, M. L.; Thompson, M. S.; Ashworth, M. A.; Lin, Y.; Vadala, T. P.; Ragheb, R.; Riffle, J. S., Heterobifunctional poly(ethylene oxide) oligomers containing carboxylic acids *Biomacromolecules* **2008**, *9*, 1035.
(27) Goff, J. D.; Huffstetler, P. P.; Miles, W. C.; Pothayee, N.; Reinholz, C. M.; Ball, S.; Davis, R. M.; Riffle, J. S., Novel Phosphonate-Functional Poly(ethylene

oxide)-Magnetite Nanoparticles Form Stable Colloidal Dispersions in Phosphate-Buffered Saline *Chem. Mater.* **2009**, *21*, 4784.
(28) Hoyle, C. E.; Bowman, C. N., Thiol-Ene Click Chemistry *Angew. Chem. Int. Edit.* **2010**, *49*, 1540.
(29) Posner, T., *Ber. Dtsch. Chem. Ges.* **1905**, *38*, 646.
(30) Lou, F. W.; Xu, J. M.; Liu, B. K.; Wu, Q.; Pan, Q.; Lin, X. F., Highly selective anti-Markovnikov addition of thiols to vinyl ethers under solvent- and catalyst-free conditions *Tetrahedron Lett.* **2007**, *48*, 8815.
(31) Cramer, N. B.; Reddy, S. K.; O'Brien, A. K.; Bowman, C. N., Thiol-ene photopolymerization mechanism and rate limiting step changes for various vinyl functional group chemistries *Macromolecules* **2003**, *36*, 7964.
(32) Kade, M. J.; Burke, D. J.; Hawker, C. J., The Power of Thiol-ene Chemistry *J. Polym. Sci. Pol. Chem.* **2010**, *48*, 743.
(33) Lowe, A. B., Thiol-ene "click" reactions and recent applications in polymer and materials synthesis *Polym. Chem.-Uk* **2010**, *1*, 17.
(34) Mishima, E.; Yamago, S., Controlled Alternating Copolymerization of (Meth)acrylates and Vinyl Ethers by Using Organoheteroatom-Mediated Living Radical Polymerization *Macromol. Rapid Comm.* **2011**, *32*, 893.

Chapter 6: Conclusions and Recommendations

In this work, three types of copolymers were synthesized as nanocarriers for drugs, iron oxide or proteins to achieve enhanced biocompatibilities. The complexes were formed via hydrophobic interactions, ligand adsorption or covalent bonds. These copolymers were assembled into core-shell nanostructures in aqueous media and their dispersions were stabilized by the hydrophilic shells comprised of poly(ethylene oxide).

Chapter 3 describes syntheses of two vinyl-functional epoxide monomers and a series of novel amphiphilic polyethers with pendent functional groups that were designed to be utilized as a platform for crosslinkable and stimuli-sensitive nanoparticles. The reaction conditions and rates of anionic ring-opening copolymerizations of the functional epoxides with 1,2-butylene oxide were investigated to understand the microstructures of these copolymers. Functional amphiphilic copolyethers with either triblock or tapered structrures were synthesized. Multiple amines and carboxylic acids were added to the copolyethers via thiol-ene additions across the vinyl groups. Investigations of the aggregation properties of these functional copolymers in aqueous media by DLS indicated that pH-sensitive micelles were formed. All CMCs of the functional copolyethers presented in this research were in the range of 0.005-0.5 mg/mL, which were greatly lower than the CMCs of some typical Pluronic triblock copolyethers. The low CMCs promoted high colloidal stabilities of the polymeric micelles, which were of great interests as drug carriers. An antiretroviral drug, ritonavir, was loaded into micelles of these copolyethers using a rapid, continuous precipitation technique yielding well-controlled nanoparticles.

Chapter 4 describes a synthetic method for making magnetic complexes with biodegradable polymers and includes both single particles and clusters. Poly(ethylene

oxide)-*b*-poly(L-glutamic acid) copolymers were synthesized and used as carriers for iron oxide nanoparticles. A mixed organic solvent comprised of a 1:1 v:v DMF:chloroform mixture was found to be a superior medium for coating the polymers onto the iron oxide nanoparticles as compared to water. The magnetic nanoparticles prepared in this mixed organic solvent were colloidally stable in simulated physiological solutions for up to a week as measured by DLS. Allyl and thiol groups were introduced to the end of PEO block and utilized as crosslink sites to make magnetic clusters. Clusters were formed from these complexes by 1) crosslinking the allyl-tipped single particles with dithiol-PEO, 2) crosslinking the thiol-tipped single particles with diallyl-PEO and 3) crosslinking two of the functional single particles with each other. The third method was determined to be best one due to the existence of iron oxide in both allyl- and thiol-functional species as well as the reduction of undesirable intra-particle crosslink by avoiding the use of bifunctional PEOs. The clusters were determined to have great potential as MRI contrast agents due to their shorter transverse relaxation times compared to the single particles.

Chapter 5 described the synthesis of a series of asymmetric triblock poly(ethylene oxide)-*b*-poly(propylene oxide)-*b*-poly(ethylene oxide) copolyethers with terminal amines and different molecular weights of each block. The triblock copolyethers were covalently bonded with superoxide dismutase (SOD1) to understand effects of polymer modification on enzyme activities. It was shown that heavy modification by polymers led to low enzymatic activities of SOD1. The conjugates were found to have higher cellular uptake than the native SOD1 in MDCK cells.

One direction of the future work could involve precise control of the release rate of ritonavir. The nanoparticles stabilized with functional copolyethers will be crosslinked via

Michael-addition of the pendent amines with PEO diacrylate. The drug release properties can be tailored by controlling the degree of crosslink. A slower release rate is expected with a higher degree of crosslink. In addition, various crosslink reaction concentrations should be tested to find an optimal condition, under which the inter-particle crosslink is diminished while maintaining an efficient reaction rate. Release rates of ritonavir from crosslinked and uncrosslinked nanoparticles will be measured and compared.

It is also interesting to make dual imaging and therapeutic complexes. We will add phosphonate side groups to the copolyethers via Michael-addition of the pendent amines with diethyl vinylphosphonate followed by removal of the ethyl groups. Ritonavir will be loaded into micelles of the copolyethers and the pendent phosphonates could be utilized to bind iron oxide nanoparticles. Another possible approach to make dual imaging and therapeutic complexes is using oleic acid-coated iron oxide as the hydrophobic nucleating agent to form drug-containing nanoparticles with the amphiphilic copolyethers. Besides loading the relatively hydrophobic drugs in the cores via hydrophobic interactions, we can also load cationic drugs (e.g. gentamicin) using the PEO-*b*-PG/iron oxide nanoparticles via electrostatic interaction with the glutamate anions. These three types of complexes are expected to have different magnetic properties since the accessibility to water has a pronounce effect on the relaxivities of the magnetic particles.

Another interesting future work is to introduce folate groups to the copolyethers by reaction of the pendent amines with *N*-hydroxysuccinimide folate. The folate-functional copolyethers could be used as drug carriers for targeting delivery of anti-cancer drugs by interaction with the folate-receptors expressed on the surfaces of cancer cells.